Sheffield Hallam University

A Sheffield Hallam University thesis

REFERENCE

ProQuest Number: 10694269

ProQuest 10694269

THE SYNTHESIS AND CHARACTERISATION OF LANGMUIR-BLODGETT FILM FORMING TCNQ ADDUCTS

by Christopher Simon Bradley

Sheffield
Hallam University

A thesis submitted in partial fulfilment of the requirements of Sheffield Hallam University for the Degree of Doctor of Philosophy.

Collaborating organisation: Health and Safety Laboratory, Sheffield.

January1999

CONTENTS

Abstract

CHAPTER ONE: Organic Electroactive Materials

CHAPTER TWO: Synthetic Work

CHAPTER THREE: Synthetic Work - Results And Discussion

CHAPTER FOUR: Langmuir-Blodgett Films

CHAPTER FIVE: Langmuir-Blodgett Films - Experimental

CHAPTER SIX: Langmuir-Blodgett Films - Results and Discussion

Acknowledgements

Abstract

Substitution reactions of TCNQ (7,7,8,8-tetracyanoquinodimethane) with suitable electron donor moieties extended the range of γ-bridged adducts R(4)Q3CNQ and R(4)P3CNQ of which the short chain Z-β-(1-butyl-4'-quinolinium)-α-cyano-4-styryldicyanomethanide (C_4H_9(4)Q3CNQ) is a typical example. These zwitterionic D-π-A materials (where D and A are electron donors and acceptors respectively) exhibit properties such as solvatochromism, molecular rectification and second harmonic generation.

Further synthetic work concentrated on modifying the donor, the acceptor and the substitution position within these zwitterions to create a series of diverse materials for non-linear optic research. Modification of the picolinium and quinolinium systems where the TCNQ substitution is in the α-position, has created the extensive analogous series- R(2)Q3CNQ and R(2)P3CNQ, their properties being compared and contrasted to the original γ-bridged adducts.

The behaviour of the materials on the subphase and their resultant Langmuir-Blodgett (LB) film fabrication was studied. The abrupt change in molecular orientation in LB films of the γ-bridged adducts occurring at R= $C_{15}H_{31}$ and above was not seen in the more flatly orientated α-bridged adducts. Further characterisation of the LB films was performed using reflectance-absorption infra-red spectroscopy (RAIRS) and surface plasmon resonance (SPR).

A number of N-alkylpyridinium benzimidazolate betaine derivatives and the related betaine-TCNQ adducts were prepared and their LB film forming properties were studied.

CHAPTER 1

Organic Electroactive Materials

1.1 Historical

Traditionally, organic materials were considered to be insulators, having conductivities of less than 10^{-10} Scm^{-1} at room temperature. However, it was suggested at the turn of the century that organic materials may exhibit conductivities comparable to metals,[1,2] though these suggestions were treated with scepticism by the scientific community. Organic materials were considered to form ordered assemblies of discrete molecules in which electrons were located within molecular orbitals which overlap only within individual molecules. Then in 1954 an unstable perylene bromide salt [1] which had a conductivity at room temperature (σ_{rt}) of ≈ 1 Scm^{-1} was prepared.[3]

[1]
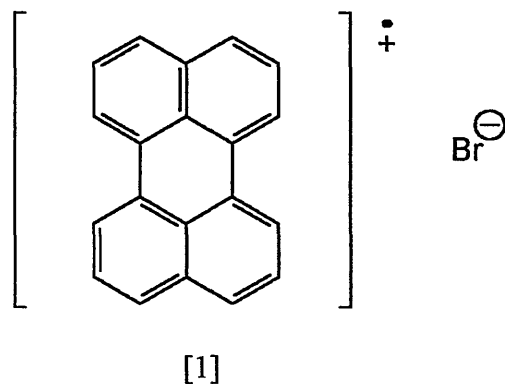
In 1960, Melby and his co-workers,[4] at duPont reported the synthesis of 7, 7, 8, 8 - tetracyano - p - quinodimethane (TCNQ) [2], a powerful new organic electron acceptor shown in Figure 1.01.
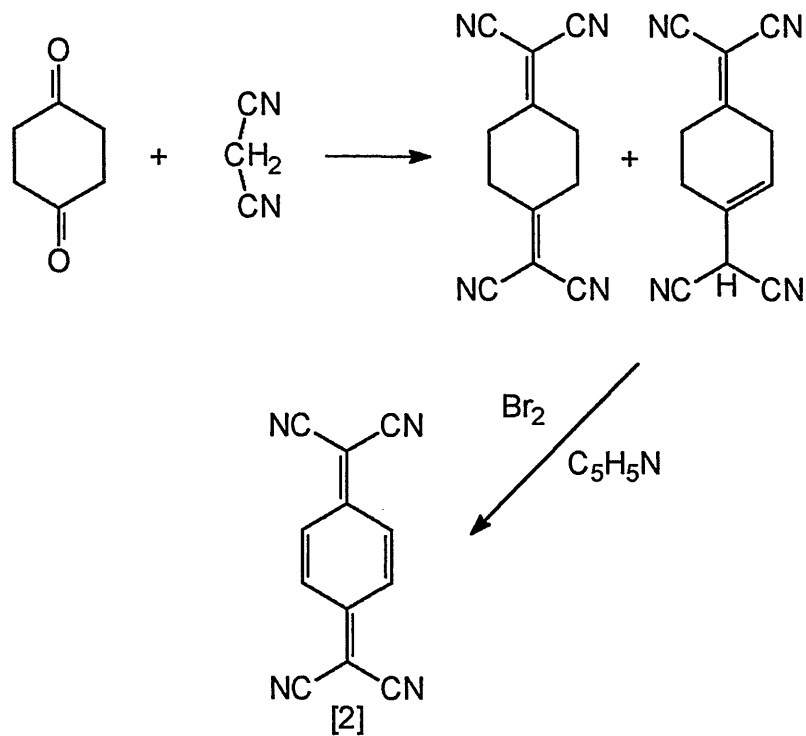
Figure 1.01 The synthesis of TCNQ from the condensation of malononitrile with 1, 4- cyclohexanedione.

TCNQ was found to yield a number of stable anion - radical derivatives, many of which were found to be semiconductors[4-9] with $\sigma_{rt} \approx 10^{-5}$ Scm^{-1}. TCNQ is a strong π acid and it forms two groups of salt-like complexes each involving a complete or partial transfer of an electron to TCNQ, with the formation of the anion - radical TCNQ$\stackrel{-}{\cdot}$ [Figure 1.02].
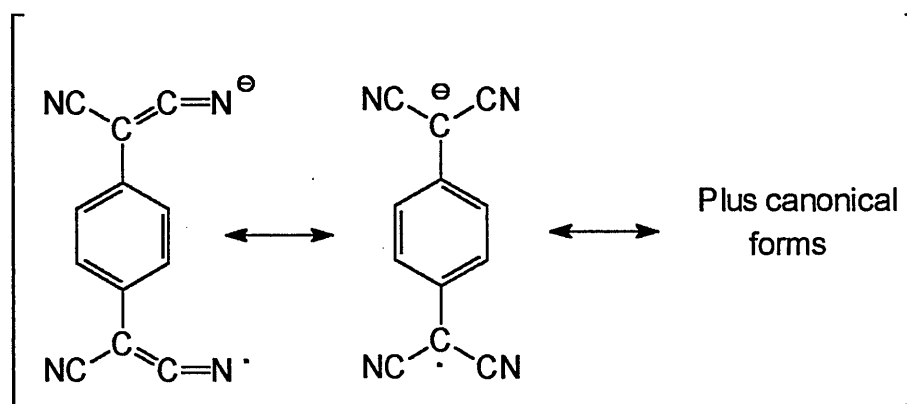
Figure 1.02 Stable TCNQ radical anions

The first group can be represented by the formula $M^+TCNQ^{\cdot-}$, e.g. LiTCNQ [3] shown in Figure 1.03, and many of these have relatively high electrical resistivities in the range 10^4 to 10^{12} Ωcm^{-1}.

$$[3]$$
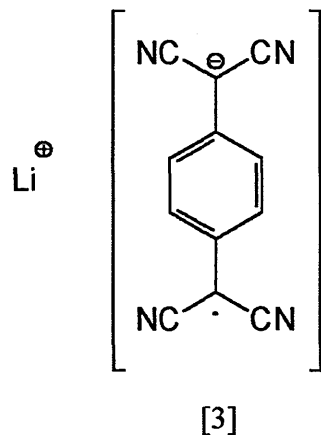
Figure 1.03 $Li^+TCNQ^{\cdot-}$ is an insulator, having a resistivity $> 10^{10}$ Ω cm^{-1}

The second group, with a molecule of neutral TCNQ in addition to the radical anion, is represented by the formula $M^+(TCNQ^{\cdot-})$ (TCNQ) e.g. [4] in Figure 1.04 and these have remarkably low resistivities of $0.01 - 100$ Ωcm^{-1}.

$$[4]$$
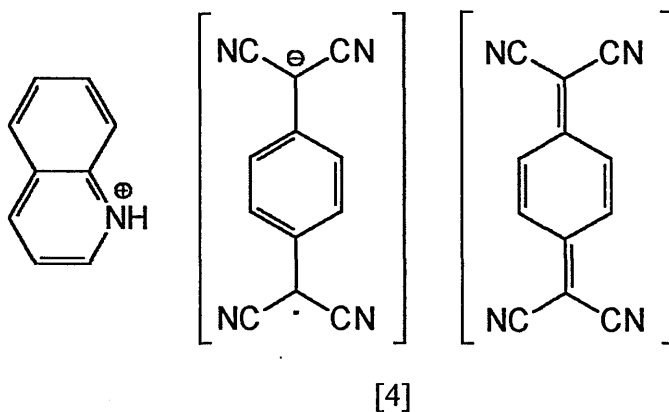
Figure 1.04 Quinolinium - TCNQ salt has a resistivity of 0.01Ω cm^{-1}, the lowest recorded by 1960 for any organic complex.

The initial research into TCNQ was itself sparked off by the discovery of the first percyanoalkene, tetracyanoethene (TCNE) [5], as this exhibited very versatile chemistry.[11]

NC   CN
   \   /
    C = C
   /   \
NC   CN
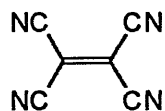
[5]

The quest for highly conducting compounds led to further work focusing on TCNQ salts.[12] It became apparent that high conductivity was associated with segregated stacks of donor (D) and acceptor (A) molecules, packing face to face, rather than mixed donor stacks (Figure 1.05).

D A D A D A   D A D A D A

A D A D A D   D A D A D A

D A D A D A   D A D A D A

A D A D A D   D A D A D A

Mixed stacks   Segregated stacks

Figure 1.05

Strong π-molecular donor and acceptor molecules can combine to produce charge transfer (CT) salts with one or both of the species being a thermodynamically stable radical ion. Conducting CT salts fall into two categories - either single chain conductors where the anion is a closed shell species, or a two-chain conductor, where both the donor and acceptor are open shell molecules that are able to form stable radical ions.

And in 1970,[13] a powerful new electron donor, tetrathiafulvalene (TTF) [6], was synthesised (Figure 1.06), with the subsequent TTF-TCNQ molecule recording the first organic metallic properties.
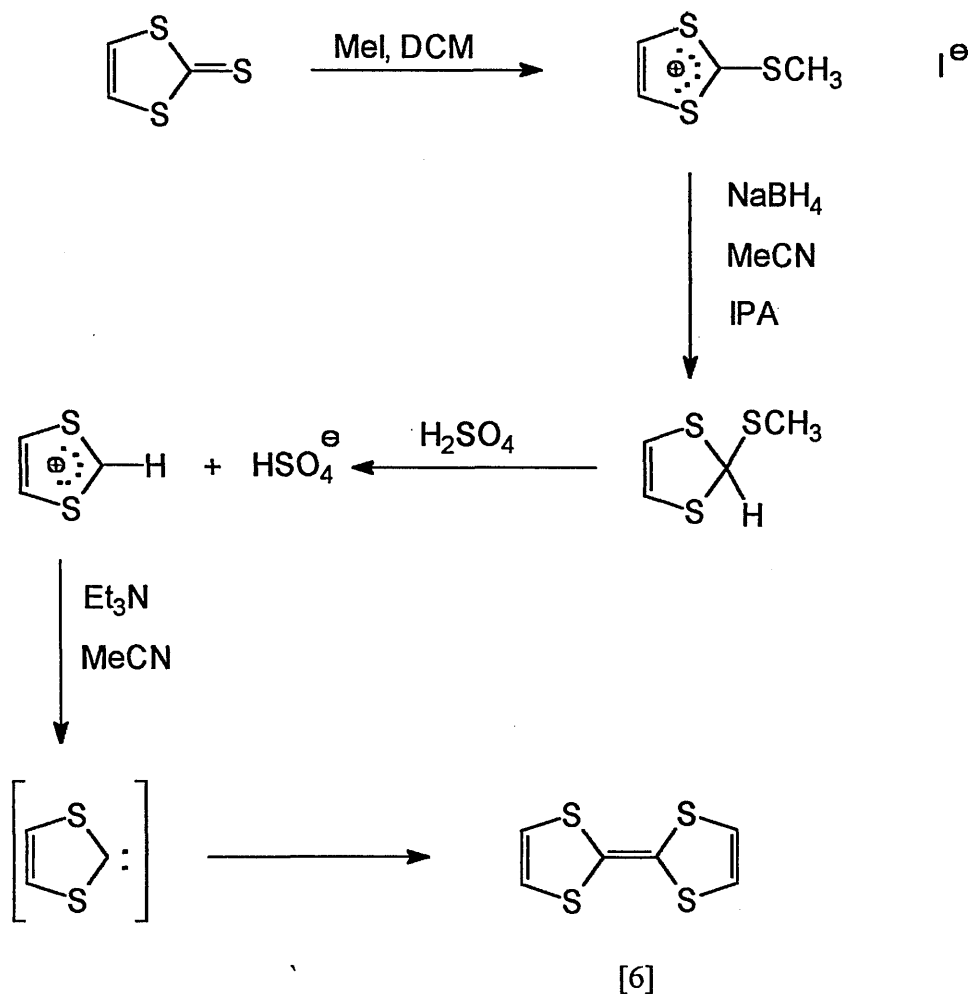
Figure 1.06 The Synthesis of TTF

1.2 Charge-Transfer Complexes

One of the earliest examples of a CT complex is that formed between iodine and benzene.[14] Although it was not a conductor, it possessed many typical features found in subsequent complexes. Its uv/vis spectrum showed characteristics associated with neither the solute nor the solvent, rather features associated with a `separate complex`. The explanation of these observations led to an extension of the Lewis acid-base theory and some of the phenomena associated with molecular complexes were forthcoming, such as very intense absorption bands in the uv/vis region of the spectra.

In the 1950's Mulliken[16] provided a molecular orbital description for electron acceptor-donor complexes. He stated that the donor (D) possesses a HOMO (Highest Occupied Molecular Orbital) and that the acceptor (A) possesses a LUMO (Lowest Unoccupied Molecular Orbital) and that charge transfer occurs between the HOMO of the donor and the LUMO of the acceptor. The bonding between the D and A was described by the following wave function:

$$\psi_N (A. D) = a\ \psi_0 (A. D) + b\ \psi_1 (A^- \text{-} D^+)$$

Here 'a' and 'b' are small integers, and $a > b$. ψ_0 is the "no-bond" contribution while ψ_1 is a dative bonding contribution. Thus $\psi_N (A. D)$ corresponds to the wave function that describes the combination of two extreme resonance forms. The above equation also implies that the degree to which charge transfer occurs may influence the nature of the complex. However it does not necessarily dictate the bonding within that complex.

In 1973 the first organic metal, TTF - TCNQ (Figure 1.07), was prepared[15] which was found to be highly conductive at room temperature ($\sigma rt = 500$ Scm^{-1}). However a dramatic increase in conductivity occurred below room temperature (- 1.47×10^4 Scm^{-1} at 66K). The 1:1 charge-transfer complex formed had the ideal electron distribution where 59% of the TTF is in the radical cation form and 59% of the TCNQ molecules are in the radical anion form, with the remaining molecules being present in the neutral form. The complex is effectively self doped by the charge-transfer that occurs between the crystals that grow in tilted, segregated stacks.
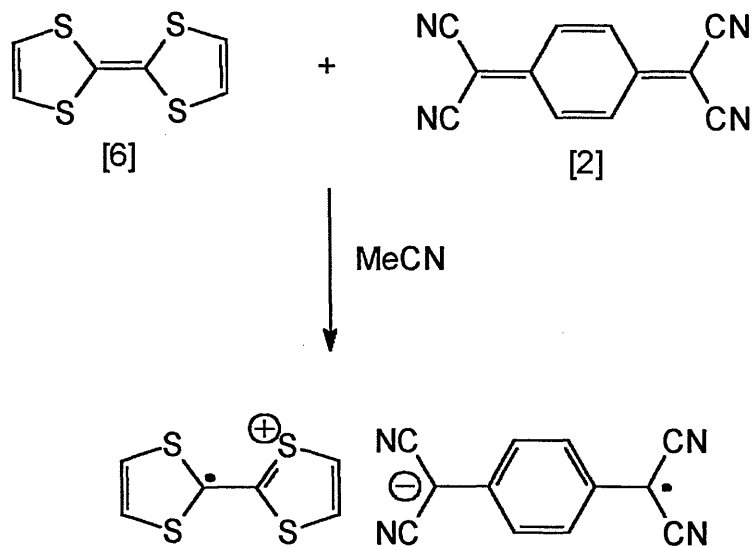
Figure 1.07 TTF-TCNQ charge transfer complex.

1.3 Conduction in Charge transfer complexes

In TCNQ-TTF the organic donor TTF is oxidised to produce the stable radical cation (Figure 1.08) :-
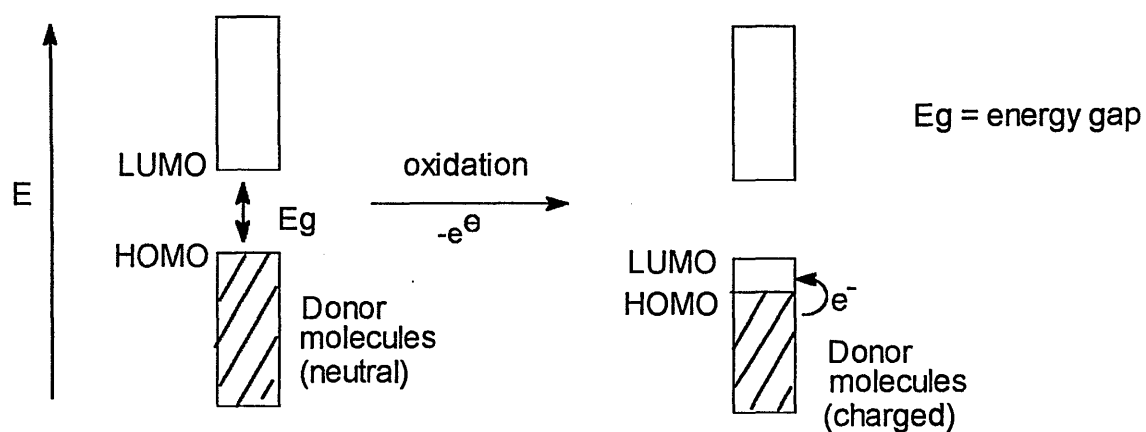
Figure 1.08 Production of the stable radical anion

Simultaneously the organic acceptor TCNQ is reduced to produce the stable radical

anion (Figure 1.09) :-
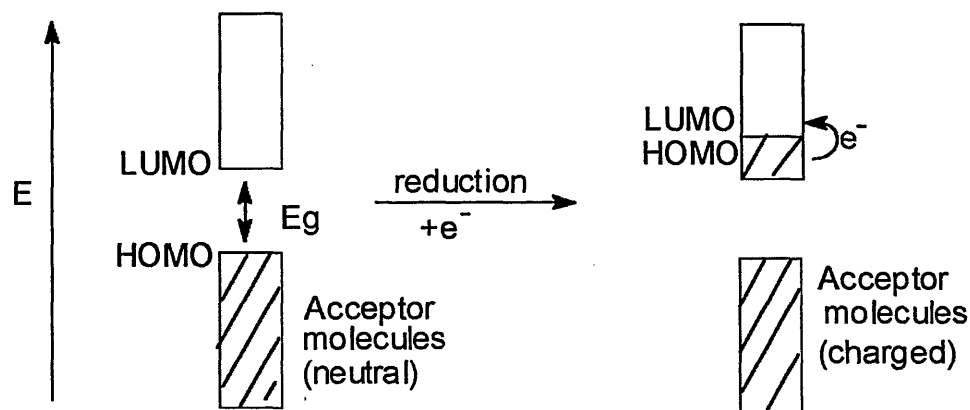
Figure 1.09 Production of the stable radical cation.

The previous mechanisms result in the TTF-TCNQ charge transfer complex

(Figure 1.10) :-
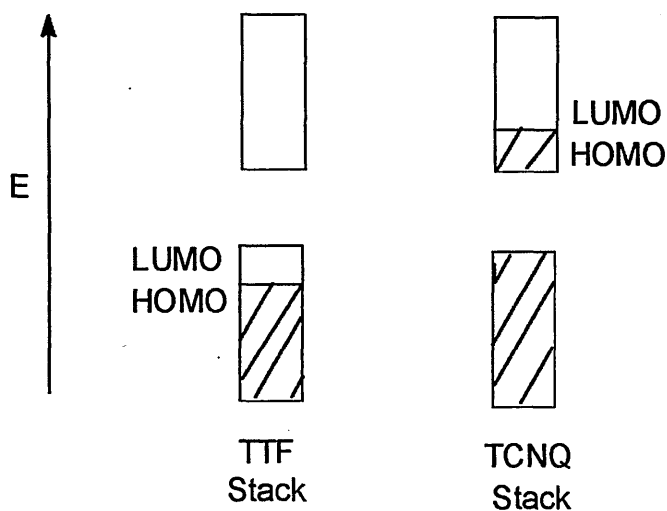
Figure 1.10 TTF-TCNQ

When the energy gap between the valence band (from the HOMO of the molecules) and the conduction band (from LUMO of the molecules) decreases, the material moves from the insulating state to a semi-conducting one, since the decrease in the energy gap allows thermally excited electrons to travel from the valence band into the conduction band. The onset of metallic behaviour requires partially filled conduction or valence bands which will allow the movement of large numbers of electrons into higher energy levels within the band. In TTF-TCNQ this metallic state is reached from the partially filled valence (HOMO) and conduction (LUMO) bands from the donor and acceptor molecules and also from electron interactions with the lattice vibrations which are governed by temperature.

For an electron transfer to take place, the energy levels of the donor and acceptor need to be matched. In solution, this can be achieved by the reorientation of the solvent around both the donor and acceptor, and in the solid by the reorientation and rotation of bonds. The energy of the transition from donor to the acceptor is dependent on the ionisation energy of the donor (I_D) and the electron affinity of the acceptor (E_A). For a strong donor/strong acceptor complex, the energy of the charge transfer is small and basically 100% charge transfer occurs. For weak donor/weak acceptor complexes, the energy required for charge transfer is much greater, the ground state is neutral and the degree of charge transfer is essentially zero. However if partial charge transfer occurs, where the energy of charge transfer is quite small and positive, the resultant conductivity is high as seen in the TTF-TCNQ complex which has a partial degree of charge transfer of 0.59.

The TTF-TCNQ complex has an important defined crystal structure. As mentioned previously, high conductivity is related to anisotropic segregated stacks of donor and acceptor species (Figure 1.11). Although the stacks are segregated, there is some interaction between the stacks and the conductivity ratio in the x, y and z axial directions

is 500: 5: 1 respectively. Therefore complexes of this nature are known as quasi-one dimensional metals.

The distance between each TCNQ and TTF molecule is very small (3.17 Å for TCNQ and 3.47 Å for TTF). The close proximity between units gives rise to supramolecular orbitals arising from the π-orbitals of the TTF and TCNQ. Ring-over-bond overlap (Figure. 1.12) also gives greater π-interaction along the stack. These sideways and vertical overlaps enhance the supramolecular orbitals, creating mass delocalisation of electrons within each segregated column.
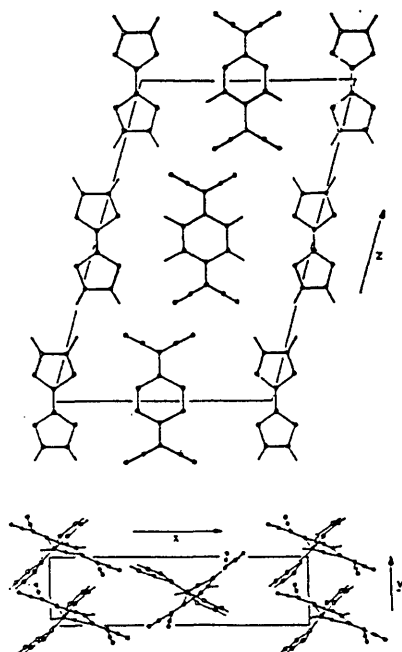
Figure 1.11 Crystal packing in TTF-TCNQ
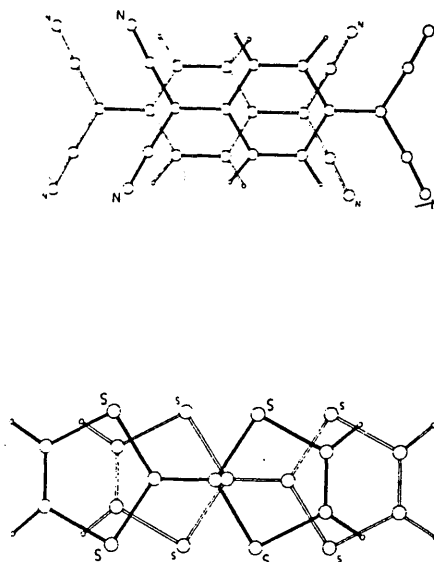
Figure 1.12 Ring-over-bond overlapping

Notice from Figure 1.13 that the TTF-TCNQ complex shows increasing metallic behaviour as the temperature decreases. The crystallinity also decreases and the π-orbital delocalisation reaches a maximum. Lattice vibrations (phonons) decrease with lowering temperature.
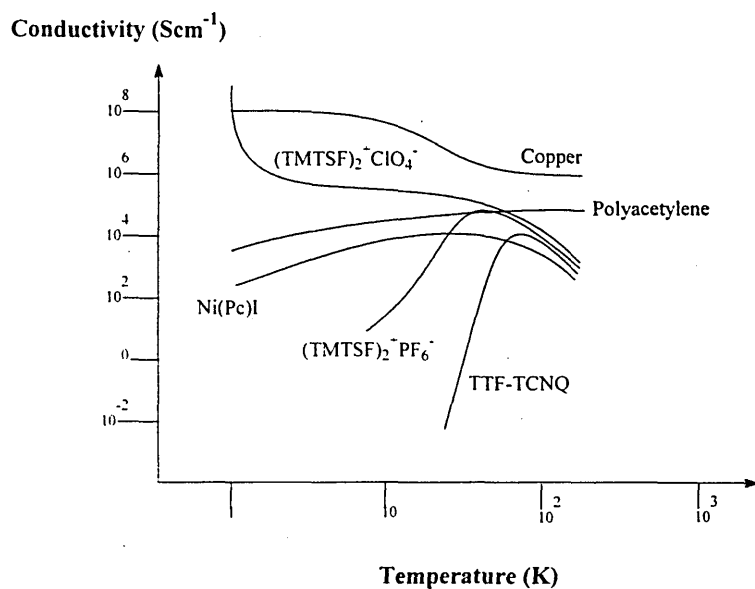
Conductivity (Scm^{-1})

Figure 1.13 Conductivity profile of TTF-TCNQ and other organic metals compared with copper

At very low temperatures this type of quasi-one dimensional metal is unable to maintain long range order due to lattice distortions.[17] A phenomenon known as Peierls distortion[18] occurs whereby the charge transfer lattice distorts into `dimers`, the metallic delocalisation is lost and an insulating state results.

1.4 Superconductivity

Since the 1970s there has been considerable development in organic conductors based on CT complexes and ion radical salts.[19, 20] Organic metals with a greater dimensionality were sought after and this led to the development of superconducting materials.

By 1978 the complex HMTSF-2,5-DMTCNQ (HMTSF = hexamethyltetraselenafulvalene[7]) was found to have the Peierls distortion suppressed under pressure ($\sigma = 10^5$ Scm^{-1} at 1 K)[21] and by 1980 the first organic superconductor had been reported - the (TMTSF)$_2$ PF$_6^-$/ClO$_4^-$ salt.[22] Essentially this was a quasi-2-dimensional material that possessed greater orbital overlap than previous systems. Superconductivity has also been observed in a number of C.T based systems containing sulphur and oxygen based donors (BEDO-TTF [8]).[23, 24] The superconductivity observed here is believed to arise from interactions of the electrons in the conductance band with lattice phonons.

[7]

[8]
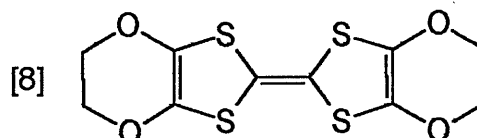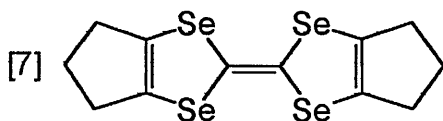
The Bardeen, Cooper and Schrieffer theory[25] of superconductivity states that super charge carriers, or highly co-ordinated electron pairs (Cooper pairs), cause superconductivity, differing from metallic conduction where individual valence electrons are the charge carriers. It is not however clear if this theory can adequately describe organic superconductivity. However there is some evidence that Cooper pairing occurs[26] and that the pairing is localised along the donor chains.

The recent discovery of the Buckminsterfullerene class of electron acceptor has led to further organic metal complexes having superconducting transitions rivalling the high

temperature ceramic superconductors.[27] For example Rb_3C_{60} acts as a metal that becomes superconducting at 30K.[28]

1.5 Conducting polymers

Conducting polymers have also attracted a lot of interest because of their perceived advantages such as processability, low costs, mechanical flexibility, etc. The first conducting polymer was found to be the initially semi-conducting poly (sulphur nitride) [9] in its polycrystalline form.[29] However, Walakta[30] found that single crystals also exhibited metallic conductivity ($\approx$ 1730 Scm^{-1}). Further research has concentrated upon polyacetylene [10], which can be synthesised to high purity, poly(paraphenylene) [11], and polypyrroles [12] and derivatives.[31-34]

Generally most polymers are closed shell species and therefore they are doped to increase their conductivity. Normally, to oxidise the polymer, halogens such as I_2 are used to accept electrons (p-type doping) and alkali metals (Li, Na and K) are used as reducing agents (n-type doping). This doping can have a great effect on the properties of the polymer and can increase the conductivity by up to 13 orders of magnitude.[35]
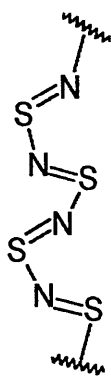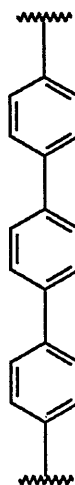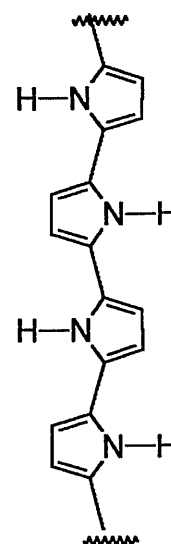
[9]   [10]   [11]   [12]

Thus far we have discussed the history and mechanisms of conductivity in organic electroactive materials. As the work reported here is concerned with the synthesis and characterisation of novel electroactive compounds, some background on the chemistry of typical systems is therefore warranted.

1.6 Organic electron donor systems

Since the discovery of the TTF-TCNQ system, there has been an explosion of interest in the behaviour of TTF and its derivatives, since certain of its salts can behave both as organic metals and superconductors.

Derivatives with an extended σ-bond framework, e.g. tetramethyltetrathiafulvalene (TMTTF [13]), and π-orbital systems were first to be studied.[36, 37] The next step was to vary the heteroatoms, e.g. replace S with Se[38] (tetraselenafulvalene-TSF [14]) or Te.[39] Here the presence of selenium d-orbitals enables the donor stack to dominate the transport properties and in general complexes of TSF, and its substituted derivatives, with TCNQ show increased stability of the metallic state compared with that of their TTF counterparts.

Modifications of the bridge between the dithiolium rings, e.g. extended conjugation [15][40] and unsymmetrical structures, have also been studied.[41] Recently the use of TTF moieties as structural building blocks in supramolecular synthesis have been investigated.[42] Other donor systems include bis-(thiadiazole)tetrathiafulvalene (BTDA-TTF) [16] which is expected to form CT salts.[43] The replacement of sulphur atoms in TTF with nitrogen has led to TTF tetraaza analogues[44] and dithiadiazafulvalenes (DTDAFs).[45] The introduction of sulphur atoms into the periphery of the polynuclear aromatic systems lowers the oxidation potentials of such structures, one example being naphthol[1,8-bc;4,5-b` c`]dithiophene [17].[46]

[13]

[14]

[15]

[16]

[17]
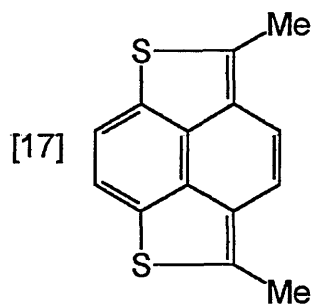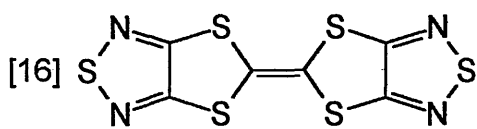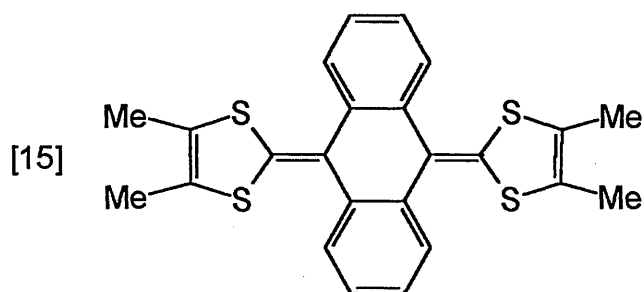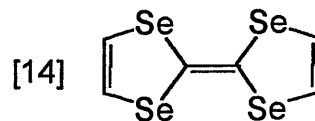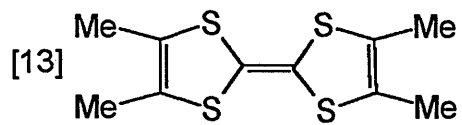
Electron Donors

1.7 Organic electron acceptor systems

A lot of effort has been expended in the development of TCNQ derivatives, however the difficult chemistry involved limits the possibilities in this area. The majority of TCNQ derivatives undergo two reversible single-electron reductions. The intermediate radical anion has a high thermal stability and its dicyanomethylene groups make TCNQ a stronger electron acceptor than say benzoquinone[47][18] though not tetracyano-1,4-benzoquinone (cyanil[19]).[48]

[18] O=⟨ ⟩=O

[19]
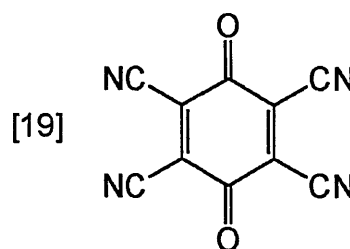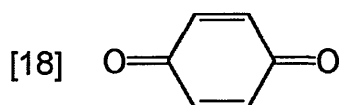
Early synthetic routes to TCNQ derivatives developed from the original work on the synthesis of TCNQ itself.[6] Wheland et al[49-51] described 21 derivatives via 1,4-bis(cyano-methyl)benzene derivatives which involved complex multistep procedures using highly toxic cyanogen chloride as the electrophilic cyanating agent. Wheland et al also discussed the formation of a number of CT complexes, but while for example the conductivity of HMTSF -TCNQ (HMTSF = hexamethyltetraselenafulvalene) was extremely high (σ_{rt} = $1500 Scm^{-1}$), the C.T complex of HMTSF with TCNQF$_4$ was comparatively low (σ_{rt} = $10^{-6} Scm^{-1}$). The presence of the highly electronegative fluorine atoms in the quinoid ring causes it to be a very strong electron acceptor and this in turn causes virtually complete charge transfer which, is not conducive to metallic conduction for the reasons outlined earlier.

At present there are three synthetic approaches available to modify the TCNQ structure. First ring substitutions which give rise to e.g. 2,3,5,6-tetrafluoro-7,7,8,8-tetracyanoquinodimethane (TCNQF$_4$ [20])[49] and 2,3,5,6-tetramethyl-7,7,8,8-tetracyanoquinodimethane (TMTCNQ [21]).[52] Second, extension of the π-electron system e.g. 9,9,10,10-tetracyanoanthraquinodimethane(9,10-TCAQ [22]) and 9,9,10,10-tetracyano-2,6-naphtho-quinodimethane (TNAP [23]).[53] Third, the incorporation of heterocyclic rings and heteroatoms into the TCNQ skeleton, such as [25].[54]

However more recently there have been newer procedures developed that have made this area more accessible. The Lehnert procedure[55] for example allows the direct bis(dicyanomethylation) of the quinone using malononitrile and TiCl$_4$ in pyridine. The Hünig method[56] for preparing N,N`-dicyanoquinonediimines (DCNQI [24]) used TiCl$_4$ to mediate the direct reaction of bis(trimethylsilyl)carbodiimide (BTC) in a simple one pot synthesis.

Bryce et al[52] used the Lehnert reagent to prepare a series of ring substituted TCNQ derivatives; TMTCNQ [21] and N,7,7-tricyanoquinodimethanimine (TCNQI) were successfully prepared using large scale recipes. Also the use of 2-chlorobenzyl thiocyanate as a source of electrophilic cyanide has provided a significantly improved synthetic approach to several TCNQ derivatives.[53]

[20]

[21]

[22]

[23]

[24]

[25]
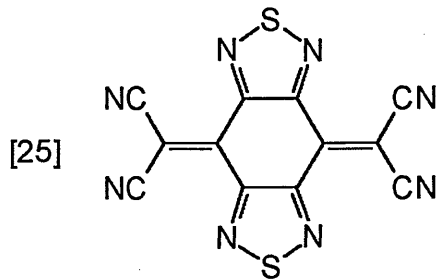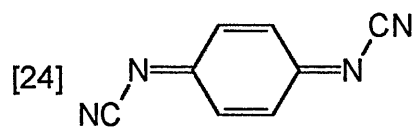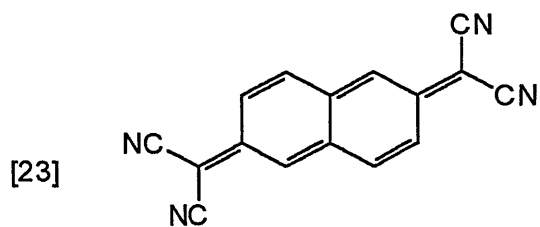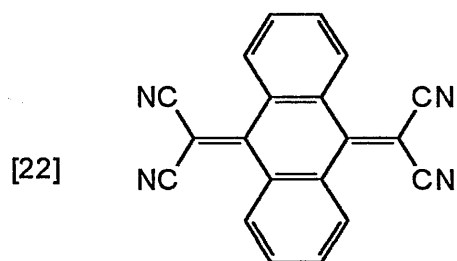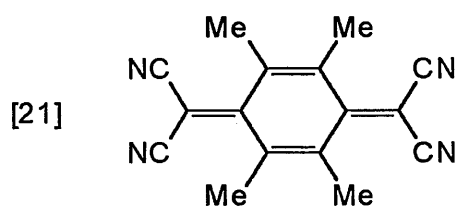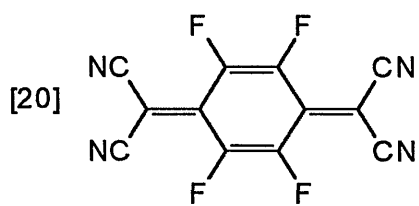
Electron Acceptors

1.8 Zwitterionic TCNQ adducts

This thesis concentrates on interactions between donor and acceptor molecules that, rather than forming a salt or complex between the two, are actually covalently bonded together. Donor pyridinium and quinolinium systems, π-bonded to TCNQ acceptors, are extensively characterised and their Langmuir-Blodgett film forming properties assessed.

The work in this thesis takes a step sideways to look at TCNQ adducts that are in the main insulators, but are able to exhibit other `exotic` properties such as second harmonic generation (SHG), solvatochromism, photochromism and molecular rectification etc.

As previously mentioned, Melby et al[6] published the first examples of TCNQ complexes with nitrogen heterocycles. In 1962 he reacted the very soluble lithium salt of TCNQ with N-methylquinolinium iodide and with similar salts of pyridinium cations producing complexes that, by today's standards, have relatively low conductivities.

The conduction mechanism in these simple TCNQ salts is dependent on the excitation of an electron from one ionic state to another, i.e.:

$$TCNQ^{-} \ TCNQ^{-} \ \text{-->} \ TCNQ^{\circ} \ TCNQ^{2-}$$

This is shown schematically in Figure 1.14:-
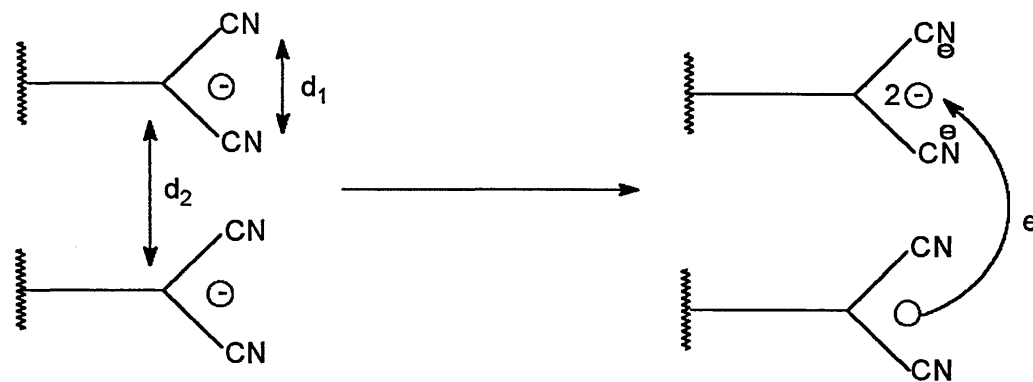
Figure 1.14 Proposed intermolecular conduction mechanism

In the above mechanism there are two conduction electrons on the same TCNQ

molecule; this is not an ideal situation and would explain the low conductivities

observed.

In such structures, the width of the band gap can be estimated if the Coulombic energy

(U) between electrons on adjacent sites is considered:-

$$U = e^2 / 4\pi E_0 d$$

Where:-

e = The charge on an electron

E_0 = The permittivity of a vacuum.

d = The distance between adjacent sites.

Therefore for 2 electrons :-

$$U = 14.4 \text{ eV} / d$$

For conduction to occur, an electron would have to shift from one acceptor unit to an adjacent acceptor unit resulting in two conduction electrons on the same TCNQ site, creating a hole in the site below. From X-ray crystallography studies, the distance d_1 is less than the distance d_2.[57] Thus, for two electrons on the same site, the repulsion energy $Ud_1 > Ud_2$ and therefore the electrical conductivity is low(insulating), as placing two electrons on the same site is energetically unfavourable.

There are many examples of addition and substitution reactions of TCNQ which have been documented for a number of years.[5-9, 58] Substitution at either, or both, of the cyano groups occurs readily with primary or secondary amines (Figure 1.15).
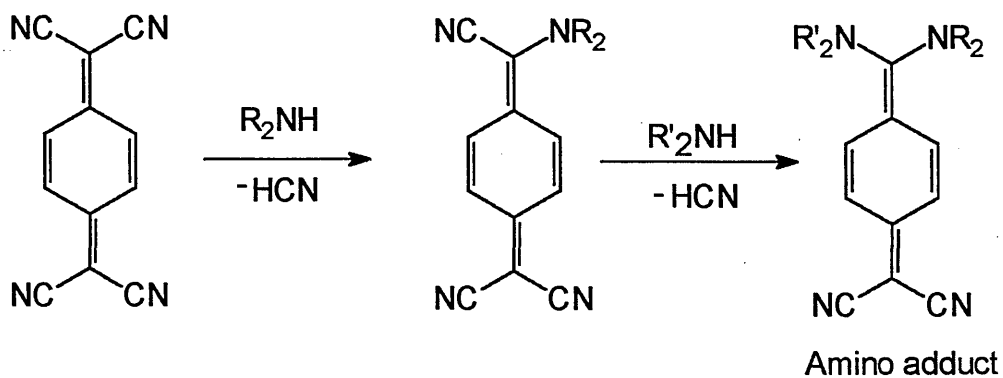
R and R' = H or alkyl, R can = R'

Fig 1.15 Reaction of TCNQ with Amines

The amine group adds to the TCNQ through nitrogen via 1,6 addition yielding a product that subsequently eliminates HCN. Mixed derivatives of TCNQ have been prepared via a similar method - the reaction of a monoamine-substituted TCNQ with an excess of a different amine. A bifunctional amine such as ethane-1,2-diamine can replace both the nitrile groups at one end of the TCNQ molecule to yield a cyclic product.

The amino adduct can be represented by the two resonance structures (Figure 1.16):
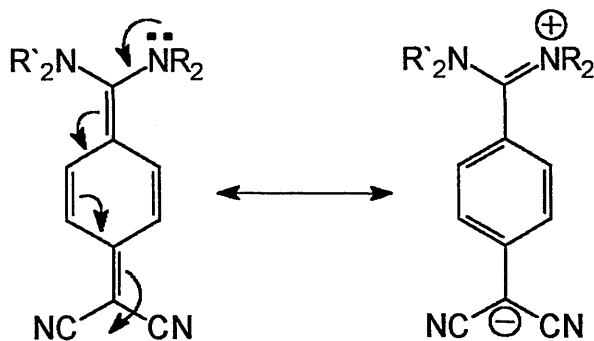
Figure 1.16 Zwitterionic canonical forms of an amino adduct

The infrared spectrum of the above adduct shows two distinct regions for the nitrile group stretching frequencies at - 2175 cm^{-1} and 2130 cm^{-1}- characteristic of a monosubstituted malononitrile anion. The uv/vis spectrum of this species in acetonitrile showed a broad band which was attributed to an intramolecular charge transfer from the donor to acceptor.

Recently a novel zwitterion DEMI [26] (Figure 1.17) was prepared via the reaction of the tertiary amine triethylamine (TEA), with TCNQ.[59] Tertiary amines are not expected to react with TCNQ as they do not possess an amino hydrogen which could be abstracted to produce the 1,6 addition intermediate. It is thought that in the above reaction the TCNQ abstracts protons from the TEA to yield an enamine and TCNQH$_2$. The enamine attacks the TCNQ in a Stork-enamine type reaction, and the subsequent elimination of HCN yields the zwitterion.
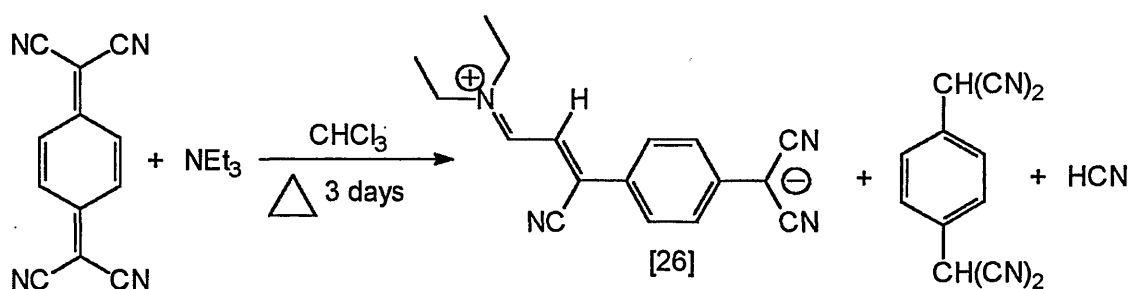
Fig 1.17 Reaction of TCNQ with a tertiary amine to produce a zwitterion

A further series of similar molecules [27-29] have been prepared with a range of ethylamines which give zwitterions with similar π-electron systems.[60,61] The spectral properties of these materials are virtually identical, comprising a broad charge transfer band in the middle of the visible region and virtually no absorbance on either side. These types of zwitterions have become known as " blue window " chromophores because of the low optical absorption between 400-500 nm.

[27]   [28]   [29]
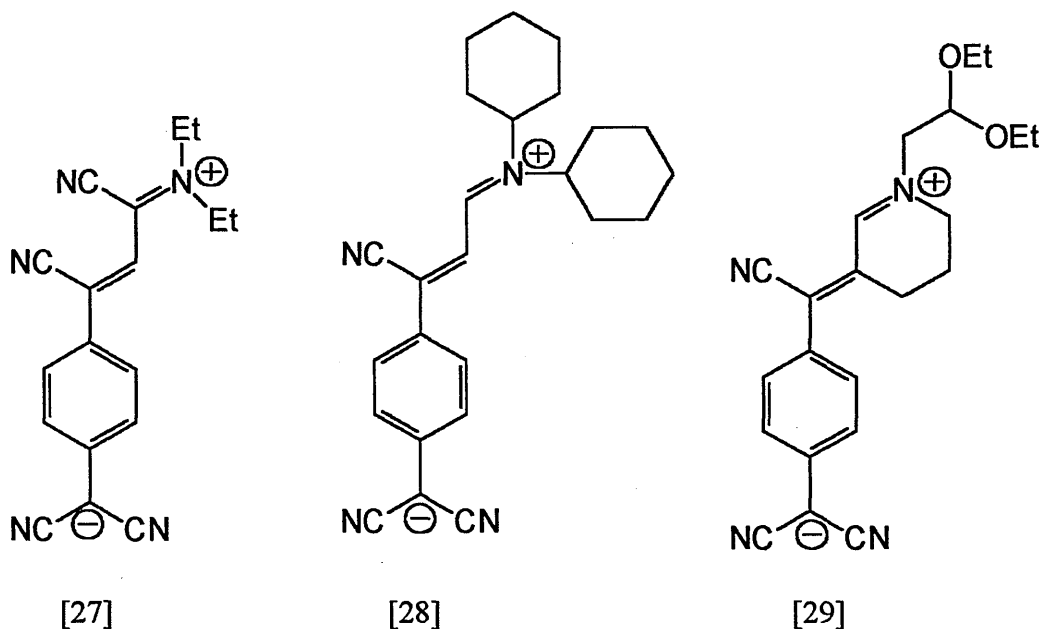
Examples of "blue window" chromophores; TCNQ adducts of tertiary ethyl amines.

The zwitterionic donor-π-acceptor TCNQ adduct Z(N-methyl-2-pyridinium)-α-cyano-4-styryldicyanomethanide [30], (trivial name picolyltricyanoquinodimethane) was first synthesised[57] in these laboratories at Sheffield Hallam University(formaily Sheffield City Polytechnic).

[30]
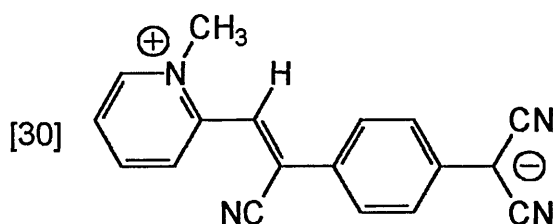
From the molecular geometry shown in Figure 1.18 the bond length between C12 and C15 shows that a double bond is present whilst the aromatic nature of the two rings is also confirmed by bond length measurements.[57] This molecule is not planar, with the pyridinium ring being twisted from the benzenoid ring from TCNQ by 10.13°. The uv/vis spectrum of this material in acetonitrile shows a broad band centred on 592nm which is thought to be an intramolecular charge transfer transition and which is now seen as typical of this type of system.
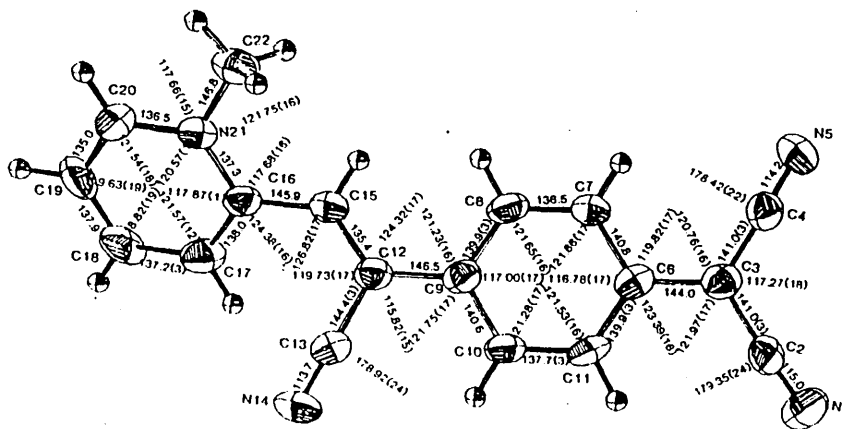
Figure 1.18 Crystal structure of picolyl-tricyanoquinodimethane
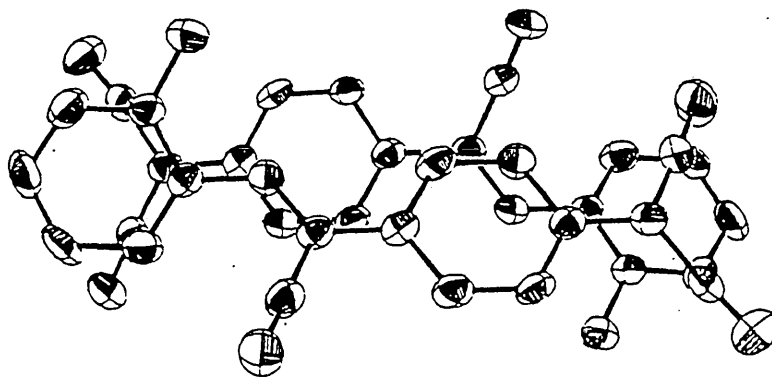
Figure 1.19 Overlap of two picolyl-tricyanoquinodimethane molecules
stacked along the b-axis

Atom in molecule calculations showed the charge distribution to be typical of a zwitterion. Evidence for such a zwitterionic structure was also obtained from the very large computed dipole moment of 26.16D. The molecule has also been studied in its solid state by polarised reflection spectroscopy.[62] An intramolecular charge transition was observed at 532 nm. The stacking arrangement of the molecules (Figure 1.19) in the solid state was found to be a head to tail arrangement.

This material was the first example of such zwitterionic D-π-A TCNQ systems and led to substantial research encompassing many areas.

The head to tail arrangement is also seen in the zwitterionic adduct formed between TCNQF$_4$ and tetramethylphenyldiamine (TMPD)[63][31]. Another related example is the pyridyl substituted pyrazino-TCNQ derivative[64] [32] where the donor molecule is attached to the pyrazine ring in order to reduce the steric hindrance and degree of non-planarity associated with the D-π-A systems examined in this thesis.

[31]

[32]
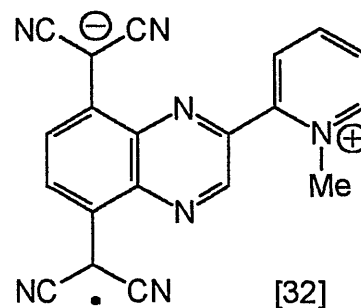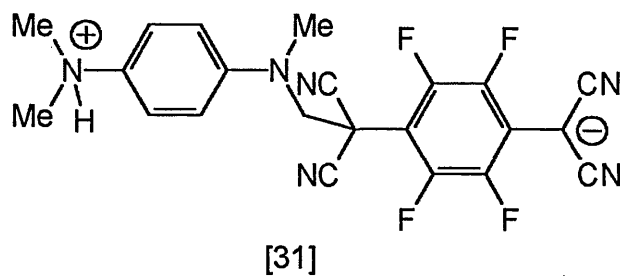
1.8.1 Nomenclature

The nomenclature used in this thesis is now explained:-

The majority of the work outlined below concerns the preparation and evaluation of a number of zwitterionic adducts prepared from quaternised N-heterocyclic donors with acceptors such as TCNQ and its derivatives. In general, adduct formation involved the creation of a new carbon to carbon double bond between a methyl carbon on the N-heterocycle ring and a dicyano carbon ($C(CN)_2$) on the acceptor moiety. A cipher nomenclature has been adopted to identify the various adducts that have been investigated. The ciphers are split into two parts, identifying the donor and the acceptor respectively.
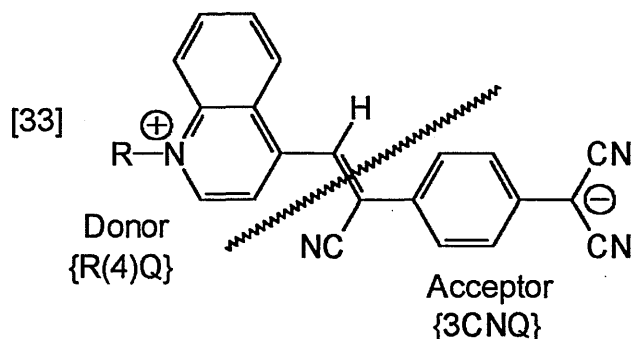
The above material [33] is given the cipher **R(4)Q3CNQ** where **R(4)Q** refers to the donor moiety {"**R**" identifies the quaternising alkyl group and **(4)Q** refers to the substitution in the **4** position of the original methyl group on the **Quinolinium** donor ring (**P** for example, would indicate a **Picolinium** donor ring)}. The **3CNQ** refers to the 3 cyano groups remaining from the TCNQ acceptor moiety.

Closely related to the α- picolinium adduct [30] is (Z)-α-cyano-β-(N-hexadecylquinolin-4-ylium)-4-styryldicyanomethanide [33, where R= $C_{16}H_{33}$], cipher form $C_{16}H_{33}(4)Q3CNQ$ which was first synthesised by Bell et al[65] and Ashwell et al.[66]

Adducts with long aliphatic chains create the necessary amphiphilic balance that enabled Langmuir-Blodgett (LB) films of these materials to be fabricated (see Chapter 5).

This quinolinium and the related picolinium systems could be prepared by the relatively time consuming method of refluxing LiTCNQ with the appropriate lepidinium/picolinium cation for, in some cases, over a hundred hours. An alternative method used neutral TCNQ in the presence of a non-nucleophilic base such as piperidine to reduce reflux times (see Chapter 2).

The subsequent chapters of this thesis deal in general with the synthesis, LB film formation and characterisation of a number of novel zwitterionic TCNQ D-π-A adducts of this general type. Research into these materials is of interest because of their potential use in areas such as molecular electronics in general and non-linear optics in particular.

1.9 Molecular Electronics - molecular rectification

Rectification is the asymmetric flow of electrons through a molecule under a potential difference in one direction but not the reverse. Rectification of an electric current was first observed nearly a century ago in vacuum diodes[67] which have been more recently replaced by semi-conductor solid state rectifiers based on p-n junctions i.e. p-doped (electron deficient) Ge with n-doped (electron rich) Ge.

Rectification by organic materials has been exhibited by junctions of layers of n-doped organic semiconductors with layers of p-doped organic semiconductors.[68-71] Kuhn et al[72] and other workers[73, 74] demonstrated electrical rectification in LB multilayers (doped with electron donors and acceptors insulated from each other by LB multilayers). Fujihira[75] produced an electrochemical photodiode, and there has also been evidence of electrochemical rectification at a monolayer modified electrode.[76, 77] However the majority of the above organic rectifiers have not been strictly at the unimolecular level.

The idea of molecular electronics, that single organic molecules or low dimensional arrays of organic molecules could mimic or replace electrical components arguably began when Aviram and Ratner proposed the construction of a simple electronic rectifier based on the use of a single organic molecule.[78, 79] These workers used molecular orbital calculations to show that, in theory, an organic molecule [34] comprising of a donor pi system and an acceptor pi system separated by a sigma bonded (methylene) bridge would allow electron transfer from donor to acceptor under a potential difference in one direction but not in the reverse.

There has been much research into providing evidence of asymmetrical electrical conduction through the molecular orbitals of a single D-σ-A molecule, where D is a good one electron donor with a low ionisation potential and A is a good electron acceptor with a high electron affinity separated by an insulating covalent bridge (σ). In theory unimolecular rectification would work in this molecule as the zwitterionic (excited state)

D^+-σ-A^- is energetically favourable compared to the neutral ground state of D-σ-A. The opposite zwitterion of D$^-$-σ-A$^+$ is energetically less favourable as it would require several electron volts more to achieve and therefore current flow in this direction is unlikely. Aviram and Ratner`s molecule [34] has never been synthesised but similar LB film forming D-σ-A materials have been, albeit without showing any evidence of rectification[80-82]apart from ambiguous results[83] that could arise from a Schottky barrier[84] formation.

DONString [Sigma Bridge] ACCEPTOR

[34]
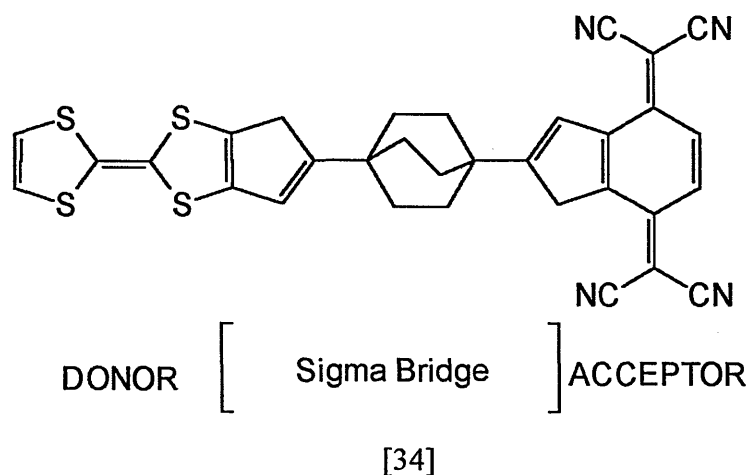
The zwitteronic D-π-A materials studied here are clearly candidates for molecular rectifiers as they fulfil Aviram and Ratner`s criteria of having good electron donor and acceptor moieties in the same molecule. Ashwell et al[85] sandwiched multilayers of $C_{16}H_{33}$(4)Q3CNQ between a noble metal electrode (Pt or Ag) and a magnesium electrode protected by an overlayer of Ag, and this exhibited rectification properties.

Structure of device:-

Pt | LB multilayer of $C_{16}H_{33}$(4)Q3CNQ | Mg | Ag

An LB monolayer of $C_{16}H_{33}$(4)Q3CNQ also exhibited rectification properties:-

Pt | LB monolayer of $C_{16}H_{33}$(4)Q3CNQ | Mg| Ag

However doubts were raised about whether a Schottky barrier was forming between the Mg electrode and the zwitterion (Mg3CNQ salt), which led to an insulating fatty acid monolayer being inserted between the Mg electrode and $C_{16}H_{33}(4)Q3CNQ$[86] - this still exhibited I-V asymmetries, indicating molecular rectification. Metzger et al[87] have recently carried out a more detailed study of $C_{16}H_{33}(4)Q3CNQ$ where the synthesis has been improved (see Chapters 2 and 3) and further proof of unimolecular rectification obtained from macroscopic and nanoscopic studies. Metzger essentially repeated previous studies (Figure 1.20), on the macroscopic level using the device:-

glass| Al | 4 LB monolayers of $C_{16}H_{33}(4)Q3CNQ$| Al
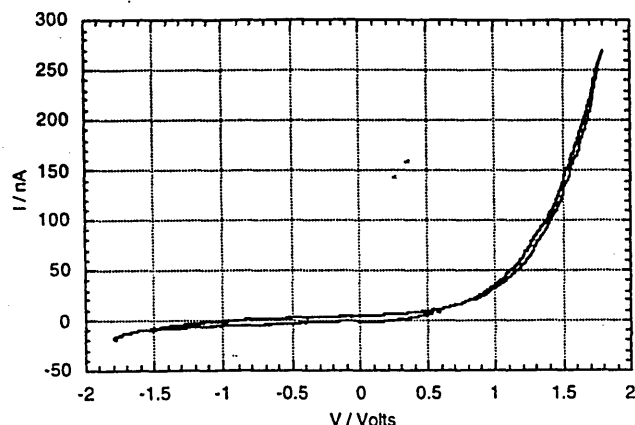
Figure 1.20 Conductivity profile of the above device. The direction of the easier electron flow is when I > 0 for V > 0 from the bottom of the electrode through the film to the top electrode. From Metzger et al.[87]

At the nanoscopic level, earlier work on monolayers of $C_{16}H_{33}(4)Q3CNQ$ on highly orientated pyrolitic graphite (HOPG) monitored by scanning tunnelling microscopy (STM), showed no reproducible rectification.[88] Metzger et al[87] have since reproduced the original work, using STM and scanning tunnelling spectroscopy (STS), where

rectification was observed in a monolayer of $C_{16}H_{33}(4)Q3CNQ$ with a higher electron flow at a positive bias from the nanotip of the STM to the HOPG.

1.10 Non-linear Optics (NLO)

Traditionally inorganic materials have dominated this area; for example guided wave optics is currently dominated by lithium niobate ($LiNbO_3$). However from more recent research it has become clear that organic materials may have some advantages over inorganics because of the versatility of the synthetic aspect, and the large optical non-linearities that can exist in organic materials.

The LB technique has prompted great interest in this area because of the ability to control, to some extent, the molecular organisation and structure of the films. Materials for NLO applications have to be of a highly polarisable nature and in many cases need to form non-centrosymmetric LB film structures. The materials studied in this thesis are highly polarised and consequently their NLO effects have been studied.[89-93]

Organic materials possessing highly conjugated and delocalised π- electron systems are able to be polarised more easily in one direction than another. These molecules are able to interact with an intense electric field generated by a laser, which causes non-linear oscillations of the electric dipoles. These non-linear oscillations lead to the emission of photons which are of a different frequency to the incident frequency. Second harmonic generation (SHG) is the generation of photons of twice the frequency of the incident light (Figure 1.21).
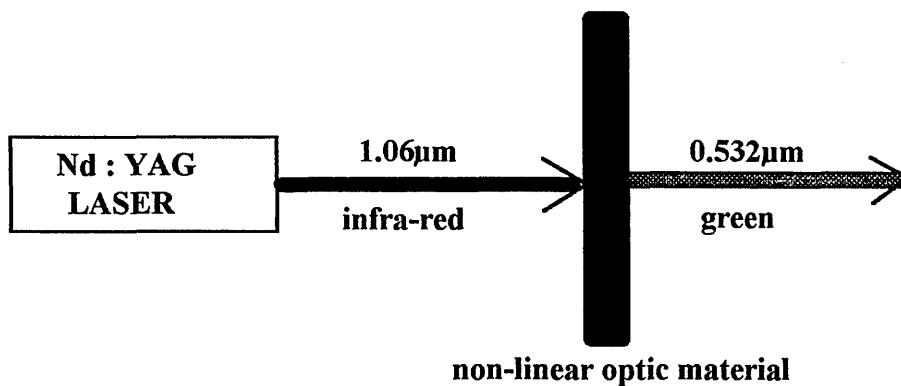
Figure 1.21 An example of SHG (doubling of the input frequency) in a noncentrosymmetric material

The general approach to the synthesis of LB film forming molecules with potential NLO application has been to join long alkyl chains to asymmetric dye molecules e. g. azobenzene and stilbene derivatives.

A lot of initial work focused on hemicyanine [35] and nitrostilbene [36] derivatives that possessed molecular hyperpolarizabilities. These were fabricated in an alternate layer ABABA type structure and they displayed a high coefficient for second-harmonic generation.[94]
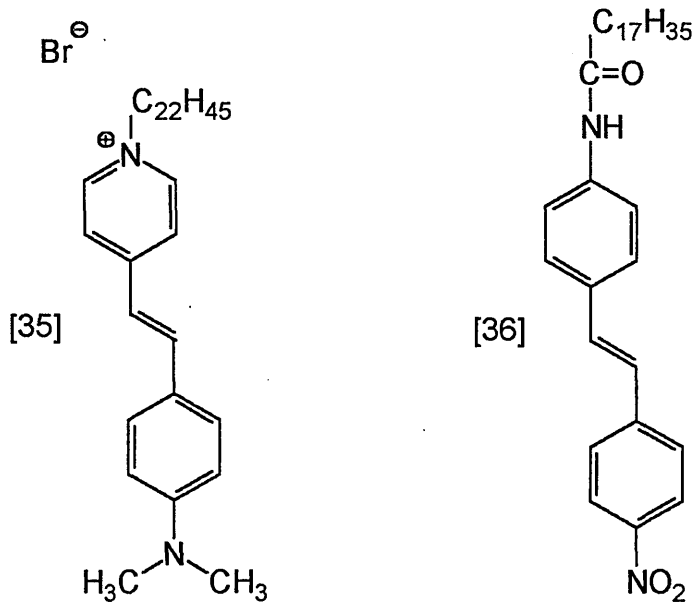
The basic theory behind NLO can be related to a number of equations beginning with the macroscopic polarisation **P** of a material comprising many individual molecules that contribute to the non linear polarisation:-

$$P = P_0 + \chi_1 (E) + \chi_2 (E^2) + \chi_3(E^3) + \text{.........} \chi_n (E^n)$$

where **P_0** is a constant, **E** is the electric field, and χ_n is the nth order susceptibility tensor. In the above equation χ_2 and χ_3 are responsible for higher order effects such as second and third harmonic generation respectively.

For individual molecules the polarising effect is expressed in terms of an induced dipole moment μ:-

$$\mu = \mu_e - \mu_g = \alpha E + \beta\, EE + \gamma\, EEE + \text{.......}$$

where μ_e and μ_g are the dipole moments in the excited and ground states respectively, **E** is the electric field and the coefficients α, β and γ are the linear, quadratic and cubic hyperpolarisabilities respectively. The hyperpolarisability coefficients are tensor quantities and thus are symmetry dependent.

The second order (quadratic) term is responsible for effects such as second harmonic generation and the Pockels' effect (the linear electrooptic effect), and a non-centrosymmetric geometry plus conjugation and intramolecular charge transfer within the material are important. In third order effects, responsible for third harmonic generation and the Kerr effect (quadratic electrooptic effect), anisotropic features, such as parallel conjugated chains, are important and the materials do not need to be non-centrosymmetric in geometry.

Second order non-linear hyperpolarisability behaviour, as well as being measured in terms of the β coefficient (individual molecules), can be measured in terms of the second order non-linear susceptibility on a macroscopic scale (χ^2) which is related to other important quantities such as electrooptic coefficients **r**, second harmonic coefficients **d**, and the refractive index **n** at a certain frequency $_w$ in the following equations.

$$\chi^2 \text{ (-w; w, 0)} = \epsilon_0 \, n_w^2 \, n_0^2 \, r \text{ (-w; w, 0)}/2$$

and

$$\chi^2 \text{ (-2w; w, 0)} = 2\epsilon 0 d$$

Related units:-

The β coefficient has SI units of $Cm^3 \, V^{-2}$; multiply by 2.7×10^{20} for e. s. u. . Second order non linear susceptibility (χ^2) has SI units of CV^{-2}; multiply by 2.7×10^{14} for e.s.u. . The SI units for the **d** and **r** coefficients are $m \, V^{-1}$.

In relation to the zwitterionic types of materials characterised in this thesis, two research groups have carried out the majority of the NLO investigations in this area. As mentioned previously Ashwell et al[89-93] have concentrated on LB films of the gamma substituted quinolinium-TCNQ adducts directly related to the materials studied here. Szablewski and co-workers[95] have researched into the "blue window chromophores" related to the TCNQ adducts of ethyl amines which have been doped into polymer films such as polymethyl methacrylate (poled polymers).

Much of the activity in this field has concentrated on increasing the magnitude of the second-order molecular hyperpolarisability, β, in these organic materials. The NLO materials reported in this work all comprise the donor (D) linked to the electron acceptor

(A) by means of a conjugated pi electron system, and can be described as having one dominant hyperpolarisability component lying in the direction of charge transfer. The degree to which the two resonance states of the molecule, the neutral D-π-A and the zwitterionic - D$^+$-π-A$^-$, contribute to the ground state of the material defines the polarisation. One popular model of NLO is Onsager's reaction field theory[96, 97] which states that the surrounding medium to the dipole is polarised and this exerts a "reaction field" back onto the molecule which acts through its linear polarisability, α, to enhance the dipole further. The evolution of higher molecular polarisabilities (such as β) as a function of the reaction field, reflects the changes in the electronic structure of the molecule. Theoretical and experimental studies of related systems have emphasised the extent to which molecular structure affects β.[98, 99]

The experimental determination of hyperpolarisabilities is usually carried out in solution using either EFISH[100, 101](Electric Field Induced Second Harmonic Generation) or hyper-Rayleigh scattering (HRS)[102] (a newer technique). In EFISH, a strong static electric field is applied to a solution of the NLO material. The interaction of the field with the permanent dipoles (μ) of the molecules causes a bias in the orientation of the chromophores. The partial removal of the isotropy allows second harmonic generation to occur. The quantity $\mu\beta$ can be determined from the intensity of the detected second harmonic light; however a separate measurement for the permanent dipole is required to calculate β.

The newer technique of HRS was developed to measure hyperpolarisabilities of unconventional non-linear molecules. HRS measurements are conducted by focusing an intense laser beam onto an isotropic solution of non-linear molecules and measuring the intensity of the frequency-doubled light. This technique has an advantage over EFISH as there is no need for an orientating electric field and thus ionic and apolar molecules are amenable to investigation.

1.11 Chapter One References

1. H. N. McCoy and W.C. Moore, *J. Am. Chem. Soc.*, **33**, 1273, 1911.

2. H. Kraus, *J. Am. Chem. Soc.*, **34**, 1732, 1913.

3. H. Akamatsu, H. Inokuchi and Y. Matsunaga, *Nature*, **173**, 168, 1954.

4. D. S. Acker, R. J. Harder, W. R. Hertler, W. Mahler, L. R. Melby, R. E. Benson and W. E. Mochel, *J. Am. Chem. Soc.*, **82**, 6408, 1960.

5. D. S. Acker and W. R. Hertler, *J. Am. Chem. Soc.*, **84**, 3370, 1962.

6. L. R. Melby, R .J. Harder, W. R. Hertler, W. Mahler, R. E. Benson and W. E. Mochel, *J. Am. Chem. Soc.*, **84**, 3374, 1962.

7. W. R. Hertler, H. D. Hartzler, D. S. Acker and R. E. Benson, *J. Am. Chem. Soc.*, **84**, 3387, 1962.

8. W. R. Hertler and R. E. Benson, *J. Am. Chem. Soc.*, **84**, 3474, 1992.

9. J. K. Williams, *J. Am. Chem. Soc.*, **84**, 3478, 1962.

10. T. L. Cairns, R. A. Carboni, D. D. Coffman, V. A. Engelhardt, R. E. Heckert, E. L. Little, E. G. McGeer, B. C. McKusick and W. J. Middleton, *J. Am. Chem. Soc.*, **79**, 2340, 1957.

11. T. L. Cairns, R. A. Carboni, D. D. Coffman, V. A. Engelhardt, R. E. Heckert, E. L. Little, E. D. McGeer, B. C. McKusick, W. J. Middleton, R. M. Scribner, C. W. Theobald and W. E. Winberg, *J. Am. Chem. Soc.*, **80**, 2775, 1958.
    plus ten other publications - Cyanocarbon chemistry II - XI., *J. Am. Chem. Soc.*, **80**, 2778 - 2846, 1958.

12. I. F. Shegolev, *Phys. Stat. Sol.*, (A), **12**, 9, 1972.

13a. F. Wudl, G. M. Smith and E. J. Hufnagel, *J. Chem. Soc.*, *Chem. Commun.*, 1453, 1970.

13b. S. Hünig, G. Kiesslich, D. Scheutzow, R. Zahradnik and P. Carsky, *Int. J. Sulphur Chem.*, *Part C*, 109, 1971.

14. H. A. Benisi and J. H. Hildenbrand, *J. Am. Chem. Soc.*, **71**, 2703, 1949.

15. J. Ferraris, D. O. Cowan, V. V. Walatka and J. M. Perlstein, *J. Am. Chem. Soc.*, **95**, 948, 1973.

16.   R. S. Mulliken and W. B. Pearson, *"Molecular Complexes"*-a lecture and reprint volume, J. Wiley and Sons Inc, London, 1969.

17.   H. Fröhlich, *Proc. R. Soc. London. , Ser. A,* **223**, 296, 1954.

18.   R. E. Peierls, `Quantum Theory of Solids`, Oxford University Press, London, 1955.

19.   M. R. Bryce, *Chem. Soc. Rev. ,* **30**, 355, 1991.

20.   M. C. Grossel and S. C. Weston, *Contemporary Organic Synthesis,* **1**, 367, 1994.

21.   C. S. Jacobson, K. Mortensen, J. R. Anderson and K. Bechgaard, *Phys. Rev. ,* **B18**, 905, 1978.

22a.   D. Jerome, A. Mazand, M. Ribault and K. Bechgaard, *J. Phys. Lett. ,* **41**, L95, 1980.

22b.   K. Bechgaard, C. S. Jacobson, K. Mortensen, H. J. Petersen and N. Thorup, *Solid State Commun. ,* **33**, 1119, 1980.

23.   G. C. Papavassilou, G. A. Mousdis, J. S. Zambounis, A. Terzis, A. Hountas, B. Hilti, C. W. Mayer and J. Pfeiffer, *Synth. Met. ,* **B27**, 379, 1988.

24.   F. Wudl, H. Yamochi, T. Suzuki, H. Isohato, C. Fite, H. Kasmai, K. Liou, G. Srdanov, P. Coppeus, K. Maly and A. Frost, *J. Am. Chem. Soc. ,* **112**, 2461, 1990.

25.   J. Bardeen, L. N. Cooper and J. R. Schreiffer, *Phys. Rev. ,* **108**, 1175, 1957.

26   K. Bechgaard and D. Jerome, *Sci. Am. ,* **247**, 50, 1982

27.   H. W. Kroto, A. W. Allaf and S. P. Balm, *Chem. Rev. ,* **91**, 1213, 1991.

28.   K. Holczer, O. Klein, S.-M. Huang, R. B. Kaner, K.-J. Fu, R. L. Whetton and F. Diedrich, *Science,* **252**, 1154, 1991.

29.   D. Chapman, R. J. Wam, A. G. Fitzgerald and A. D. Yoffe, *Trans. Faraday Soc.,* **60**, 294, 1964.

30.   V. V. Walakta, *Physics Review Lett. ,* **31**, 1139, 1973.

31.   J. H. Edwards and W. J. Feast, *Polymer,* **21**, 595, 1980.

32.   D. M. Ivory, G. G. Miller, J. M. Sowa, L.W. Schacklette, R. R. Chance and R. H. Baughman, *J. Chem. Phys.* , **71**, 1506, 1979.

33.   A. F. Diaz, J. Crowley, J. Bargan, G. P. Gardini and J. B. Torrance, *J. Electroanal. Chem.* , **121**, 355, 1981.

34.   K. K. Kanazawa, A. F. Diaz, R. H. Geiss, W. D. Gill, J. F. Kwak, J. A. Logan, J. F. Rabolt and G. B. Street, *J. Chem. Soc. , Chem. Commun.* , 854, 1979.

35a.   H. Shirakawa, E. J. Louis, A. G. MacDiarmid, C. K. Chiang and A. J. Heeger, *J. Chem. Soc. , Chem. Commun.* , 578, 1977.

35b.   C. K. Chiang, C. R. Fincher, Jr. , Y. W. Park, A. J. Heeger, H. Shirakawa, E. J. Louis, S. C. Gau and A. G. MacDiarmid, *Phys. Rev. Lett.* , **39**, 1098, 1977.

36.   R. L. Greene, J. J. Mayerle, R. Schumaker, G. Castro, P. M. Chaikin, E. Etemad and S. J. Laplaca, *Solid State Commun.* , **20**, 943, 1976.

37.   Y. Ueno, A. Nakayama and M. Okawara, *J. Chem. Soc. , Chem. Commun.* , 74, 1978.

38.   T. J. Kistenmacher, T. J. Emge, P. Shu and D. O. Cowan, *Acta Cryst,* **B35**, 772, 1979.

39.   F. Wudl and E. Aharon-Shalom, *J. Am. Chem. Soc.* , **104**, 1154, 1982.

40a.   A. J. Moore and M. R. Bryce, *Synthesis,* **26**, 1991.

40b.   E. Cerrada, M. R. Bryce and A. J. Moore, *J. Chem. Soc. , Perkin Trans.* **1**, 537, 1993.

41.   For example: S. Ikegawa, K. Mujawaki, T. Nogami and Y. Shirota, *Bull. Chem. Soc. Jpn.* , **66**, 2770, 1993.

42.   T. Jorgsensen, T. K. Hansen and J. Becher, *Chem. Soc. Rev.* , **23**, 41, 1994.

43.   A. E. Underhill, I. Hawkins, S. Edge, S. B. Wilkes, K. S. Varma, A. Kobayashi and H. Kobayashi, *Synth. Met.* , **55**, 1914, 1993.

44.   R. P. Thummel and V. Goulle, B. Chen, *J. Org. Chem.* , **54**, 3052, 1989.

45.   For example: G. V. Tormos, M. G. Bakker, P. Wang, M. V. Lakshmikantham, M. P. Cava and R. M. Metzger, *J. Am. Chem. Soc.* **117**, 8528, 1995.

46.   A. Moradpour, *J. Chem. Soc. , Perkin Trans.* 1, 7, 1993.

47.　For example: M. E. Peover, *J. Chem. Soc.* , 4540, 1962

48.　C. Vasquez, J. Calabrese, D. A. Dixon and J. S. Miller, *J. Org. Chem.* , **58**, 65, 1993.

49.　R. C. Wheland and E. L. Martin, *J. Org. Chem.* , **40**, 3101, 1975.

50.　R. C. Wheland and J. L. Gulson, *J. Am. Chem. Soc.* , **98**, 3916, 1976.

51.　R. C. Wheland, *J. Am. Chem. Soc*, **98**, 3926, 1976.

52.　M. R. Bryce, S. R. Davies, A. M. Grainger, J. Hellberg, M. B. Hursthouse, M. Mazid, R. Buchmann and F. Gerson, *J. Org. Chem.* , **57**, 1690, 1992.

53.　M. R. Bryce, A. M. Grainger, M. Hasan, G. J. Ashwell, P. A. Bates and M. B. Hursthouse, *J. Chem. Soc.* , *Perkin Trans,* **1**, 611, 1992.

54.　T. Suzuki, Y. Yamashita, C. Kabuto and T. Miyashi, *J. Chem. Soc.* , *Chem. Commun.* , 1102, 1989.

55a.　W. Lehnert, *Tetrahedron Lett.* 473, 1970.

55b.　W. Lehnert, *Synthesis*, 667, 1974.

56.　A. Aumüller and S. Hünig, *Liebigs. Ann. Chem.* 165, 1986.

57.　R. M. Metzger, N. E. Heimer and G. J. Ashwell, *Mol. Cryst.* , *Liq. Cryst.* , **107**, 133, 1984.

58.　B. P. Bespalov and V. V. Titov, *Russ. Chem. Rev.* , **44**, 1091, 1975.

59.　M. Szablewski, *J. Org. Chem.* , **59**, 954, 1994.

60.　J. C. Cole, J. A. K. Howard, G. H. Cross and M. Szablewski, *Acta Crystallogr.* , Sect. C, **C51**, 715, 1995.

61.　G. H. Cross, D. Bloor and M. Szablewski, *Nonlinear Opt.* **14**, 219, 1995.

62.　S. Akhtar, J. Tanaka, R. M. Metzger and G. J. Ashwell, *Mol. Cryst.* , *Liq. Cryst.* , **107**, 133, 1984.

63.　J. S. Miller and J. C. Calabrese, *J. Chem. Soc.* , *Chem. Commun.* , 63, 1988.

64.　Y. Tsubata, T. Suzuki, T. Miyashi and Y. Yamashita, *J. Org. Chem.* , **57**, 6749, 1992.

65.　N. A. Bell, R. A. Broughton, J. S. Brooks, T. A. Jones and S. C. Thorpe, *J. Chem. Soc.* , *Chem. Commun.* , 325, 1990.

66. G. J. Ashwell, E. J. C. Dawnay and A. P. Kuczynski, *J. Chem. Soc. , Faraday Trans. ,* **86**, 1117, 1990.

67. J. A. Fleming, U. K. Patent 24.850 (appl. Nov. 16, 1904): U.S. Patent 803.684 (granted Apr. 19, 1905).

68. J.E. Meinhard, *J. Appl. Phys.* **35**, 3059, 1964.

69. T. L. Anderson, G. C. Komplin and W. Pietro, *J. Phys. Chem.* **97**, 6577, 1993.

70. W. Pietro, *Adv. Mater.* **6**, 239, 1994.

71. S. Hamm and H. Wachtel, *J. Chem. Phys.* **103**, 10689,1994.

72. H. Kuhn, E. E. Polymeropoulos and D. Möbius, *Thin Solid Films,* **68**, 173, 1980.

73. M. Sugi, K. Sakai, M. Saito, Y. Kawabata and S. Iizima, *Thin Solid Films,* **132**, 69, 1985.

74. C. M. Fischer, M. Burghard, S. Roth and K. Klitzing, *Europhys. Lett. ,* **28**, 129, 1194.

75. M. Fujihira, K. Nishiyama and H. Yamada, *Thin Solid Films,* **132**, 77, 1986.

76. Y. Sato, H. Itoigawa and K. Uosaki, *Bull. Chem. Soc. Jpn. ,* **66**, 1032, 1993.

77. K. S. Alleman, K. Weber and S. E. Creager, *J. Phys. Chem.* **100**, 17050, 1996.

78. A. Aviram and M. A. Ratner, *Bull. Am. Phys. Soc. ,* **19**, 341, 1974.

79. A. Aviram and M. A. Ratner, *Chem. Phys. Lett. ,* **29**, 277, 1974.

80. R. M. Metzger and C. A. Panetta, *New J. Chem. ,* **15**, 209, 1991.

81. R. M. Metzger, *In Molecular and Biomolecular Electronics*; R. R. Birge, Ed. , ACS Advances in chemistry Series 240; American Chemical Society: Washington, DC, 81, 1994.

82. R. M. Metzger, *Mater. Sci. Eng. ,* **C3**, 277, 1995.

83. N. J. Geddes, J. R. Sambles, D. J. Jarvis, W. G. Parker and D. J. Sandman, *J. Appl. Phys. Lett.* **56**, 1916, 1990.

84. N. J. Geddes, J. R. Sambles, D. J. Jarvis, W. G. Parker and D. J. Sandman, *J. Appl. Phys. ,* **71**, 756, 1992.

85. G. J. Ashwell, J. R. Sambles, A. S. Martin, W. G. Parker and M. Szablewski, *J. Chem. Soc. , Chem. Commun. ,* 1374, 1990.

86. A. S. Martin, J. R. Sambles and G. J. Ashwell, *Phys. Rev. Lett,* **70**, 218, 1993.

87. R. M. Metzger, B. Chen, U. Höpfner, M. V. Lakshmikantham, D. Vuillaume, T. Kawai, X. Wu, H. Tachibana, T. V. Hughes, H. Sakurai, J. W. Baldwin, C. Hosch, M. P. Cava, L. Brehmer and G. J. Ashwell, *J. Am. Chem. Soc.*, **119**, 10455, 1997.

88. L. X. Wu, M. Shamsuzzoha, R. M. Metzger and G. J. Ashwell, *Synth. Met.*, **55**, 3836, 1993.

89. G. J. Ashwell, E. J. C. Dawnay, A. P. Kuczynski, M. Szablewski, I. M. Sandy, M. R. Bryce, A. M. Grainger and M. Hasan, *J. Chem. Soc.*, *Faraday Trans.*, **86**, 1117, 1990.

90. G. J. Ashwell, C. R. Hargreaves, C. E. Baldwin, C. S. Bahra and C. R. Brown, *Nature(London)*, **357**, 393, 1992.

91. G. J. Ashwell, P. D. Jackson and W. A. Crossland, *Nature (London)*, **368**, 438, 1994.

92. G. J. Ashwell, G, Jeffries, E. J. C. Dawnay, A. P. Kuczynski, D. E. Lynch, Yu Gongda and D. G. Bucknall, *J. Mater. Chem.*, **5**, 975, 1995.

93. G. J. Ashwell, "*In Organic Materials for Non-Linear Optics*": G. J. Ashwell and D. Bloor, Eds. : Royal Soc. of Chem. : Cambridge, **31**, 1993.

94. D. B. Neal, M. C. Petty, G. G. Roberts, M. M. Ahmed, W. J. Feast, I. R. Girling, N. A. Cade, P. V. Kolinsky and I. R. Peterson, *Electron. Lett.*, **22**, 460, 1986.

95. M. Szablewski, P. R. Thomas, A. Thornton, D. Bloor, G. H. Cross, J. M. Cole, J. A. K. Howard, M. Malagoli, F. Meyers, J. L. Bredas, W. Wenseleers and E. Goovaerts, *J. Am. Chem. Soc.*, **119**, 3144, 1997.

96. L. Onsager, *J. Am. Chem. Soc.* **58**, 1486, 1936.

97. C. J. F. Böttcher, *Theory of Electric Polarization*; Elsevier: Amsterdam, Vol. **1**, 1973; Vol. **2**, 1978.

98a. S. R. Marder, D. N. Beratan and L. T. Cheng, *Science,* **252**, 1030, 1991.

98b. S. R. Marder, J. R. Perry, G. Bourhill, C. B. Gorman, B. G. Tiemann and K. Mansour, *Science,* **261**, 186, 1993.

99.   F. Meyers, S. R. Marder, B. M. Pierce and J. L. Brédas, *J. Am. Chem. Soc.*, **116**, 10703, 1994.

100. B. F. Levine and C. G. Bethea, *J. Chem. Phys.*, **63**, 2666, 1975.

101. K. D. Singer and A. F. Garito, *J. Chem. Phys.*, **75**, 3572, 1981.

102. K. Clays and A. Persoons, *Phys. Rev. Lett.*, **66**, 2980, 1991.

CHAPTER 2

Synthetic Work

Reagents

All reagents used were purchased from Aldrich Chemicals and Avocado and they were
not further purified prior to use unless stated.

Instrumentation:-

Infra-red spectroscopy

Infra-red spectra were recorded as Nujol mulls and KBr disks using a Phillips PU 9706
spectrophotometer and an ATI Mattson Genesis series FTIR instrument.

Mass Spectrometry

Mass spectra were recorded using a VG Micromass 7070F mass spectrometer utilising electron impact and fast atom bombardment as ionisation techniques. The solvents used were glycerol and N, N'-methylenebisacrylamide (MBA).

NMR Spectroscopy

^{1}H and ^{13}C nmr spectra were recorded on a Bruker AC 250 and Joel PX60 nmr spectrometers. Samples were dissolved in a range of deuterated solvents.

Combustion Analysis

Microanalyses were carried out by the Department of Chemistry at Brunel University.

2.1   Quinolinium and Picolinium Zwitterions

The initial stages of this project involved the preparation of a series of long chain R(4)Q3CNQ [33], R(4)P3CNQ [37], R(2)Q3CNQ [38]and R(2)P3CNQ [39] analogues to enable a comparative detailed LB study to be carried out. The gamma substituted quinolinium analogues have been well documented in the literature.[1-7] However synthetic and LB film studies of the other adducts, especially the long chain alpha quinolinium derivatives, have not been reported because of synthetic difficulties. The literature methods for the synthesis of R(4)Q3CNQ[1-7] were used as the basis for the synthetic work carried out.

[33]

[37]

[38]

[39]
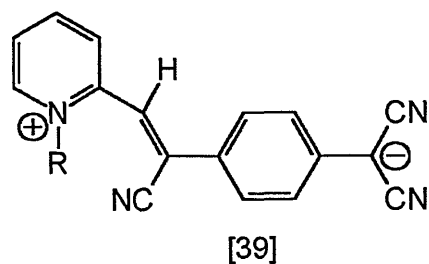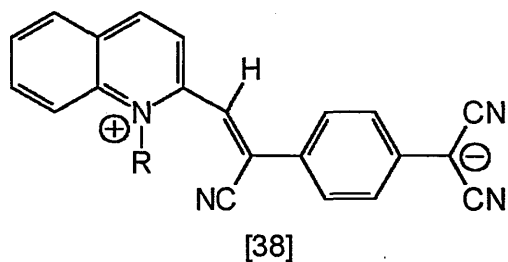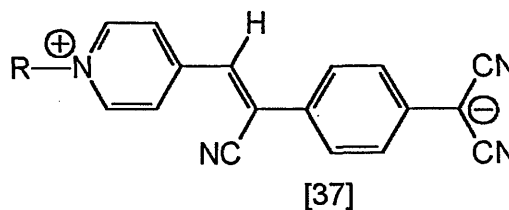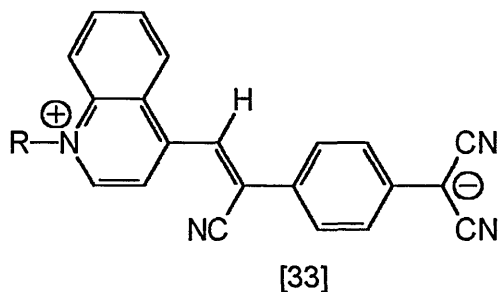
Initially a range of quinolinium and picolinium donor analogues were prepared via the Menschutkin reaction[8] as precursors to zwitterionic adducts of TCNQ.

2.1.1 *Preparation of N-alkyl-4 and -2-methyl quinolinium and pyridinium cations:*

Scheme 2.1:
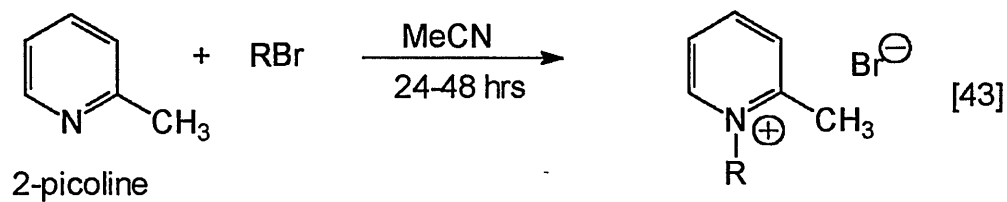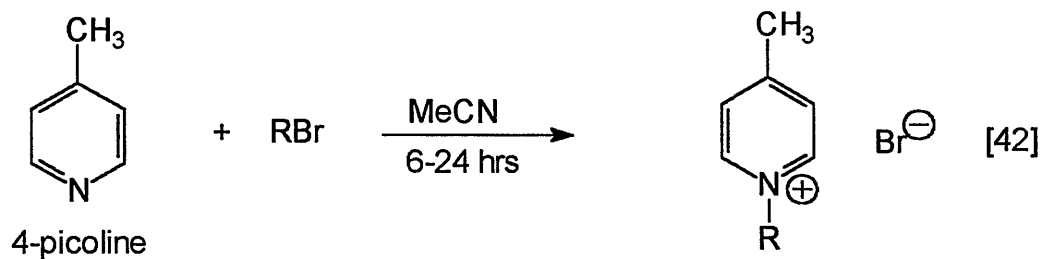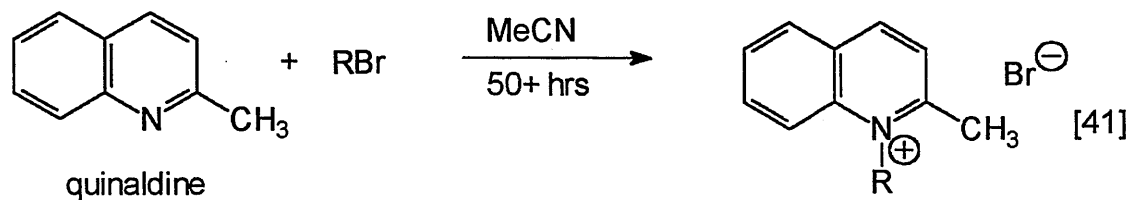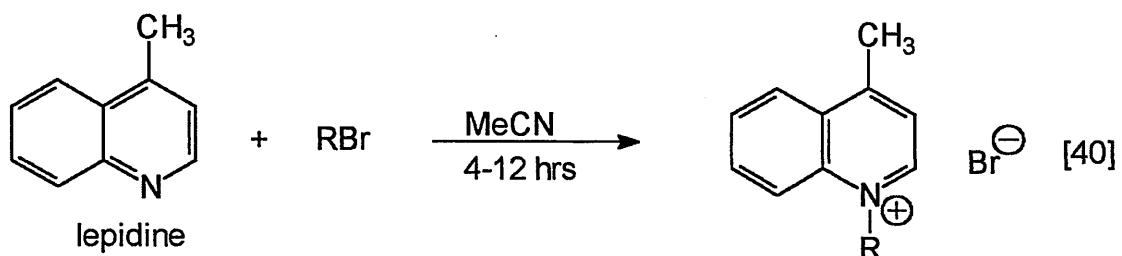
2.1.1.1 *Preparation of N-Hexadecyl-4-methylquinolinium bromide [40 where*
R=$C_{16}H_{33}$]

1-Bromohexadecane (4.24g, 0.014 moles) and lepidine (2g, 0.014 moles) were refluxed together in dry acetonitrile (25 mls) for 6 hours. The initial yellow coloured solution became darker and more viscous as the reaction progressed, producing a mauve solution. The reaction mixture was then cooled and on the addition of ether, the salt formed as a white precipitate which was filtered off under suction and washed with ether. Off-white platelets were obtained, which were recrystallised from hot methanol. Yield: 4.75g (76%) off white platelets. Melting point 110-115°C. See Table 2.01

2.1.1.2 *Preparation of N-Hexadecyl-2-methylquinolinium bromide [41 where*
R=$C_{16}H_{33}$]

1-Bromohexadecane (10.00g, 0.032 moles) and quinaldine (4g, 0.028 moles) were refluxed together in dry acetonitrile (10 mls) for 168 hours. The initial pale brown colouration darkened as the reaction progressed, producing a red solution. The reaction mixture was then cooled and on the addition of ether, the salt formed as a pink precipitate. The precipitate was filtered off under suction and washed with ether. Light pink platelets were obtained which were recrystallised from hot methanol. Yield:- 4g (32%) off white platelets. Melting point 120-123°C.

2.1.1.3 *Preparation of N-Hexadecyl-4-picolinium bromide [42 where R=$C_{16}H_{33}$]*

1- Bromohexadecane (30g, 0.1 moles) and 4-picoline (10.3g, 0.1 moles) were refluxed together in dry acetonitrile (75 mls) for 6 hours. The initial pale yellow solution changed to a deep red solution as the reaction progressed. The reaction mixture was then cooled and on the addition of ether, a light yellow precipitate formed. The precipitate was filtered off under suction and washed with ether. The product was then recrystallised

from hot acetonitrile and washed again with ether. Yield: 28g (70%) off white platelets.

Melting point 53-56° C.

2.1.1.4 *Preparation of N-Hexadecyl-2-picolinium bromide [43 where R=$C_{16}H_{33}$]*

1-Bromohexadecane (32g, 0.12 moles) and 2-picoline (10.3g, 0.1 moles) were refluxed together in dry acetonitrile (100 mls) for 36 hours. The initial off white solution changed to a deep red as the reaction progressed. The reaction mixture was then cooled and on the addition of ether, the salt formed as a white precipitate. The precipitate was filtered off under suction and washed with ether. The product was then recrystallised from hot acetonitrile and washed again with ether. Yield: 35g (80%). Melting point 127-131°C.

The synthetic procedures for the other analogues of the quinolinium/picolinium donor cations were obviously similar and, for brevity have not been included here. However their reaction times and yields have been summarised in the following tables:-

Table 2.01 N-alkyl-4-methylquinolinium cations [40]:

R group	Reaction time (hrs)	Yield (%)
C_4H_9	4	90+
C_5H_9	4	90+
C_6H_{13}	4	90+
C_8H_{17}	4	86
$C_{10}H_{21}$	4	84
$C_{11}H_{23}$	4	86
$C_{12}H_{25}$	4	80
$C_{13}H_{27}$	6	80
$C_{14}H_{29}$	6	75
$C_{15}H_{31}$	6	70
$C_{16}H_{33}$	6	76
$C_{18}H_{37}$	12	65
$C_{20}H_{41}$	12	60
⟨_⟩-CH$_2$–	4	90+
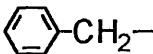
Table 2.02 N-alkyl-2-methylquinolinium cations [41]:

R* group	Reaction time (hrs)	Yield
C_4H_9	50	65
C_5H_{11}	50	65
C_6H_{13}	50	60
C_8H_{17}	72	60
$C_{10}H_{21}$	72	56
$C_{11}H_{23}$	72	45
$C_{12}H_{25}$	100	43
$C_{13}H_{27}$	100	34
$C_{14}H_{29}$	120	30
$C_{15}H_{31}$	168	35
$C_{16}H_{33}$	168	32
$C_{18}H_{37}$	200+	12
$C_{20}H_{41}$	200+	10
⟨◯⟩-CH₂–	50	60
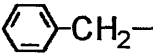
* The corresponding haloalkane was used in slight excess during the reaction.

Table 2.03 N-alkyl-4-picolinium cations [42]:

R group	Reaction time (hrs)	Yield
C_4H_9	6	90+
C_5H_{11}	6	90+
C_6H_{13}	6	90+
C_8H_{17}	6	85
$C_{10}H_{21}$	6	86
$C_{11}H_{23}$	6	85
$C_{12}H_{25}$	12	80
$C_{13}H_{27}$	12	70
$C_{14}H_{29}$	12	70
$C_{15}H_{31}$	12	70
$C_{16}H_{33}$	12	75
$C_{18}H_{37}$	24	65
$C_{20}H_{41}$	-	-
⟨◯⟩-CH₂–	6	90+

Table 2.04 N-alkyl-2-picolinium cations [43]:

R* group	Reaction time (hrs)	Yield
C_4H_9	24	80
C_5H_{11}	24	85
C_6H_{13}	24	80
C_8H_{17}	24	80
$C_{10}H_{21}$	24	80
$C_{11}H_{23}$	24	80
$C_{12}H_{25}$	24	80
$C_{13}H_{27}$	36	80
$C_{14}H_{29}$	36	75
$C_{15}H_{31}$	36	75
$C_{16}H_{33}$	36	60
$C_{18}H_{37}$	48	35
$C_{20}H_{41}$	-	-
$\langle\rangle$-CH$_2$-	24	70
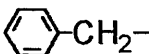
* The corresponding haloalkane was used in slight excess during the reaction.

2.1.2 *Preparation of N-alkyl-2 and -4-quinolinium\picolinium zwitterionic TCNQ adducts:*

N.B. C,H,N Analytical data are summmarised in Tables 2.09 - 2.10 (pages 62-63)

Method 1 - Using LiTCNQ

Scheme 2.2

R(4)Q3CNQ

R(2)Q3CNQ

R(4)P3CNQ

[43] + LiTCNQ $\xrightarrow[\text{100+ hrs}]{\text{MeCN}}$

R(2)P3CNQ   [39]
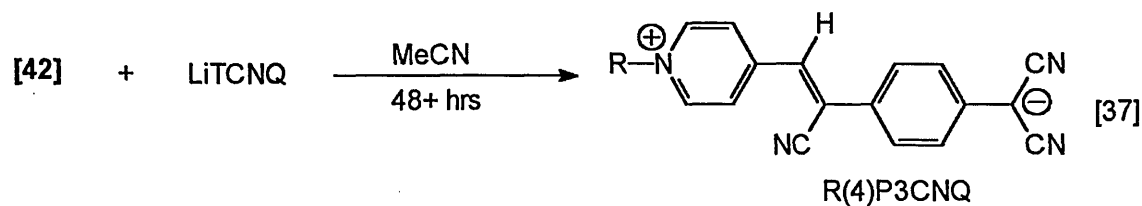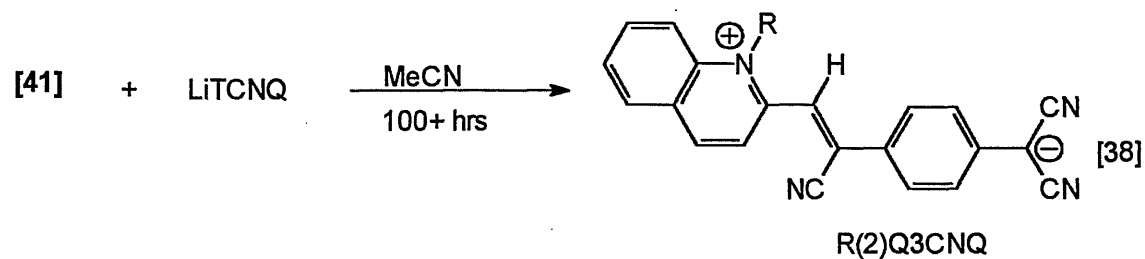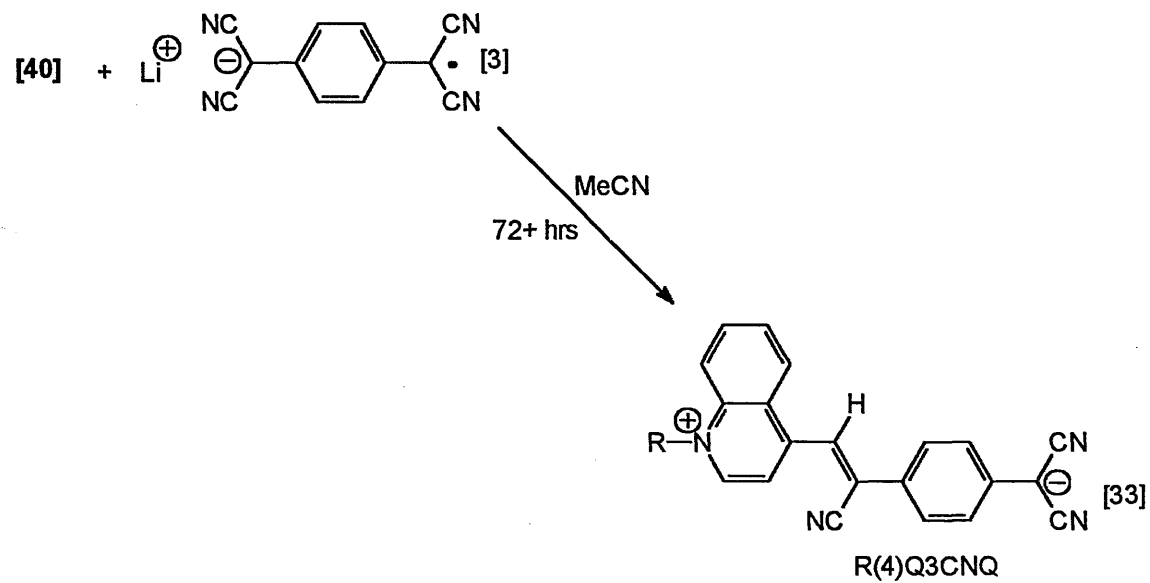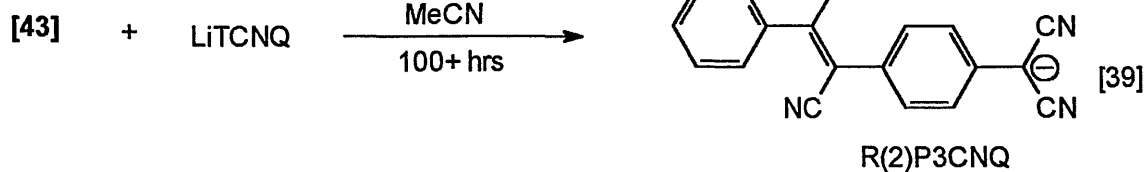
* All the above reactions yielded LiBr also.

2.1.2.1 *Preparation of Lithium-TCNQ* [3]

Scheme 2.3 :-

LiI + $\xrightarrow[\text{Reflux 3 hours}]{\text{MeCN}}$ Li$^{\oplus}$
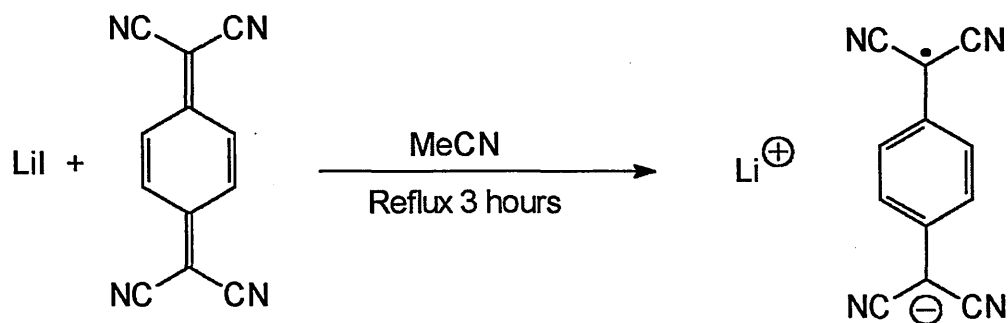
Lithium iodide (19.70g, 0.147 moles) was dissolved in dry acetonitrile(250 mls) and refluxed for 10 minutes. 7, 7, 8, 8- Tetracyanoquinodimethane (30.0g, 0.147 moles), dissolved in acetonitrile (250 mls) was added dropwise to the refluxing lithium iodide solution. Due to the hygroscopic nature of lithium iodide the reaction was performed under nitrogen and the mixture was refluxed for a further 3 hours. A purple precipitate formed, which was filtered off under suction and washed with toluene and ether to remove any unreacted TCNQ, before drying *in vacuo*.

The characteristic U.V/Vis spectrum was observed in acetonitrile.

Yield: 25g (80%) of fine purple crystals.

2.1.2.2 *Preparation of Z-β-(1-hexadecyl-4'-quinolinium)-α-cyano-4-styryl dicyanomethanide* - $C_{16}H_{33}$(4)Q3CNQ [33, where R=$C_{16}H_{33}$]

Hexadecyl-4-methylquinolinium bromide (0.429g, 0.000474 moles), dissolved in hot water (15 mls), was added dropwise to a refluxing solution of LiTCNQ (0.2g, 0.000474 moles) in acetonitrile (25 mls) over a 2 hour period. This deep green solution was refluxed for a further 5 days. The progress of the reaction was monitored every 12hrs using visible spectrophotometry to observe the disappearance of the TCNQ⁻ band at approximately 840 nm and the appearance of a broad CT band between 450 and 800 nm as the reaction progressed. The deep green solution gradually became darker over the period of reflux until a blue solution was obtained and a gold film was observed on the surface of the reaction mixture. The solution was then evaporated to a small volume and cooled in ice, yielding metallic green crystals. The product was then filtered under suction, washed with toluene, ether and hot water, recrystallised from hot acetonitrile, and finally dried *in vacuo* at 110°C.

yield : 180mgs (69%) - metallic green microcrystals. Melting point 285 - 288°C

UV/Vis (MeCN) - broad charge-transfer band at λmax = 712 nm

IR (cm⁻¹): 2910, 2180, 2140, 1600, 1500

^{1}H nmr (DMSO-d$_6$): δ 9.4 (d, 1H); 8.8 (d, 1H); 8.6 (d, 1H); 8.5 (d, 1H); 8.4 (t, 1H); 8.2 (t, 1H); 8.0 (s, 1H); 7.8 (d, 2H); 6.9 (d, 2H); 5.3 (t, 2H); 2.1(m, 2H); 1.6 -1.2(m, 26H); 0.85 (t, 3H).

MS: m/z 544 (M^+, 10%), 320 (M^+ -$C_{16}H_{33}$, 50%), 255 (M^+ - $C_{16}H_{33}$-C(CN)$_2$, 100%).

Analytical data for $C_{37}H_{44}N_4$ Theory: C, 81.58 %; H, 8.14 %; N, 10.28 %. Found: C, 81.61%; H, 8.10%; N, 10.29%.

2.1.2.3 *Preparation of Z-β-(1-hexadecyl-2'-quinolinium)-α-cyano-4-styryl dicyanomethanide* -$C_{16}H_{33}(2)Q3CNQ$ [38, where R=$C_{16}H_{33}$]

Hexadecyl-2-methylquinolinium bromide (2.3g, 0.0051 moles), dissolved in a minimum volume of hot water (5 mls) was added dropwise to a refluxing solution of $Li^+ TCNQ^-$ (1g, 0.0047 moles) in a minimum volume of acetonitrile (20 mls) over a 4 hour period. The initial deep green solution, attributed to the TCNQ radical anion, was refluxed for at least another 14 days. During this period the reaction was continually monitored (uv-vis) for the disappearance of this $TCNQ^-$ anion at 840 nm and the appearance of a broad charge transfer band over the range of 400 - 900 nm. The reaction was also monitored by TLC using a 7:3 DCM:methanol mobile phase. As the reaction progressed (7 days) the deep green solution became darker and a red tinge developed in the reaction mixture. At this point the broad CT band begian to develop and after approximately a further 48 hours reflux, the formation of gold solid in the solution was observed. The reaction mixture was then cooled in ice, solid formation being aided by scratching the side of the reaction flask with a glass rod and then the reaction mixture was refrigerated for a further 72 hours. The gold solid was then filtered off under suction, washed with ether, recrystallised from hot methanol and dried *in vacuo* at 110°C for 72 hours.

Yield: 220 mgs (9%) of metallic gold platelets. Melting point 192 - 195 °C.

UV/Vis (MeCN) - broad charge transfer band at λmax = 698 nm

IR (cm^{-1}): 2910, 2180, 2140, 1600, 1500

^{1}H nmr ((CD_3)$_2$CO): δ 9.4 (d, 1H); 8.9 (d, 2H); 8.7 (d, 1H); 8.55 (t, 1H), 8.4 (t, 1H), 8.05 (s, 1H); 7.95 (d, 2H); 7.3 (d, 2H); 5.5 (t, 2H); 2.1 - 1.0 (m, 31H).

MS: m/z 544 (M^+, 25%),

Analytical data for $C_{37}H_{44}N_4$ - Theory: C, 81.58 %; H, 8.14 %; N, 10.28 %. Found: C, 80.44 %; H, 8.15 %; N, 10.00 %.

2.1.2.4 *Preparation of Z -β-(1-tridecyl-4'-pyridinium)-α-cyano-4-styryldicyanomethanide - $C_{13}H_{27}(4)$-P3CNQ [37, where R=$C_{13}H_{27}$]*

LiTCNQ (0.5g, 0.0024 moles) was refluxed in acetonitrile (75 mls). To this refluxing solution, N-tridecyl-4-picolinium bromide (0.85g, 0.0024 moles) dissolved in warm water (50 mls) was added dropwise over a period of 2 hours. The reaction was left to reflux for 72 hours by which time a colour change of dark green to turquoise was observed. As with the quinolinium TCNQ adducts the reaction was monitored using UV/VIS (350-900 nm). The reaction mixture was then cooled in ice. On addition of cold water(50 mls) the product precipitates out as metallic blue/black platelets. The product was then isolated by suction filtration, washed with hot water (2 x 20 mls), toluene (2 x 10 mls) and ether (2 x 10 mls) to remove any unreacted cation and LiTCNQ. The product was then dried *in vacuo* at 110°C for 72 hrs.

Yield: 481 mgs (44.6%) blue/black platelets. Melting point 161 - 164 °C

UV/Vis (MeCN) - broad charge-transfer band at λ max = 636 nm

IR (cm^{-1}): 2910, 2160, 2120, 1580, 1500.

^{1}H nmr (DMSO-d$_6$): δ 8.85 (d, 2H); 8.3 (d, 2H); 7.85 (s, 1H); 7.6 (d, 2H); 6.85 (d, 2H); 4.8(d, 2H); 1.3 (m, 22H); 0.8 (t, 3H)

MS: m/z 452 (M$^+$,)

Analytical data for $C_{30}H_{36}N_4$ - Theory: C, 79.61 %; H, 8.02 %; N, 12.38 %; Found: C, 78.22 %; H, 8.03 %; N, 12.38 %.

2.1.2.5 *Preparation of Z-β-(1-tridecyl-2'-pyridinium)-α-cyano-4-styryldicyanomethanide* -$C_{13}H_{27}(2)P3CNQ$ [39, where $R=C_{13}H_{27}$]

LiTCNQ (0.5g, 0.0024 moles) was refluxed in acetonitrile (40 mls). To this refluxing solution, N-tridecyl-2-picolinium bromide (0.85g, 0.0024 moles) dissolved in warm water (10mls) was added dropwise over a period of 6 hours. The reaction was left to reflux for a further 168 hours with regular monitoring by UV/VIS (350 - 900 nm). During this period a colour change from dark green to turquoise was observed. The reaction mixture was then cooled in ice and on the addition of cold water (25 mls) the product precipitated out as blue/black platelets. The product was then isolated by suction filtration, washed with hot water (2 x 10 mls), toluene (2 x 10 mls) and ether (2 x 10 mls) to remove any unreacted cation and LiTCNQ. The product was then dried in vacuo at 110°C for 72 hrs.

Yield: 105 mgs (10%)-blue/black platelets. Melting point 141 - 143 °C

UV/Vis (MeCN)- broad charge transfer band at λmax = 600 nm

IR (cm^{-1}): 2910, 2160, 2120, 1580, 1500.

^{1}H nmr (DMSO-d_6): δ 9.05 (d, 1H); 8.6 (t, 1H); 8.45 (d, 1H); 8.05 (t, 1H); 7.85 (s, 1H); 7.55 (d, 2H); 6.85 (d, 2H); 4.7 (t, 2H); 1.3 (m, 22H); 0.8 (t, 3H).

MS: m/z 452 (M^+)

Analytical data for $C_{30}H_{36}N_4$ - Theory: C, 79.61 %; H, 8.02 %; N, 12.38 %; Found C, 79.01 %; H, 8.07 %; N, 11.95 %.

A series of zwitterionic quinolinium/picolinium TCNQ analogues, ranging from R = C_4H_9 to $C_{20}H_{41}$ were made to create a stock of compounds for a comparative Langmuir-Blodgett film study. The synthetic procedures for the other quinolinium/picolinium TCNQ analogues were obviously similar and have been omitted here for brevity, however their reaction times and yields have been summarised in the following Tables where an increase in reaction time and decrease in yield for an increase in chain length can be clearly seen, which is further emphasised with the sterically hindered alpha analogues.

Table 2.05 R(4)Q3CNQ zwitterions with LiTCNQ.

R Group	Reaction Time	% Yield
C_4H_9	72 hours	65
C_5H_{11}	72 hours	65
C_6H_{13}	72 hours	55
C_8H_{17}	72 hours	60
$C_{10}H_{21}$	72 hours	56
$C_{11}H_{23}$	72 hours	60
$C_{13}H_{27}$	5 days	63
$C_{14}H_{29}$	5 days	58
$C_{15}H_{31}$	5 days	64
$C_{16}H_{33}$	5 days	68
$C_{18}H_{37}$	20 days	35
$C_{20}H_{41}$	no reaction	no reaction
$\langle \rangle$-CH$_2$-	70 hours	70
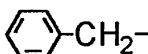
Table 2.06 R(2)Q3CNQ zwitterions with LiTCNQ.

R Group	Reaction Time (hrs)	% Yield
C_4H_9	5 days	50
C_5H_{11}	5 days	60
$C_{10}H_{21}$	10 days	43
$C_{11}H_{23}$	10 days	45
$C_{13}H_{27}$	5 days	37
$C_{14}H_{29}$	5 days	23
$C_{15}H_{31}$	20 days	15
$C_{16}H_{33}$	14 days	<10
$C_{18}H_{37}$	20 days	<10
$C_{20}H_{41}$	no reaction	no reaction
⬡-CH_2-	10 days	30
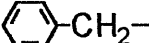
Table 2.07 R(4)P3CNQ zwitterions with LiTCNQ.

R Group	Reaction Time (hrs)	% Yield
C_4H_9	36 hours	58
C_5H_{11}	36 hours	60
$C_{10}H_{21}$	72 hours	42
$C_{11}H_{23}$	72 hours	61
$C_{12}H_{25}$	72 hours	20
$C_{13}H_{27}$	72 hours	43
$C_{14}H_{29}$	72 hours	30
$C_{15}H_{31}$	72 hours	15
$C_{16}H_{33}$	72 hours	<10
$C_{18}H_{37}$	72 hours	<10
$C_{20}H_{41}$	no reaction	no reaction
⬡-CH_2-	12 hours	70
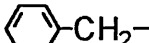
Table 2.08 R(2)P3CNQ zwitterions with LiTCNQ.

R Group	Reaction Time (hrs)	% Yield
C_4H_9	4 days	34
C_5H_{11}	4 days	43
$C_{10}H_{21}$	5 days	27
$C_{11}H_{23}$	5 days	25
$C_{13}H_{27}$	7 days	12
$C_{14}H_{29}$	7 days	<10
$C_{15}H_{31}$	10 days	<10
$C_{16}H_{33}$	10 days	<10
$C_{18}H_{37}$	10 days	<10
$C_{20}H_{41}$	pure pdt not obtained	pure pdt not obtained
$\langle \underline{} \rangle$–$CH_2$–	24 hours	40
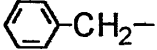
Method 2:-

An alternative method for preparation of the zwitterions

Due to the inefficiency of the previous methods in terms of some yields and reaction times, another literature method[2-7] was also investigated. The requirement for acid behaviour by a proton on the quinolinium/picolinium cation led to the use of a suitable base - namely piperidine in these reactions. Ashwell et al[3-6] and Bell et al[2,7] used piperidine to synthesise the γ-quinolinium-TCNQ derivatives for subsequent LB studies.

Scheme 2.4
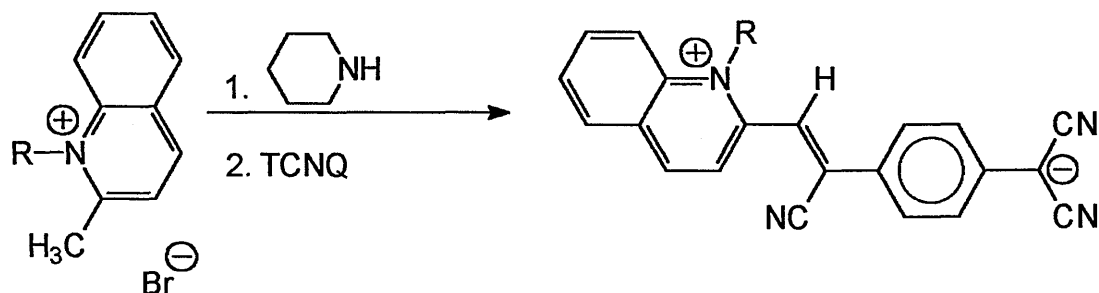
General Method (see Scheme 2.4) :-

Acetonitrile was refluxed with piperidine (0.001 mole), for 10 minutes. The γ-quinolinium or picolinium bromide (0.001 mole) dissolved in acetonitrile (20 mls) was added dropwise over a period of 2 hours to the refluxing solution. TCNQ (0.001 mole) was added to the blue solution and refluxed for a further 3-20 hours using UV/VIS to monitor the reaction. A colour change from an intense blue to green was observed after just an hour's reflux which darkened to a brown colour on completion of the reflux. At this point the product precipitated out as dark green / black platelets. The reaction mixture was cooled and the product isolated by filtration under suction. The crude product was washed with toluene (2 x 10 mls) to remove any unreacted TCNQ, and ether (2 x 10 mls) and then recrystallised from hot methanol. Yields of between 20-50%

of dark green platelets for the γ-quinolinium adducts and dark blue/black platelets for the γ- picolinium adducts, were obtained.

Although the above method substantially decreased reaction times and in some cases increased yields (i.e. for the longer chain gamma analogues), the method was flawed in some respects for its repeated failure to produce substantially pure products for use as LB film materials (see Chapter 3) no doubt due to competitive addition and substitution reactions between amines and TCNQ. The sterically hindered α-quinolinium (Scheme 2.4) and α-picolinium analogues proved virtually impossible to synthesise using this method.

DBU, DBN and N-methyl piperidine[9] were also tried as bases in the above reaction with varying degrees of success. However the same problem was encountered with the purity of the final products for suitable LB film work.

Table 2.09 Analytical data for quinolinium zwitterions

zwitterion	calculated			found		
	%C	%H	%N	%C	%H	%N
C_4H_9(4)-Q3CNQ	79.76	5.35	14.88	79.81	5.39	14.62
C_5H_{11}(4)-Q3CNQ	79.97	5.68	14.35	80.13	5.64	14.13
$C_{10}H_{21}$(4)-Q3CNQ	80.83	7.00	12.16	80.72	6.53	12.34
$C_{11}H_{23}$(4)-Q3CNQ	80.98	7.22	11.80	81.25	7.30	11.65
$C_{13}H_{27}$(4)-Q3CNQ	81.24	7.62	11.15	81.86	7.77	10.87
$C_{14}H_{29}$(4)-Q3CNQ	81.35	7.80	10.84	81.10	7.78	10.42
$C_{15}H_{31}$(4)-Q3CNQ	81.46	7.97	10.55	81.05	7.95	10.99
$C_{16}H_{33}$(4)-Q3CNQ	81.58	8.14	10.28	81.61	8.10	10.29
$C_{18}H_{37}$(4)-Q3CNQ	81.77	8.45	9.78	81.80	8.21	9.50
Benzyl(4)-Q3CNQ	81.95	4.39	13.66	not obtained		
C_4H_9(2)-Q3CNQ	79.76	5.35	14.88	79.31	5.89	14.57
C_5H_{11}(2)-Q3CNQ	79.97	5.68	14.35	79.03	5.64	14.61
$C_{10}H_{21}$(2)-Q3CNQ	80.83	7.00	12.16	80.25	6.92	12.32
$C_{11}H_{23}$(2)-Q3CNQ	80.98	7.22	11.80	81.23	6.89	10.85
$C_{13}H_{27}$(2)-Q3CNQ	81.24	7.62	11.15	80.14	8.95	9.99
$C_{14}H_{29}$(2)-Q3CNQ	81.35	7.80	10.84	80.87	8.12	10.65
$C_{15}H_{31}$(2)-Q3CNQ	81.46	7.97	10.55	81.25	7.95	10.99
$C_{16}H_{33}$(2)-Q3CNQ	81.58	8.14	10.28	80.44	8.15	10.00
$C_{18}H_{37}$(2)-Q3CNQ	81.77	8.45	9.78	81.33	8.64	10.02
$C_{20}H_{41}$(2)-Q3CNQ	81.95	9.72	9.32	81.05	8.65	10.12
Benzyl(2)-Q3CNQ	81.95	4.39	13.66	82.20	5.34	13.89

Table 2.10. Analytical data for picolinium zwitterions

zwitterion	calculated			found		
	%C	%H	%N	%C	%H	%N
C_4H_9(4)-P3CNQ	77.28	5.56	17.17	79.65	5.45	16.38
C_5H_{11}(4)-P3CNQ	77.62	5.92	16.46	79.67	5.34	16.78
$C_{10}H_{21}$(4)-P3CNQ	78.99	7.37	13.65	79.48	7.43	13.84
$C_{11}H_{23}$(4)-P3CNQ	79.21	7.60	13.20	79.05	6.98	12.74
$C_{13}H_{27}$(4)-P3CNQ	79.61	8.02	12.38	78.22	8.03	12.98
$C_{14}H_{29}$(4)-P3CNQ	79.79	8.21	12.01	78.19	8.35	13.77
$C_{15}H_{31}$(4)-P3CNQ	79.96	8.39	11.66	78.35	8.13	11.97
$C_{16}H_{33}$(4)-P3CNQ	80.12	8.56	11.32	79.23	8.24	11.89
$C_{18}H_{37}$(4)-P3CNQ	80.41	8.87	10.72	80.04	8.97	10.25
Benzyl(4)-P3CNQ	80.45	3.91	15.64	not obtained		
C_4H_9(2)-P3CNQ	77.28	5.56	17.17	not obtained		
C_5H_{11}(2)-P3CNQ	77.62	5.92	16.46	77.20	6.24	18.02
$C_{10}H_{21}$(2)-P3CNQ	78.99	7.37	13.65	78.45	7.42	13.97
$C_{11}H_{23}$(2)-P3CNQ	79.21	7.60	13.20	79.65	7.09	13.98
$C_{13}H_{27}$(2)-P3CNQ	79.61	8.02	12.38	79.01	8.07	11.95
$C_{14}H_{29}$(2)-P3CNQ	79.79	8.21	12.01	78.98	8.74	12.58
$C_{15}H_{31}$(2)-P3CNQ	79.96	8.39	11.66	79.52	8.65	12.23
$C_{16}H_{33}$(2)-P3CNQ	80.12	8.56	11.32	79.40	8.92	12.10
$C_{18}H_{37}$(2)-P3CNQ	80.41	8.87	10.72	80.00	8.98	10.66
Benzyl(2)-P3CNQ	80.45	3.91	15.64	81.62	4.03	16.20

2.2   Altering the electron donor moiety:-

Further work involved looking initially at changing the electron donating group. Initially we looked at the following benzothiazolium, pyridazine and pyrazine derivatives which were commercially available.
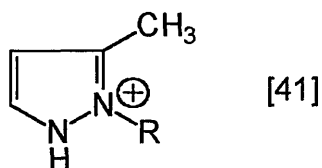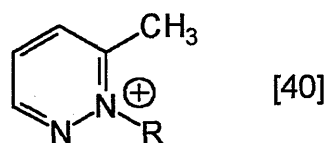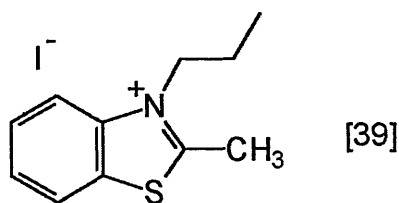
These were 2-methyl-3-propylbenzothiazolium iodide [39], 3-methyl pyridazine* [40] and 3-methyl pyrazine* [41] derivatives whose structures are shown above.

* commercially available in un-alkylated forms.

2.2.1 Preparation of *N-hexadecyl-3-methylpyridazinum bromide* [44, where R is

n-$C_{16}H_{33}$]

Scheme 2.5 :-

[44]
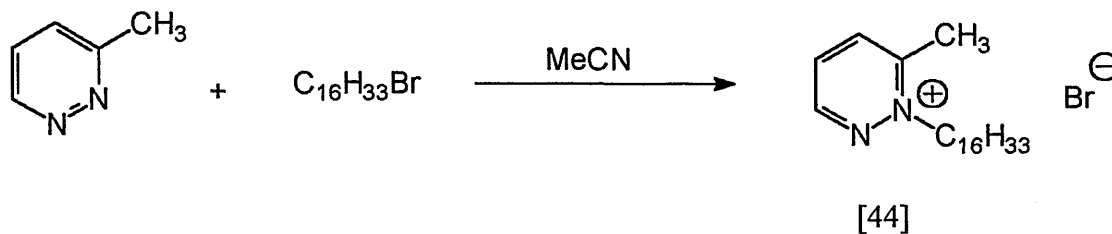
3-Methylpyridazine (0.5g, 0.0053 moles) and bromohexadecane (1.6g, 0.0053 moles) were refluxed together in acetonitrile (15mls). After 1 hr the initially clear solution developed an orange/brown colour. The solution was refluxed for a further 48 hours and then cooled in ice. An orange precipitate developed which was filtered off under suction and washed with ether (2 x 20 mls). The product was dried *in vacuo* to yield orange platelets (1.8g, 85% yield).

2.2.2 Preparation of *N-hexadecyl-3-methylpyrazole* [45, where R is n-$C_{16}H_{33}$]

Scheme 2.6 :-

[45]
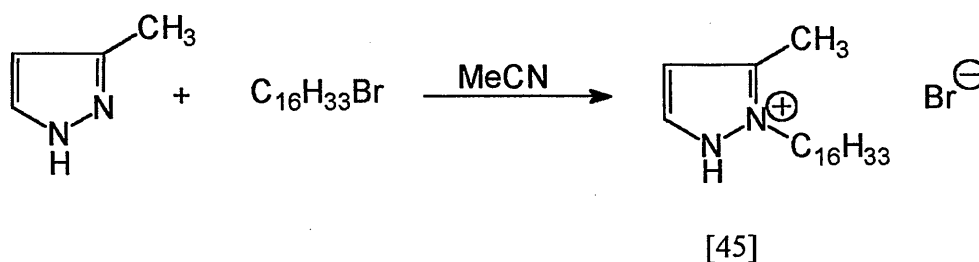
3-Methylpyrazole (0.5g, 0.0061 moles) and 1-bromohexadecane (1.86g, 0.0061 moles) were refluxed for 48 hours in dry acetonitrile (15 mls) to give a light blue solution. The acetonitrile was rotary evaporated off at reduced pressure to give a green solid. The solid was washed with ether (2 x 20mls) and dried *in vacuo* to yield light green platelets (1.2g, 51% yield).

2.2.3 Preparation of a zwitterionic N-hexadecylpyridazinium TCNQ adduct (C₁₆H₃₃-(2)Pdz3CNQ) [46].

2.2.3 *Preparation of a zwitterionic N-hexadecylpyridazinium TCNQ adduct*

(C₁₆H₃₃-(2)Pdz3CNQ) [46].

Scheme 2.7:-

Using method 1

[46]
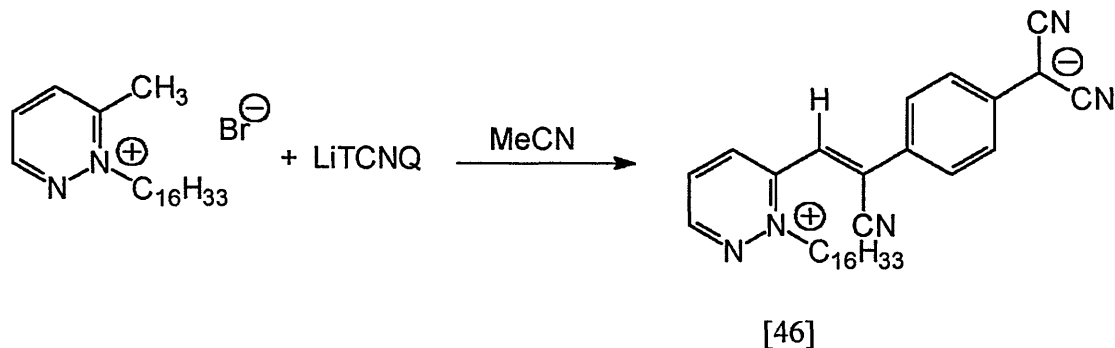
To a refluxing acetonitrile solution (30 mls) of lithium TCNQ (0.54g, 0.0026 moles), the quaternary salt (1g, 0.0026 moles) dissolved in acetonitrile (10mls) was added slowly over a period of 4 hours. The reaction mixture was refluxed for a further 48 hours during which time the initial deep green solution developed into a deep blue one. A blue precipitate formed upon cooling which was filtered off under suction, washed with ether(2 x 20 ml), recrystallised from dichloromethane and dried *in vacuo*.

Yield (0.45g, 35 %) blue platelets. Melting point 180 - 185°C

UV/vis (MeCN)- Sharp charge transfer band at λmax = 480 nm

IR (cm⁻¹):2910, 2180, 2120, 1580, 1500

^{1}H nmr (CDCl₃/DMSO-d₆ (60:40)) : δ 9.9 (d, 1H); 8.45 (t, 1H); 8.4 (d, 1H); 7.85 (s, 1H); 7.5 (d, 2H); 6.8 (d, 2H)

MS: m/z 495 (M⁺, 25%)

Analytical data for C₃₂H₄₁N₅- Theory: C, 77.54 %; H, 8.34 %; N, 14.13 %. Found: C, 78.66 %; H, 8.57 %; N, 15.02 %.

2.2.4 Preparation of a zwitterionic N-hexadecylpyrazolium TCNQ adduct (C₁₆H₃₃(2)-Prz3CNQ) [47]

2.2.4 Preparation of a zwitterionic N-hexadecylpyrazolium TCNQ adduct
(C$_{16}$H$_{33}$(2)-Prz3CNQ) [47]

Scheme 2.8:-

Using method 1.

[47]
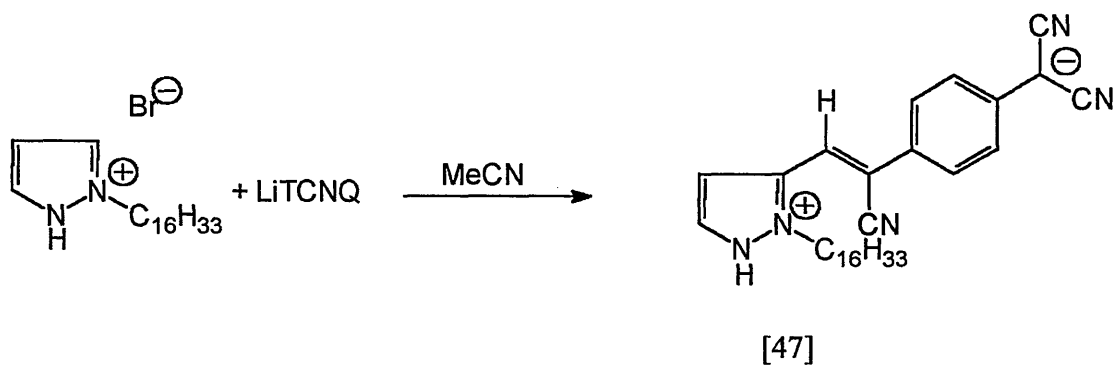
To a refluxing solution acetonitrile solution (30 mls) of lithium TCNQ (0.53g, 0.0021

moles), the quaternary bromide (1g, 0.0026 moles) dissolved in acetonitrile (10 mls) was

added slowly over a period of 2 hours. The reaction mixture was refluxed for a further

24 hours during which the dark green solution became lighter in colour. The acetonitrile

was reduced in volume using a rotary evaporator. A blue/green precipitate formed upon

cooling (24 hours) which was filtered off under suction, washed with ether (2 x 20 mls),

recrystallised from methanol and dried *in vacuo*.

Yield: (0.3g, 30 %) blue/green lustrous platelets. Melting point 172 - 176°C

IR (cm^{-1}): 2190, 2170.

^{1}H nmr: Resolution not adequate for interpretation.

MS: m/z 483 (M$^+$, 20%)

Analytical data for C$_{31}$H$_{41}$N$_5$ - Theory: C, 76.98 %; H, 8.54 %; N, 14.48 %. Found: C,

78.02 %; H, 8.97 %; N, 15.60 %.

2.2.5 *Synthesis of a zwitterionic N-propylbenzothiazolium TCNQ adduct (C₃H₇(2)Bz3CNQ)* [48]

Scheme 2.9:-

Using method 2.

[48]
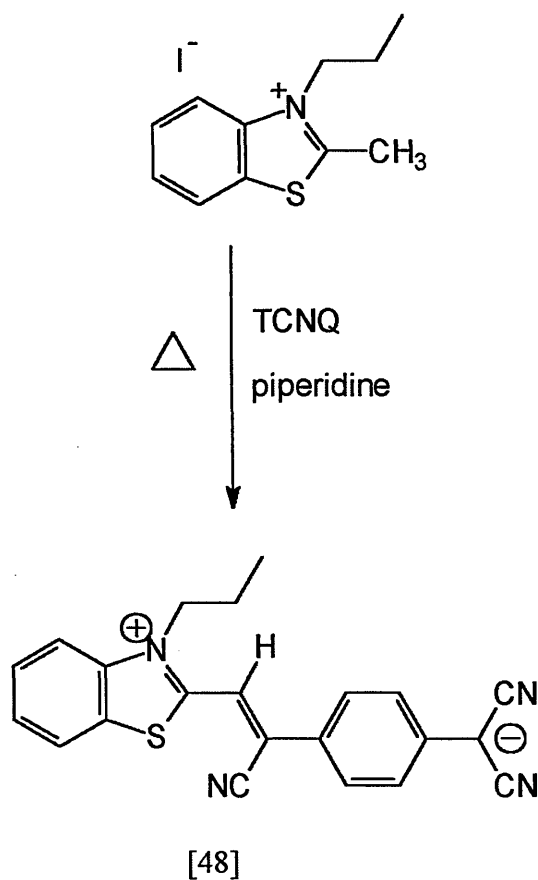
Acetonitrile was refluxed with TCNQ (0.50g, 0.0025 moles) and piperidine (0.21g, 0.0025 moles) for 10 minutes to form a deep blue solution. 2-Methyl-3-propyl-benzothiazolium iodide (0.78g, 0.0025 moles) was added to form a green precipitate. The reaction mixture was refluxed for another 30 minutes before being cooled in ice, filtered under suction, washed with toluene and ether and dried in *vacuo*.

Yield : 760 mgs (80+%) - green platelets. Melting point > 300 °C

UV/Vis (MeCN) - A twin peaked broad charge-transfer band at λmax = 770 nm

IR (cm⁻¹): 2910, 2860, 2195, 2180, 1600, 1530, 1500.

¹H nmr : Material too insoluble for adequate interpretation.

Analytical data for $C_{22}H_{16}S_1N_4$ - Theory: C, 71.52%; H, 4.38%, N, 15.21%, S, 8.70%. Found: C, 73.21%; H, 4.60%; N, 15.75%; S, 9.02%.

2.3   Altering the electron acceptor moiety

As mentioned in Chapter 1, a lot of recent research work has focused on altering

the electron acceptor group - in this case the TCNQ framework.

2.3.1 *Synthesis of 11,11,12,12-tetracyano-9,10-anthraquinodimethane*(TCAQ) [49][10]

Scheme 2.10 :-

1. $TiCl_4$ / $CHCl_3$ / N_2 / Δ

2. C_5H_5N / $CH_2(CN)_2$ / $CHCl_3$

3. 13 hour reflux

[49]
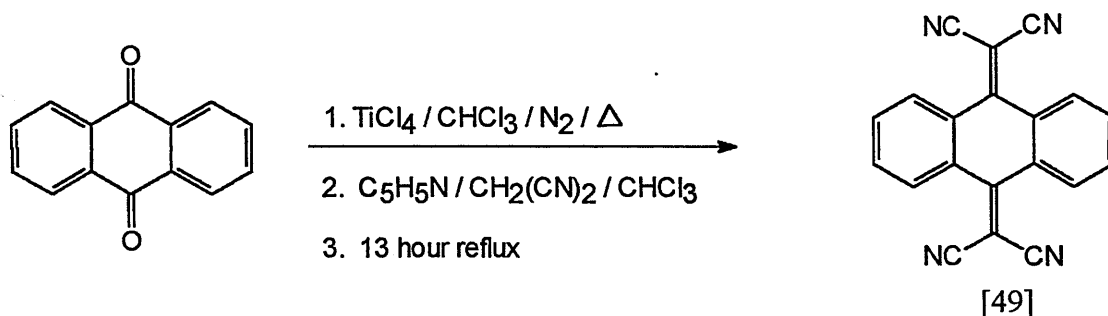
Titanium (iv) chloride (3.8g, 2.2 mls, 0.02 moles) was added via a syringe to a solution

of anthraquinone (2.08g, 0.01 moles) in dry chloroform (200 mls). The light yellow

suspension was refluxed for 1 hour. This suspension was then added to a solution of

malononitrile (13.2g, 12.58 mls, 0.02 moles) and pyridine (31.8g, 32.48 mls, 0.04 moles)

in dry chloroform (150 mls). The black reaction mixture was then refluxed for a further

13 hours. Upon cooling in ice, the suspension was poured into cold water (150 mls) and

further chloroform was added (100 mls). The resultant layers were separated and the

aqueous layer was extracted with chloroform (3 x 50 mls). The organic extracts were

combined and washed with 10% sodium bicarbonate solution (3 x 50 mls), water (3 x 50

mls) and dried over magnesium sulphate. The yellow organic extract was reduced in

volume to approximately 30 mls. A yellow precipitate formed on addition with petroleum

ether which was filtered off under suction and recrystallised from DMSO to yield yellow

metallic crystals (1.2 g, 39 %): Melting point > 360 °C

UV - Vis (DMSO) 344nm, 304nm, 280 nm;

IR (KBr): 2229 cm^{-1} (C≡N), 1581, 1556, 1546 cm^{-1}(C=C);

^{1}H-NMR (DMSO-d$_6$): 7.91-8.36(m, 8H, aromatic-H);

MS: m/z 304 (M$^+$, 100%), 277 (M$^+$, 21% -HCN), 250 (M$^+$, 11% -2HCN);

Analytical data for C$_{20}$H$_8$N$_4$: Theory: C, 78.94; H, 2.65; N, 18.40. Found: C, 78.69; H, 2.60; N, 18.31.

2.3.2 *Synthesis of N-alkyl-4 and -2-methylquinolinium adducts of TCAQ*

Scheme 2.11:-

Using method 2

[50]

Scheme 2.12:-

[51]
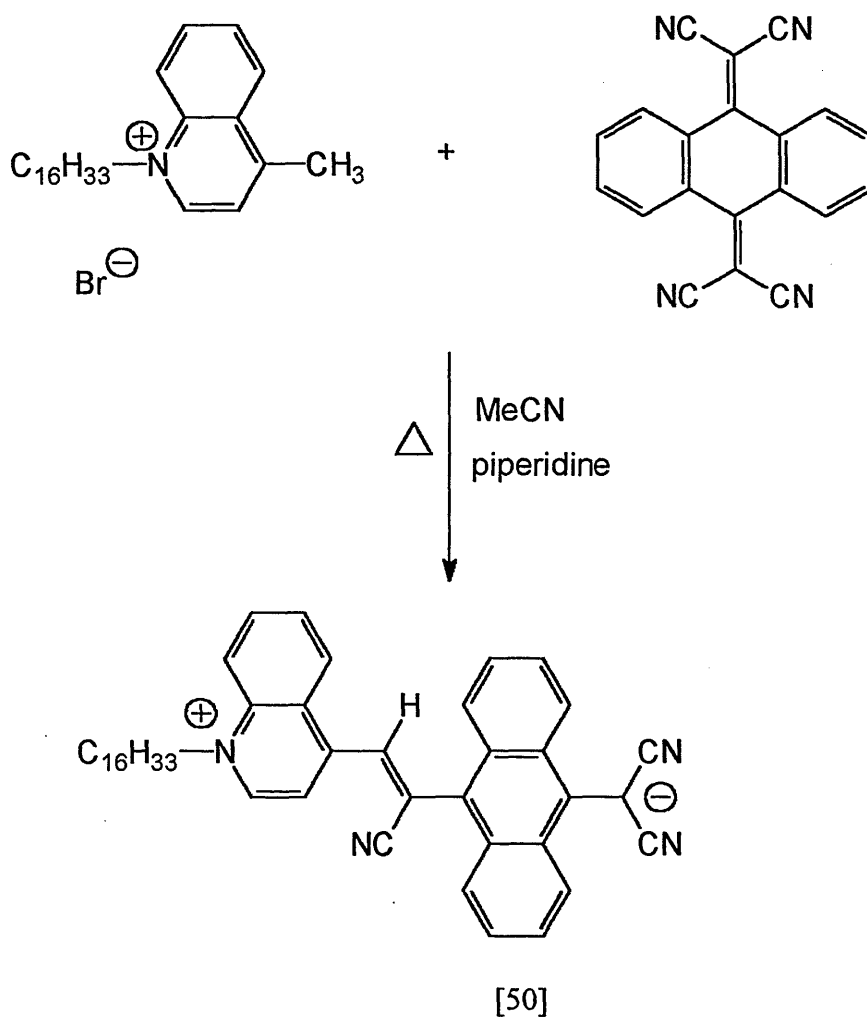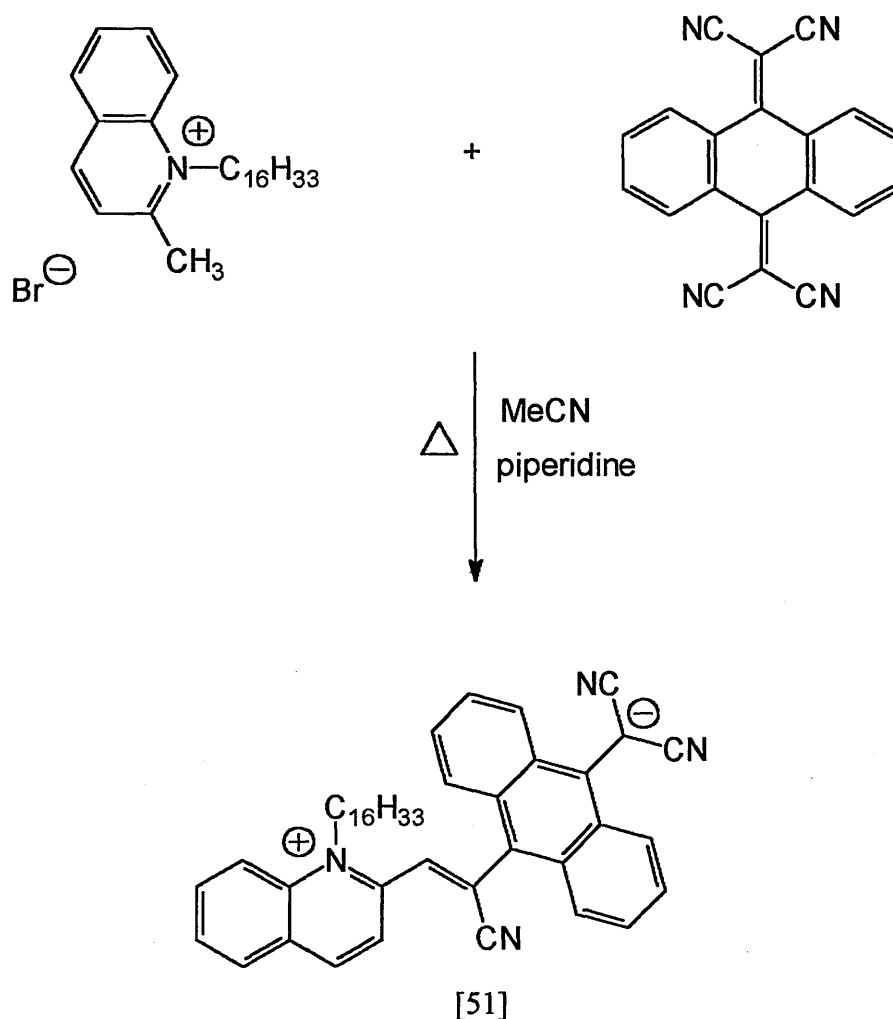
The cation, - N-hexadecyl-4-methylquinolinium bromide or N-hexadecyl-2-methylquinolinium bromide (0.5g, 0.0016 moles) dissolved in acetonitrile (5 mls) was added dropwise over a period of 2 hours to a refluxing solution of TCAQ (0.5g, 0.0016 moles) and piperidine in acetonitrile (20 mls). The reaction progressed until a colour change from yellow to red to black was observed. A black precipitate formed on cooling which was filtered under suction to yield a black microcrystalline solid (typically <10%).

Evidence for a zwitterionic material was not conclusive (see Chapter 3).

2.4   Related synthetic work - N-alkylpyridinium benzimidazolate betaine derivatives *

Further to the study of zwitterionic TCNQ adducts, additional research focused on heterocyclic betaine derivatives in which both positive and negative charges are delocalised within the π-electron system. Amphiphilic derivatives were sought after for possible LB film fabrication.

N-Alkylpyridinium benzimidazolate derivatives of type [52] and [53] were synthesised along with the related betaine-TCNQ charge transfer complexes of the above e.g [54] :-

[52]   [53]

[54]
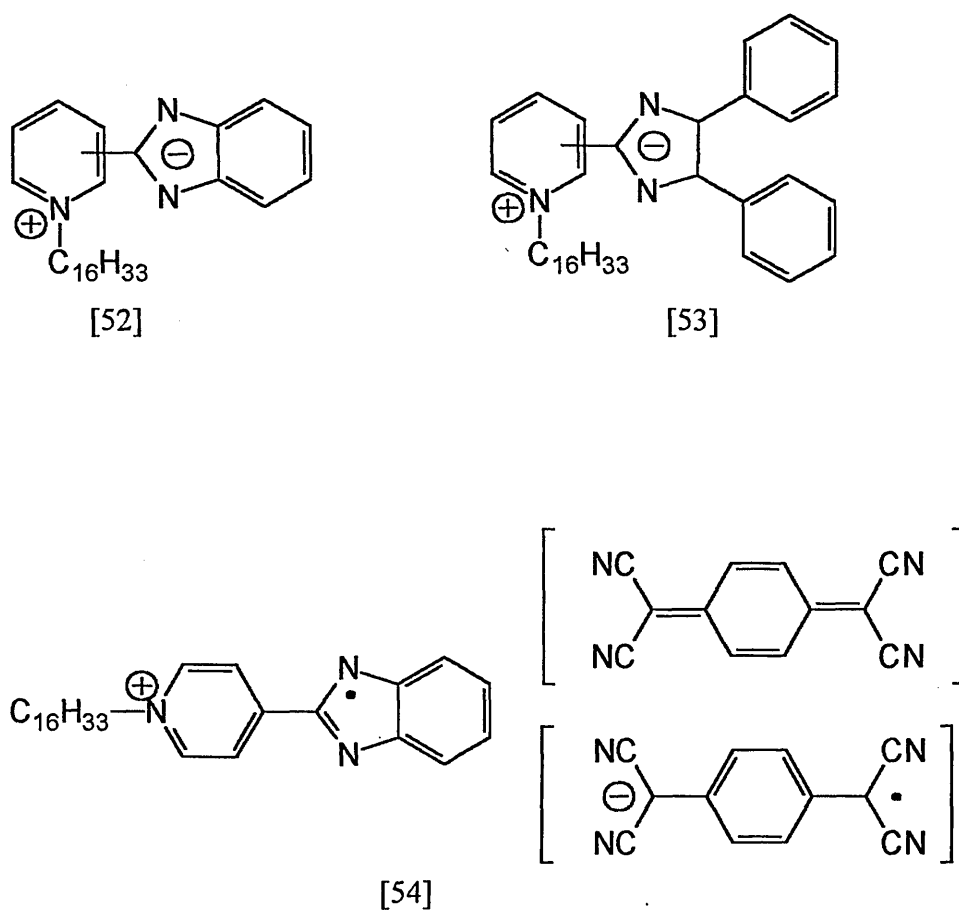
* work carried out in collaboration with Professor D. W. Allen and J. Hawkrigg at SHU

2.4.1 *Synthesis of 2-(1-hexadecylpyridinium-3-yl) benzimidazolate:-*

Scheme 2.15 :-
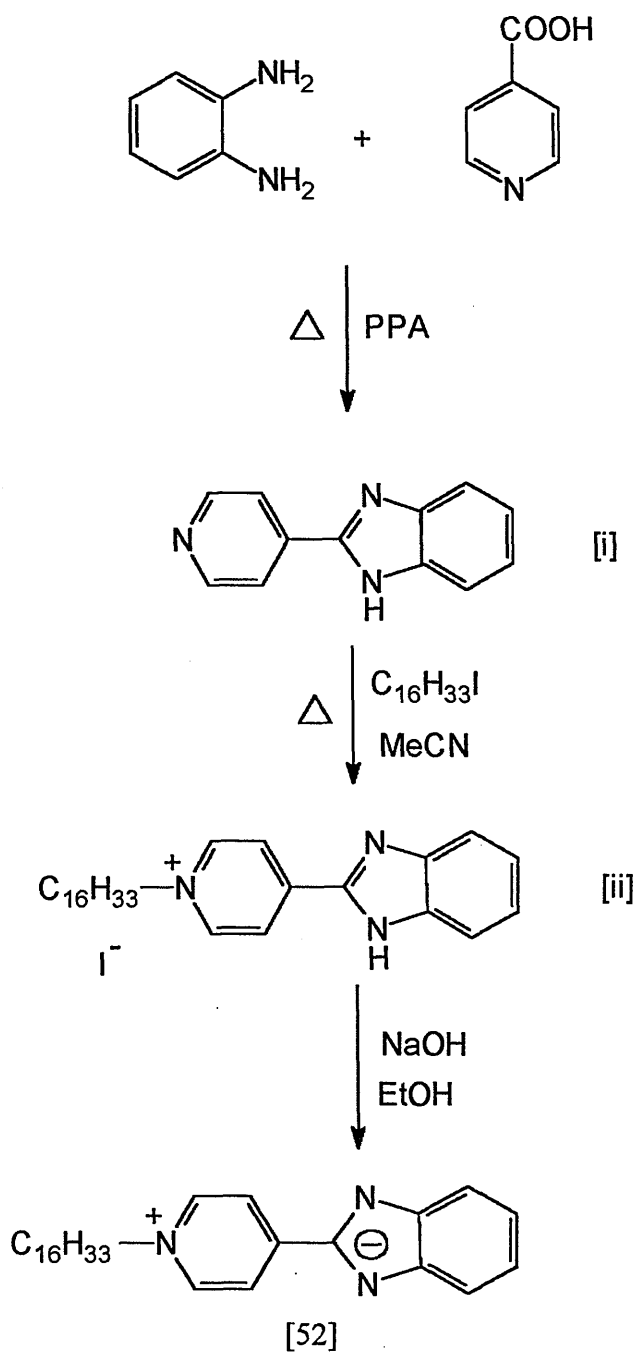
2.4.1.1 *Preparation of 2-(4'-pyridyl)-1H-benzimidazole (i)*

Pyridylbenzimidazole (i) was prepared essentially as described by Alcalde et al[10] via the condensation of pyridine-4-carboxylic acid with 1,2- phenylenediamine in a suspension of polyphosphoric acid and heated in an oil bath at 160 -180°C for 3-4 hours. The reaction mixture was then poured into ice-water to yield a tacky mixture which solidified in the ice. After 12 hours a grey solid was produced which was neutralised with aqueous ammonia, filtered under suction, washed with water and recrystallised from methanol to yield off white platelets.

2.4.1.2 *Preparation 1-hexadecyl-4-(2-benzimidazolyl)pyridinium iodide (ii)*

Pyridylbenzimidazole (i) (1.0g, 0.0051 moles) and 1-iodohexadecane (2.0 g, 0.0057 moles) were refluxed in acetonitrile (30 mls) for 3 hours. On cooling a yellow precipitate formed which was filtered under suction and recrystallised from methanol.

Yield :- 1.2g (43%)- yellow micro needles.

2.4.1.3 *Preparation of 2-(1-hexadecylpyridinium-3-yl) benzimidazolate* [52]

An aqueous solution of sodium hydroxide (2 mls) was added dropwise to a solution of the above salt (ii) (1g, 0.0018 moles) in ethanol. Immediately a yellow solid precipitated out which was filtered under suction and washed repeatedly with aqueous ethanol to give the betaine.

Yield : 850 mgs (86.5 %) - yellow microcrystals. Melting point 261 - 263 °C

[1]H nmr (CD_3OD): δ 9.10 (d, 2H); 8.45 (d, 2H); 7.60 (m, 2H); 7.05 (m, 2H); 4.75 (t, 2H); 2.10(m, 2H); 1.3 (s, 26H); 0.85 (t, 3H).

MS: m/z 420 (M^++ 1, 100%).

2.4.2 *Synthesis of 2-(1-hexadecyl-pyridinium-3-yl)-4,5-diphenyl imidazolate* [53]

Scheme 2.16:-

$$CH_3COONH_4 \quad + \quad$$

Benzil | Glacial Acetic acid $\triangle$

[i]

$\triangle$ | $C_{16}H_{33}I$
MeCN

[ii]

I^-

$C_{16}H_{33}$

NaOH
EtoH

$C_{16}H_{33}$

[53]
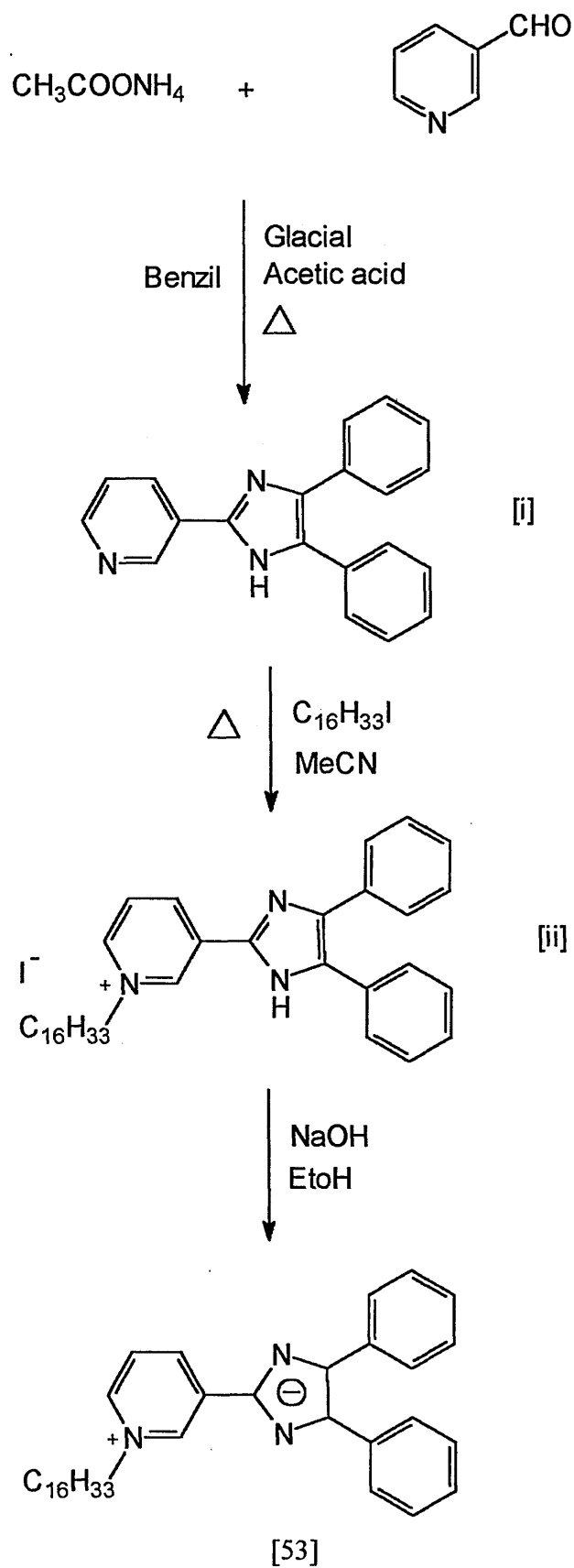
2.4.2.1 Preparation of 2-(3-pyridyl)-4,5-diphenyl imidazole (i).

3-Pyridinecarboxaldehyde and benzil were refluxed in the presence of ammonium acetate, using glacial acetic acid as the solvent. After a 6 hour reflux the reaction mixture was poured into ice-water and neutralised with aqueous ammonia to yield a yellow solid.

2.4.2.2 Preparation of 2-(1-hexadecylpyridinium-3-yl)-4,5-diphenyl imidazole bromide (ii).

Pyridyldiphenyl imidazole (i) (0.5g, 0.0017 moles) and 1-iodohexadecane (0.7g, 0.0020 moles) were refluxed in acetonitrile (30 mls) for 3 hours. The reaction mixture was then cooled for 12 hours during which time a deep yellow precipitate formed which was filtered under suction and recrystallised from methanol.

Yield:- 530 mgs (48%), yellow platelets.

2.4.2.3 Preparation of 2-(1-hexadecyl-pyridinium-3-yl)-4,5-diphenylimidazolate [53]

An aqueous solution of sodium hydroxide (3mls, 0.1mole) was added dropwise to a solution of the above salt (ii) (0.19g, 0.00029 moles) in ethanol (15 mls). Cold water (100 mls) was added to the reaction mixture producing a light orange oily solution. On cooling in ice for 2 hours an orange precipitate formed which was filtered under suction and washed with ethanol to give the betaine.

Yield:110 mgs (73 %), dark orange platelets. Melting point 278-282 °C

[1]H nmr (CDCl$_3$) δ 9.30 (s, 1H); 8.90 (d, 1H); 7.75 (d, 4H); 7.6 (d, 1H); 7.40 (m, 6H); 7.35 (d, 1H); 4.10 (t, 2H); 1.90 (m, 2H); 1.40 (s, 26H); 1.00 (t, 3H).

MS: m/z 522 (M$^+$+ 1, 100%)

2.4.3 *Preparation of N-alkylpyridinium betaine-TCNQ charge transfer complexes*

Scheme 2.17:-
(assuming a 1:1 TCNQ:betaine ratio)

[54]
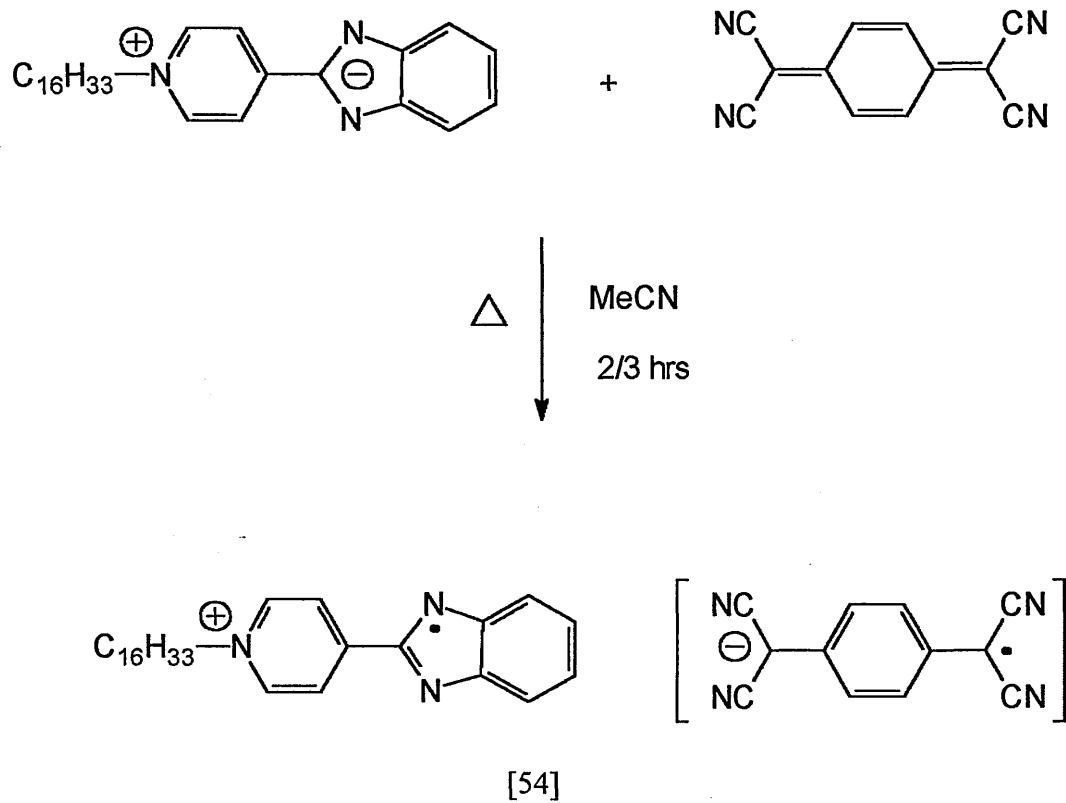
Scheme 2.18:-
(assuming a 2:1 TCNQ: betaine ratio)

[55]
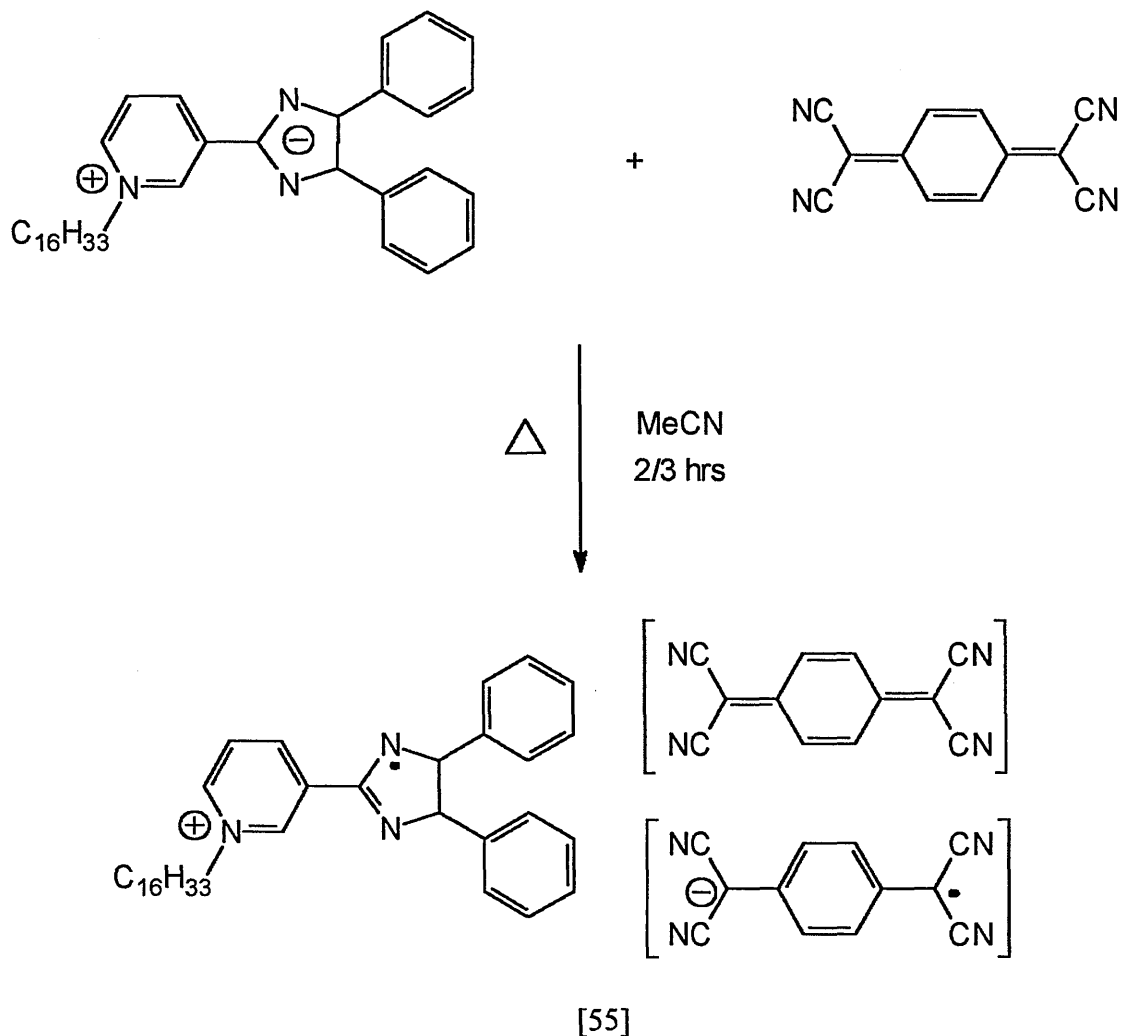
The adducts were prepared by refluxing together the betaines [52] or [53] with TCNQ in equimolar quantities for 2-3 hours in acetonitrile. After cooling for 12 hours the dark solution yielded on addition of petroleum ether, the product which was filtered off under suction.

2-(1-Hexadecylpyridinium-3-yl) benzimidazolate - TCNQ adduct [54]

Yield:- 70 %, black microcrystalline solid.

Analytical data for $C_{42}H_{45}N_7$(1:1 betaine:TCNQ ratio) Theory: C, 77.01 %; H, 7.27 %; N, 15.72 %. $C_{42}H_{45}N_7$.MeCN(1:1 betaine:TCNQ ratio) Theory: C, 75.90 %; H,

7.23 %; N, 16.87 %. $C_{54}H_{49}N_{11}$.MeCN(1:2 betaine:TCNQ ratio) Theory: C, 75.31 %;

H, 5.87 %; N, 18.82%. Found: C, 75.10 %; H, 6.71 %; N, 16.57 %. IR(cm^{-1}): 2190,

2170 (radical anionic C≡N stretching frequencies)

2-(1-hexadecylpyridinium-3-yl)-4,5-diphenyl imidazolate - TCNQ adduct [55]

Yield:- 75%, dark blue metallic microcrystalline solid.

Analytical data for $C_{48}H_{51}N_7$ (1:1 betaine:TCNQ ratio) Theory: C, 76.67 %; H, 6.02

%; N, 13.51. $C_{48}H_{51}N_7$.MeCN (1:1 betaine:TCNQ ratio) Theory: C, 78.30 %, H, 7.10

%, N, 14.51 %. $C_{50}H_{55}N_{11}$. MeCN (1:2 betaine:TCNQ ratio) Theory: C, 76.67 %, H,

6.02 %, N, 17.31 %. Found: C, 77.80 %; H, 7.08 %, N, 14.90%.

IR (cm^{-1}): 2190, 2170 (radical anionic C≡N stretching frequencies).

2.5   Chapter Two References

1.   R. M. Metzger, N. E. Heimer and G. J. Ashwell, *Molecular Crystals Liquid Crystals*, **107**, 133, 1984.

2.   N. A. Bell, R. A. Broughton, J. S. Brooks, T. A. Jones, S. C. Thorpe and G. J. Ashwell, *J. Chem. Soc. , Chem. Commun. ,* **325**, 1990.

3.   G. J. Ashwell, *Thin Solid Films,* **186**, 155, 1990.

4.   G. J. Ashwell, E. J. C. Dawnay, A. P. Kuczynski, M. Szablewski, I. M. Sandy, M. R. Bryce, A. M. Grainger and M. Hasan, *J. Chem. Soc. , Faraday Trans. ,* **86**, 1117, 1990.

5.   G. J. Ashwell, G. Jefferies, E. J. C. Dawnay, A. P. Kuczynski, D. E. J. Lynch, Y. Gongda and D. G. Bucknall, *J. Mater. Chem. ,* **5**, 975, 1995.

6.   G. J. Ashwell, E. J. C. Dawnay and A. P. Kuczynski, *J. Chem. Soc. , Chem. Commun. ,* **1355**, 1990.

7.   N. A. Bell, R. A. Broughton, J. S. Brooks, T. A. Brooks and S. C. Thorpe. *Int. J. Electronics,* **76**, 751, 1994.

8.   N. Menschutkin, *Z.Phys. Chem. ,* **6**, 41, 1890.

9.   M. Szablewski, PhD Thesis. Cranfield Institute of Technology. 1992.

10.   E. Alcalde, *Adv. Heterocycl. Chem. ,* **60**, 197, 1994 and refs. therein.

CHAPTER 3

Synthetic Work - Results and Discussion

3.1 Zwitterionic TCNQ adducts

3.1.1 Synthesis and mechanisms

The synthesis of R(4) and R(2) picolinum and quinolinium TCNQ adducts provided the main body of materials required for this study. In theory the preparation of these compounds should be relatively straightforward with the synthesis of R(4)Q3CNQ and R(4)P3CNQ systems being well documented.[1-7]However, in general the synthetic procedures encountered in the literature were found to be inconsistent and unreliable in terms of reproducibility.

The synthesis of these zwitterions followed a two stage process, beginning with the cation formation and then reaction with TCNQ or LiTCNQ to produce the adduct.

The preparation of the N-alkylated 4- and 2-methylquinolinium/picolinium bromide salts were essentially N-alkylation reactions involving the Menschutkin[8] reaction where the bromine atom of the alkyl halide is displaced by the nucleophilic atom of the quinoline ring system (Figure 3.01). The production of γ and α - substituted cations followed a similar mechanism:-
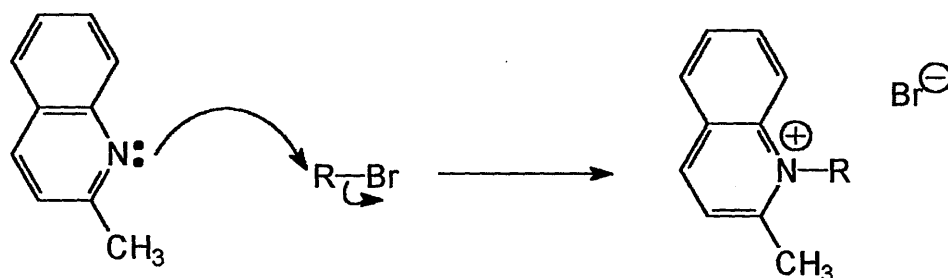
Figure 3.01 N-alkylation mechanism

An analogous series of N-alkylated cations was prepared where the R group varied from C_4H_9 to $C_{20}H_{41}$ and also benzyl to create a series of amphiphilic materials for subsequent LB film fabrication.

Reaction times and yields for these simple cations varied dramatically depending on substitution and chain length. With regards to the γ-cations, reaction times were relatively short (4-6 hours), increasing to 12 hours for the $C_{20}H_{41}$ analogue, with yields between 60-90%. However, due to increased steric hindrance (Figure 3.02), reaction times for the α-cations increased massively with increasing chain length e.g 50 hours for C_6H_{13} rising to 200+ hours for the $C_{20}H_{41}$ analogue:-
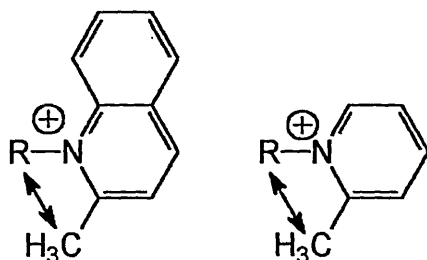
Figure 3.02 Steric crowding in quinolinium and picolinium cations.

Another consequence of steric crowding was a loss in yield (less than 30% for the α-$C_{16}H_{33}$ quinolinium cation) in comparison to the corresponding γ-derivatives (76 % for γ-$C_{16}H_{33}$ quinolinium cation).

Preparations of α-cations from quinaldine and 2-picoline worked best with excess nucleophile and, especially for long chain alkyl halides, concentrated solutions in acetonitrile.

The quinolinium/picolinium cations possess an acidic proton on the methyl group which is readily removed by an appropriate base to form an apparent carbanion that is in fact a vinyl amine. The well documented method[1,3-5] of using piperidine as a base was originally tried to obtain analogues of R(4)Q3CNQ. Here the piperidine removes the acidic methyl proton from the cation to form a vinyl amine which is resonance stabilised and can be represented by two resonance forms (Figure 3.03), a zwitterion and the other form where a lone pair of electrons is situated on the electron deficient nitrogen which is an enamine:-
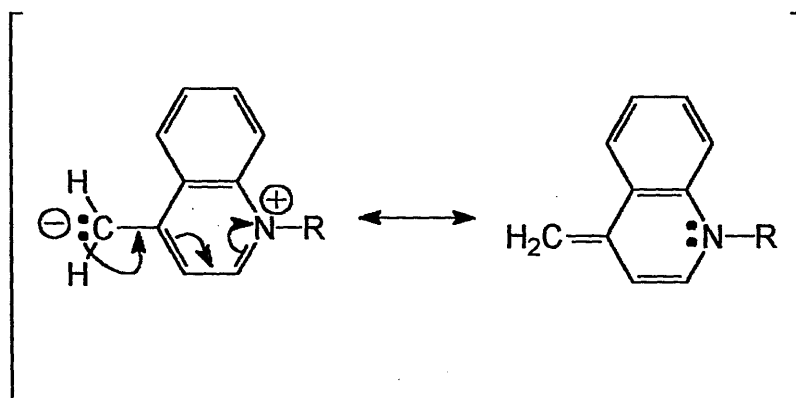
Figure 3.03 Possible resonance of zwitterion/enamine forms.

If the methyl group is β (or in the 3 position) to the hetero atom, no proton removal would be possible as resonance stabilisation would not exist (i.e the enamine could not form). This methyl proton abstraction results in an extremely reactive homo-aromatic

base which is highly nucleophilic via the exocyclic carbon. The use of a polar aprotic

solvent such as acetonitrile rather than a polar protic solvent such as methanol reduces

any hydrogen bonding to the carbanionic resonance structure, thus aiding the progression

of the reaction. The addition of TCNQ results in the reaction which is believed to occur

via one of two mechanisms (Figures 3.04 and 3.05). The addition reaction which results

in the creation of the zwitterion is very similar to a cyanoethylation reaction[9] which is a

variant of the Michael addition reaction,[10] in which a carbanion typically reacts with an

α, β-unsaturated carbonyl system.
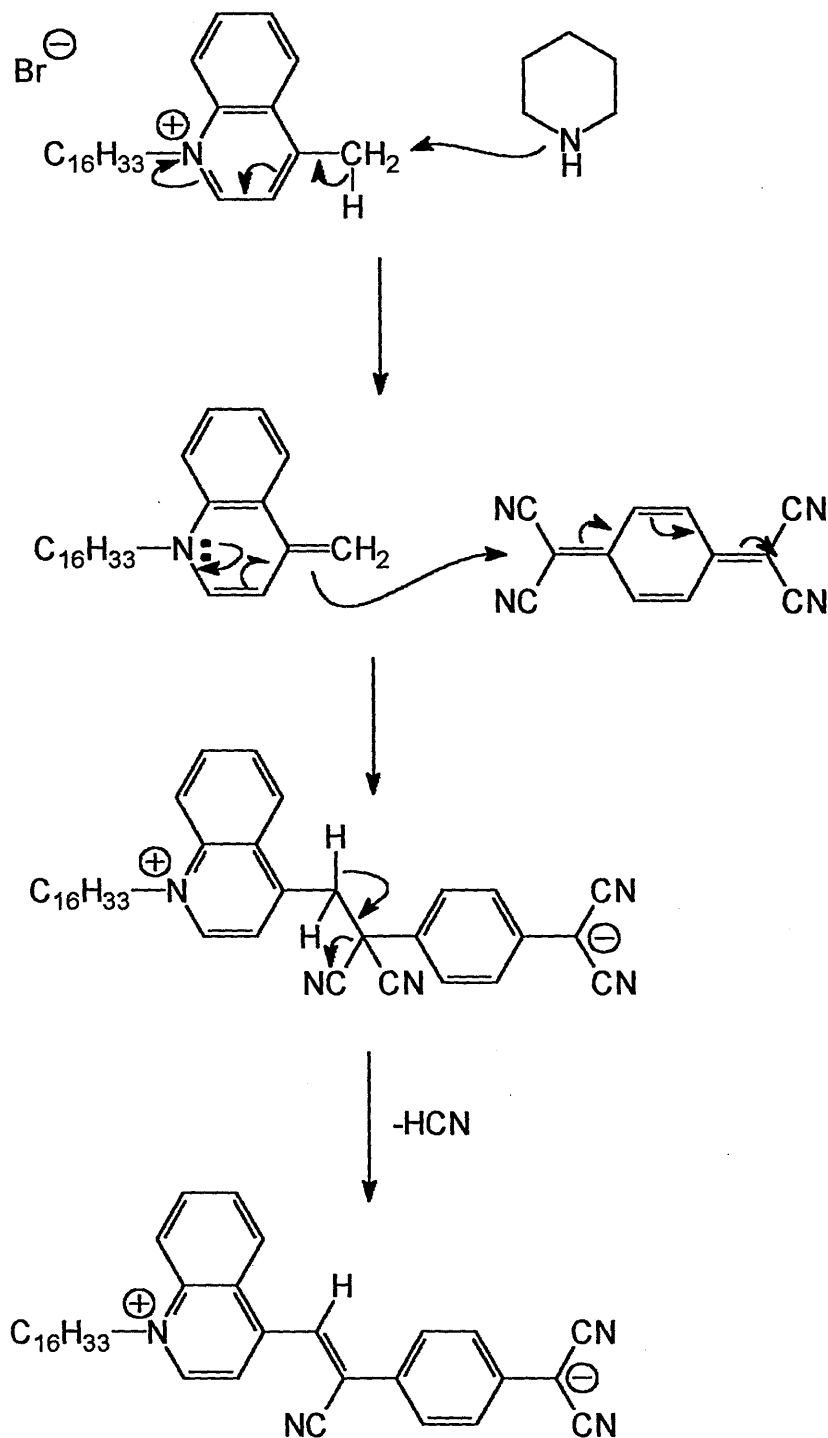
Figure 3.04 Mechanism 1 involving piperidine as base

In Figure 3.04 the piperidine[11] removes the acidic proton from the methyl group of the cation forming the highly reactive enamine (the Michael donor). This then attacks the TCNQ molecule (the Michael acceptor) which is acting as a conjugated nitrile. Spontaneous loss of HCN from the adduct produces the fully conjugated zwitterion.
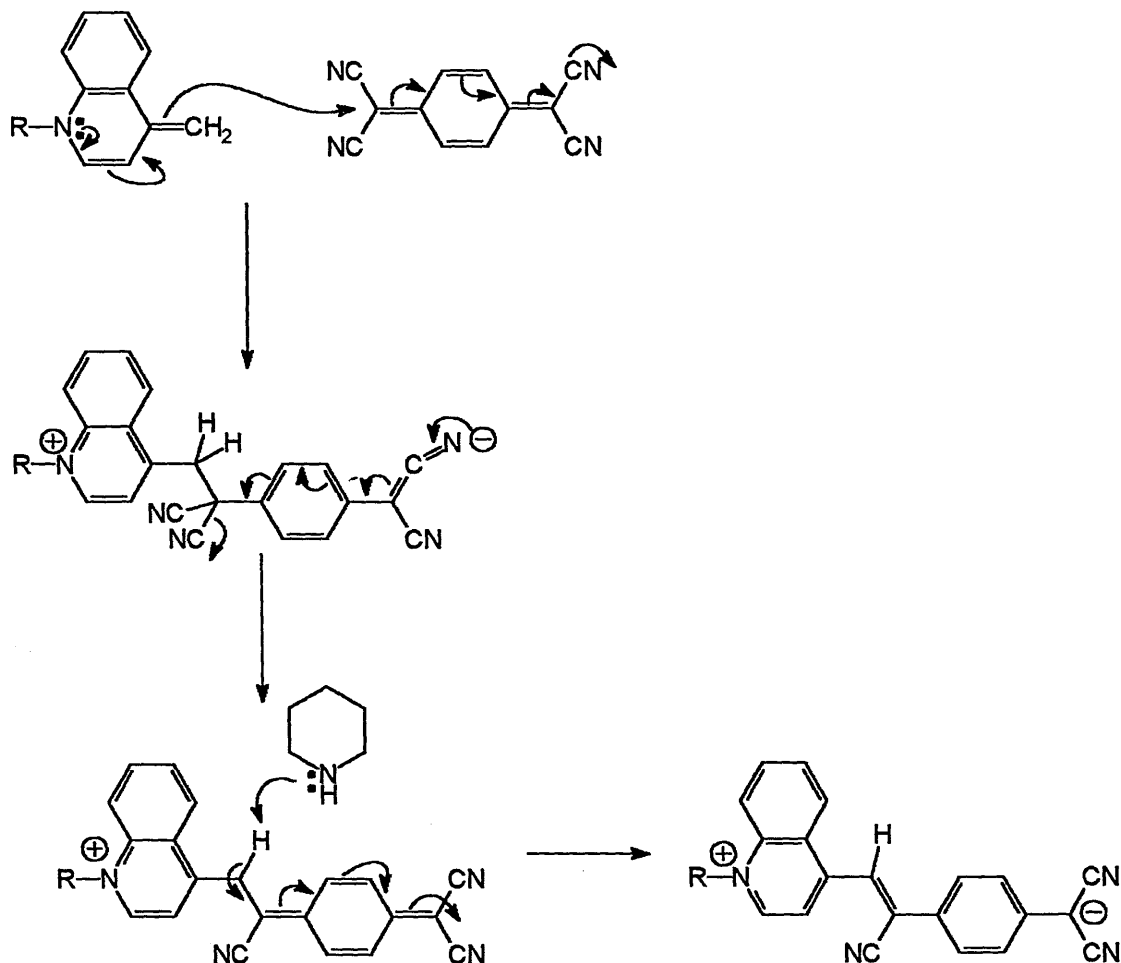
Figure 3.05 Mechanism 2 using piperidine as base

The other mechanism (Figure 3.05)[12] which has been suggested by a number of workers in this field shows a second molecule of piperidine removing a further proton from the D-π-A framework to produce the zwitterion. However this mechanism is probably flawed as the piperidine in this Michael type addition reaction is acting more like a catalyst rather than a stoichiometric base and thus a second mole of base would be unnecessary. This would explain why only very small amounts of piperidine or N-methyl piperidine are needed for these reactions and the driving force behind this reaction is the formation of a new carbon - carbon bond and the conversion of the quinoid structure of the TCNQ moiety to a predominantly benzenoid one.

The piperidine method however was effectively flawed in this study for three main reasons:-

1. None of the alpha substituted derivatives R(2)Q3CNQ and R(2)P3CNQ required for this study were produced by this method.

2. The use of piperidine as base led to problems regarding competitive addition reactions between piperidine and TCNQ resulting in impurities in the final product which affected LB film studies.

3. This method was generally unreliable in terms of reproducibility.

It was therefore clear from the above problems that this method was unsuitable for this study. This is perhaps not surprising as piperidine is a secondary amine, and it was clear from early work that TCNQ can react with secondary amines (see Chapter 1) this caused an obvious problem. Substitution reactions of TCNQ with primary or secondary amines yield products in which one or two of the cyano groups are replaced. The amine group would add to the TCNQ through the nitrogen in the manner of a 1, 6- addition yielding a product which eliminates HCN resulting in a mono- or a bisamino substitution product.

Originally Broughton[12] used a minimal amount of piperidine (2-3 drops with 0.001 moles of reactants) which would minimise the chance of side reactions with TCNQ but this typically kept yields low [30% for the $C_{16}H_{33}(4)Q3CNQ$ adduct] and, as mentioned above, only a small amount of base is necessary to catalyse the reaction. Reactions times were also minimal with this method - not more than 15 hours for the $C_{20}H_{41}(4)Q3CNQ$ adduct. Ashwell et al[5] and Szablewski[13] used the tertiary amine, N-methyl piperidine, in an attempt to reduce these competitive side reactions and obtained yields of 40 % for the

an attempt to reduce these competitive side reactions and obtained yields of 40 % for the

$C_{16}H_{33}(4)Q3CNQ$ adduct. Typically reaction times increased using this base to

approximately 35 hours for the $C_{16}H_{33}(4)Q3CNQ$ derivative. Tertiary amines are not

expected to react with TCNQ as they are sterically hindered and possess no amino

hydrogen which could be abstracted from a reaction intermediate. However it has since

been shown that the tertiary amine - triethylamine (TEA) does react with TCNQ in

chloroform to produce the related zwitterion.[14]

Piperidine was originally used for synthesis of the analogous series of R(4)Q3CNQ and

R(4)P3CNQ. However this general method was abandoned when it became impossible

to produce enough material of sufficient purity for LB studies and also because of its

repeated failure to yield alpha substituted zwitterions. The vastly increased steric

hindrance of the alpha substituted systems must have contributed to this fact.

The original method of using LiTCNQ with the quaternary salts, which historically was

first used to synthesise $CH_3(2)PQ3CNQ^2$ was evaluated and found to provide a

relatively simple and reproducible method which crucially yielded the alpha analogous

series that the piperidine method had failed to. However, its inefficiency was evident

from the fact that reaction times could approach weeks in the case of the sterically

hindered long chain alpha substituted adducts, e.g. 2 weeks for $C_{16}H_{33}(2)Q3CNQ$, and

have been reported to approach several months for related materials.[12]

The first step of the mechanism (Figure. 3.06) using LiTCNQ proceeds via removal of

the acidic methyl proton, in this case by the $TCNQ^-$ anion, probably resulting in the

production of neutral TCNQ and $TCNQH_2$ or $TCNQH^-$ to form the highly reactive

homo-aromatic base. $TCNQH_2$ and TCNQH are examples of products/intermediates of

1,6-addition reactions which are typical of reactions of TCNQ and can be compared with

nucleophilic addition to a carbon-carbon double bond.
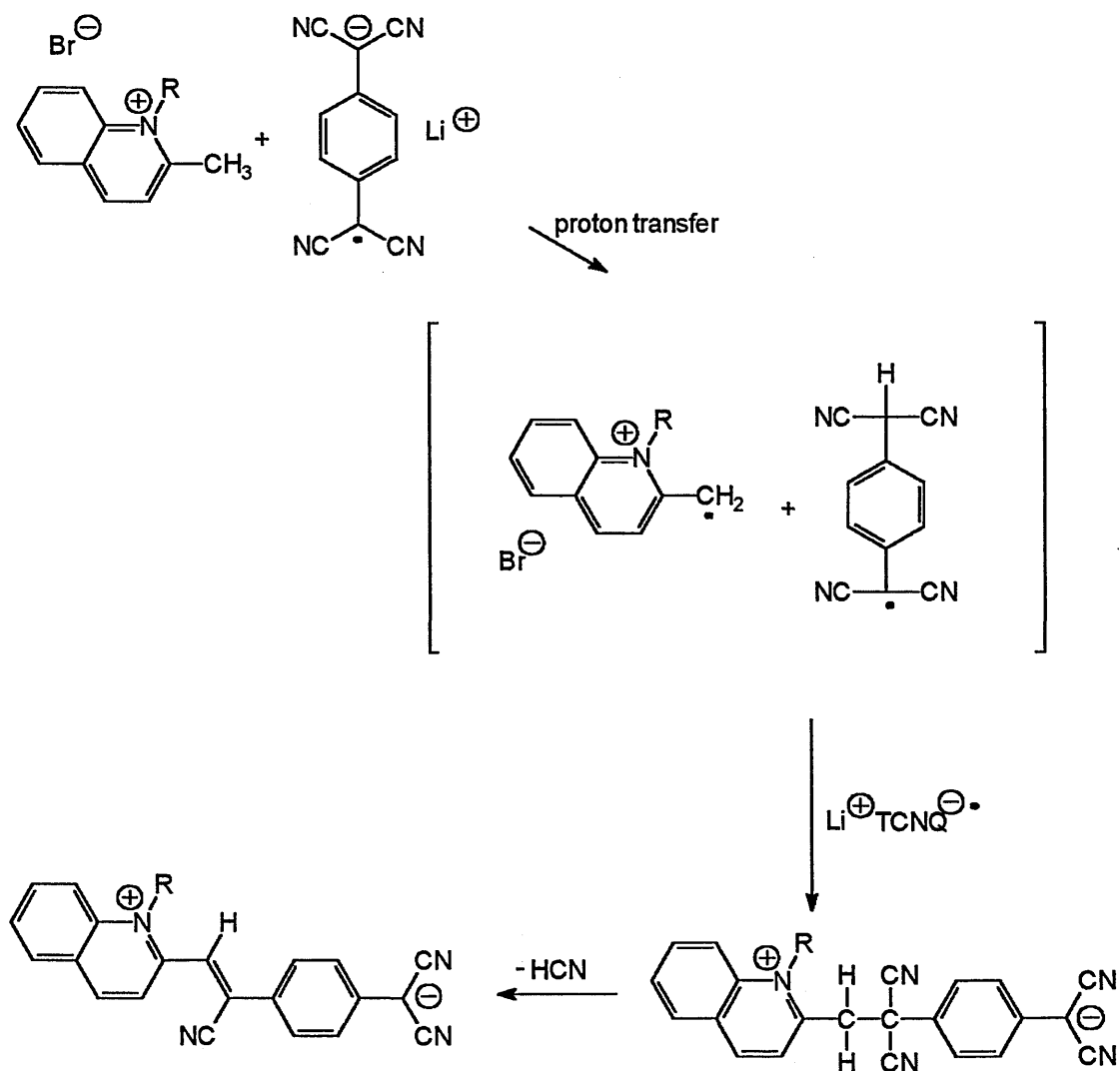
Figure 3.06 Mechanism 3 using LiTCNQ

The carbanion is then believed to attack TCNQ or free LiTCNQ in the same manner as in mechanism 1 (Figure. 3.04) followed by spontaneous loss of HCN to produce the zwitterion. The reactions with LiTCNQ were only successful in small quantities of acetonitrile where starting material concentration was high. An analogous series of alpha substituted adducts was produced using this method but with yields that were typically low, as expected for the long chain derivatives e.g. <10% for $C_{16}H_{33}(2)Q3CNQ$. As minute quantities of pure material were required for subsequent L.B film work (typically 0.01mg - 0.1 mg per experiment), it was only necessary to produce enough material for

this and for their characterisation; thus further optimisation of this method was deemed unnecessary at this point.

Metzger et al[15] have reported a further method for the synthesis of the gamma quinolinium/picolinium adducts which is a variant of the original LiTCNQ synthesis. Here N-hexadecyl-4-methylquinolinium tosylate and LiTCNQ are refluxed in dry dimethylsulphoxide in the presence of pyridine to produce the adduct. The mechanism of this reaction is believed to occur via an electron transfer process (Fig. 3.07). The quinolinium cation loses H• to LiTCNQ, being converted to the radical cation salt, which then couples with free LiTCNQ to give an intermediate that spontaneously loses HCN to produce the product. Reaction times using this procedure have been reduced to approximately 20 hours, with a yield of 60% for the $C_{16}H_{33}(4)Q3CNQ$ analogue. LiTCNQ was used in a 2:1 excess and it would appear that 1 mole was being used up as the base. However, as reported in this thesis, such an excess of LiTCNQ was not required and in the first instance the LiTCNQ could be acting as a catalyst for the reaction. This is analogous to the role of piperidine in Michael type addition reactions. This idea of electron/proton transfer may explain mechanisms 3 and 4 (Figures. 3.06 and 3.07) with LiTCNQ and has previously been suggested for 1,6 addition reactions of TCNQ.[16] (Figure 3.08)
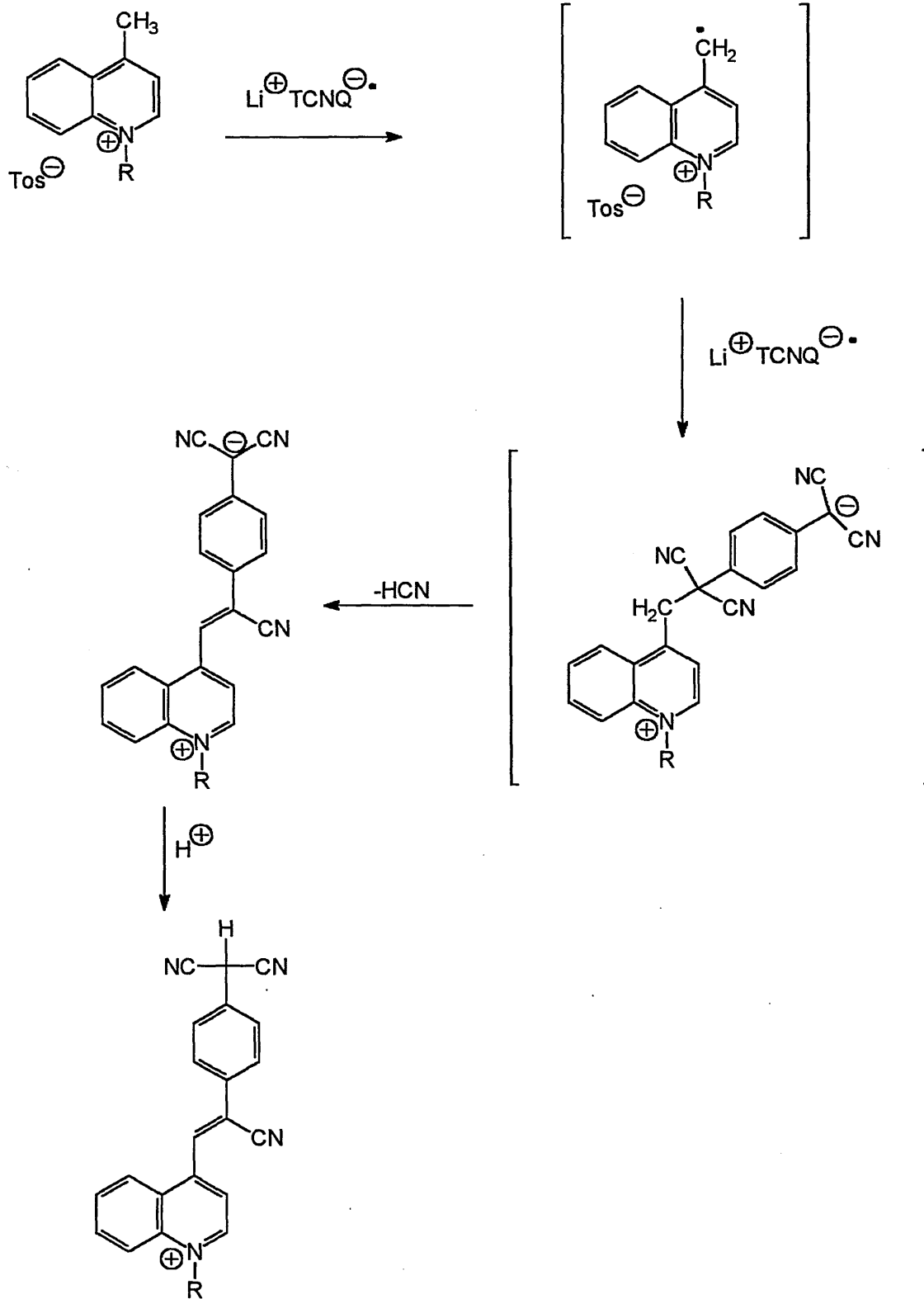
Figure 3.07 Mechanism 4 using LiTCNQ [15]
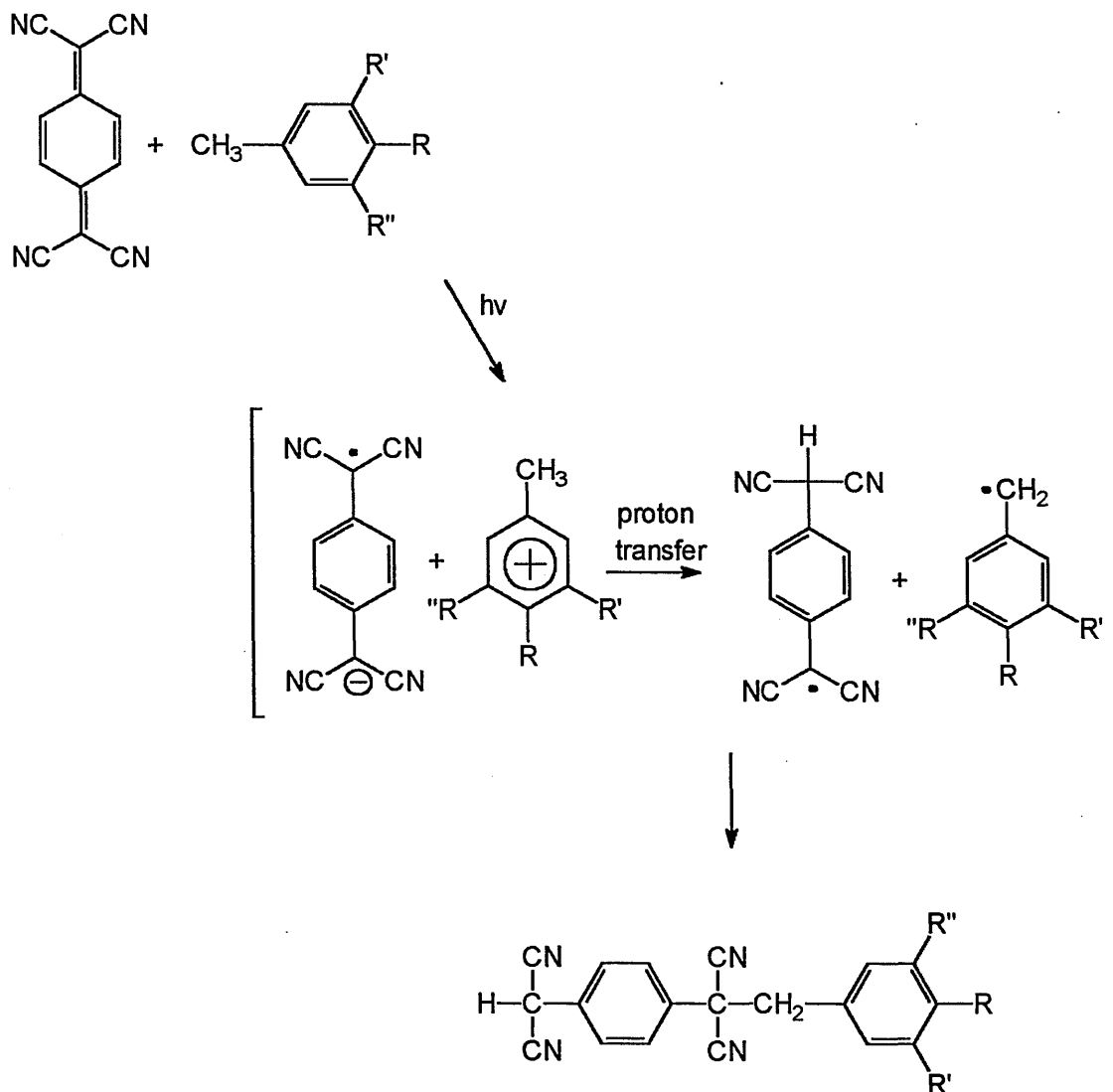
Figure 3.08 A suggested mechanistic route for a TCNQ addition reaction[16]

3.1.2 Reaction Progression

The progress of the reactions could in all cases be monitored using ultra violet/visible

spectroscopy.(Figure 3.09) Initially the uv/vis spectra show sharp bands characteristic of

the TCNQ⁻ radical anion at ca 420nm and 720 - 840 nm and the reaction mixture is

typically green in colour. These TCNQ⁻ bands gradually reduce during the reaction and a

very characteristic broad charge transfer band appears between 400 and 900 nm. A deep

blue colouration develops in all the solutions once this charge transfer band begins to appear. The reaction can be deemed to be nearing completion once a gold film is seen on the surface of the reaction mixture as this is some of the product precipitating out.

3.1.3 Characterisation

The quinolinium/picolinium and the related zwitterionic adducts could all be identified by three distinct characteristics: First, a distinct broad intramolecular charge transfer band in the solution UV/vis spectra; second, two environments for the $C \equiv N$ stretching in the infrared spectra and third, the lustrous metallic appearance of the crystals/micro-needles in the solid state. The structure of these materials was also unequivocally proven by a solid state crystal structure, supported by diagnostic mass spectrometry and ^{1}H nmr data.

3.1.3.1 Ultraviolet/visible Spectroscopy

In solution the charge transfer spectrum is dominated by an intense broad transition between 400 and 900 nm and also two lesser transitions at ca 300 and 400 nm. This broad transition is attributed to an intramolecular process from the negatively charged dicyanomethanide group to the positively charged donating moiety, rather than an intermolecular one. This process has been substantiated by a linear relationship being observed for plots of absorbance against concentration in accordance with Beer's law. For an intermolecular process this would not be the case as the interaction between chromophores would cause a significant deviation from Beer's law.

This intramolecular process is independent of chain length as the active component of the material is the same in every case. However substitution of electron withdrawing components (e.g fluorine), into the alkyl chain lowers the electron donating effect of the
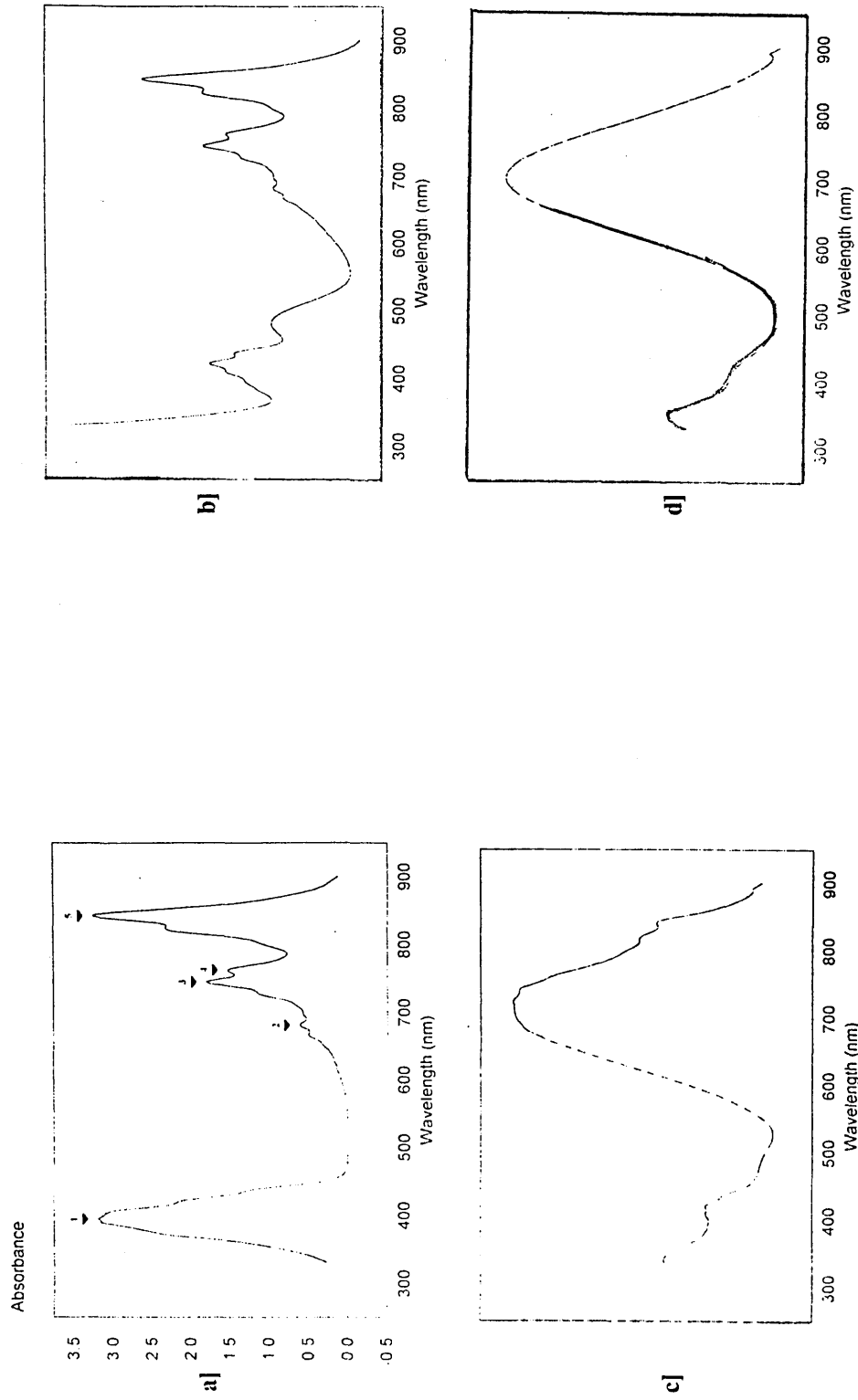
Figure 3.09 UV/vis spectra of $C_{16}H_{33}(2)Q3CNQ$ with LiTCNQ. (a) LiTCNQ; (b) Reactants after 1 day reflux; (c) 10 days reflux and (d) purified product after 14 days reflux. Note disappearance of LiTCNQ bands at 400 nm and between 700–900 nm with increasing reflux time.

donor causing a shift in λ_{max} to a longer wavelength (lower energy), e.g. the molecule $C_{10}F_{17}H_4(4)P3CNQ$ has a λ_{max} of 672 nm in MeCN[12] compared to 638 nm for $C_{10}H_{21}(4)P3CNQ$ Table 3.03). The λ_{max} of the intramolecular charge transfer band does increase marginally for increasing chain length and there is a difference between the α and γ systems (tables 3.01-3.04). The α systems (Figure 3.10) exhibit a decrease in the λ_{max} of the charge transfer band compared to the γ systems and this is more pronounced in the picolinium systems where $C_{16}H_{33}(2)P3CNQ$ has a λ_{max} of 592nm in MeCN compared to 641nm for the corresponding $C_{16}H_{33}(4)P3CNQ$. An increase in the electron donating power of the alpha substituted moieties may be a reason for the higher energy shifts of the charge-transfer band.

Table 3.01 Uv/Vis data for gamma substituted quinolinium TCNQ adducts.

Zwitterion	λ_{max} in MeCN (nm)
$C_4H_9(4)Q3CNQ$	705
$C_5H_{11}(4)Q3CNQ$	706
$C_6H_{13}(4)Q3CNQ$	705
$C_8H_{17}(4)Q3CNQ$	708
$C_{10}H_{21}(4)Q3CNQ$	710
$C_{11}H_{23}(4)Q3CNQ$	710
$C_{13}H_{27}(4)Q3CNQ$	710
$C_{14}H_{29}(4)Q3CNQ$	712
$C_{15}H_{31}(4)Q3CNQ$	712
$C_{16}H_{33}(4)Q3CNQ$	712
$C_{18}H_{37}(4)Q3CNQ$	710
$Bz(4)Q3CNQ$	708

Table 3.02 Uv/Vis data for alpha substituted quinolinium TCNQ adducts.

Zwitterion	λ_{max} in MeCN (nm)
$C_4H_9(2)Q3CNQ$	695
$C_5H_{11}(2)Q3CNQ$	694
$C_6H_{13}(2)Q3CNQ$	698
$C_8H_{17}(2)Q3CNQ$	708
$C_{10}H_{21}(2)Q3CNQ$	698
$C_{11}H_{23}(2)Q3CNQ$	698
$C_{13}H_{27}(2)Q3CNQ$	699
$C_{14}H_{29}(2)Q3CNQ$	697
$C_{15}H_{31}(2)Q3CNQ$	698
$C_{16}H_{33}(2)Q3CNQ$	698
$C_{18}H_{37}(2)Q3CNQ$	700
$C_{20}H_{41}(2)Q3CNQ$	700
Bz(2)Q3CNQ	696

Table 3.03 Uv/Vis data for gamma substituted picolinium TCNQ adducts.

Zwitterion	λ_{max} in MeCN (nm)
$C_4H_9(4)P3CNQ$	638
$C_5H_{11}(4)P3CNQ$	638
$C_6H_{13}(4)P3CNQ$	638
$C_8H_{17}(4)P3CNQ$	642
$C_{10}H_{21}(4)P3CNQ$	638
$C_{11}H_{23}(4)P3CNQ$	638
$C_{13}H_{27}(4)P3CNQ$	640
$C_{14}H_{29}(4)P3CNQ$	640
$C_{15}H_{31}(4)P3CNQ$	640
$C_{16}H_{33}(4)P3CNQ$	641
$C_{18}H_{37}(4)P3CNQ$	644
Bz(4)P3CNQ	641

Table 3.04 Uv/Vis data for alpha substituted picolinium TCNQ adducts.

Zwitterion	λ_{max} in MeCN (nm)
$C_4H_9(2)P3CNQ$	590
$C_5H_{11}(2)P3CNQ$	590
$C_6H_{13}(2)P3CNQ$	588
$C_8H_{17}(2)P3CNQ$	588
$C_{10}H_{21}(2)P3CNQ$	590
$C_{11}H_{23}(2)P3CNQ$	591
$C_{13}H_{27}(2)P3CNQ$	592
$C_{14}H_{29}(2)P3CNQ$	592
$C_{15}H_{31}(2)P3CNQ$	592
$C_{16}H_{33}(2)P3CNQ$	592
$C_{18}H_{37}(2)P3CNQ$	594
Bz(2)P3CNQ	597

Table 3.05 Uv/Vis data for related zwitterionic TCNQ adducts.

Zwitterion	λmax in MeCN (nm)
$C_{16}H_{33}(2)PRD3CNQ$	480
$C_{16}H_{33}(2)PRZ3CNQ$	502
$C_3H_7(2)BT3CNQ$	738
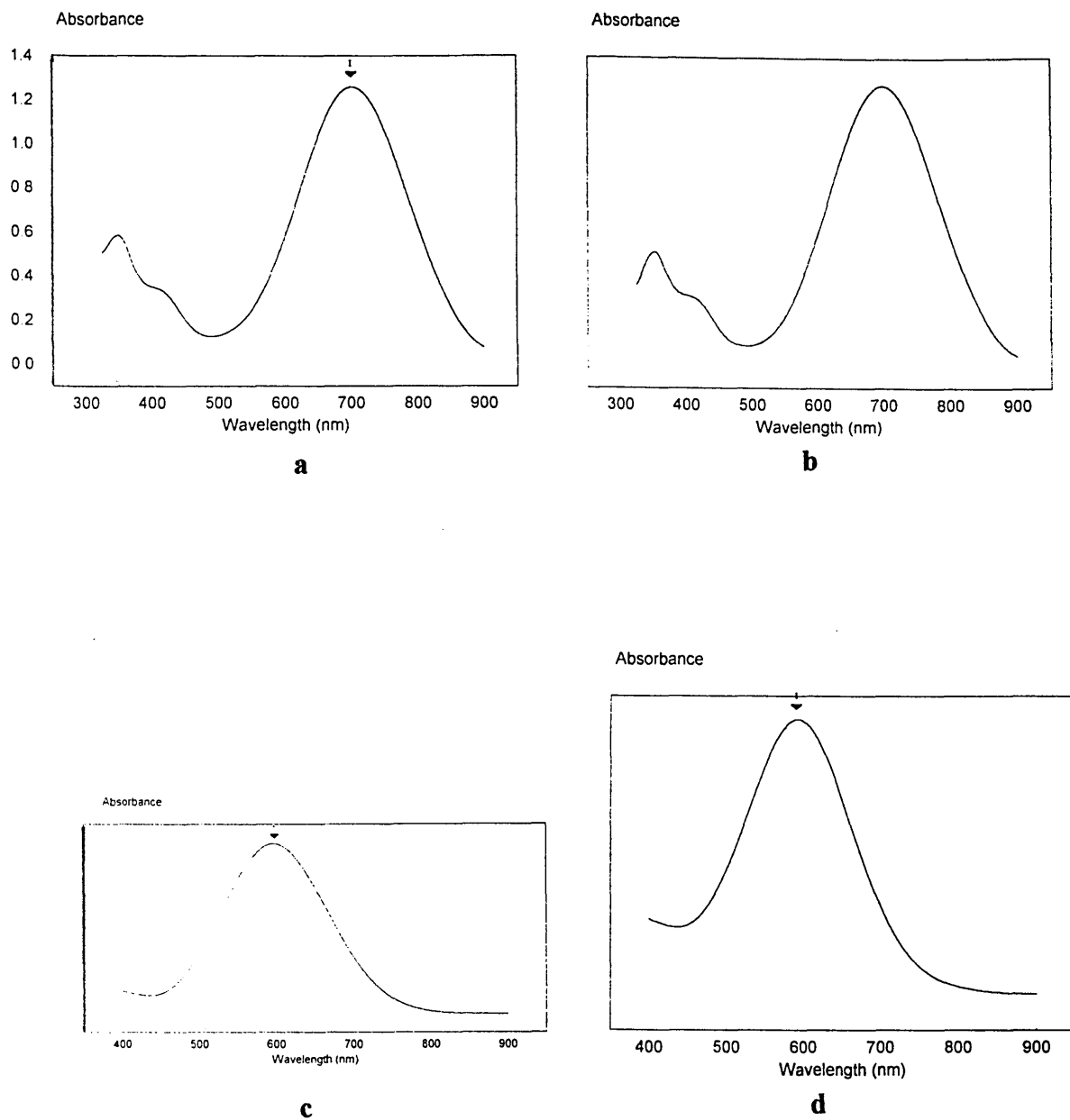
Figure 3.10 UV/Vis Spectra of charge transfer bands for selected alpha substituted TCNQ adducts in acetonitrile: a] $C_{18}H_{37}(2)Q3CNQ$ b] $C_{10}H_{21}(2)Q3CNQ$ c] $C_{18}H_{37}(2)P3CNQ$ d] $C_{15}H_{31}(2)P3CNQ$.

3.1.3.2 Solvatochromism, photochromism and pH effects

The picolinium and quinolinium adducts studied here exhibit solvatochromism: that is the values of λ_{max} are solvent dependent. In solution the zwitterions will interact with the solvent in different ways; such solute-solvent interactions can be due to a number of factors:[17]

a) Dipole-dipole interactions between polar solvent and solute.

b) Solute dipole-solvent induced dipole interactions where the solute is polar and the solvent is not.

c) Solvent dipole-solute induced dipole interactions where the solvent is polar and the solute is not.

d) Dispersion interactions.

e) Specific interactions such as hydrogen bonding and charge transfer.

f) Solvent cage effects.

These interactions are largely dependent on solvent polarity and this would be expected in view of the very large dipole moment of the zwitterionic species (26.16 D for Me(2)P3CNQ[2]). All the above interactions influence the energy and hence the wavelength of the charge transfer band.

Theory predicts[17] that solvatochromism in polar solutes is dependent on the solute dipole moment in the ground state and its change on excitation and, therefore, an increase in dipole moment on excitation should lead to a bathochromic (red) shift. The charge transfer band in these zwitterions was found to shift hypsochromically (blue shift) with increasing solvent polarity (see Figure 3.11 and Table 3.06). This is due to the decrease in dipole moment from the zwitterionic ground state to the neutral excited state of these materials. This phenomenon has been observed in other highly polar complexes[18] which also undergo a reduction in dipole moment on charge transfer.
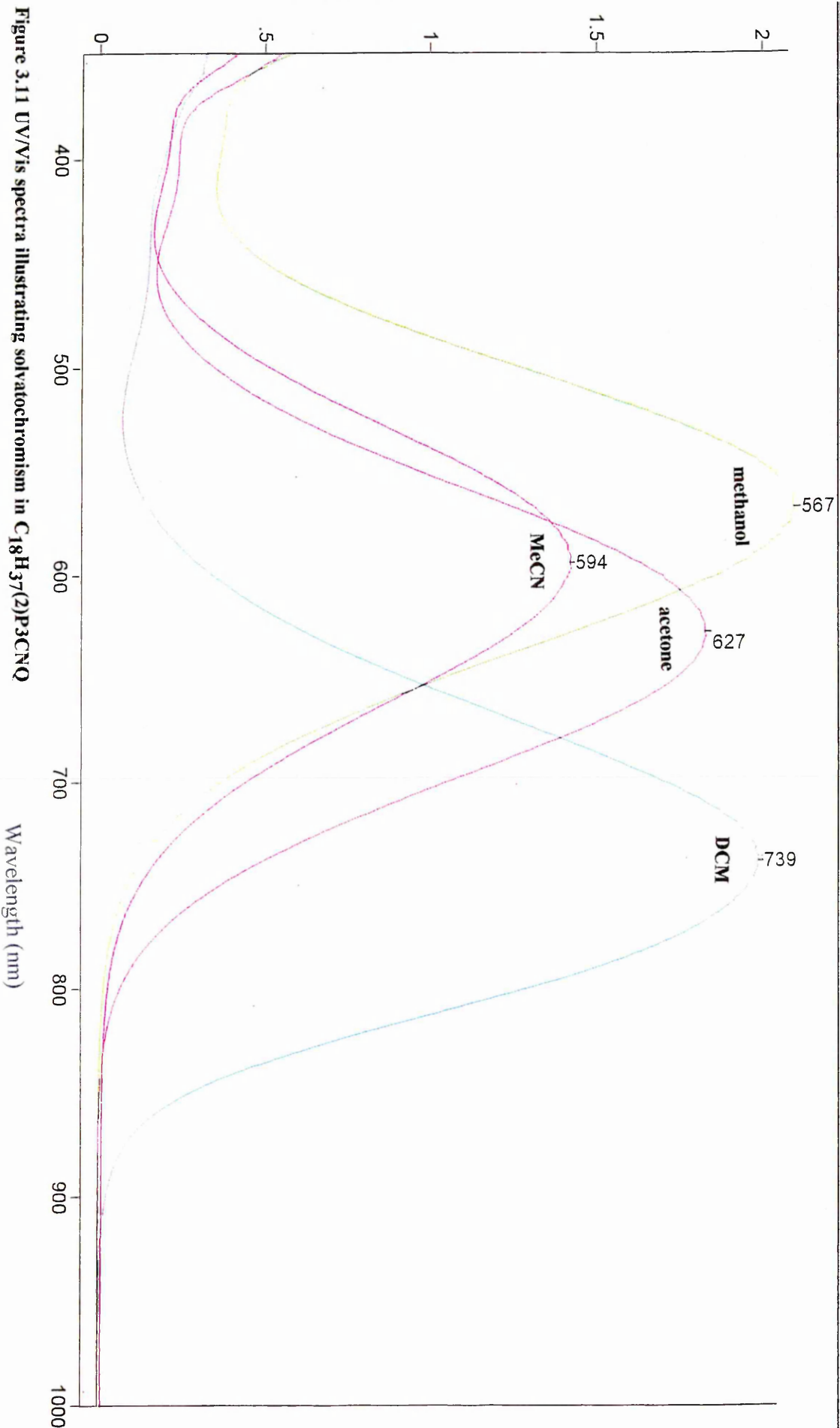
Figure 3.11 UV/Vis spectra illustrating solvatochromism in $C_{18}H_{37}(2)P3CNQ$

Table 3.06 Position of the charge transfer band verses the solvent dielectric constant (ε) for $C_{16}H_{33}(2)Q3CNQ$.

solvent	ε	λmax (nm)
acetonitrile	37.5	698
methanol	32.7	666
acetone	20.7	738
dichloromethane	8.9	852
chloroform	4.8	874

Table 3.07 Position of the charge transfer band verses the solvent dielectric constant (ε) for $C_{18}H_{37}(2)P3CNQ$ (see figure 3.11).

solvent	ε	λmax (nm)
acetonitrile	37.5	594
methanol	32.7	567
acetone	20.7	627
dichloromethane	8.9	739

Polar protic solvents such as methanol cause a greater hypsochromic (negative) shift than would be expected from the above trend. Hydrogen bonding between the polar protic solvent and the solute would probably increase the energy difference between the zwitterion and its excited neutral state and thus cause these deviations. There was no noticeable difference between the alpha and gamma systems in terms of their solvatochromism. These solvatochromic trends are also seen in DEMI and its related adducts of tertiary amines with TCNQ.[19]

Changes in pH greatly affect the charge transfer bands in these materials. Acidification (pH 1) of a typical adduct in an acetonitrile solution with sulphuric acid bleaches the

originally deep blue solution. The broad charge transfer band disappears completely but the lesser transition between 300 - 400 nm increases. On addition of sodium hydroxide, the deep blue colour and the charge transfer band are regenerated albeit at a lesser intensity.

The bleaching of the solution is due to the protonation of the TCNQ moiety in the adduct, resulting in a 1,6-addition type product. The proton in this type of product is extremely labile[20] and subsequent addition of base removes it to regenerate the zwitterion, although not completely.

These materials can also be bleached by visible light (Figure 3.12), however the charge transfer band does not return on addition of a base, indicating that a different mechanism is occurring. The charge transfer band regenerates slowly when the solution is left in the dark.

The mechanism suggested for this photochromic reaction[3] states that when the zwitterion is irradiated with a wavelength of light which overlaps that of the charge transfer band, an intramolecular back charge transfer (IABCT) occurs from the negatively charged acceptor moiety to the positively charged donor moiety. Such a mechanism would result in a planar, conjugated and neutral system. It was seen from the CH3(2)P3CNQ adduct[2, 28] that in the solid state (charge separated ground state) the C-H and the $C-C \equiv N$ groups from the $-CH=C(CN)-$ bridge are out of plane from the rest of the molecule. The dihedral angles are 36.1° between the N-methylpyridinium cation and the bridge unit, and 5.0° between the bridge unit and the dicyanomethanide anion, and also 31.1° between the cation and the anion. It is thought that rotation of the above units occurs with IABCT to yield a planar system (Figure 3.13).

It has been observed in gamma quinolinium systems that bleaching and recolouration follow first order kinetics and that substitution of the π-bridge affects the rate of bleaching.[13]
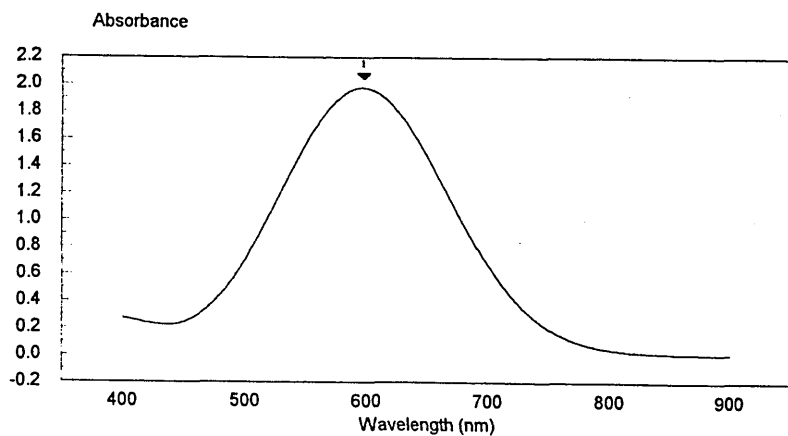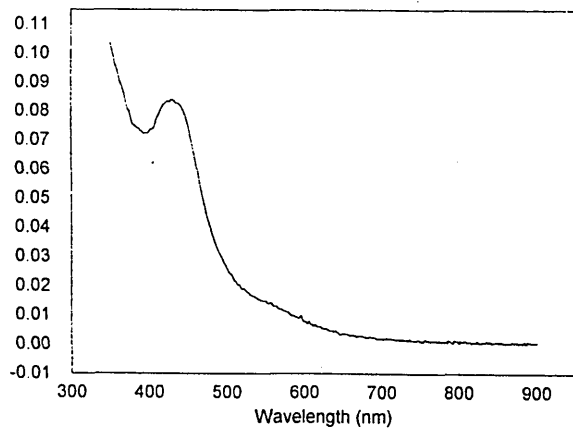
Figure 3.12 Bleaching of C$_{18}$H$_{37}$(2)P3CNQ (McCN solution)
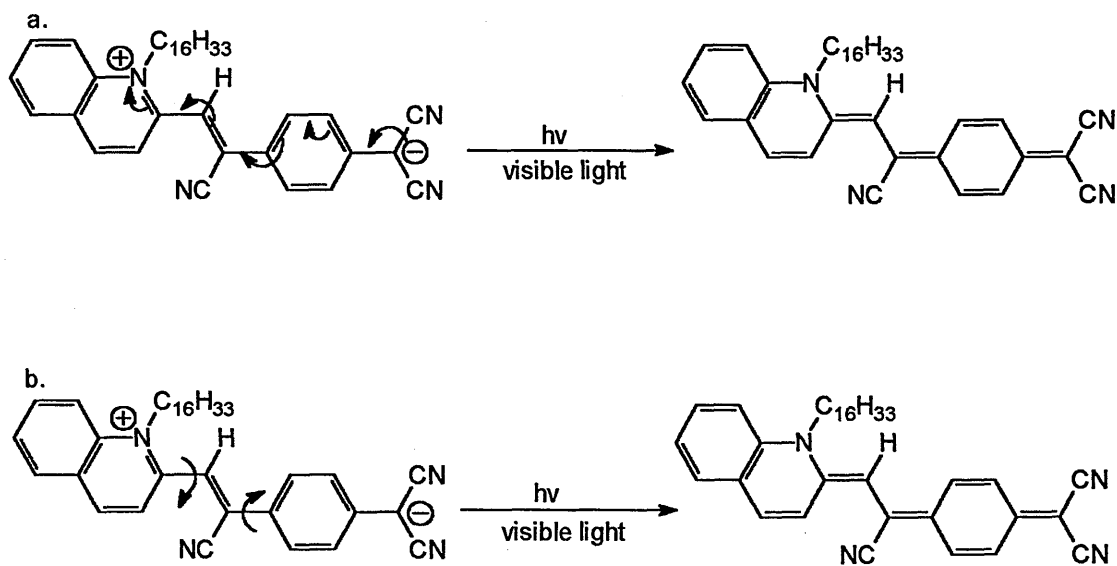
Figure 3.13 Proposed photochromic mechanism in $C_{16}H_{33}(2)Q3CNQ$.

a. intramolecular back charge transfer (IABCT) and b. formation of a planar system via the

rotation of the C-H and C-C≡N groups in the bridge unit to position them into the planes of the

quinolinium ring and the phenyl dicyanomethanide unit.

3.1.3.2 Infrared Spectroscopy

As expected all the quinolinium/picolinium and the related pyridazine, pyrazole and

benzothiazolum adducts gave similar infrared spectra typical of this type of system. The

most important features of the spectra are the two C≡N stretching bands between ca.

2200 cm^{-1} and 2120 cm^{-1}. Neutral nitriles normally occupy the range 2260 to 2200

cm[-1]. The presence of the two cyano stretching frequencies indicates two different cyano group environments. The band at 2200 cm^{-1} therefore represents the neutral environment whereas the band at for example 2240 cm-1 represents the dicyanomethanide 3-carbon unit over which the negative charge is delocalised. This delocalisation of charge reduces the strength of the bond and thus the stretching frequency is reduced correspondingly.

3.1.3.3 [1]Hnmr studies

The NMR spectra of the picolinum/quinolinium systems and the related adducts corroborates the UV/Vis and IR data to give further evidence of a dipolar ground state. The alkene proton on the π-bridge is seen as a singlet between δ 7.8 ppm and δ 8.05 ppm in all the adducts. Where resolution proved possible the quinolinium/picolinium protons in the alpha and gamma systems exhibit aromatic rather than quinoidal type signals. To illustrate this it has been observed that the H-2 proton in a 4-cyanovinyl N-alkylquinoline methide appears at δ 7.90 ppm[15]. The equivalent H-2 protons in the gamma and the H-3 protons in the alpha systems resonate between δ 9.0 - δ 9.4 ppm (Figure 3.14).

R— C_4H_7 to $C_{20}H_{41}$

R'—C(CN)—pH—C(CN)$_2$
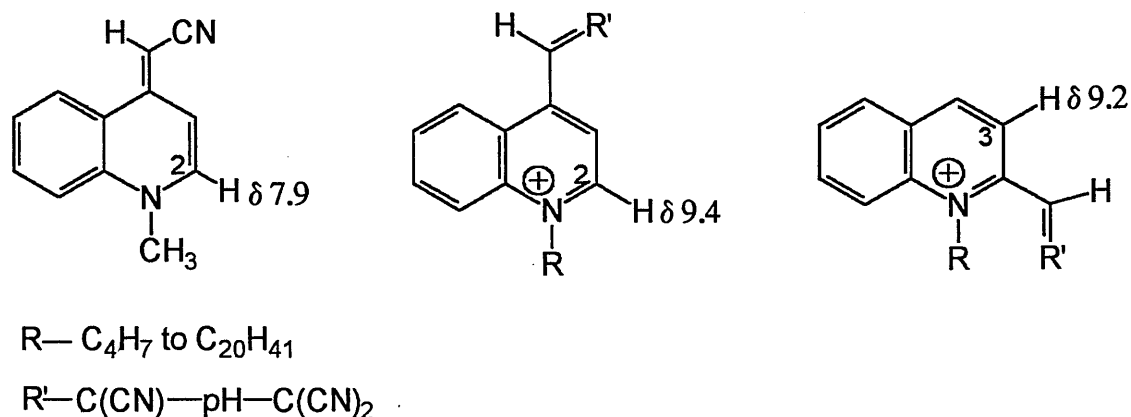
Figure 3.14 Illustrating H-2 and H-3 proton resonances in 4-cyanovinyl N-methylquinoline methide, R(4)Q3CNQ and R(2)Q3CNQ systems respectively

3.2 Pyridazine, Pyrazole and Benzothiazolium adducts

These three types of zwitterions were synthesised from commercially available reagents to contrast and compare properties with the gamma and alpha quinolinium/picolinium systems and provide further materials for LB studies. Their general insolubility however made most work impossible. Their general spectroscopic properties were very similar to the quinolinium/picolinium systems, yielding similar IR and NMR profiles to indicate dipolar ground states. The benzothiazolium derivative proved the only material that could be synthesised consistently, using neutral TCNQ with piperidine/N-methyl piperidine or with LiTCNQ and a reaction time of less than 40 minutes in either method. Second harmonic generation from LB films of a long chain benzothiazolium TCNQ derivative has been reported.[21]

3.3 Tetracyanoanthraquinone adducts

The preparation of TCAQ[22] was achieved by a Knoevenagel[23] type condensation reaction using Lehnerts procedure[24] to convert the quinone to the quinodimethane derivative. The Lewis acid, titanium (iv) chloride, activates the carbonyl group of the quinone by forming a metal - oxygen bond, thus increasing the polarisation in the carbon-oxygen bond, making it more susceptible to nucleophilic attack (Figure 3.15).
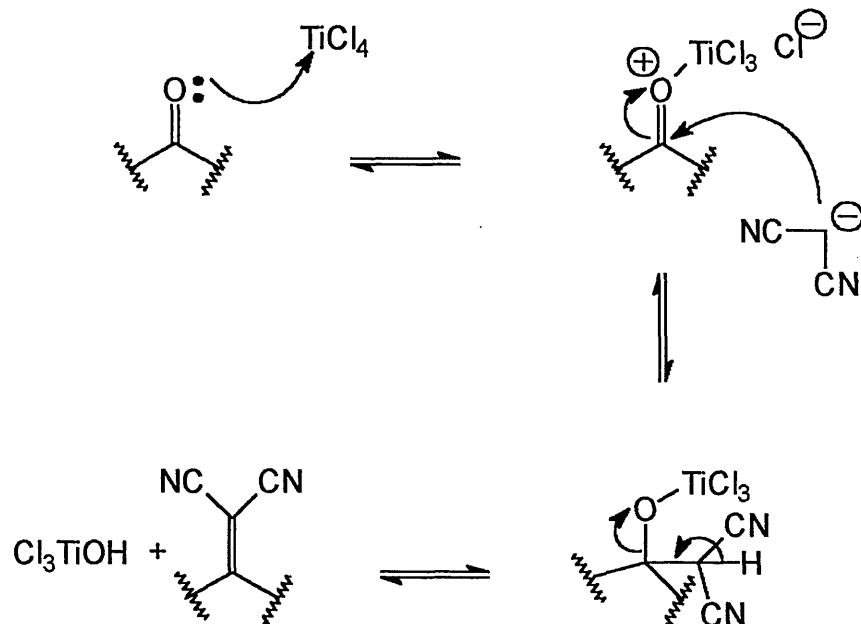
Figure 3.15 TiCl₄ mediated condensation

The titanium (iv) chloride mediated condensation does not give complete conversion of the quinone to the quinodimethane as there are a number of suspected competing side reactions (Figure 3.16) which ultimately reduce the final yield of the desired product.

Figure 3.16 Suspected side product from the TiCl₄ mediated reaction with anthraquinone and malononitrile

The attempted preparation of tetracyanoanthraquinone adducts was deemed a failure as the products formed failed to provide any evidence of zwitterionic ground states. In comparison with TCNQ, TCAQ is in fact a poor electron acceptor[25] due to the positive

induction effects of the two extra aromatic rings. There is also a loss of planarity in TCAQ to avoid interactions between the cyano groups and the aromatic peri hydrogens. To alleviate the strain the TCAQ adopts a butterfly conformation where the benzene rings fold upwards ("wings of a butterfly") and the cyano units point downwards.[26] This loss of planarity and the increased size of the TCAQ moiety compared to TCNQ itself increase the steric crowding of the reaction site. Coupled with the reduced electron accepting potential of TCAQ, this could explain the failure of these reactions.

However certain features of the zwitterions were observed, such as two cyano environments in the infrared spectra and weak charge transfer bands in the visible region.[27] The black platelets isolated which are distinctive of many TCNQ open shell systems, may also support evidence for a charge transfer salt (Figure 3.17). Analytical (combustion analysis) data proved inconclusive due to solvent being trapped in the final product.
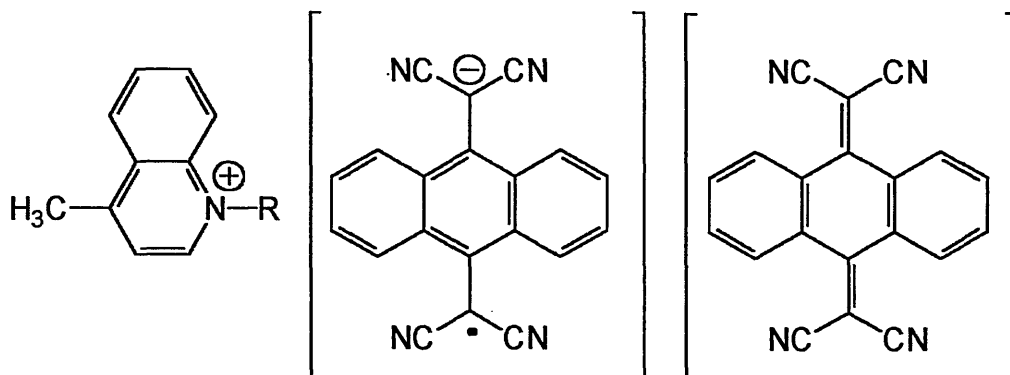
Figure 3.17 A quinolinium - tetracyanoanthraquinone charge transfer salt.

3.4 N-Alkylpyridinium benzimidazole betaines

Among the few other materials that have exhibited analogous properties to the zwitterions studied here are DEMI and its related derivatives, the merocyanine dyes[29] and certain heterocyclic betaines.[30] As with the quinolinium/picolinium zwitterions, N-alkylpyridinium benzimidazole betaines are examples of NLO materials that exhibit negative solvatochromism, that is in an increasingly polar medium the charge transfer band in the UV/visible absorption spectrum moves to shorter wavelengths. The synthesis of the N-alkylpyridinium benzimidazole betaines was first explored by Alcalde,[30] creating systems which exhibited short range charge transfer from a charged aromatic donor to a directly linked, charged aromatic acceptor group. Unlike the related materials mentioned above, however, these betaines possess no π-electron bridge between the donor and acceptor in the ground state.

The synthetic routes used to prepare the N-alkylated betaines [52] and [53] are outlined in Schemes 2.15 and 2.16 (Chapter 2, pages 73 -76). During the preparation of [52] and [53], the pyridylbenzimidazole (Section 2.4.1.1) and pyridyldiphenylimidazole (Section 2.4.2.1) were prepared essentially as described by Alcalde et al.[31]
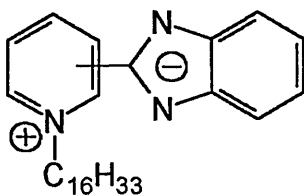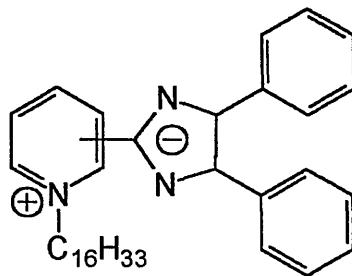
[52]   [53]

Conversion of the pyridylbenzimidazole and pyridyldiphenylimidazole into the corresponding N-alkylated salts (sections 2.4.1.2 and 2.4.2.2) was carried out using hexadecyl bromide under standard conditions. Treatment of the salts with equimolar proportions of sodium hydroxide in ethanol yielded the stable betaines [52] and [53]. Reaction of betaines [52] and [53] with TCNQ in acetonitrile yielded black microcrystalline adducts typical of TCNQ charge transfer salts. Unfortunately combustion analysis did not clarify the betaine:TCNQ ratio and it was assumed that a 1:1 or 1:2 betaine to TCNQ ratio could exist.

3.5 Solid State Studies

Crystal structures of the zwitterionic series R(4)Q3CNQ, R(4)PQ3CNQ, R(2)Q3CNQ and R(2)P3CNQ have previously been limited to just one of the original zwitterions Me(2)P3CNQ.[2] Difficulties have been encountered growing crystals of these materials due to their general insolubility and their tendency to form suspensions in solvents. As with Metzger et al,[15] often small metallic micro-needles were obtained that just would not diffract or gave superpositions of diffraction patterns.

However here we report the crystal structure[31] which was obtained for the long chain $C_{10}H_{21}(2)Q3CNQ$ adduct (Figure 3.18) crystallised from an acetonitrile solution which was refluxed for 3 months and then left to cool slowly to yield metallic gold crystals that produced a diffraction pattern.
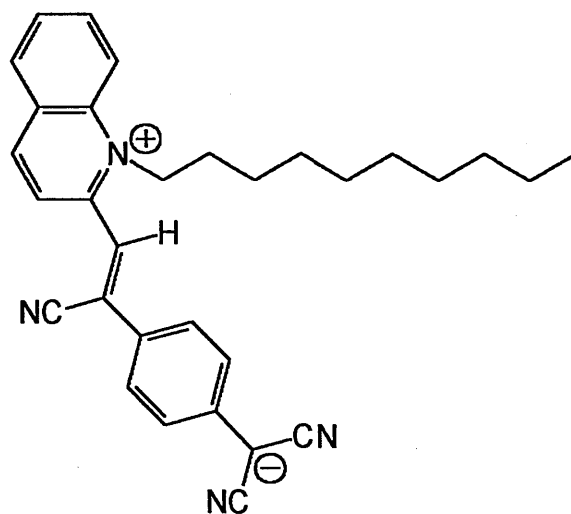
Figure 3.19 $C_{10}H_{21}(2)Q3CNQ$

Table 3.08 Crystal data and structure refinement for $C_{31}H_{32}N_4$

Empirical formula	$C_{31}\ H_{32}\ N_4$
Formula weight	460.61
Temperature	150 (2) K
Wavelength	0.71069 A
Crystal system	Orthorhombic
Space group	Pbca
Unit cell dimensions	$\alpha = 22.824$ (5) A
	$\beta = 7.4540$ (10) A
	$\gamma = 29.516$ (6) A
Volume	5022 (2) A^3
Z	8
Density (calculated)	1.219 mg/m^3
Absorption coefficient	0.072 mm^{-1}
F (000)	1968
Crystal size	0.16 x 0.12 x 0.10 mm
Theta range for data collection	2.26 to 24.77 deg
Index ranges	-23<=h <=24, -8 <=k<=6, -32<=1<=31
Reflections collected	10634
Independent reflections	3083 [R(int) = 0.1247]
Refinement method	Full- matrix least-squares on F^2
Data/ restraints / parameters	3083 / 12 / 317
Goodness-of-fit on F^2	0.704
Final R indices [I>2sigma (I)]	R1 = 0.0535, wR2 = 0.0981
R indices (all data)	R1 = 0.1594, wR2 = 0.1170
Largest diff. peak and hole	0.192 and -0.165 $e.A^{-3}$

Table 3.09 Bond lengths for C$_{10}$H$_{21}$(2)Q3CNQ

Bonds	Bond length (Å)	Bonds	Bond length (Å)
N(1) - C(1)	1.358(5)	N(1) - C(9)	1.394(5)
N(1) - C(22)	1.497(5)	N(2) - C(12)	1.136(5)
N(3) - C(20)	1.151(6)	N(4) - C(21)	1.131(5)
C(1) - C(2)	1.387(6)	C(1) - C(10)	1.453(6)
C(2) - C(3)	1.366(6)	C(3) - C(4)	1.387(6)
C(4) - C(9)	1.411(6)	C(4) - C(5)	1.424(6)
C(5) - C(6)	1.344(6)	C(6) - C(7)	1.422(6)
C(7) - C(8)	1.371(6)	C(8) - C(9)	1.404(6)
C(10) - C(11)	1.360(6)	C(11) - C(13)	1.447(6)
C(12) - C(13)	1.454(7)	C(13) - C(18)	1.400(6)
C(13) - C(14)	1.412(6)	C(14) - C(15)	1.371(6)
C(15) - C(16)	1.409(6)	C(16) - C(17)	1.410(6)
C(16) - C(19)	1.426(6)	C(17) - C(18)	1.359(6)
C(19) - C(20)	1.383(7)	C(19) - C(21)	1.421(7)
C(22) - C(23)	1.497(5)	C(23) - C(24)	1.524(6)
C(24) - C(25)	1.521(6)	C(25) - C(26)	1.506(6)
C(26) - C(27)	1.573(7)	C(27) - C(28)	1.516(7)
C(28) - C(29)	1.516(8)	C(29) - C(30)	1.284(8)
C(30) - C(31)	1.530(7)		

Table 3.10 Bond angles for C$_{10}$H$_{21}$(2)Q3CNQ

Bonds	Angles(°)	Bonds	Angles(°)
C(1) - N(1) - C(9)	122.6(4)	C(1) - N(1) - C(22)	119.1(4)
C(9) - N(1) - C(22)	118.2(4)	N(1) - C(1) - C(2)	118.2(5)
N(1) - C(1) - C(10)	119.6(4)	C(2) - C(1) - C(10)	122.2(5)
C(3) - C(2) - C(1)	121.3(5)	C(2) - C(3) - C(4)	120.8(5)
C(3) - C(4) - C(9)	118.8(5)	C(3) - C(4) - C(5)	123.0(5)
C(9) - C(4) - C(5)	118.2(5)	C(6) - C(5) - C(4)	120.7(5)
C(5) - C(6) - C(7)	120.8(5)	C(8) - C(7) - C(6)	120.0(6)
C(7) - C(8) - C(9)	119.7(5)	N(1) - C(9) - C(8)	121.3(5)
N(1) - C(9) - C(4)	118.2(5)	C(8) - C(9) - C(4)	120.5(5)
C(11) - C(10) - C(1)	127.4(5)	C(10) - C(11) - C(13)	124.5(5)
C(10) - C(11) - C(12)	119.4(5)	C(13) - C(11) - C(12)	116.0(5)
N(2) - C(12) - C(11)	175.2(6)	C(18) - C(13) - C(14)	114.5(5)
C(18) - C(13) - C(11)	124.3(5)	C(14) - C(13) - C(11)	121.2(5)
C(15) - C(14) - C(13)	123.3(5)	C(14) - C(15) - C(16)	121.2(5)
C(15) - C(16) - C(17)	115.7(5)	C(15) - C(16) - C(19)	122.4(5)
C(17) - C(16) - C(19)	121.9(5)	C(18) - C(17) - C(16)	122.3(5)
C(17) - C(18) - C(13)	123.0(5)	C(20) - C(19) - C(21)	117.5(5)
C(20) - C(19) - C(16)	121.1(5)	C(21) - C(19) - C(16)	121.4(5)
N(3) - C(20) - C(19)	176.6(6)	N(4) - C(21) - C(19)	179.3(5)
C(23) - C(22) - N(1)	113.6(3)	C(22) - C(23) - C(24)	111.0(3)
C(25) - C(24) - C(23)	114.7(5)	C(26) - C(25) - C(24)	113.4(5)
C(25) - C(26) - C(27)	112.1(5)	C(28) - C(27) - C(26)	111.1(5)
C(29) - C(28) - C(27)	116.5(6)	C(30) - C(29) - C(28)	128.4(8)
C(29) - C(30) - C(31)	119.3(7)		
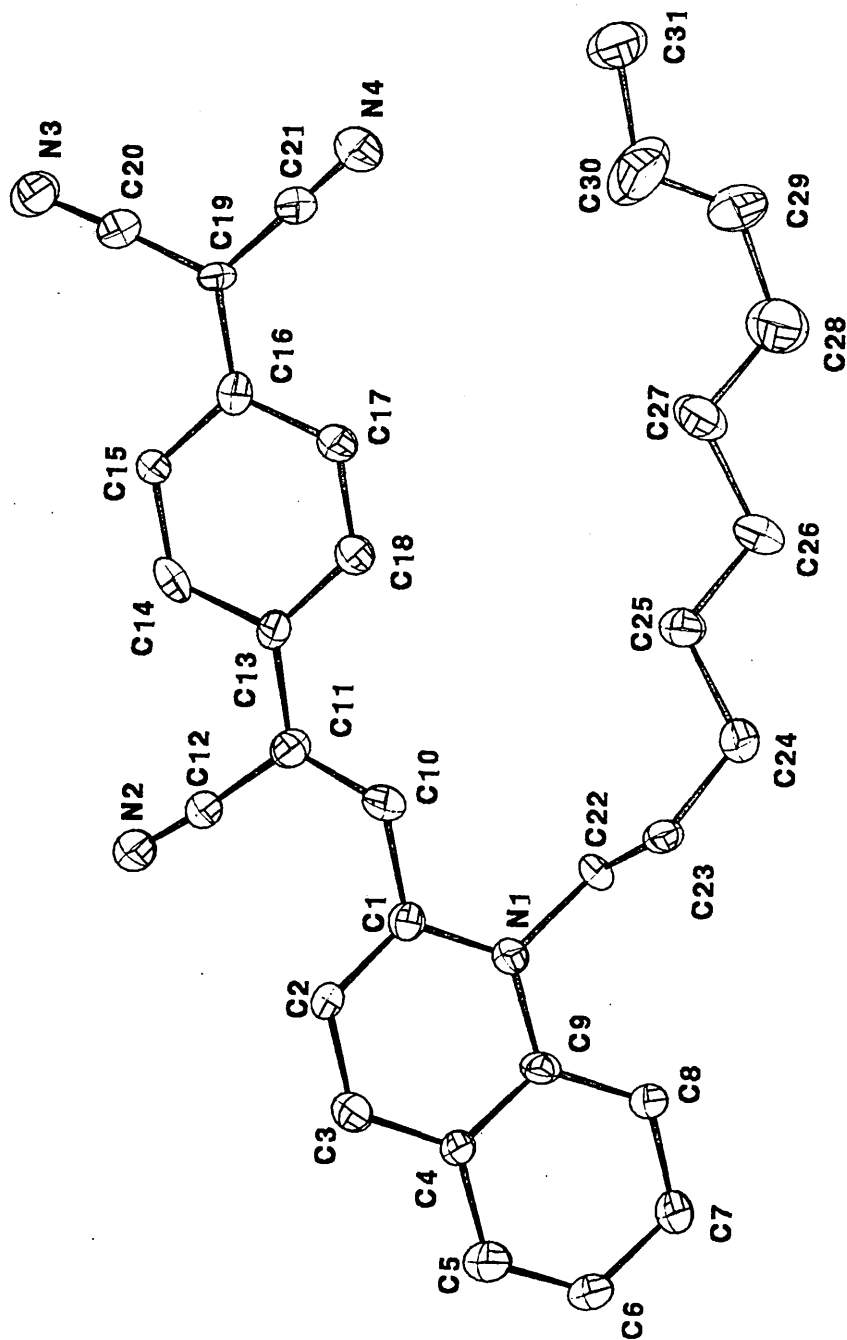
Figure 3.18 X-Ray crystal structure of $C_{10}H_{21}(2)Q3CNQ$

The crystal structure of $C_{10}H_{21}(2)Q3CNQ$ is shown in Figure 3.18. The bond lengths and angles are given in Tables 3.09 and 3.10 respectively. The bond lengths within the tricyanoquinodimethane portion of the molecule (Table 3.11) and within the quinolinium ring are benzenoid rather than quinoid in character. The bond length between C10 and C11 (1.360 Å) clearly indicates the double bond π-bridge separating the quinolinium and tricyanomethane groups. The lengths of bonds C11 - C13 and C16 - C19 indicate single bonds, thus ruling out a quinoidal ground state.

Table 3.11 Significant bond lengths in $C_{10}H_{21}(2)Q3CNQ$

Bonds	Bond lengths (Å)
C10 - C11	1.360
C11 - C13	1.447
C14 - C15	1.371
C16 - C19	1.426
C18 - C17	1.359

Table 3.12 Significant bond lengths in $CH_3(2)P3CNQ$ (see Chapter 1 and diagram 1.18) from Metzger et al.[2]

Bonds	Bond lengths (Å)
C3 - C6	1.440
C7 - C8	1.365
C10 - C11	1.377
C12 - C9	1.465
C12 - C15	1.354

Comparisons with the crystal structure data[2] of the original zwitterion (CH3(2)P3CNQ), indicate a very similar ground state structure (Table 3.12) thus providing further unequivocal evidence of a charge separated ground state.

Figures 3.21 to 3.24 show packing diagrams of the molecules along the a, b and c axes with eight molecules being present per unit cell.

The molecules appear to stack along the b-axis and the unit cell in Figures 3.22 and 3.24 shows that the positive donor centre overlaps the negative dicyanomethane swallow tail, thus creating a zero net dipole for the overlapping molecules (Figure 3.20).
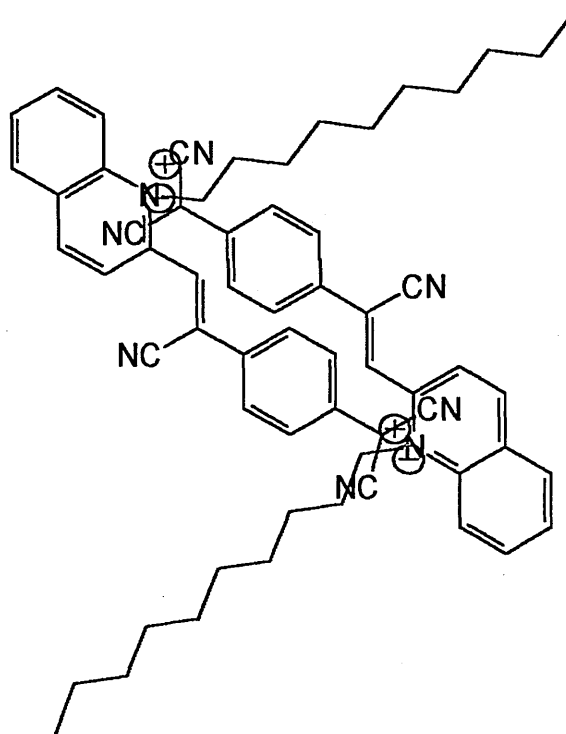
Figure 3.20 Overlapping of two molecules of $C_{10}H_{21}(2)Q3CNQ$ stacked along the b-axis.
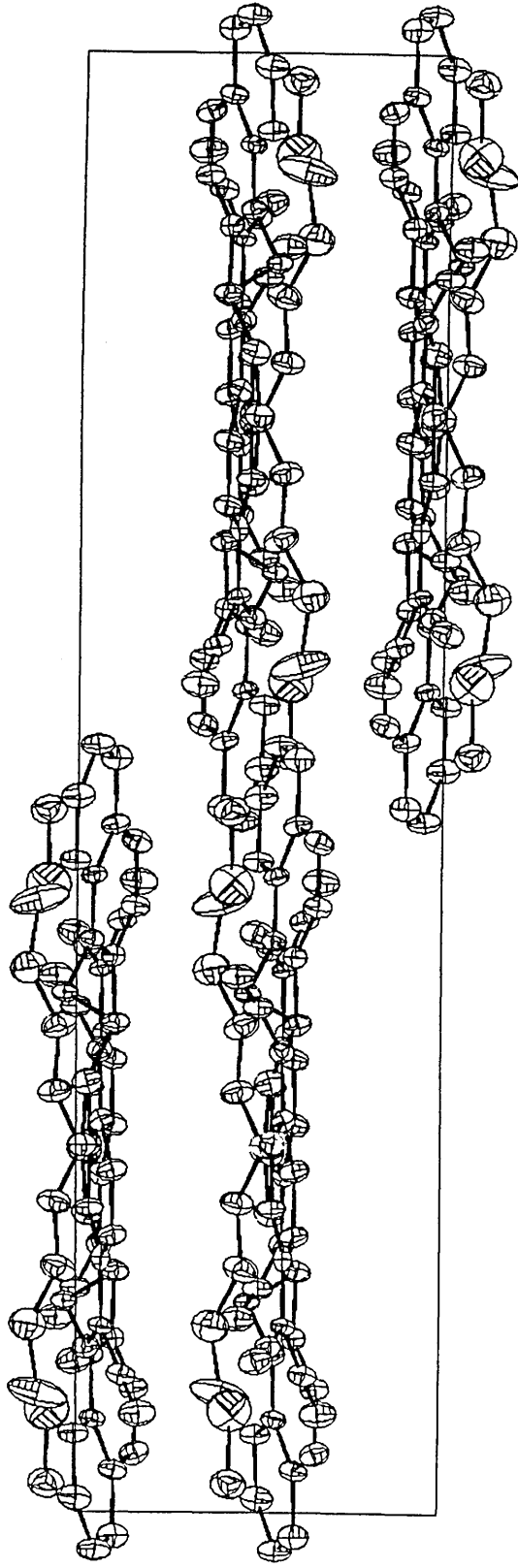
Figure 3.21 Packing diagram showing molecules of $C_{10}H_{21}(2)Q3CNQ$ stacked along the a-axis
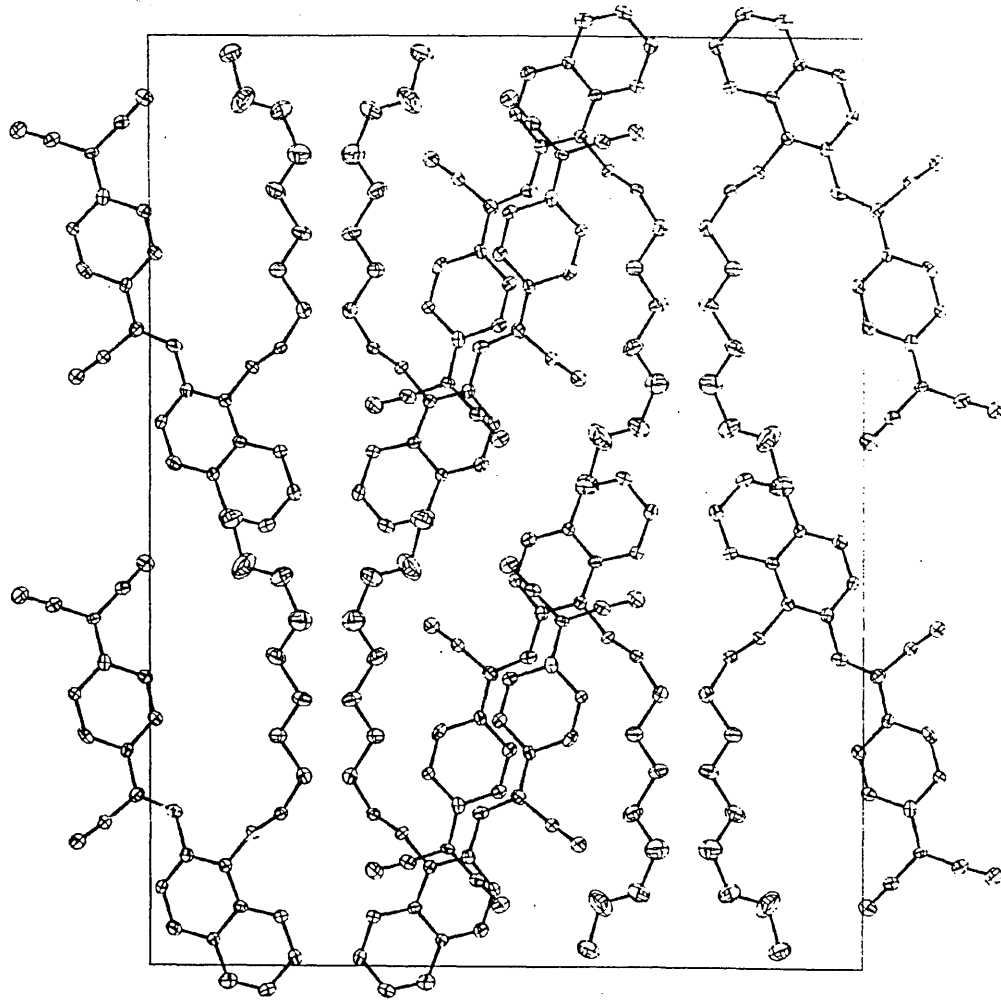
Figure 3.22 Packing diagram showing molecules of $C_{10}H_{21}(2)Q3CNQ$ stacked along the b-axis
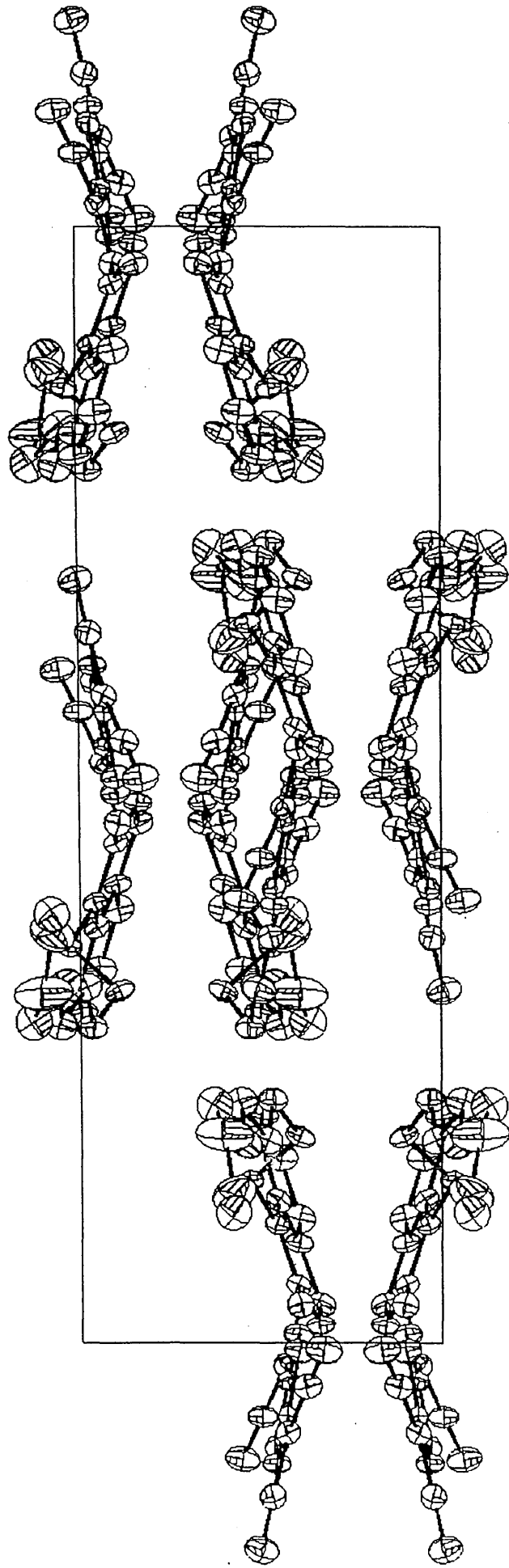
Figure 3.23 Packing diagram showing molecules of $C_{10}H_{21}(2)Q3CNQ$ stacked along the c-axis
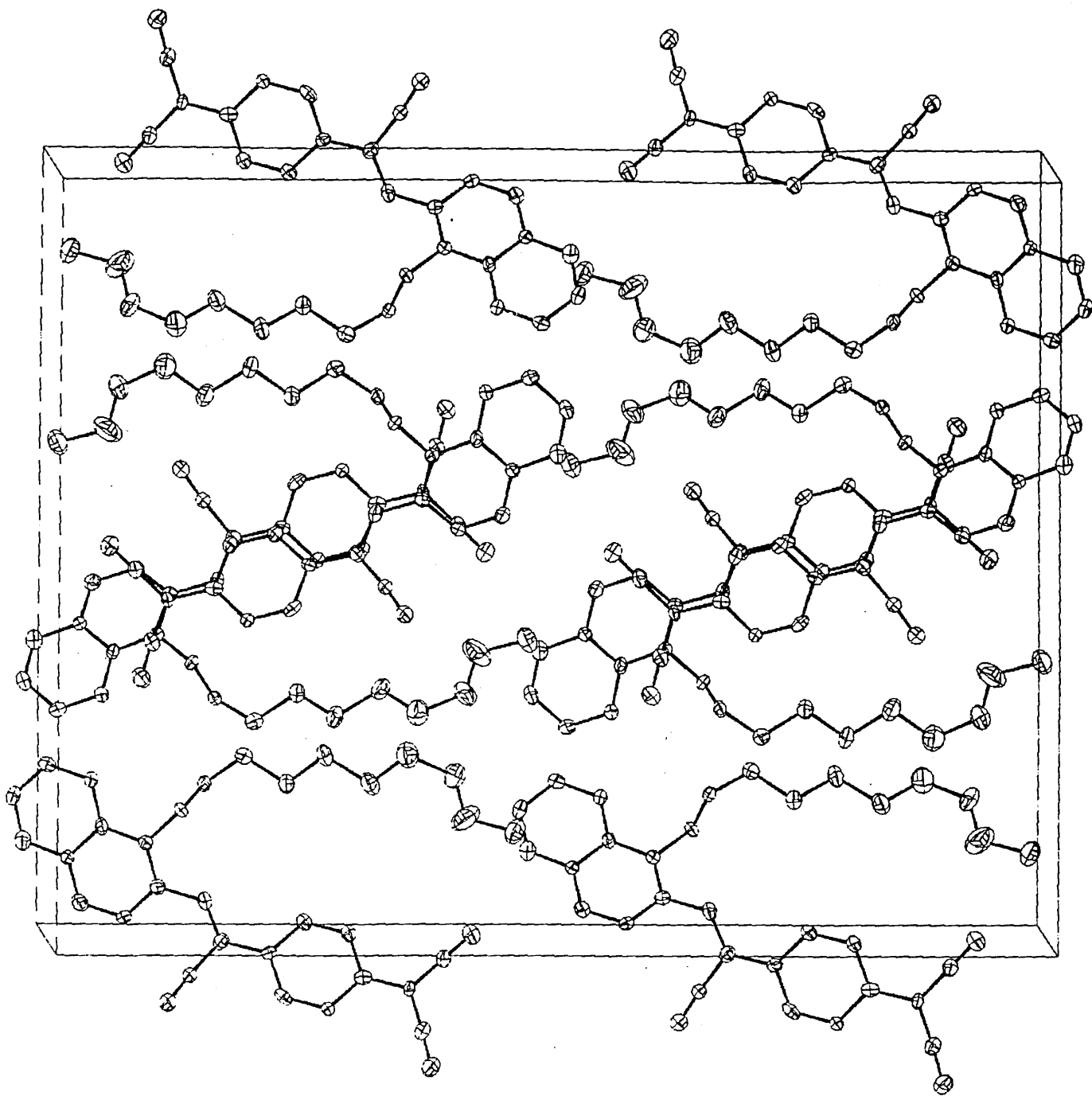
Figure 3.24 Packing diagram of $C_{10}H_{21}(2)Q3CNQ$

3.6 Chapter Three References

1. N. A. Bell, R. A. Broughton, J. S. Brooks, T. A. Jones and S. C. Thorpe, *J. Chem. Soc. , Chem. Commun. ,* 325, 1990.

2. R. M. Metzger, N. E. Heimer and G. J. Ashwell, *Molecular Crystals Liquid Crystals,* **107**, 133, 1984.

3. G. J. Ashwell, *Thin Solid Films,* **186**, 155, 1990.

4. G. J. Ashwell, E. J. C. Dawnay, A. P. Kucynski, M. Szablewski, I. M. Sandy, M. R. Bryce, A. M. Grainger and M. Hasan, *J. Chem. Soc. , Faraday Trans. ,* **86**, 1117, 1990.

5. G. J. Ashwell, G. Jefferies, E. J. C. Dawnay, A. P. Kuczynski, D. E. J. Lynch, Y. Gongda and D. G. Bucknall, *J. Mater. Chem. ,* **5**, 975, 1995.

6. G. J. Ashwell, E. J. C. Dawnay and A. P. Kuczynski, *J. Chem. Soc. , Chem. Commun. ,* 1355, 1990.

7. N. A. Bell, R. A. Broughton, J. S. Brooks, T. A. Jones and S. C. Thorpe, *Int. J. Electronics,* **76**, 751, 1994.

8. N. Menschutkin, *Z. Phys. Chem.* **6**, 41, 1890.

9. H. A. Bruson, *Organic Reactions,* **5**, 79, 1949.

10. E. D. Bergmann, D. Ginsberg and R. Rappo, *Organic Reactions,* **10**, 179, 1959.

11. R. Connor and W. R. McClellan, *J. Org. Chem. ,* **3**, 570, 1938.

12. R. A. Broughton, Sheffield Hallam University, PhD Thesis, 1993.

13. M. Szablewski, Cranfield Institute of Technology, PhD Thesis, 1992.

14. M. Szablewski, *J. Org. Chem. ,* **59**, 954,1994.

15. R. M. Metzger, B. Chen, U. Hopfner, M. V. Lakshmikanthan, D, Vuillaume, T. Kawai, X, Wu, H. Tachibana, T. V. Hughes, H. Sakurai, J. W. Baldwin, C. Hosch, M. P. Cava, L. Brehmer and G. J. Ashwell, *J. Am. Chem. Soc. ,* **119**, 10455, 1997.

16. B. P. Bespalov and V. V. Titov, *Russian Chem. Revs. ,* **44**, 1091, 1975.

17.	K. M. C. Davis in *"Molecular Association"*, Vol. 1, Ed - R. Foster, Academic Press, 1985.

18.	D. J. Sandman, A. F. Garito, *J. Org. Chem.* **39**, 1165, 1974.

19.	M. Szablewski, P. R. Thomas, A. Thornton, D. Bloor, G. H. Cross, J. M. Cole, J. A. K. Howard, M. Malagoli, F. Meyers, J-L. Bredas, W. Wenseleers and E. Goovgerts, *J. Am. Chem. Soc.* , **119**, 3144, 1997.

20.	B. P. Bespalov, V. V. Titov, *Russian Chem. Revs.* **44**, 1091, 1975.

21.	G. J. Ashwell, M. Malhotra, M. R. Bryce and A. M. Grainger, *Synthetic Metals,* **41-43**, 3173, 1991.

22.	A. Aumüller and S. Hünig, *Liebigs Ann. Chem.* , **618**, 1984.

23.	G. Jones, *Organic Reactions,* **15**, 232, 1967.

24a.	W. Lehnert, *Synthesis,* **667**, 1974 and references therein.

24b.	W. Lehnert, *Tetrahedron Letters,* **54**, 4723, 1970.

25.	M. C. Grossel and S. C. Weston, *Contemporary Organic Synthesis,* **1**, 367, 1994.

26.	U. Schubert, S. Hunig and A. Aumuller, *Liebigs Ann Chem,* 1216, 1985.

27a.	D. J. Crouch, Sheffield Hallam University, BSc project report, 1995.

27b.	D. J. Crouch, Sheffield Hallam University, internal publication, 1997.

28.	S. Akhtar, J. Tanaka, R. Metzger and G. J. Ashwell, *Mol. Cryst. Liq. Cryst.* **139**, 353, 1986.

29.	A. Fort, C. Runser,C. Barzoukas, C. Cambellas, C. Suba and A. Thiebault, *Proc. SPIE,* **5**, 2285, 1984.

30.	E. Alcalde, *Adv. Heterocycl. Chem.* , **60**, 97, 1994 and references cited therein.

31.	E. Alcalde, I. Dinares, L. I. Perez-Garcia, T. Roca, Synthesis, 395, 1992.

32.	D. E. Hibbs and M. B. Hursthouse, Personal Communication, 1997.

CHAPTER 4

Langmuir- Blodgett Films

4.1 Historical

The phenomenon of oil spreading on water has been known for thousands of years. The Babylonians in the 18th century BC were known to pour oil on water (or water on oil) and observe its effects as a form of divination.[1] The Greeks, who looked at the effects of examining liquid in a bowl a thousand years later, called it lecanomancy, from lekani = bowl and manteia = divination. Pouring oil onto stormy seas was documented as early as AD 429 and 651 when its calming properties were observed.[2] However this was attributed to divine intervention rather than the effects of the oil itself. According to Scott,[3] a theory attributed to Aristotle and Plutarch was that "the oil produces calm by smoothing the water surface so that the wind can slip over it without making an impression".

In the eighteenth century the American statesman Benjamin Franklin (1706 - 1790) noted the spreading effect of oil on a pond at Clapham Common, again its calming influence being observed.[4] This account was the basis of much research in the 19th century. An extract from this colourful account reads:-

"........At length being at Clapham where is, on the common, a large pond, which I observed to be one day very rough with the wind, I fetched out a cruet of

oil, and dropped a little of it on the water. I saw it spread itself with surprising

swiftness upon the surface....... I then went to the windward side, where [the

waves] began to form; and there the oil, though not more than a teaspoonful,

produced an instant calm over a space several yards square, which spread

amazingly, and extended itself gradually till it reached the lee side, making all that

quarter of the pond, perhaps half an acre, as smooth as a looking glass........"

In the second half of the 19th century Shields (1822-1890), who was the owner of a linen

mill, carried out a series of experiments using undersea pipes to deliver quantities of oil to

the surface when required and he even took out a number of patents in this area.[5] Shields

findings were never reported in the scientific press; however they were widely recorded in

local media of the day and were subjects of discussions in Parliament.[6] However, it

became clear that numerous practical difficulties were encountered from damage to the

piping system by underwater currents, resulting in the high costs of the proposed projects.

It is believed that the first scientist to work seriously in this area was John Aitken (1839 -

1919) whose interest must have been fuelled by Shields' work. He was a graduate in

engineering from the University of Glasgow and he designed his own laboratory in order

to research into natural phenomena. He devised and constructed apparatus to test theories

of the calming action of oil on water.[7] One such experiment was to measure the amount of

torsion of different currents of air on clear water surfaces, and water surfaces having a thin

oil film on them. He found that the oil does not reduce "....the bite, grip or friction of air

on the surface......," thus contradicting the long held wave damping theory. Aitken then

devised a series of experiments to explain this phenomenon.[8]

However it was not until the 1880's when Lord Rayleigh (1842 - 1919) began to realise

that these surface films were of a molecular thickness that the concept of monolayer

science was born.[9] Rayleigh's initial interest in sound waves led him to observe the

behaviour of colliding water jets and water drops and the effect of static electricity upon

them.[10] He also added soap to the water and observed the effects. In later papers,[11] he

began to realise that monolayers were being formed by fatty acids in the soap and also that

layers of olive oil affected the surface tension of the water's surface. From these

publications it was obvious that he was beginning to realise that these films were of

molecular thickness. He believed that, if the thickness of these films could be determined,

it would give the first direct measurement of the size of an organic molecule but he had

not found a method of doing so.

Agnes Pockels (1862 - 1935) was the first to make a direct measurement of molecular

sizes. She designed a simple apparatus based on a kitchen sink, which is today the basis of

the Langmuir trough.[12] She also published the first pressure-area isotherms which were of

fatty acids. In fact Pockels' experimental methods described in a letter to Rayleigh in

1891, have to this day remained the essentials of monolayer research.

Due to Pockels' and Rayleigh's findings there was an increased level of activity in this

field. Hardy,[13] for instance, found that polar functional groups were required in the oils to

form monolayers and he was the first to consider the molecular orientation of the polar

molecules on the subphase and of the potential use of this field in lubrication. He also

considered the nature of the cohesive forces between these molecules and incorrectly

found them to be long range. Devaux,[14] measured the thickness of various films using

different methods and found that they represented molecular diameters. He was the first to

spread polymers as films using protein and cellulose and he also reported that egg albumen

spreads on water to give an extremely elastic monolayer.

Irving Langmuir (1881 - 1957) fully developed the theory of monolayers and for this work he was awarded the Nobel Prize. Langmuir published a paper in 1917[15] which described the design of his trough and how it could be used to determine the molecular area and orientation of monolayers at the air-water interface. Langmuir also surmised that the cohesive forces between molecules were short range (not long range as stated by Hardy[13]) and acted only between molecules in contact.

Katherine Blodgett (1898 - 1979), who worked with Langmuir on the properties of floating monolayers developed the technique of sequentially building up monolayer upon monolayer on a substrate producing multilayer films. These are now known as Langmuir-Blodgett(LB) films.[16,17] Blodgett also developed anti reflection coatings[18] and step thickness gauges,[19] which were the first practical uses of LB films.

Research interest in LB films remained very quiet until the 1960s when Kuhn and Mobius published a series of papers[20] which showed how monolayers could be used to construct precise supra-molecular structures. They used the LB technique to demonstrate the fluorescence and quenching of dye molecules attached to fully saturated fatty acids under UV light. This seminal work and the publication of "Insoluble Monolayers at Liquid Gas Interfaces" by Gaines[21] initiated a revival in the field and this resulted in thousands of publications in this area over the last 30 years. Many applications of LB films are currently being investigated in fields that include: electronics/microelectronics, non linear optics, biotechnology and molecular electronics.

4.2 Monolayers

Certain organic molecules can orientate themselves at the boundary between a liquid and a gas, i.e. the air-water interface, and also between two liquid phases, to reduce their free energy. This excess of free energy is due to the difference in environment between the molecules at the boundary and those in the bulk phase.[21-23] The resulting film, known as a monolayer, is one molecule thick.

The surface tension (γ) of a planar interface is given by:-

$$\gamma = (\delta G/\delta s)_{T,P,n_i}$$

where **G** is the Gibbs free energy of the system, **s** is the surface area, and temperature **T**, pressure **P** and composition **ni** are held constant. The surface tension of pure water is 73 mN/m at 20°C and atmospheric pressure. This value is extremely high and is the reason why water is used as the liquid phase in most monolayer/LB film experiments.

Suitable monolayer forming materials are molecules which possess two distinct regions. These two regions are a hydrophilic head group (water soluble) and a hydrophobic tail group (water insoluble). The `classic` monolayer forming material is stearic acid (octadecanoic acid) which has a long hydrophobic alkyl chain group and a hydrophilic acid head group, as shown in Figure 4.01. Other materials of this type have been widely studied such as arachidic acid ($C_{19}H_{39}COOH$) and behenic acid ($C_{21}H_{43}COOH$).[24] These fatty acids of the general formula $C_nH_{2n+1}CO_2H$ have been shown[25] to form stable monolayers where n > 12, as these materials have the correct amphiphilic balance which will prevent the material from slowly dissolving into the subphase.

$$C_{17}H_{35}COOH$$

hydrophobic alkyl chain length   hydrophillic
                                        acid group
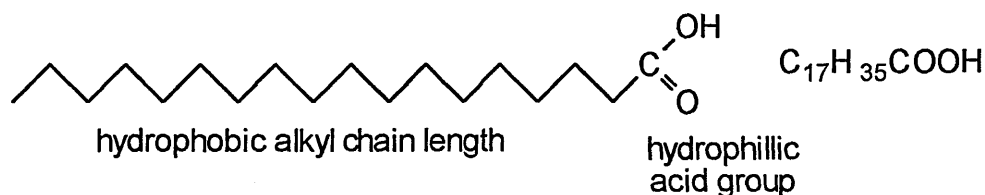
Figure 4.01 Stearic acid (octadecanoic acid)

When a material such as stearic acid (usually dissolved in a fairly non polar solvent such as chloroform or dichloromethane) is placed on the water's subphase, it spreads across the surface until the surface pressure reaches an equilibrium. As the solvent evaporates, this leaves behind a monolayer where the polar head group (acid group) is in the subphase and the non polar group (alkyl chain) is resting on the surface of the subphase (a "2 dimensional gas"). On compression of the monolayer (Figure 4.02) the organic molecules orientate themselves to eventually form a "two dimensional solid".

The presence of this monolayer on the liquid subphase will affect the surface tension (Figure 4.03). In the case of a water subphase any contamination will reduce the surface tension: therefore in most monolayer /LB experiments (see chapter 5 and 6) the strength of this reduction in the pure water surface tension by the monolayer is measured by the surface pressure (Π), i.e.,

$$\Pi = \gamma0 - \gamma$$

where $\gamma0$ is the surface tension of the pure water or liquid subphase and γ is the surface tension of the monolayer.
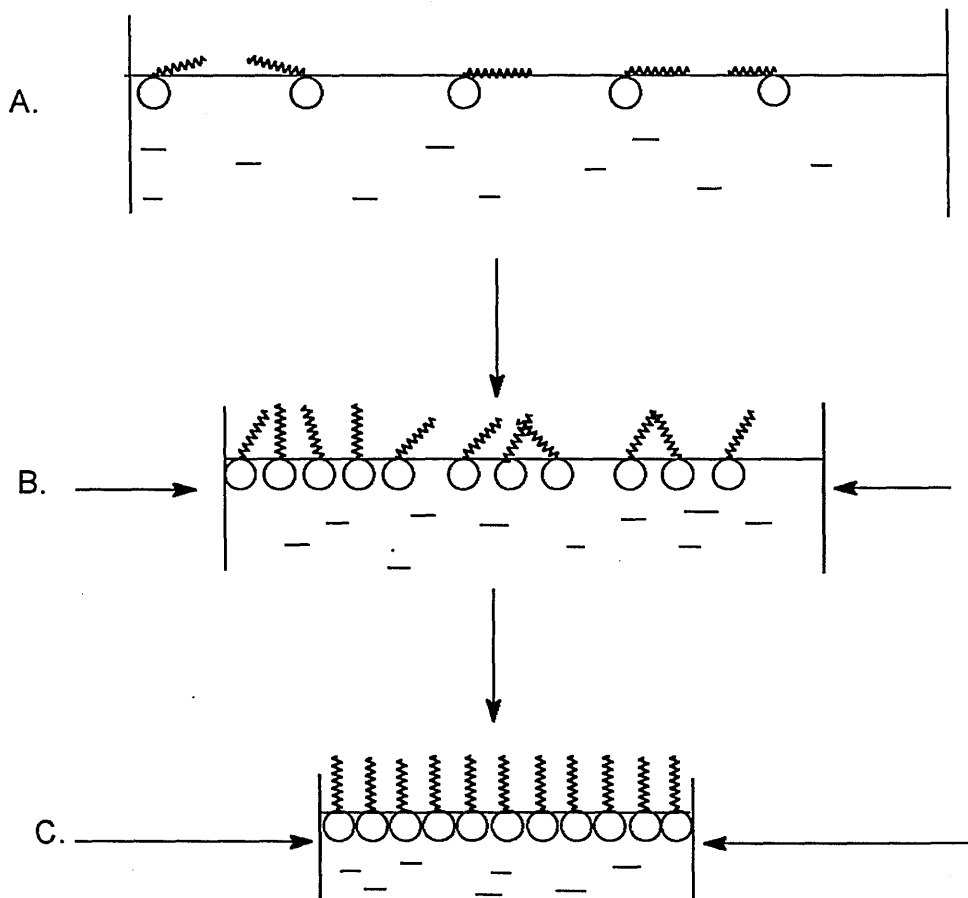
Figure 4.02 Compression of a monolayer of stearic acid to produce a "2" dimensional solid: (A) Expanded monolayer where the polar head groups of the acid have dissolved into the subphase and the non-polar alkyl chain groups are lying on the surface. (B) Partial compression. (C) Total compression to yield a "2" dimensional solid.
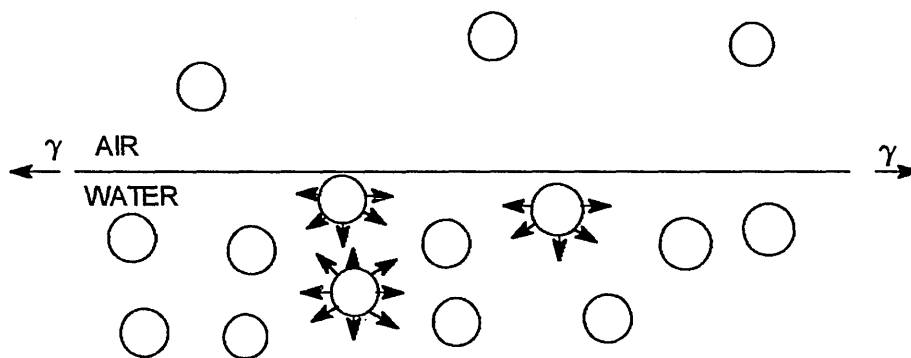
Figure 4.03 Forces acting on molecules in the subphase and at the air/water interface. The line of force acting on the molecules is the surface tension (γ)

4.3 Isotherms

The surface tension can be defined as "the work required to expand the surface isothermally by unit area" (i.e. mN/m). Surface-active molecules tend to accumulate at the interface and this favours expansion of the interface which in turn will lower surface tension. Therefore the surface pressure, as a function of the area occupied per molecule, can be determined provided the number of molecules is known. Thus -

$$Å^2 = AM/CN_AV = A/cN_AV$$

where $Å^2$ is the area per molecule (angstrom units squared), A is the film area (angstrom units squared), M is the molecular weight of the material, C is the concentration of the spreading solution in mass per unit volume, c is the specific molar concentration of the solution, V is its volume and N_A is Avogadro's number (6.022×10^{23}).

The characteristics of monolayer behaviour on the water subphase can be studied by measuring surface tension changes on compression of the monolayer. Surface pressure readings are made using, for example, the Wilhelmy plate technique (see chapter 5). Pressure-area isotherm plots are obtained (so called because compression occurs at constant temperature) which provide a two-dimensional `fingerprint` of a particular molecule (Figure 4.04).
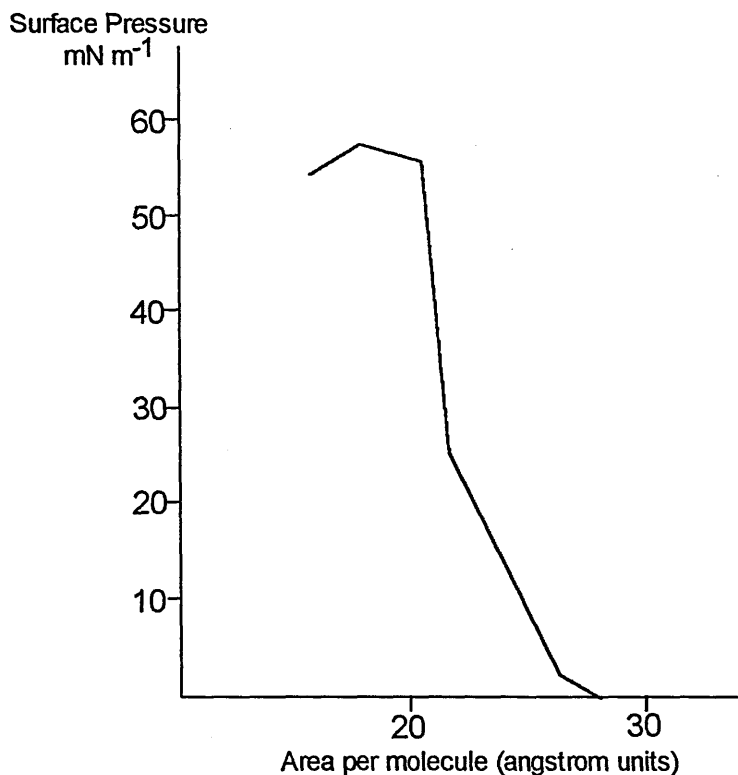
Figure 4.04 An idealised stearic acid isotherm

During compression the monolayer undergoes a number of phase changes (Figure 4.04);

these could be described as being virtually analogous to that of three dimensional gases,

liquids and solids. The molecules before compression are far enough apart on the air/water

interface to exert little or no influence on each other (a 'gaseous phase', refer to A, Figure

4.03); at this point the area per molecule will be large. The molecules at the interface then

pass into a 'liquid' phase, often referred to as the 'expanded phase' (B, figure 4.02). Here

the polar headgroups are dissolved in the subphase and the alkyl chains are in an irregular

orientation. In the stearic acid isotherm (Figure 4.04) as the surface pressure increases

above 20 mN/m, the gradient of the isotherm increases abruptly as the molecules orientate

themselves into a more ordered 'two dimensional solid' arrangement (C, Figure 4.03). If

this part of the isotherm is extrapolated to zero pressure it gives the hypothetical structure

of the two dimensional solid, uncompressed. Thus an idea of the area occupied by a single

stearic acid molecule can be obtained; in the case of the above isotherm it would be $\approx$ 22Å².

As compression continues further and the area per molecule continues to decrease, collapse of the monolayer eventually occurs as the molecules begin to pass over each other and disordered multilayers are formed (Figure 4.05).
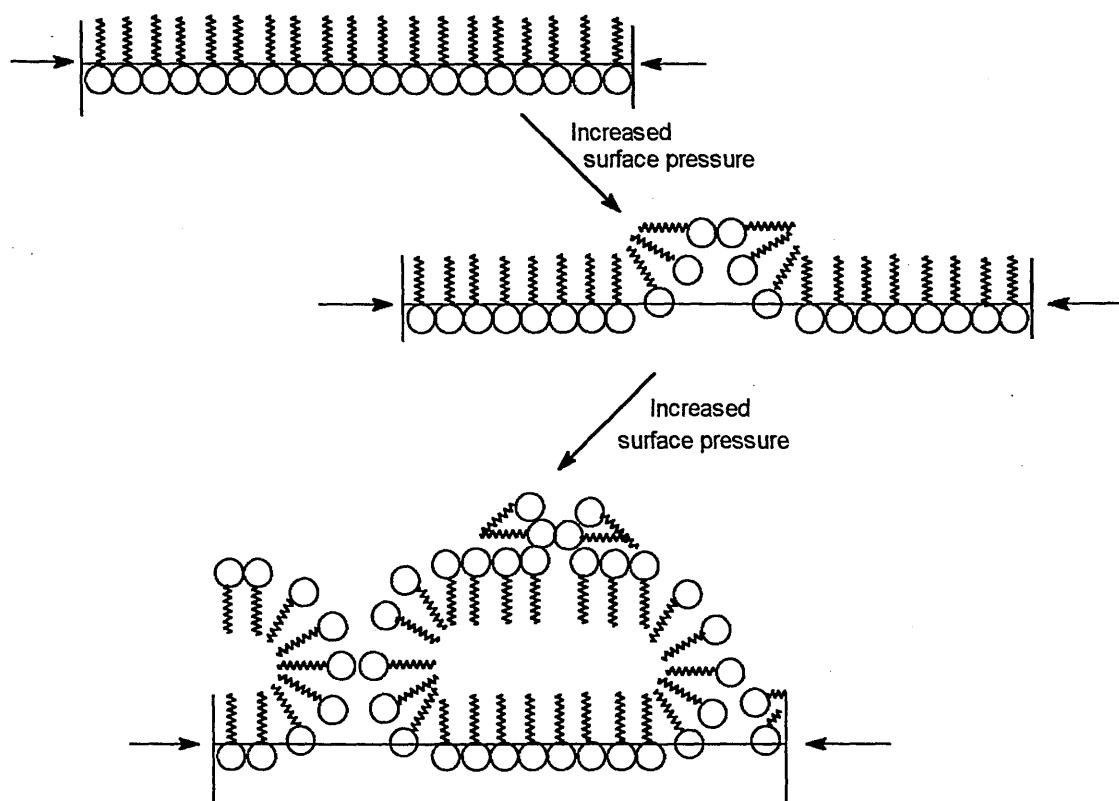
Figure 4.05 Collapse of the monolayer.

4.4 Surface pressure measurement

Surface pressure in the trough can be measured by a number of techniques, including that of a sensitive micro balance linked to a piece of filter paper - the Wilhelmy plate method.

The forces acting on the plate are gravity, surface tension downwards and the buoyancy due to the displaced water upwards.
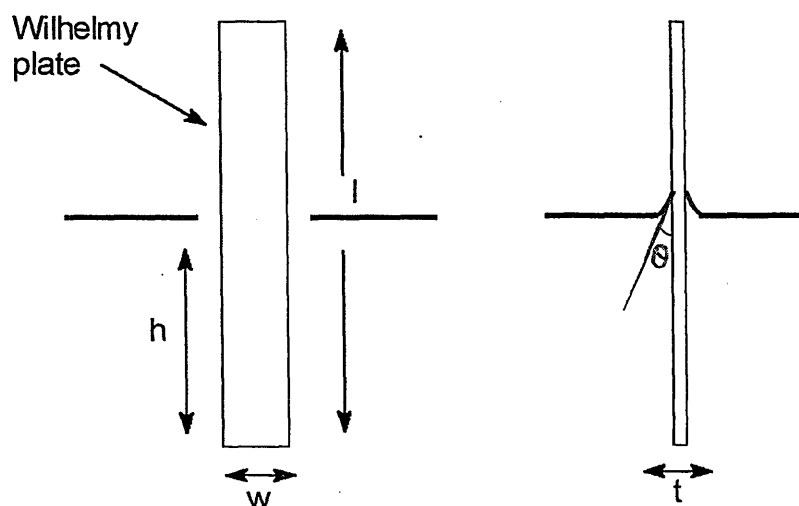
Fig 4.06 The Wilhelmy plate

From a consideration of figure 4.06 the plate has dimensions of l, w and t and is of density ρ_p, immersed to a depth h.

Therefore the net downward force is given by:-

$$F = \rho_p glwt - \rho_0 + 2y(t + 1) \cos\theta$$

Where y is the liquid surface tension, θ is the contact angle (usually zero, thus $\cos\theta = 1$), g is the gravitational constant and ρ_0 is the surface density. The surface pressure π is

generally considered to be equal to the reduction of the pure liquid surface tension by the film. The surface tension of pure water is 73 mN/m at 20°C and atmospheric pressure. This is an exceptionally high value compared to most other liquids and explains water's pre-eminence as a subphase.

So, $\pi = y_0 - y_1 = \delta y$, where y_0 is the surface tension of the pure liquid and y_1 is the surface tension of the liquid when covered with the film. The depth **h** and the plate dimensions remain constant and thus the first two terms in the above equation remain unchanged.

Therefore:-

$$\Delta F = 2(y_0 - y_1)(t+w)$$

If the plate is of negligible thickness and has a width of 1 cm then,

$$\Delta F = 2\Delta y$$

i.e., the weight measured in mgs is equal to twice the surface pressure in mN/m.

4.5 Langmuir-Blodgett film formation

Depending on the monolayer behaviour of a particular molecule, it is possible to extend these Langmuir film studies to the study of Langmuir-Blodgett films. When a suitable solid substrate is passed through the monolayer, in a controlled fashion the material can attach itself to the substrate by a number of mechanisms. Subsequent layers can be successively deposited to build up a multilayered structure - a Langmuir-Blodgett film (Figure 4.07). The transfer ratio will give an indication of how well the material is being deposited and also the type of film structure that is being produced. The transfer ratio η is defined as:

$$\eta = \frac{\text{Decrease in area of subphase covered by film}}{\text{Area of substrate covered by the monolayer}}$$

This leads to several deposition types (Figure 4.08):-

If η up = 0, η down = 1, then deposition type = X

If η up = 1, η down = 1, then deposition type = Y

If η up = 1, η down = 0, then deposition type = Z

Figures 4.07 , 4.08 and 4.09 show a deposition process and resultant LB structure possibilities respectively.

UP DOWN UP
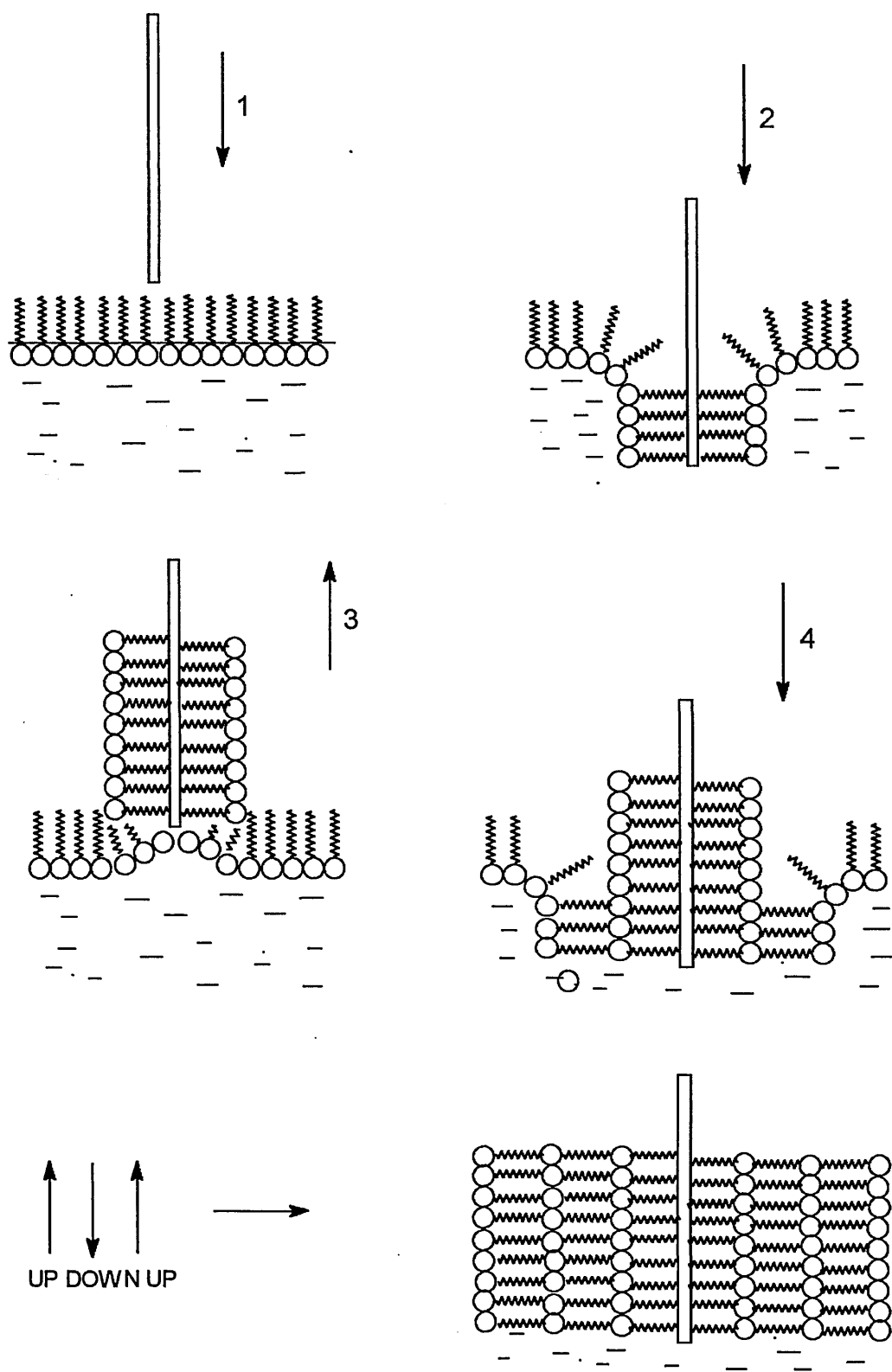
Figure 4.07 An example of X-type deposition on a hydrophobic substrate
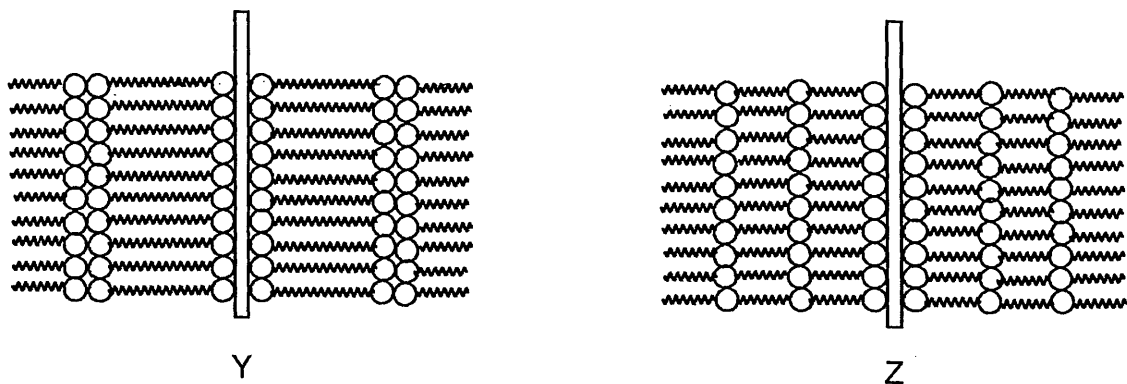
Figure 4.08 Examples of Y and Z type deposition on hydrophilic substrates
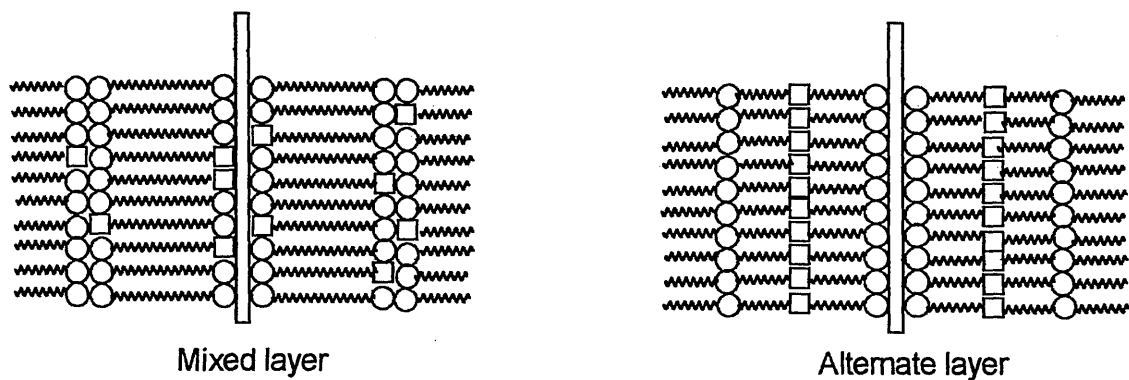
Figure 4.09 Examples of mixed and alternate layered film structures on hydrophilic substrates.

Another type of film deposition exists - the horizontal lifting technique, where the substrate is held horizontally and lowered into the monolayer from above

4.6 Materials

As well as the "classic" monolayer forming materials such as stearic acid/arachidic acid etc. , many other materials are able to be fabricated into LB films. Derivatives of long chain fatty acids with double bonds incorporated into them have been extensively studied, for example ω-tricosenoic acid [56] polymerises when exposed to an electron beam.[25] These films show excellent thermal and mechanical stability. Diacetylenes can be easily polymerised by γ or uv radiation [57] yielding good quality Y-type LB films.[26]

In the last twenty years Langmuir-Blodgett research has moved on from studying naturally occurring fatty acids to investigating aromatic, heterocyclic and supramolecular materials and assemblies which have had implications in many fields of research.

From a synthetic point of view, it is relatively straight forward to add long hydrophobic chain groups to molecules that contain hydrophilic head groups to create an amphiphilic balance that will enable the material to be fabricated into an LB film. However attachments of long alkyl chains to molecules can severely undermine the stability of the materials and may even "dilute" their properties. More recently molecules containing much less aliphatic character have been fabricated into LB films. These have included porphryins [58] [27] and phthalocyanines [59],[28, 29] which have been extensively used as chemical sensors. Studies of these type of materials have shown that they generally produce films that have an imperfect structure compared to that of the `classic` LB film forming materials.

Much co-ordinated work on the structure property relationships in materials has been carried out. Perhaps the first schematic study of this type was carried out on anthracene derivatives[60] by scientists at Durham and ICI,[30] who systematically altered the

hydrophobic and hydrophilic groups of the material to produce LB films. Thus a conclusion from this work was that the size of the aliphatic chain could be reduced if polycyclic systems were incorporated into anthracene.

Replacing a carbon with a nitrogen in the benzene ring increases the molecules' hydrophilicity and subsequent quaternisation of the nitrogen creates a very effective polar head group. The pyridine ring system is relatively electron deficient and the surplus negative charge on the nitrogen gives the molecule a large dipole moment (2.3 D). For example the bispyridinium salt [61] has been deposited as mixed multilayers with stearic acid. The material has two positive charges on the hydrophilic head group with two hydrophobic chains and has been used for photo induced electron transfer processes.[31]

Cyanine[62] type dyes which contain two nitrogen heterocycles with positive charge delocalised between the two atoms have been extensively studied because of their interesting optical properties.[32, 33]

More recently still it has been shown that derivatives of many of the charge transfer complexes and salts mentioned earlier in Chapter 1 can be fabricated into LB films. TCNQ-pyridinium salts [63][34] with long alkyl chain R groups were fabricated into films which exhibited conductivities of $\sigma_{rt} = \sim 10$ Scm^{-1} when doped with iodine. By 1986 TTF-TCNQ type films [64] were fabricated by Japanese scientists[35] which undoped had conductivities approaching $\sigma_{rt} = 10^{-2}$ Scm^{-1}. An example of a TTF-TCNQ derivative film [65] which exhibited a decrease in conductivity from $\sigma_{rt} = 10^{-3}$ Scm^{-1} to $\sigma_{rt} = 10^{-6}$ Scm^{-1} when doped with iodine is known.[36] This decrease was attributed to molecular re-orientation within the film caused by the iodine. Doped TTF neutral films [66][37] have been prepared where the dopant does not affect the orientation of the film. However it slowly

becomes semi-conducting when the TTF molecules become fully oxidised and the iodine is released, forming a mixed valence conducting state.

Organometallic films such as Au(dmit)$_2$ [67][38] have been fabricated from a 50% icosanoic acid solution using the horizontal lift technique, which exhibited high conductivity - σ_{rt} = 25 Scm^{-1} when doped with Br$_2$.

[56] $CH_2 = CH - (CH_2)_{20} C\overset{O}{\underset{OH}{}}$

[57]

[58]

[59]

[60]

[61] $C_{18}H_{37}$—N⊕ =⟨pyridinium⟩—⟨pyridinium⟩—N⊕—$C_{18}H_{37}$

2 X⊖

[62] ⟨indoline⟩—CH=CH—CH=⟨indoline⟩

$C_{18}H_{37}$ $C_{18}H_{37}$

X⊖

[63] ⟨pyridinium⟩
R

NC, CN, ⊖, NC, CN

[64] Me—S, S—Me

Me—S, S—Me

NC, CN, NC, CN

$C_{18}H_{37}$

[65] ⟨dithiole⟩ OH—$C_{17}H_{35}$

NC, CN, NC, CN

[66] ⟨dithiole⟩—O—$C_{15}H_{31}$

[67] $\left[S=\overset{\displaystyle S}{\underset{\displaystyle S}{\diagup}}\overset{\displaystyle S}{\underset{\displaystyle S}{\diagdown}}Au\overset{\displaystyle S}{\underset{\displaystyle S}{\diagup}}\overset{\displaystyle S}{\underset{\displaystyle S}{\diagdown}}=S \right]^{-}$ $MeN^{+} (C_{10}H_{21})_3$
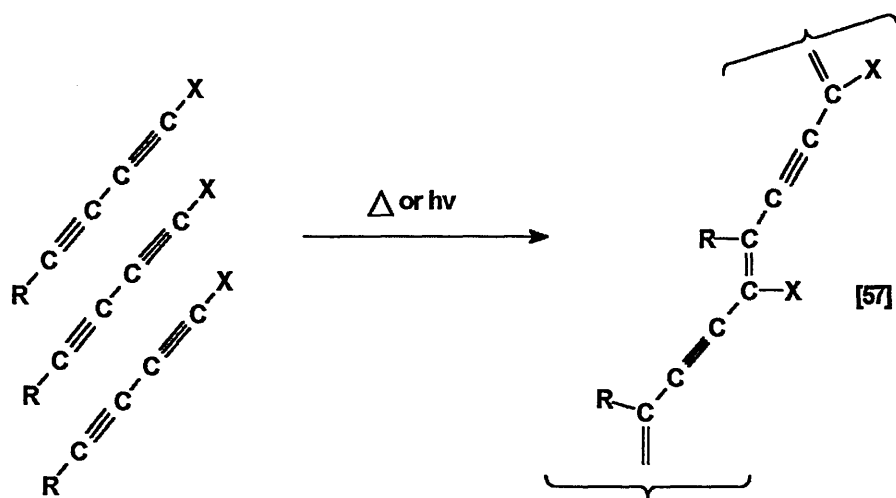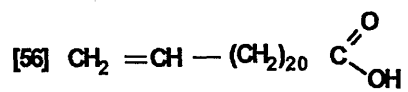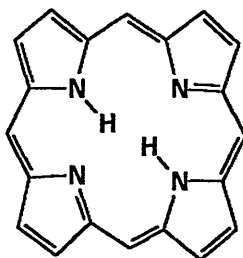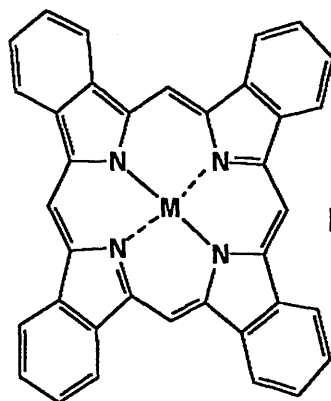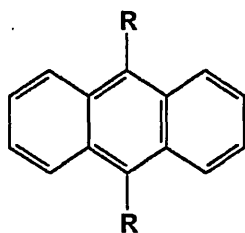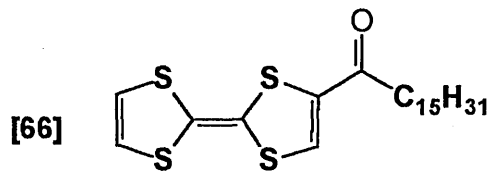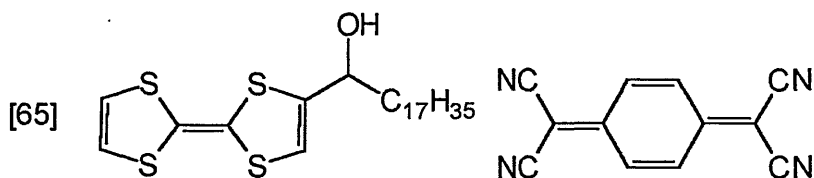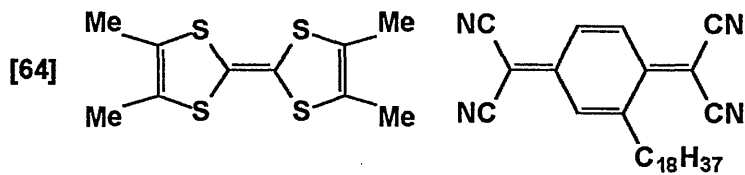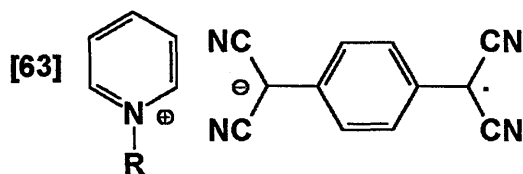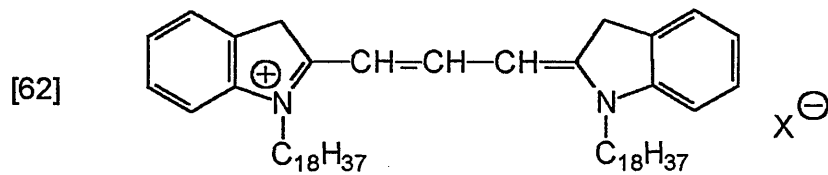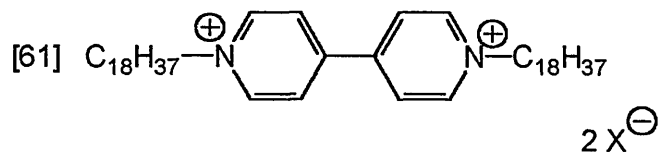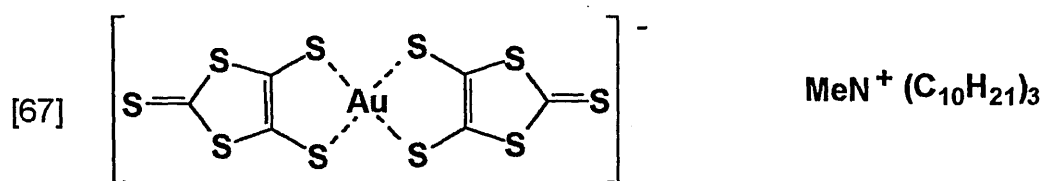
4.7 Applications

The first potential commercial applications of LB films were recognised by Katherine Blodgett who published and patented a number of possible devices; these included anti-reflection coatings on glass,[35-39] whereby the refractive index of the glass was lowered using skeletonised LB films of cadmium arachidate to reduce the effect of glare. Further work on skeletonised films included Blodgett patenting a step gauge device to determine film thicknesses.[40]

However, in the fifty years since the above work was published many potentially good ideas have appeared in many fields using LB films but not one commercially viable device or application is available. One of the main problems at present is that the technology does not really exist to enable the fabrication of films in viable quantities to justify commercial exploitation. Also the reproducibility and stability of known and unknown materials is difficult to control. However because the scope for producing suitable organic materials is virtually endless along with the elegance and great control this technique yields, it can only be a matter of time before a suitable application is exploited.

Much fundamental LB work has concentrated on biological systems, as in essence LB films mimic biological cell membranes - a cell membrane can consist of phospholipids (amphiphilic molecules), carbohydrates and proteins.[41] Photophysical research has seen Kuhn et al[42] study fluorescence from mixed monolayers containing synthetic dye molecules in a fatty acid matrix. Yoshikawa et al[43] used monomolecular layer assemblies of donor and acceptor molecules to `harvest' light energy, by a process of electron transfers used to produce oxygen. There has also been a lot of interest in immobilising biological molecules including enzymes and proteins which can bind specific ions or molecules, with a resulting change in physical or chemical properties, which may then be used in the development of biological sensors.[44]

Other work has involved the use of LB films as micro lithographic positive and negative resists.[45] As integrated circuit technology is constantly developing with components becoming smaller and smaller, plus the need for faster and greater memory storage increasing, techniques for patterning components on semiconducting wafers is constantly changing. Photolithographic techniques are being replaced by X-rays, electron and ion-beams. Very thin resists are a useful way of reducing scattering of substrate material when electron and ion-beams are used. Very good resolution has been achieved using fatty acids and also ω-tricosenoic acid which polymerises when irradiated.

LB films also make excellent insulators and there has been much research into field effect semiconductors.[46] They may also find use as active insulators on compound semiconductors.[47]

Their potential, as lubricants, has long been known from Lord Rayleigh's work. Seto et al,[48] found that 7 layers of barium stearate would reduce the friction between a cobalt magnetic tape and the recording head. Bowden et al[49] have also carried out research into

the lubrication effects of LB films where the sliding friction between two monolayers was studied using molecularly smooth mica substrates.

4.8 Zwitterionic TCNQ adducts

During this project the vast majority of Langmuir-Blodgett film work was directed towards analogues of the synthesised TCNQ adducts (see chapter 2). LB films of these systems were first prepared at Sheffield Hallam University in the 1980s.[50, 51] Ashwell et al[52-57] further developed this field to encompass the non-linear optical aspects hinted at in the earlier publications. The interest in these materials stems from their highly polarised `push-pull' nature deriving from their donor-pi-acceptor structure (see Chapters 1 and 2). This behaviour gives the films of these materials many possible applications in the electronics industry; these include second harmonic generation,[52-54] photochromism[53,54] and molecular rectification[55-57].

Langmuir-Blodgett films of the R(4)Q3CNQ systems where (R is an alkyl chain length of 8 to 20 carbon units) have been studied.[50-52] An abrupt change in film behaviour occurs where alkyl chain length is greater than 14 carbon atoms (see table 4.01).

R	Area per molecule (Å^2)	λ_{max} (nm)	HWHM (nm)
C_8H_{17}	32	616	37±2
C_9H_{19}	30	617	37±2
$C_{10}H_{21}$	34	616	37±2
$C_{11}H_{23}$	30	616	37±2
$C_{12}H_{25}$	30	613	37±2
$C_{13}H_{27}$	31	615	37±2
$C_{14}H_{29}$	31	615	37±2
$C_{15}H_{31}$	40	561	22±2
$C_{16}H_{33}$	44	565	22±2
$C_{18}H_{37}$	42	565	22±2
$C_{20}H_{41}$	48	565	22±2

Table 4.01 A table showing the area per molecule, λ_{max} and half width at half maxima (HWHM) observed in LB films of R(4)Q3CNQ analogues. Note a sharp change in the parameters when R > $C_{14}H_{29}$[51].

The reason for this dramatic change in behaviour is not clear but the molecular orientation of these molecules appears to play a part. They have an orientation that lies between the perpendicular (area per molecule is approximately 100 Å^2) and being completely parallel (area per molecule is approximately 20 Å^2) to the subphase; thus the molecules suddenly adopt a more parallel orientation with this increase in chain length.

These materials were considered to form predominantly Y-type film structures.[50,51]

However Ashwell et al found $C_{16}H_{33}(4)Q3CNQ$ to orientate itself in a Z-type manner, from scanning tunnelling microscopy which revealed an array of negatively charged - $CN(CN)_2$ groups.[59] This non-centrosymmetric structure is actually partially stabilised by Coulomb repulsion which would theoretically repel if there was a totally Y-type (centrosymmetric) structure.

This predominantly non-centrosymmetric alignment is an important condition for second harmonic generation and the molecular orientation within the film structure has been seen to be influenced by the alkyl chain lengths.[51,58] It has been found that films produced from shorter chain homologues of $C_n \leq 14$, not only exhibit a large bathochromic shift in their visible absorption spectra (λ_{max} = 615nm ± 2, HWHM = 37±2 nm for $C_8H_{17}(4)$-Q3CNQ to $C_{14}H_{29}(4)$-Q3CNQ) and smaller area per molecule (30Å² ±4 for $C_8H_{17}(4)$-Q3CNQ to $C_{14}H_{29}(4)$-Q3CNQ) but also show a weak second order susceptibility ($\chi_{zzz}^{(2)}$ = 6 pm V⁻¹ for $C_{10}H_{21}(4)$-Q3CNQ). This is believed to be due to anti parallel arrangements of chromophores within the Langmuir film and also in the deposited LB film or a change in their molecular tilt.[51,53,58]

The molecular orientation alters in films where $C_n \geq 15$ (λmax =565 ±3 nm, HWHM = 22± 1 nm and area per molecule of 40 - 48Å² for $C_{15}H_{31}(4)$-Q3CNQ to $C_{20}H_{41}(4)$-Q3CNQ). These films also exhibit a much greater second order susceptibility, $\chi_{zzz}^{(2)}$ = 180 pm V⁻¹ in 200+ layer films of $C_{16}H_{33}(4)$-Q3CNQ.[53] The molecular alignment in films of $C_n \geq 15$, is predominantly non-centrosymmetric where the Z-type structure of the film is stabilised by the negative charge on the terminal dicyanomethanide group. However these materials can be deposited as predominantly Y-type structures[51] and it is thought some reorganisation takes place during deposition to reduce the coulombic repulsion of a totally Y-type structure.

LB films of these materials exhibit photochromism, and possess narrow, switchable charge

transfer bands and thus maybe suitable for use in a multifrequency optical memory.[54,55]

Also, monolayers and multilayers of $C_{16}H_{33}(4)$-Q3CNQ sandwiched between platinum

and magnesium electrodes exhibit asymmetrical current-voltage characteristics and this

behaviour is ascribed to molecular rectification.[55, 56] Further work[57] demonstrated that

the transition of the ground state zwitterion to an excited-state of a neutral conformer is

responsible for rectification of the multilayered LB film between two aluminium

electrodes. The intramolecular tunnelling in a monolayer is consistent with the modified

Aviram-Ratner mechanism.[60-62]

4.9 Chapter Four References

1.   D. Tabor, *J. Colloid. Interface Sci.* , **75**, 240, 1980.

2.   G. D. Fulford, *Isis,* **59**, 198, 1968.

3.   J. C. Scott in *"History of Technology"* (A. R. Hall and N. Smith, eds.), **3**, 163, Mansell, London, 1978

4.   B. Franklin, *Philos. Trans. R. Soc.* London. , **64**, 445, 1774.

5a.   J. Shields, British Patent 3490, 1879; cf. US. Patent 289720, 1883 and US. Patent 334295, 1886.

5b.   J. Shields, British Patent 1112 (1882); cf. French Patent 148160 (1882)

6a.   C. H. Giles and S. D. Forrester, *Chem. Ind.* (London), 80, 1970.

6b.   C. F. Gordon Cumming, *The 19th Century*, **11**, 572, 1882.

6c.   Hansards' Parliamentary Debates, 3rd series, 273, cols. 6-15, Corrielius Buek, London, 1882.

7.   J. Aitken, *Proc. R. Soc.* Edinburgh, **12**, 56, 1882-1884

8.   C. H. Giles and S. D. Forester, *Chem. and Ind.* London. , **43**, 1971.

9.   Lord Rayleigh, *Proc. R. Soc.* London. , **47**, 364, 1890.

10a.   S. D. Forrester and C. H. Giles, *Chem. and Ind.* London, 469, 1979.

10b.   Lord Rayleigh, *Proc. Lond. Math. Soc.* , **10**, 4, 1879.

10c.   Lord Rayleigh, *Proc. R. Soc.* London, **28**, 406, 1879.

11a.   Lord Rayleigh, *Proc. R. Soc.* London, **47**, 281, 1890.

11b.   Lord Rayleigh, *Proc. R. Soc.* London, **47**, 364, 1890.

11c.   Lord Rayleigh, *Proc. R. Soc.* London, **13**, 85, 1890.

11d.   Lord Rayleigh, *Proc. R. Soc.* London, **48**, 127, 1890.

11e.   Lord Rayleigh, *Philos. Mag.* , **30**, 386, 1890.

12a.   A. Pockels, *Nature* (London), **43**, 437, 1891.

12b.   A. Pockels, *Nature* (London), **46**, 418, 1892.

12c.   A. Pockels, *Nature* (London), **48**, 152, 1893.

13a.   W. B. Hardy, *Proc. R. Soc.* London, Ser. A, **86**, 610, 1912.

13b.   W. B. Hardy, *Proc. R. Soc.* London, Ser. A, **88**, 303, 1913.

13c.   W. B. Hardy, *Collected Scientific Papers,* 508, 550, Cambridge University Press, 1939.

14a.   H. Devaux, *Kolloid-2.* , **58**, 260, 1932.

14b.   H. Devaux, *Annu. Rep. Smithsonian Inst.* , 261, 1913.

15a.   I. Langmuir, *J. Am. Chem. Soc.* , **39**, 1848, 1917.

16a.   K. B. Blodgett, *J. Am. Chem. Soc.* , **56**, 495, 1934.

16b.   K. B. Blodgett, *J. Am. Chem. Soc.* **57**, 107, 1935.

17.   K. B. Blodgett, *Phys. Rev.* , **51**, 964, 1937.

18.   K. B. Blodgett, *Physical Review*, **55**, 391, 1939.

19.   K. B. Blodgett, *Rev. Sci. Instrum.* **12**, 10, 1941.

20a.   H. Kuhn, *Pure Appl. Chem.* , **11**, 345, 1965.

20b.   H. Bucher, K. H. Drexhage, M. Fleck, H. Kuhn, D. Mobius, F. P. Schafer, J. Sondermann, W. Sperling, P. Tillmann and J. Wiegand, *Mol. Cryst.* , **2**, 199, 1967.

20c.   H. Kuhn, D. Möbius and H. Bucher, *Physical Methods in Chemistry*, **1**, 577, 1972

21.   G. L. Gaines Jr. , "*Insoluble Monolayers at Liquid Gas Interfaces*", Wiley, New York, 1966.

22.   W. Adamson, "*Physical Chemistry of Surfaces*", 4th edition, Wiley, New York, 1982.

23.   A. J. Walton, "*Three Phases of Matter*", McGraw-Hill, Maidenhead, 1976

24.   H. E. Ries, Jr. and W. A. Wimball, *J. Phys. Chem.* , **59**, 94, 1955

25.   A. Baraud, C. Rosilio and A. Raude-Texier, *J. Colloid Interface Sci*, **62**, 509, 1977.

26.   B. Tieke, H. J. Graf, G. Wegner, B. Naegele, H. Ringsdorf, A. Banerjie, D. Day and J. B. Lando, *Colloid Polym. Sci.*, **255**, 521, 1977.

27.   R. H. Tredgold, S. D. Evans, P. Hodge, R. Jones, M. G. Stocks and M. C. J. Young, *Brit Polym J*, **19**, 397, 1987.

28.   S. Baker, M. C. Petty, G. G. Roberts and M. U. Twigg, *Thin Solid Films*, **99**, 53, 1982.

29.   H. Laurs and G. Heiland, *Thin Solid Films*, **149**, 129, 1987.

30.   P. S. Vincent, W. A. Barlow, F. T. Boyle, J. A. Finney and G. G. Roberts, *Thin Solid Films*, **60**, 265, 1979.

31.   D. Mobius, Ber. Bunsenges. *Phys. Chem.*, **82**, 848, 1978.

32.   H. Kuhn, *Pure Appl. Chem.*, **51**, 341, 1979.

33.   D. Mobius, *Acc. Chem. Res.*, **14**, 63, 1981.

34.   A. Barraud, P. Lesieur, A. Ruaudel-Teixier and M. Vanddevyver, *Thin Solid Films*, **133**, 125, 1985.

35.   M. Fujiki and H. Tabei, *Synth. Metals*, **18**, 815, 1987.

36.   A. S. Dhindsa, C. Pearson, M. R. Bryce and M. C. Petty, *J. Phys. D. Appl. Phys.*, **22**, 1586, 1989.

37.   A. S. Dhindsa, M. R. Bryce, J. P. Lloyd and M. C. Petty, *Thin Solid Films*, **165**, L97, 1988.

38.   T. Nakamura, K. Kojima, M. Matsumoto, H. Tachibana, M. Tanaka, E. Manda and Y. Kawabata, *Chem. Lett.*, 367, 1989.

39a.   K. B. Blodgett, U. S. Patent 2, 220, 860, 1940

39b.   K. B. Blodgett, U. S. Patent 2, 220, 861, 1940.

39c.   K. B. Blodgett, U. S. Patent 2, 220, 862, 1940

40.   K. B. Blodgett, U. S. Patent 2, 587, 282, 1952.

41. N. P. Franks and K. A. Snook, *Thin Solid Films*, **99**, 139, 1983.

42. H. Kuhn, *Pure Appl. Chem.*, **51**, 341, 1979.

43. K. Yoshikawa, M. Mahino, S. Nakata and T. Ishii, *Thin Solid Films*, **180**, 117, 1989.

44. For example:- T. Morizumi, *Thin Solid Films*, **160**, 413, 1988.

45a. M. Vekita, H. Awaji, M. Murata and S. Mizuma, *Thin Solid Films*, **180**, 271, 1989.

45b. H. Kato, M. Tawata, S. Morita and S. Hattori, *Thin Solid Films*, **180**, 299, 1989.

46. For example:- G. L. Larkins Jr. , C. D. Fung and S. E. Richert, *Thin Solid Films*, **180**, 217, 1989.

47. J. P. Lloyd, M. C. Petty, G. G. Roberts, P. G. Lecomber and W. E Spear, *Thin Solid Films*, **99**, 297, 1982

48. J. Seto, T. Nagai, C. Ishimoto and H. Watanabe, *Thin Solid Films*, **134**, 101, 1985.

49. F. B. Bowden and D. Tabor, *Proc. R. Soc.* London, Ser. A, **169**, 371, 1939

50. N. A. Bell, R. A. Broughton, J. S. Brooks, T. A. Jones and S. C. Thorpe, *J. Chem. Soc. , Chem. Commun.* , 325, 1990.

51. N. A. Bell, R. A. Broughton, J. S. Brooks, T. A. Jones and S. Thorpe, *Int. J. Electronics*, **76**, 5, 751, 1994.

52. G. J. Ashwell, E. J. C. Dawnay, A. P. Kuczynski, M. Szablewski, I. M. Sandy, M. R. Bryce, A. M. Grainger and M. Hasan, *J. Chem. Soc. , Faraday Trans.* , **86**, 1117, 1990.

53. G. J. Ashwell, E. J. C. Dawnay and A. P. Kuczynski, *J. Chem. Soc. , Chem. Commun.* , 1355, 1990.

54. G. J. Ashwell, *Thin Solid Films*, **186**, 155, 1990.

55. G. J. Ashwell, J. R. Sambles, A. S. Martin, W. G. Parker and M. Szablewski, *J. Chem. Soc. , Chem. Commun.* , 1374, 1990.

56.   A. S. Martin, J. R. Sambles and G. J. Ashwell, *Thin Solid Films,* **210**, 313, 1992.

57.   R. B. Metzger, B. Chen, U. Hopfner, M. V. Lakshmikantham, D. Vuillaume, T. Kawai, X. Wu, H. Tachibana, T. V. Hughes, H. Sakurai, J. W. Baldwin, C. Hosch, M. P. Cava, L. Brehmer and G. J. Ashwell, *J. Am. Chem. Soc.* , **119**, 10455, 1997.

58.   G. J. Ashwell, G. Jefferies, E. J. C. Dawnay, A. Kuzynski, D. E. J. Lynch, Y. Gongda and D. G. Bucknall, *J. Mater. Chem.* , **5**, 975, 1995.

59.   X-L. Wu, M. Shamsuzzoha, R. M. Metzger and G. J. Ashwell, *Synth. Met.* , 55-57, 3836, 1993

60a.   A. Aviram and M. A. Ratner, *Bull. Am. Phys. Soc.* , **19**, 341, 1974.

60b.   A. Aviram and M. A. Metzger, *Chem. Phys. Lett.* , **29**, 277, 1974.

61.   R. M. Metzger and C. A. Panetta, *Synth. Met.* , **28**, 807, 1989.

62.   R. M. Metzger, *Advances in Chem. Series,* **240**, 81, 1994.

CHAPTER 5

Langmuir-Blodgett Films - Experimental

5.1 The Langmuir-Blodgett trough

The films produced in this work were fabricated using two different designs of trough:-

1. The Joyce-Loebl Langmuir Trough 4 (section 5.1.1)

2. The Nima 622d (section 5.1.2)

5.1.1 The Joyce-Loebl Langmuir Trough 4

The initial work in this thesis was performed using this design. An important feature of this trough is the PTFE coated, constant perimeter glass fibre barrier used to control the surface area (fig 5.01). Enclosing the monolayer between a continuous band minimises the

problem of contamination and film leakage. The subphase is contained in a thick glass

trough, clamped into position and sealed with PTFE end plates. The compression barrier

(the PTFE belt) is held by a system of six PTFE rollers which are secured by two mobile

overarms. These overarms are moved symmetrically inwards or outwards by means of a

highly geared motor and thus the PTFE barrier is kept taut.

The trough (Figure 5.02) is based on a design developed by scientists at ICI and Durham

University using an idea by Blight et al.[1]
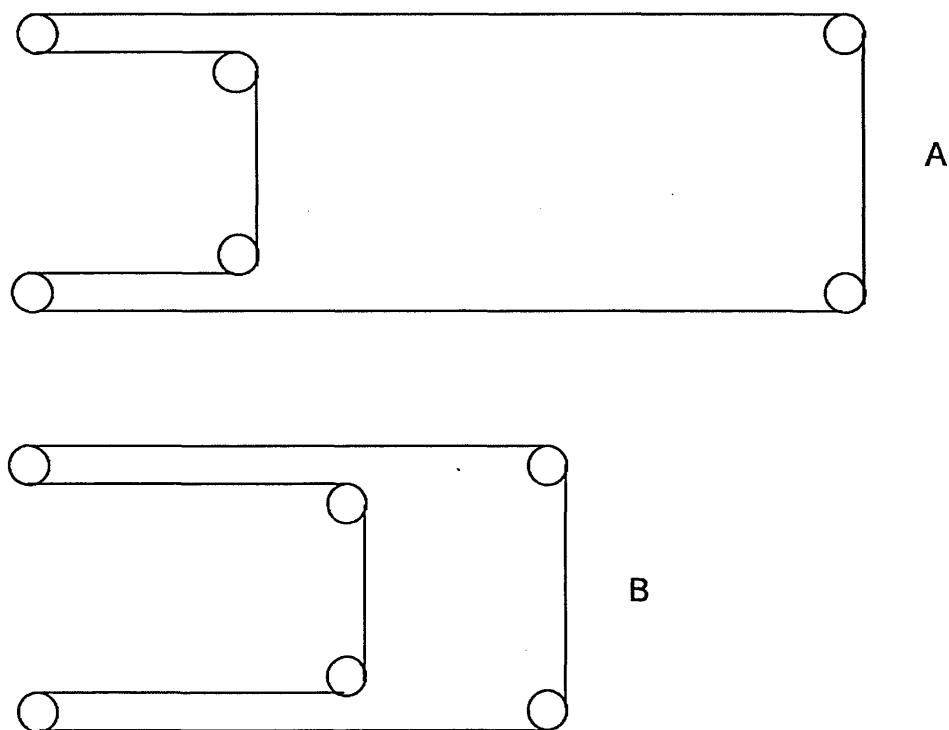
Figure 5.01 Maximum (A) and minimum (B) area configurations of the constant perimeter PTFE

        glass fibre barrier which defines the working area of the air/water interface, found in

        the Joyce Loebl 4 trough.
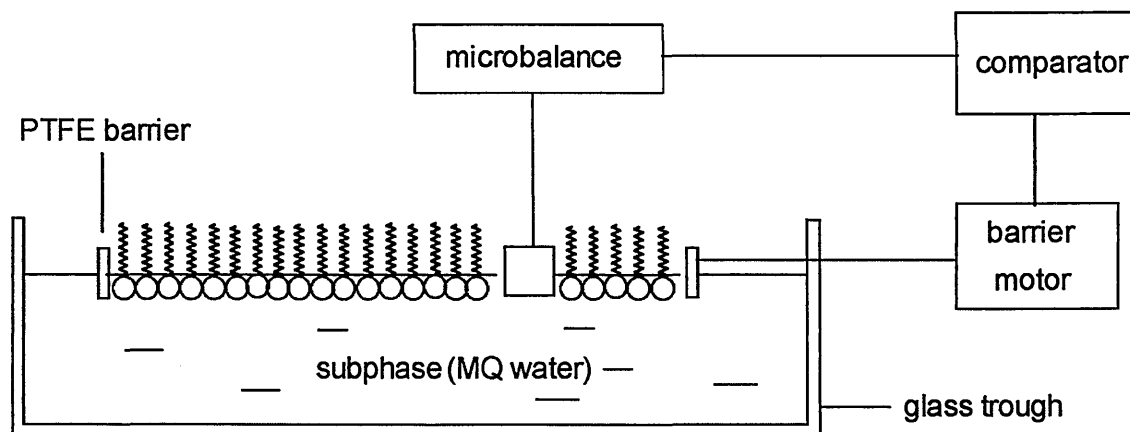
Figure 5.02 Schematic diagram of the features of a Joyce Loebl 4 trough.

5.1.2 Nima 622D Trough

Towards the later stages of this work, this particular trough (Fig 5.03) was used inside a class 100 clean room. The experiments and cleaning procedures were essentially the same as those performed on the Joyce-Loebl trough. This trough and barriers were fabricated from polytetrafluoroethylene (PTFE), as this polymer is essentially inert. Thus it will not leach plasticiser and it is also the most hydrophobic polymer available. The trough was subjected to very rigorous cleaning procedures. The subphase capacity of the this trough-1500mls, was much less than the Joyce-Loebl model (5000mls) reducing the demand for ultra-pure de ionised water, making cleaning quicker and easier and most importantly reducing the risk of contamination.

Because of the smaller surface area available on the Nima trough, experiments were modified slightly as only 10-12 layers could be deposited in any one experiment. This is

compared to approximately 40 layers on the Joyce-Loebl trough. In practice this meant

that the experiment had to be stopped, the barriers reopened and more material applied.

The class 100 clean room environment for this trough provides for idealised conditions for

film preparation as external contamination was at a minimum.
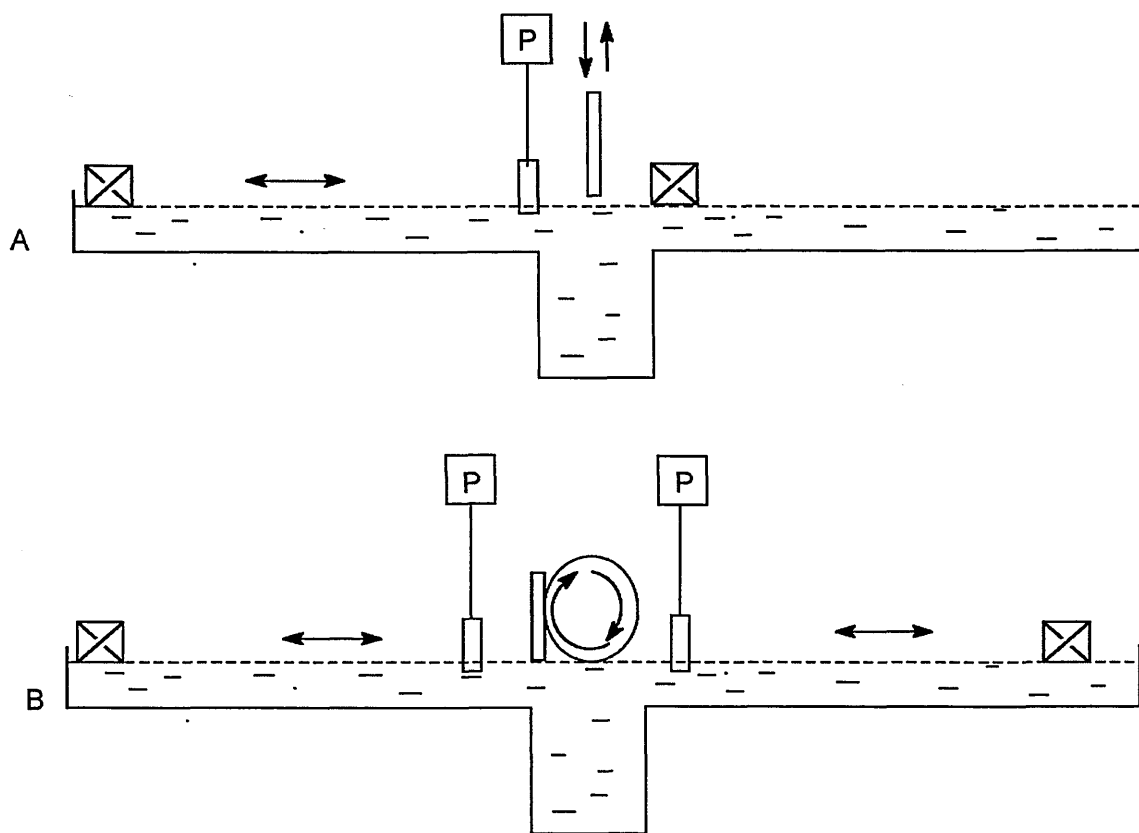
Figure 5.3 The Nima 622D type trough in a conventional set-up with one pressure sensor -A, and in

an alternate layer set-up, with two pressure sensors - B. This trough is much smaller than

the Joyce Loebl having a dipping well, with the trough itself and the barriers being made

from PTFE.

5.2 Surface Area Calibration

Before any detailed experiments were carried out, all separate instruments:- pH meter, micro balance, MQ water system, chart recorder and the trough - were calibrated according to manufacturers instructions. For reproducible isotherms and area per molecule data, the maximum and minimum surface area of the trough had to be known accurately. The approximate values for the Joyce Loebl trough were $1000cm^2$ and $100cm^2$ respectively. Because the speed at which the barrier is moving prior to attaining the maximum and minimum areas affects exactly when the micro switches trip, the speed used for the area calibrations was that at which the isotherm measurement takes place.

5.3 Surface Pressure Calibration

The micro balance is calibrated using standard weights and then the surface pressure is related to the micro balance reading using the dimensions of the Wilhelmy plate - if the plate used is 1cm wide, of negligible thickness and has a zero contact angle with the surface, then a 2mg weight will correspond to a surface pressure of 1 mN/m(see Section 4.4).

5.4 The Subphase

In all the experiments carried out in this work, water was used as the subphase, although it is possible to use other subphases such as glycerol or to add ions like the divalent Cd^{2+} in the form of $CdCl_2$ to stabilise certain films. Because the water had to be of the highest purity and quality, the quantity of particles, ions and surface active materials had to be kept to a minimum. The water was first distilled and then purified using a Millipore water "Milli-Q" water system which fed low resistivity water - 18 mega ohms, directly into the trough when required. The millipore system makes use of an initial reverse osmosis stage

followed by a system of "polishing" filters which ultimately remove contaminants at the biological level and then ion-exchange units which remove any unwanted ions from the water. Fresh water was produced for every experiment.

5.5 Preparation and Cleaning Procedures

5.5.1 Trough and Subphase

For reproducible results, the level of surface and subphase contamination had to be kept to a minimum. Before and between experiments the trough was rigorously cleaned. For this purpose organic solvents were used in small quantities. First, the trough was wiped using a `dust` free tissue with chloroform (Aristar grade), then with isopropyl alcohol (Aristar grade) and then the trough was washed out twice more with MQ water. The trough was then filled with fresh MQ water. Before any monolayer material was spread the subphase surface had to be cleaned. This was routinely done by using a Pasteur pipette attached to a self priming water pump and literally `sucking` off the top subphase layer, thus removing any fibres or surface active contaminants that are present. To check the quality of the subphase the barrier on the trough was set to the maximum surface area, the micro balance was then zeroed and then the surface was compressed until the minimum configuration was reached. Any surface contamination manifested itself as an increase in the surface pressure. If the surface pressure increased by more than 0.1 mN/m, the cleaning process was repeated until it was satisfactory.

This cleaning technique has however been criticised by Albrecht[2], who stated that any system that cannot be closed to give an absolute zero, could have an area left that on

compression would show contamination. This problem can be overcome by spreading a material that has been well characterised e.g. stearic acid and observing any deviations from the standard isotherm, though in practice this would just prove time consuming, as the cleaning process would have to be started again to remove the unwanted stearic acid.

5.5.2 Substrates

The quality of the first layer deposited on the substrate is critical as this determines the deposition properties of all the subsequent layers. Defects in the first layer can be passed through to subsequent layers. Therefore thorough cleaning of the substrates is crucial. Microscope slides were used as the basic substrates in all experiments. Standard BDH and Dow Corning microscope slides were used for the majority of the experiments as well as unwashed (removed from the manufacturing process before cleaning with detergents) microscope slides. All cleaning solvents used were Aristar grade.

The substrates were initially wiped with Kimberley-Clarke "Kimwipe" surfactant-free tissues soaked in dichloromethane to remove any larger contaminants. The slides were then washed in isopropyl alcohol and then de-ionised water. The slides were then left to soak for at least 24 hours in the strong oxidising agent chromic acid to remove further grease and other surface active agents. Further rinsing followed with de-ionised water and dichloromethane or chloroform, followed by cleaning in boiling IPA using a Soxhlet vessel and finally further rinsing in de-ionised water. The slides were then rendered hydrophilic by soaking the slides for 12 hours in a $1g.dm^{-3}$ sodium hydroxide solution, followed by a rinsing in ultra pure water and drying under a stream of white spot nitrogen.

Although hydrophilic substrates were predominantly used for the experiments, hydrophobic substrates were obtained by exposing the slides to a few drops of hexamethyl disilazane.

5.5.3 Metal Coating Of Slides

Gold, silver and aluminium were evaporated or sputter coated onto the clean slides for infrared and surface plasmon resonance studies using vapour deposition and plasma sputter coating techniques. Metal thicknesses of 100 to 200 nm were required for infrared and 40 to 50 nm for SPR experiments. Gold plating rendered the substrates hydrophobic and this had to be taken into account in SPR experiments

5.6 Monolayer Formation- Experimental

The monolayer was formed on the surface of the subphase by dissolving the material in a suitable solvent (see Table 5.01) and spreading the resultant solution dropwise (via a syringe) onto the water surface. Each drop was allowed to evaporate before the next was added and the drops were distributed evenly around the trough.

Table 5.01 Properties of a number of solvents used for LB work

Solvent	Melting point (°C)	Boiling point (°C)	Solubility in water (g/kg)
n- hexane	-94	69	0.01
cyclohexane	6.5	81	0.07
chloroform	-64	61	8
benzene	5.5	80	1.8
diethyl ether	-116	35	75
acetone	-93.4	56	∞
dichloromethane	-98	40	1.3

The volatility of the solvent is important because the evaporation time must be short but not too short that the concentration of the solution cannot be determined due to evaporation. The boiling point of any ideal solvent should lie in or near the range 40 - 80 °C.

Organic solvents such as acetone that are soluble in water were avoided as they can carry amphiphilic material into the subphase and cause the material to precipitate out. The use of such solvents meant the use of much more of the material to counteract the above effect. Thus accurate molecular area interpretation from using water soluble solvents would be impossible.

The spreading process once the drop of solution is on the subphase can occur in a number of ways. A thin film of material dissolved in the solvent usually forms immediately, whilst the Langmuir film forming material aligns itself at the air-water interface. The solvent evaporates leaving behind the monolayer. Sometimes the deposited droplet does not spread over the subphase but instead a thin film of dilute solution of monolayer forming material spreads from its edges; as solvent evaporates more film spreads from the droplet.

Spreading can continue until the surface pressure of the monolayer is equal to the `equilibrium spreading pressure`. When this point is reached, all the available surface is covered in monolayer. Any further attempts at adding more material will cause patches of undistributed material which can be clearly visible to the naked eye - to form on top of, or in, the monolayer. This undispersed material can be deposited as bulk aggregates if not removed.

5.7 Characterisation Experiments

5.7.1 Reflection Absorption Infrared Spectroscopy (RAIRS)

RAIRS (also known as external reflection spectroscopy (ERS) or grazing angle spectroscopy) is a surface selective infrared sampling technique and was used as a characterisation method for the LB films fabricated in this project. The geometry of an experiment is shown in Figure 5.04.
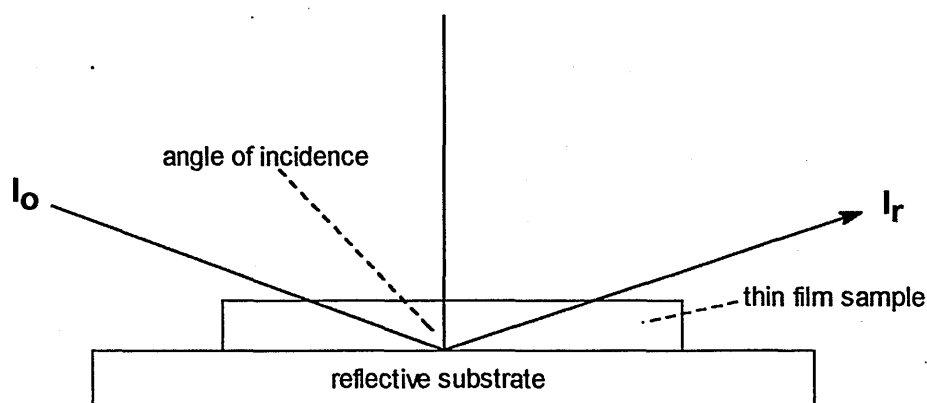
Figure 5.04 A schematic diagram of the geometry in a RAIRS experiment, where I_0 is the incident radiation and I_r is the reflected radiation

RAIRS is confined to thin sample films on totally reflective surfaces. Therefore LB films on gold, silver and alumina substrates provided good samples for this technique. RAIRS has been used for many years to characterise monolayers or multilayers.[3,4] RAIRS is highly sensitive to the angle of incidence, polarisation of the incident radiation and the orientation of the electric dipoles associated with the sample.

The principle advantage of this technique is the so called "metal surface infrared selection rule" [5,6] (Figures 5.05 and 5.06) which arises because of the different phase shifts experienced by s and p components of the incident radiation as a function of the incident angle. Light polarised with its electric vector perpendicular to the surface normal (TE or S polarised) results in a low intensity electric field at the film metal interface at all incident angles. This is because the electric field dipole and its image dipole are anti parallel and of equal magnitude (i.e. equal field strength). Thus this prevents absorption of TE polarised light by a molecule in a surface thin film.

Conversely however, light polarised with its electric field vector component parallel to the surface normal (TM or P polarised light) has a non zero electric field vector component perpendicular to the surface. This is maximised at the Brewster angle (ϕ) which is approximately 89.5° for aluminium, silver and gold. However, practically only angles of around 85° are possible. The Brewster angle is given by the following equation:-

$$SIN\phi.TAN\phi = \frac{\sqrt{2}}{1.05 \times 10^{-6} (v.\varepsilon.\rho)^{1/2}}$$

where ε is the dielectric constant

        v is the frequency of incident radiation

        ρ is the resistivity of the metal

The surface infrared selection rule states that only vibrating dipoles with a non zero component perpendicular to the substrate will be excited by TM polarised infrared radiation (see Figure 5.05). Hence this is a good method for the determination of the average orientation of molecules on a surface.

TM/p polarised

TE/s polarised

Reflective substrate
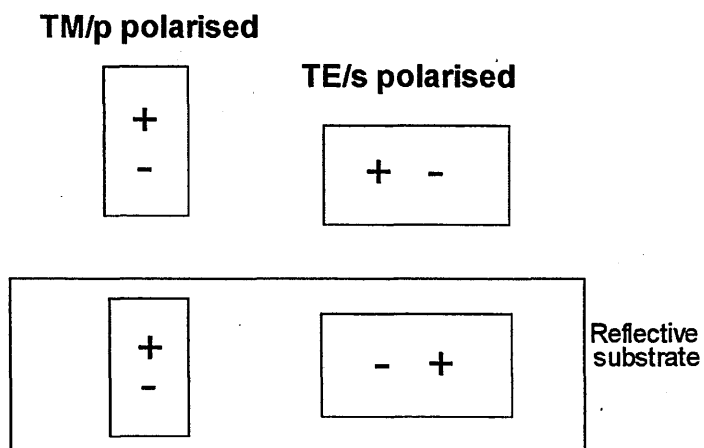
Figure 5.05 A schematic diagram of the infrared selection rule For TE/s polarised light in the

incident, its electric-field dipole and its image dipole cancel out. In contrast the dipole

has a non zero component normal to the surface in TM/ p polarised light. The larger the

incident angle, the larger the total electric field dipole for TM light (maximised at the

Brewster angle).
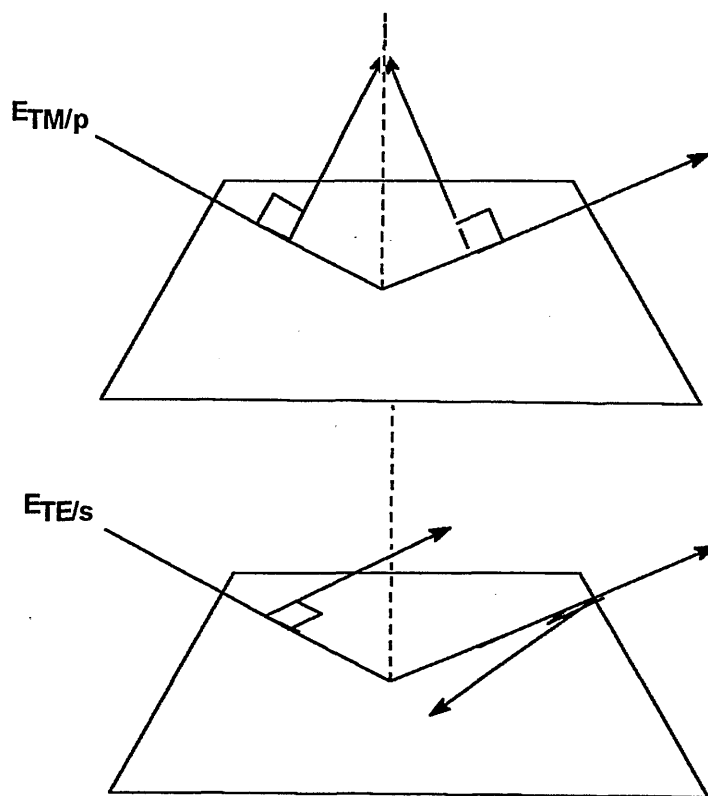
Figure 5.06 A schematic diagram of the incident and reflected vector geometries on the metal

surface at the grazing angle of incidence. There is no field at the surface for the

perpendicular component (TE) due to a 180° phase shift. However enhancement in the

parallel component (TM) due to a 90° phase shift is noted.

Unfortunately RAIRS suffers from signal to noise problems when compared against other infrared techniques such as ATR (attenuated total reflectance), as the thin organic films only contribute weak signals but the noise levels remain constant. RAIRS also only permits one reflection, whereas with ATR multiple reflections are possible, thus reducing the strength of the signal reaching the detector.

However signal to noise (S/N) problems can be reduced by filtering out the TE component of the infrared radiation. This is effective as the signal that is observed emanates from the interaction of the sample with the TM polarised infrared radiation and the only contribution that TE polarised light makes to the detector signal is noise.

Experiments were carried out on silver, aluminium and gold coated substrates prepared as previously mentioned (see Sections 5.5.2 and 5.5.3) coated with between 3 and 40 layers of selected quinolinium/picolinium zwitterions and N-alkyl pyridinium benzimidazolate betaine-TCNQ systems. The FTIR spectra were recorded on a Mattson Sirius 100 instrument with a polariser fitted.

5.7.2 Surface Plasmon Resonance

Further LB film characterisation was carried out using surface plasmon resonance (SPR). Surface plasma waves are electromagnetic waves which are collective oscillations of the free electrons at the interface of a metal (or a semiconductor) and a dielectric; their quanta are known as surface plasmons.

Surface plasmons may be excited by several methods but the most popular and the one used in this experimental work utilises the photon reflectance technique.[7] Resonance is observed by changing the angle of incidence of the light and measuring the amount of light reflected from the metal surface. Resonance occurs when the wave vector and frequency of the incident light coincide with those of the surface plasmon. The angle at which this resonance occurs is dependent on the wavelength of the light used and the refractive index of the glass, but it is typically in the region of 43°, which is above the critical angle.

The ATR (attenuated total reflectance) method was used, utilising a glass prism in the Kretchman configuration (Figure 5.07)[8] to create an inclined incident surface. The experimental principle was to coat the base of the prism with a thin evaporated layer of metal (e.g silver or gold) between 40 and 50 nm thick. For a particular value of the angle of incidence θ_i inside the prism, the tangential component of the wave vector of the evanescent wave matches that of the surface plasmon, which is thus excited. When the coupling is at an optimum the total incident energy is dissipated through diffusion of the plasmon wave in the metal. As a result of this the reflection coefficient falls to zero. This resulting dip in the reflection as a function of the incident angle is attributed to the surface plasmon resonance.
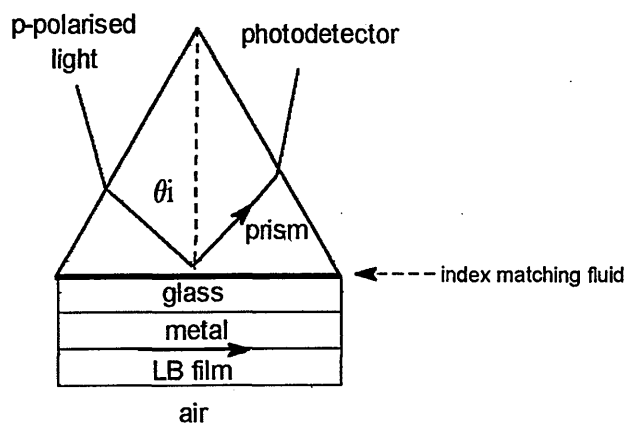

Figure 5.07 The Kretchmann configuration for observing SPR. The light can couple to the surface plasmons across the thin metal layer. The metal thickness (40-50 nm) must be thick enough to reduce re-radiation into the prism but thin enough to permit the field to penetrate the opposite surface.

SPR measures both the dielectric constants of the metal and the sample. It is ideal for measuring the properties of LB films that are deposited on metal coated slides. The plasma surface (the metal) allows group resonant oscillation of free electrons and this produces a charge density wave propagating along the surface. This transverse wave is known as the surface plasmon. Its oscillating field vector is normal to the surface, thus p-polarised light (light polarised parallel to the incident plane) is used to excite the surface plasmon. Resonance occurs when the wave vector and frequency of the incident light coincide with those of the surface plasmon.

5.7.2.1 SPR Equipment

A monochromatic plane polarised Spectra Physics He-Ne ($\lambda = 632.8$ nm) gas laser was used to illuminate the prism. To ensure that the light was of an optimum collimation, intensity and polarisation, it was passed through an aperture, a neutral density filter and a polariser. The beam was modulated via a mechanical beam chopper to produce a step signal (on/off) at a frequency of 1.6 kHz, to help to eliminate noise from sources of lower frequency e.g. laboratory light sources. A beam splitter was then used to divert a small fraction of the beam intensity to a reference photo detector. The reflected beam was detected by a photo detector and then the reflected signal is passed together with the reference signal to a Stanford Research Systems SR830 DSP Lock-in Amplifier. The use of the reference beam compensated for any drift in the light source intensity and removed the background dc level from the modulated signal, thus noise levels were highly reduced. Figure 5.08 shows the experimental configuration.
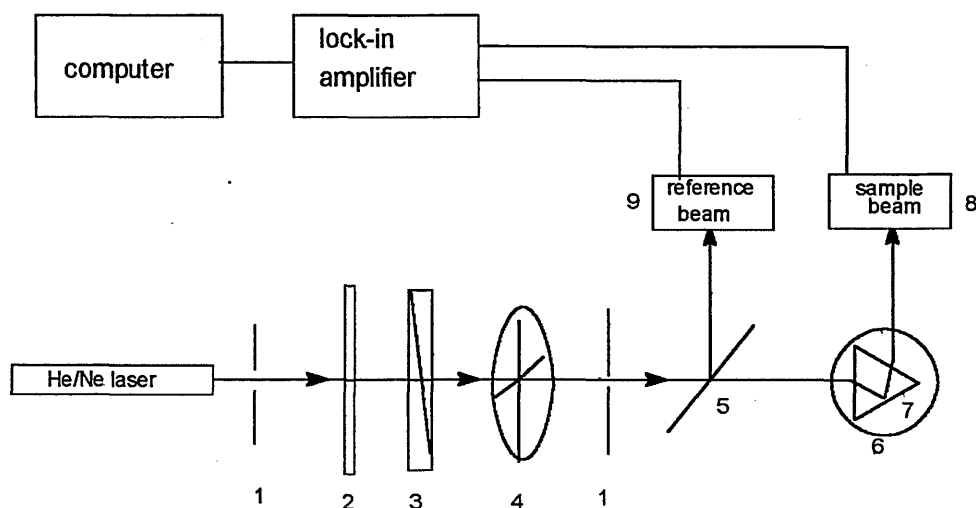
Components of an SPR experiment:-

1. Aperture, 2. Neutral Density Filter, 3. Polariser, 4. Beam Chopper, 5. Beam Splitter, 6. Turntable, 7. Sample/Prism Assembly, 8. Photo detector (Sample beam), 9. Photo detector (Reference beam).

Figure 5.08 A schematic diagram of an SPR experiment.

The sample slides were cleaned using the standard procedures (see Section 5.5.2) and coated via vapour deposition or sputter coating with gold at a thickness of between 40-50nm before multilayer LB film deposition. Methyl benzoate was used as index matching fluid. The data was corrected for reflections at the entrance and exit faces of the prism and analysed by comparison to the Fresnel reflection formulae using a curve fitting routine performed by O. Omar from the Physical Electronics and Fibre-optics Research Laboratories, School of Engineering, Sheffield Hallam University.

5.8 Chapter Five References

1. L. Blight, C. W. N. Campbell and V. J. Kyte, *J. Colloid Sci.* **20**, 393, 1965.

2. O. Albrecht, *Thin Solid Films*, **178**, 563, 1989

3. P. A. Chollet, J. Messier and C. Rosilio, *J. Chem. Phys.* **64**, 1042, 1976.

4. M. K. Debe, *J. Vacuum Sci. Technol.* , **21**, 74, 1982.

5a. R. G. Greenler, *J. Chem. Phys.* , **44**, 310, 1966.

5b. R. G. Greenler, *J. Chem. Phys.* , **50**, 1963, 1969.

6. N. V. Richardson and N. Sheppard in J. T. Yates and T. E. Madey (Eds),

   "Vibrational Spectroscopy of Molecules on Surfaces", Plenum, New York, 1987

   and references cited therein.

7. H. Raether, *Phys. Thin Films*, **9**, 145, 1977

8. E. Kretschmann and H. Raether, *Z. Natureforsch.* , **23a**, 2135, 1968.

CHAPTER 6

LANGMUIR-BLODGETT FILMS

RESULTS AND DISCUSSION

6.1 Isothermal Studies

6.1.1 The Gamma Series (R(4)Q3CNQ and R(4)P3CNQ)

Initial LB film studies were performed on the gamma substituted quinolinium and picolinium TCNQ adducts to compare and contrast their properties with those in the current literature. Langmuir-Blodgett films of the gamma quinolinium (R(4)Q3CNQ) systems have been extensively studied in the past decade (refer to Chapter 4)[1-8].

Initial experiments involved spreading solutions of the R(4)Q3CNQ and R(4)P3CNQ materials in Aristar dichloromethane at concentrations between 0.5 - 1.0 mg/ml onto the pure water subphase. Due to their poor solubility in chlorinated solvents, an ultrasonic bath had to be employed to aid dissolution, and the materials were filtered before they could be spread onto the subphase. Appropriate volumes of the solutions were delivered dropwise onto the subphase using a micrometer syringe. A time period of five minutes

was allowed between each drop for the dichloromethane to evaporate and for the materials to associate with the subphase. The amount of material added to the subphase depended on the concentration of the material and the size of the LB trough subphase area. Once all the material had been added, a further time period of 15 minutes was allowed for complete solvent evaporation. The monolayer was then compressed to obtain isotherms of the materials.

Typical experimental conditions for production of an isotherm:-

System Parameters:-

Single or multi compression	Single
Number of excursions	1
Minimum surface pressure (mN/m)	0.00
Maximum surface pressure (mN/m)	45.00
Barrier area compression rate (cm^2/min)	0.5
Barrier area expansion rate (cm^2/min)	0.5

Run Details (for $C_{18}H_{37}(4)Q3CNQ$):-

Temperature (°C)	20
Subphase	MQ water
Subphase pH	5.8
Material	$C_{18}H_{37}(4)Q3CNQ$
Molecular weight	572
Volume of material (mls)	0.15
Concentration (mg/ml)	0.95
Amount of material	2.6×10^{-7} moles

Area per molecule data were calculated from the isotherms by both the Joyce Loebl and Nima software systems, using various system parameters. These were the maximum and minimum areas of the subphase enclosed by the barriers, which are set internally during the calibration routines, the concentration of the solution added to the subphase and Avagadro's number.

The area per molecule was calculated using the following formula (see Chapter 4):-

$$Å^2 = AM/CN_AV = A/cN_AV$$

For the above example of $C_{18}H_{37}(4)Q3CNQ$, its molecular cross sectional area (where P=0 on the isotherm) would lie between the area per molecule calculated for the maximum and minimum subphase areas.

Thus at the maximum subphase area:-

Say $A = 960$ cm^2 $\equiv 9.6 \times 10^{18}$ Å^2

Then:- $Å^2 = \dfrac{9.6 \times 10^{18} \ Å^2}{6.023 \times 10^{23} \times 2.6 \times 10^{-7} \text{ moles}}$

$= 60.8$ Å^2

If the minimum subphase area is 1.55×10^{18} Å^2 , then the area per molecule would be 9.82 Å^2 and therefore the materials cross sectional area has to lie between 9.82 and 60.8 Å^2.

These early experiments on the gamma quinolinium systems were repeated to obtain accurate area per molecule data. However it was apparent that the area per molecule - for example, for the gamma C16 and C18 quinolinium analogues- varied widely at P=25 mN/m from 15 Å² to 58 Å².

On investigation, the gamma system's sparing solubility in dichloromethane was found to cause widely varying area per molecule values and filtering the solutions prior to spreading was removing undissolved pure adduct, compounding inaccurate results. Using polar solvents such as methanol or acetone, or even acetone/dichloromethane mixtures was discounted as the polar solvent would cause the material to be pulled into the subphase as the solvent mixed with the water, the material precipitating out as solid aggregates, with resulting poor quality Langmuir films.

Thus very dilute solutions (0.5 - 0.01 mg/ml) of all the gamma adducts were used in Aristar grade dichloromethane or chloroform, ensuring dissolution and removed the need of any further filtration. This in turn increased the volumes of solvent that were applied to the subphase.

In order to produce LB multilayers successfully, it was vital that the isotherms of the materials being investigated exhibited reproducible pressure-area profiles so that the behaviour of the monolayers under pressure is assured.

Figure 6.01 shows an isotherm of $C_{18}H_{37}(4)Q3CNQ$ and is typical of the gamma quinolinium - TCNQ systems. Compression at 20°C, in the dark, yielded an isotherm that rose steeply until the film collapsed at a pressure (Π_c) > 40 mN/m. The gamma quinolinium/picolinium systems (figure 6.02) all yielded similar isothermal profiles that deviated from the classical stearic acid profile of defined phase changes. The isotherms

were generally featureless and any features such as bumps or plateau indicated poor

Langmuir films for these systems.

Isotherm of C18H37(4)Q3CNQ
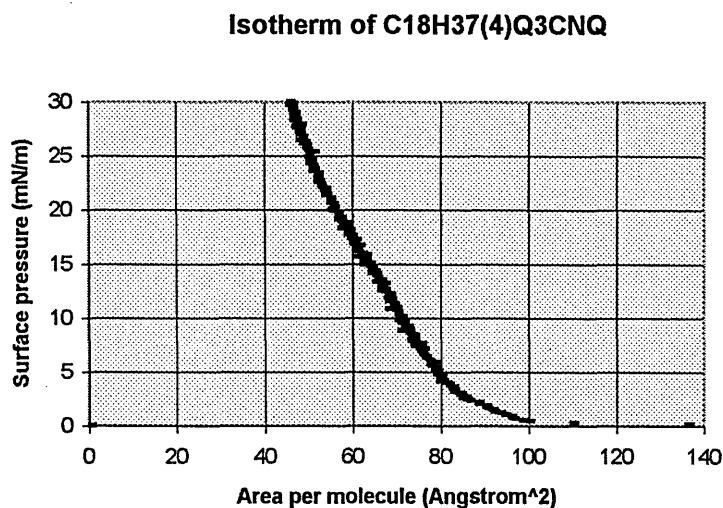
Figure 6.01 A pressure-area per molecule isotherm of $C_{18}H_{37}$(4)Q3CNQ

The area per molecule data for the R(4)Q3CNQ systems (Table 6.01) agrees with the

current literature.[1-6] (see Section 4.08) The marked increase in molecular areas as the

alkyl chain length increases above $C_{14}H_{29}$ by more than 10 Å² is indicative of

considerable molecular reorientation, even though the alkyl chain length has increased by

only one carbon unit. The shorter alkyl chain analogues (between C_4H_9 and $C_{14}H_{29}$)

occupy approximately the same molecular areas of between 28 and 29 Å² and thus the

alkyl chain length for these particular analogues does not appear to affect their molecular

orientation within the Langmuir film, as they are occupying the minimum area possible.

The van der Waals cross sectional area of the widest part of these adducts is 30 Å² (the

cross sectional area of the quinolinium group) [3,9] and in theory it is impossible for any of

the gamma and alpha quinolinium analogues to occupy a smaller area.

As the alkyl chain length increases above $C_{14}H_{29}$, the 10 $Å^2$ jump in molecular area is followed by a steady increase in molecular areas for subsequent analogues and would therefore imply that above $C_{14}H_{29}$, their alkyl chain length does affect their molecular orientation.

Table 6.01 Area per molecule data for R(4)Q3CNQ adducts where Π= 25mN/m.

TCNQ Adduct	Area per molecule ($Å^2$)
$C_4H_9(4)Q3CNQ$	28
$C_5H_{11}(4)Q3CNQ$	28
$C_{10}H_{21}(4)Q3CNQ$	29
$C_{11}H_{23}(4)Q3CNQ$	29
$C_{13}H_{27}(4)Q3CNQ$	28
$C_{14}H_{29}(4)Q3CNQ$	28
$C_{15}H_{31}(4)Q3CNQ$	38
$C_{16}H_{33}(4)Q3CNQ$	41
$C_{18}H_{37}(4)Q3CNQ$	44
Benzyl(4)Q3CNQ	28

The gamma picolinium adducts (table 6.02) and the other analogous series' (tables 6.03 and 6.04) do not exhibit the above phenomenon. The R(4)P3CNQ series exhibit a seemingly slight increase in molecular areas from approximately 20$Å^2$ for the short chain to 24-26 $Å^2$ for the long chain derivatives. The minimum cross sectional area of the picolinium group[10] is approximately 24$Å^2$ (from the $C(CN)_2$ swallowtail) and therefore is in good agreement with the experimental results. No gross molecular reorientation is observed.

Table 6.02 Area per molecule data for R(4)P3CNQ adducts where Π=25mN/m

| TCNQ Adduct	Area per molecule ($Å^2$)
C_4H_9(4)P3CNQ	21
C_5H_{11}(4)P3CNQ	20
$C_{10}H_{21}$(4)P3CNQ	23
$C_{11}H_{23}$(4)P3CNQ	22
$C_{13}H_{27}$(4)P3CNQ	25
$C_{14}H_{29}$(4)P3CNQ	24
$C_{15}H_{31}$(4)P3CNQ	24
$C_{16}H_{33}$(4)P3CNQ	26
$C_{18}H_{37}$(4)P3CNQ	26
$C_{20}H_{41}$(4)P3CNQ	-
Benzyl(4)P3CNQ	20

6.1.2 The Alpha Series (R(2)Q3CNQ and R(2)P3CNQ)

The R(2)Q3CNQ and the R(2)P3CNQ analogous series' were much more soluble in chlorinated solvents than the corresponding gamma adducts. However the experimental conditions were kept the same for both the alpha and gamma systems so a valid comparison could be made. Again very dilute solutions were used (between 0.5 and 0.01 mg/ml) to avoid any undissolved material entering the subphase and possible aggregation of the molecules.

Isotherms of the materials compressed at 20°C, in the dark, rose steeply until film collapse. The isotherms (Figures 6.02-6.04) for these materials were again featureless but film collapse occurred above 35 mN/m which was considerably lower than that observed in the gamma systems.

Isotherm of C15H31(2)Q3CNQ
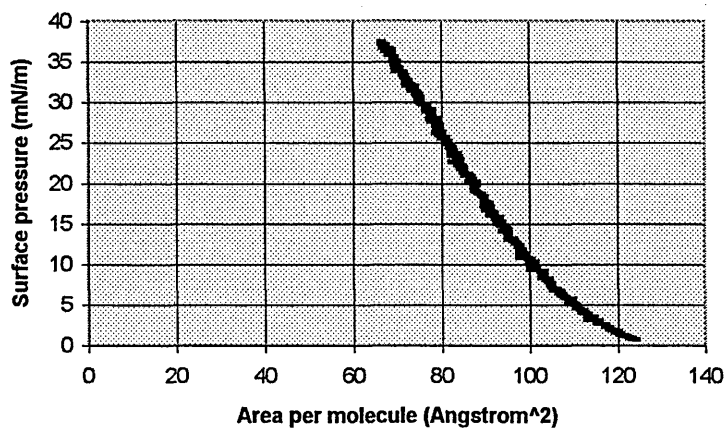

Isotherm of C18H37(2)Q3CNQ
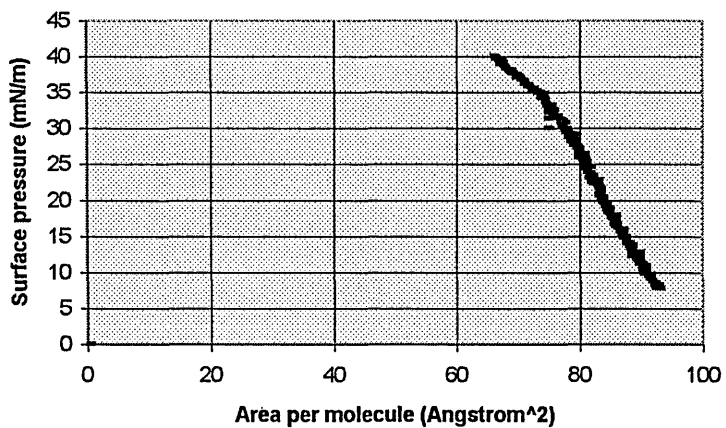
Figure 6.02 Pressure-area per molecule isotherms of $C_{15}H_{31}$ and $C_{18}H_{37}$ α-bridged quinolinium-TCNQ adducts

Isotherm of C15H31(2)P3CNQ
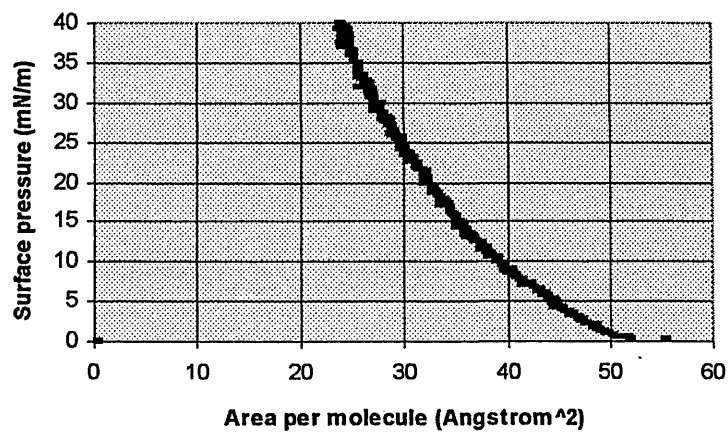
Isotherm of C18H37(2)P3CNQ
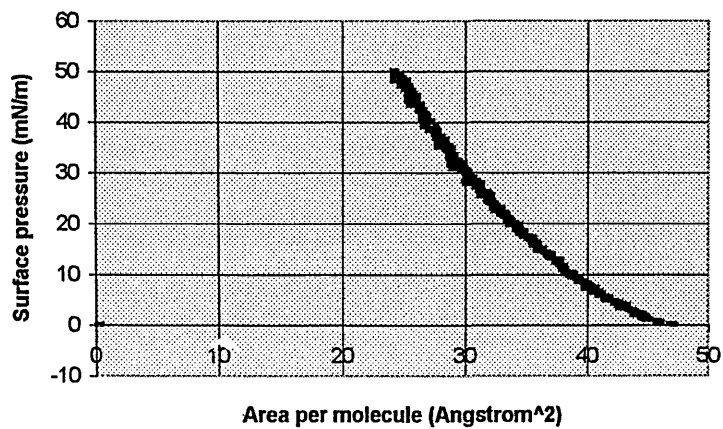
Figure 6.03 Pressure-area per molecule isotherms of $C_{15}H_{31}$ and $C_{18}H_{37}$ α-bridged picolinium-TCNQ adducts.
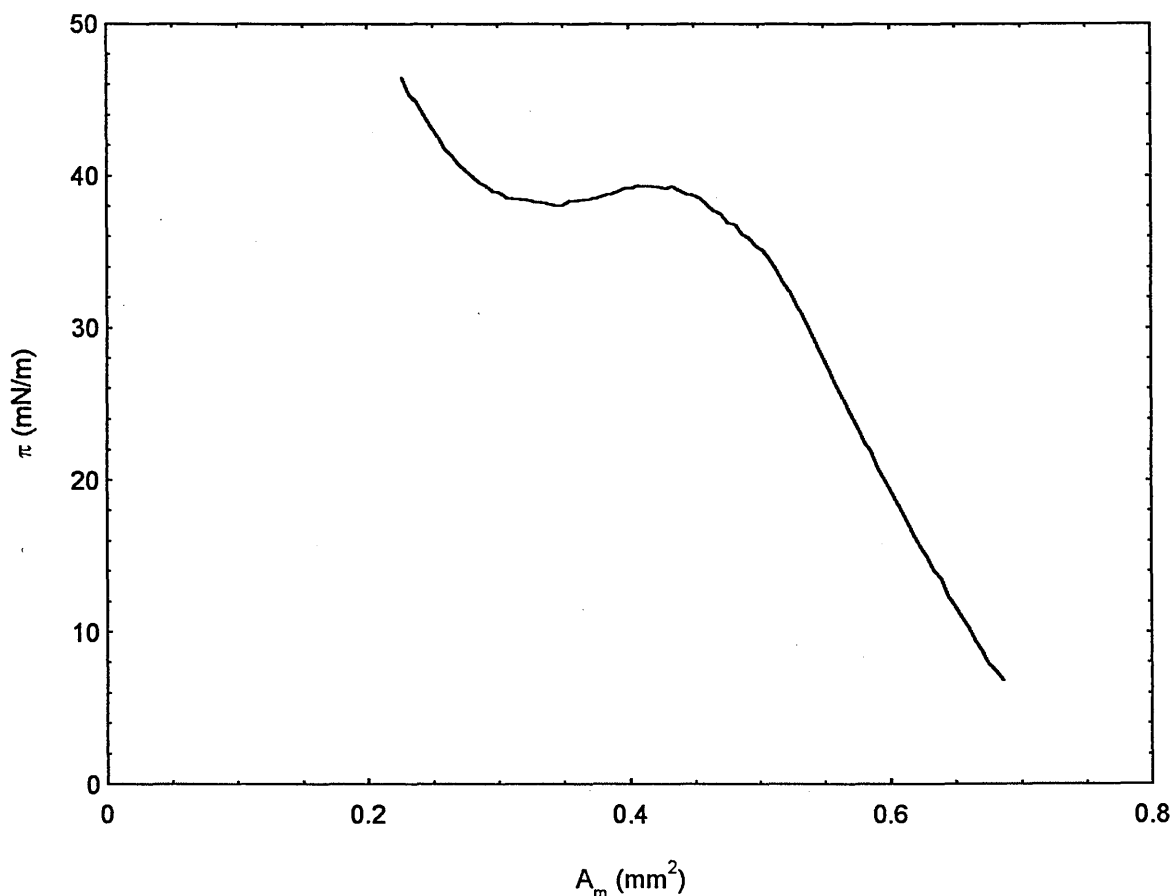
Figure 6.04 A pressure- area isotherm of $C_{16}H_{33}(2)Q3CNQ$ showing film collapse at > 35 mN/m

A steady increase in molecular areas as alkyl chain length increased was observed for the R(2)Q3CNQ and R(2)P3CNQ adducts (Tables 6.03 and 6.04). What is also obvious however is the large increase in molecular areas for the α-quinolinium systems compared to the corresponding γ-analogues, for example $C_{16}H_{33}(4)Q3CNQ$ occupied 30Å^2 less than $C_{16}H_{33}(2)Q3CNQ$ at a surface pressure of 25 mN/m. A similar phenomenon was observed in the picolinium analogues but it was not as pronounced. This increase in molecular areas is indicative of differing molecular orientations within the Langmuir film. As the area per molecule increased a "flatter" tilt angle of the materials on the subphase is observed (Section 6.2). The benzyl analogues in both systems occupied similar areas to

the short chain analogues ($< C_6H_{13}$). The benzyl group is therefore exerting an equivalent amphiphilic balance as say a C_6H_{13} alkyl chain group.

Table 6.03 Area per molecule data for R(2)Q3CNQ adducts where Π= 25 mN/m

TCNQ Adduct	Area per molecule ($Å^2$)
$C_4H_9(2)Q3CNQ$	62
$C_5H_{11}(2)Q3CNQ$	63
$C_{10}H_{21}(2)Q3CNQ$	64
$C_{11}H_{23}(2)Q3CNQ$	68
$C_{13}H_{27}(2)Q3CNQ$	64
$C_{14}H_{29}(2)Q3CNQ$	65
$C_{15}H_{31}(2)Q3CNQ$	66
$C_{16}H_{33}(2)Q3CNQ$	71
$C_{18}H_{37}(2)Q3CNQ$	69
Benzyl(2)Q3CNQ	65

Table 6.04 Area per molecule data for R(2)P3CNQ adducts where Π=25mN/m

TCNQ Adduct	Area per molecule ($Å^2$)
$C_4H_9(2)P3CNQ$	29
$C_{10}H_{21}(2)P3CNQ$	33
$C_{11}H_{23}(2)P3CNQ$	33
$C_{13}H_{27}(2)P3CNQ$	32
$C_{14}H_{29}(2)P3CNQ$	29
$C_{15}H_{31}(2)P3CNQ$	33
$C_{16}H_{33}(2)P3CNQ$	38
$C_{18}H_{37}(2)P3CNQ$	34
Benzyl(2)P3CNQ	32

6.2 Molecular orientation within the Langmuir film

As the area per molecule becomes greater the orientation of the molecules within the Langmuir film changes. An increase in molecular area will cause a decrease in the tilt angle (θ) of the molecules within the Langmuir film (see Figure 6.05).
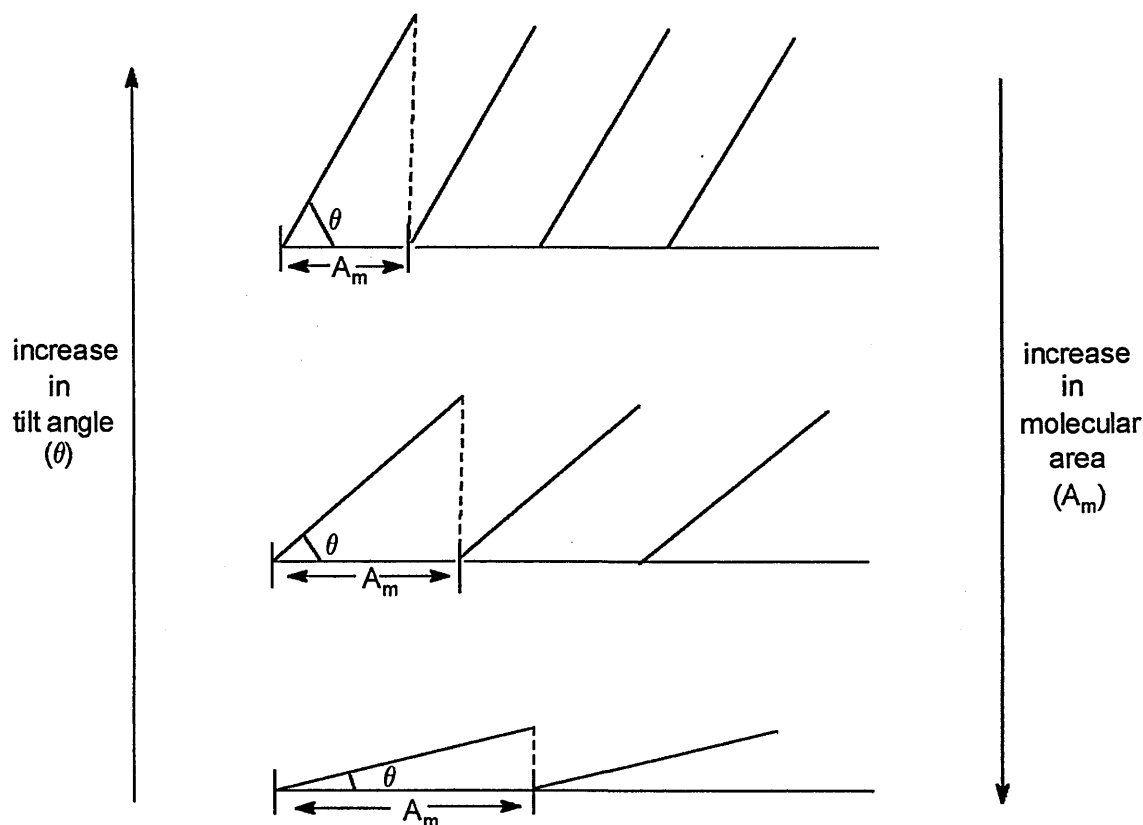
Figure 6.05 Representation of how an increase in molecular area (Am) can decrease the molecular tilt angle (θ) within a Langmuir film.

A decrease in the tilt angle (θ) would quite reasonably lead to a more favourable electrostatic organisation where the positive portion of the zwitterion lies above the negative portion of the adjacent molecule thus Coulombic repulsion is minimised (see Figure 6.06)
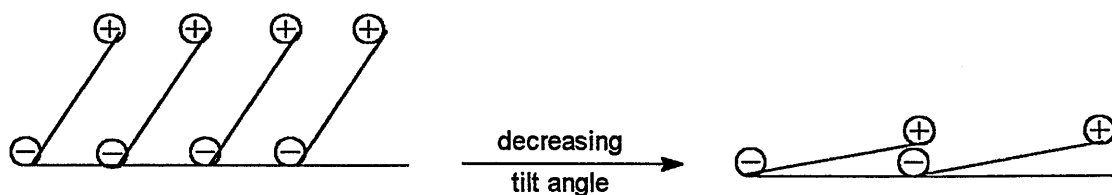
Figure 6.06 Increasing electrostatic interactions with decreasing tilt angles within the Langmuir film.

The tilt angle (θ), which is the angle between the plane of the subphase and the long axis of the chromophore was calculated using a formula based upon the simple geometrical model of Nabok et al[11]:-

$$\theta = \sin^{-1} [A_w/A_m]$$

where A_w is the van der Waals area of the widest part of the chromophore and A_m is the area per molecule.

As already stated for the quinolinium zwitterions the widest part of the chromophore is the quinolinium portion which occupies an area of approximately 30Å^2, whereas the widest part of the picolinium chromophore is the area occupied by the terminal -C(CN)$_2$-"swallowtail" - approximately 24Å^2.

Table 6.05 Approximate molecular tilt angles in the Langmuir film for R(4)Q3CNQ adducts

TCNQ Adduct	Tilt Angle (θ) (°)
$C_4H_9(4)Q3CNQ$	approaching 90
$C_5H_{11}(4)Q3CNQ$	approaching 90
$C_{10}H_{21}(4)Q3CNQ$	approaching 90
$C_{11}H_{23}(4)Q3CNQ$	approaching 90
$C_{13}H_{27}(4)Q3CNQ$	approaching 90
$C_{14}H_{29}(4)Q3CNQ$	approaching 90
$C_{15}H_{31}(4)Q3CNQ$	52
$C_{16}H_{33}(4)Q3CNQ$	47
$C_{18}H_{37}(4)Q3CNQ$	43
Benzyl(4)Q3CNQ	approaching 90

Table 6.06 Approximate molecular tilt angles in the Langmuir film for R(4)P3CNQ adducts

TCNQ Adduct	Tilt Angle (θ) (°)
$C_4H_9(4)P3CNQ$	approaching 90
$C_5H_{11}(4)P3CNQ$	approaching 90
$C_{10}H_{21}(4)P3CNQ$	approaching 90
$C_{11}H_{23}(4)P3CNQ$	approaching 90
$C_{13}H_{27}(4)P3CNQ$	approaching 90
$C_{14}H_{29}(4)P3CNQ$	approaching 90
$C_{15}H_{31}(4)P3CNQ$	approaching 90
$C_{16}H_{33}(4)P3CNQ$	67
$C_{18}H_{37}(4)P3CNQ$	67
Benzyl(4)P3CNQ	approaching 90

Table 6.07 Approximate molecular tilt angles in the Langmuir film for R(2)Q3CNQ adducts.

TCNQ Adduct	Tilt Angle (θ) (°)
$C_4H_9(2)Q3CNQ$	29
$C_5H_{11}(2)Q3CNQ$	28
$C_{10}H_{21}(2)Q3CNQ$	28
$C_{11}H_{23}(2)Q3CNQ$	26
$C_{13}H_{27}(2)Q3CNQ$	28
$C_{14}H_{29}(2)Q3CNQ$	27
$C_{15}H_{31}(2)Q3CNQ$	27
$C_{16}H_{33}(2)Q3CNQ$	27
$C_{18}H_{37}(2)Q3CNQ$	27
Benzyl(2)Q3CNQ	27

Table 6.08 Approximate tilt angles in the Langmuir film for R(2)P3CNQ adducts.

TCNQ Adduct	Tilt Angle (θ) (°)
$C_4H_9(2)P3CNQ$	56
$C_{10}H_{21}(2)P3CNQ$	47
$C_{11}H_{23}(2)P3CNQ$	47
$C_{13}H_{27}(2)P3CNQ$	47
$C_{14}H_{29}(2)P3CNQ$	56
$C_{15}H_{31}(2)P3CNQ$	47
$C_{16}H_{33}(2)P3CNQ$	39
$C_{18}H_{37}(2)P3CNQ$	45
Benzyl(2)P3CNQ	48

The "flatter" molecular orientation of the α-bridged adducts compared to that of the γ-bridged adducts can be clearly seen from the tables of molecular tilt angles (Tables 6.05-6.08).

The sudden change in molecular orientation in the R(4)Q3CNQ systems is illustrated in Table 6.05 where R $\geq C_{15}H_{31}$, where the angle of tilt changes abruptly from being nearly 90° to approximately 50°, this is also linked to the sudden increase in molecular areas.

Langmuir films of the γ-bridged shorter chain quinolinium homologues (R $\leq C_{14}H_{29}$ to C_4H_9) and the R(4)P3CNQ homologues have molecular areas at 25mN/m which are in close agreement to the cross-sectional van der Waals area of the widest part of the chromophores ($30Å^2$ and $24Å^2$ respectively). From this it is possible to speculate that the chromophores are positioned on their "ends", i.e. nearly perpendicular to the substrate. Therefore as the molecular areas at 25mN/m become greater and approach that of the face area of the chromophore (between 100 - 120 $Å^2$), the chromophores become tilted towards the plane of the substrate as in the case of the R(2)Q3CNQ and R(2)P3CNQ analogues. The less linear α-bridged adducts appear to adopt this "flatter" orientation as the hydrophobic alkyl chains lie back across the molecules, forcing the chromophores into the subphase leading to a smaller tilt angle (Tables 6.07 and 6.08).

The reason the molecular alignment alters so markedly in the R(4)Q3CNQ adducts is unclear, although it has been suggested that the $C_{15}H_{31}$ alkyl chain group is approximately the same length as the long axis of the quinolinium chromophore[12] and this would have some bearing on the electrostatic and amphipathic balances. Therefore when the alkyl chain is less than 15 carbon atoms the hydrophilic moiety is longer than the hydrophobic moiety and for alkyl chains greater than 15 carbon units the hydrophilic portion is shorter. The $C_{15}H_{31}$ group is the shortest alkyl chain capable of filling the space along the full length of the chromophore.

From the isotherms of the long chained γ-bridged quinolinium analogues ($C_{15}H_{31}$ – $C_{18}H_{37}$) (for example see Figure 6.01) and the whole α-bridged quinolinium series (for example see Figure 6.02), it can be seen that the molecular areas at which surface pressure starts to increase (110 -130 Å^2) are comparable to the face area of the Q3CNQ chromophore (114Å^2). Therefore it can be concluded that these particular analogues lie face down in the subphase before any compression has taken place.

Isotherms of the shorter chained γ-bridged quinolinium[13] analogues (C_4H_9 to $C_{14}H_{29}$) and all the γ- and α-bridged picolinium analogues (for example see Figure 6.03) studied here are characterised by a smaller molecular area at which surface pressure begins to increase (50-70 Å^2). From the face area of the Q3CNQ chromophore and that of the P3CNQ chromophore (100 Å^2 [10]) it can be seen that these molecules adopt a more perpendicular orientation before any subsequent compression.

6.3 Langmuir Blodgett film multilayer deposition

For both α- and γ-bridged quinolinium/picolinium systems films were deposited at a surface pressure of 25 mN/m. This was found to be the optimum pressure for the α-bridged systems and by other workers[1-8] for the γ-bridged quinolinium/picolinium analogues. This deposition or dipping pressure was chosen on the basis of the behaviour of the floating monolayers of the zwitterions under pressure. For compacted molecules/monolayers to be deposited, rather than unorganised monolayers, the point where the molecules are behaving as a quasi-solid, and are consequently most ordered, was taken. The monolayers also had to be stable at this pressure to ensure consistent film

deposition. All the adducts studied here exhibited long term monolayer stability at the deposition pressure (24+ hrs).

A clean hydrophilically treated microscope slide (see Chapter 5) was passed through the condensed film (held at 25mN/m) at speeds of 5 to 10 mm min^{-1}. The transfer of the monolayers occurred on both the upstroke and the down stroke until a predetermined number of layers had been deposited. After deposition of the first layer a drying time of 15 minutes was ensured. Imperfections in this first layer may seriously affect the quality of the LB film as this is the foundation for the rest of the molecular structure. The next layer and all subsequent layers were given shorter drying times of less than 20 seconds.

LB films of the quinolinium zwitterions were obtained for chain lengths of C_6H_{13} and greater, whereas LB films of the picolinium adducts were obtained for chain lengths of C_8H_{17} and greater. Langmuir films of zwitterions where R is C_4H_9 and C_5H_{11} have been obtained, but production of multilayer films of reproducible structural integrity was not possible.

LB film UV/Vis spectra for both α and γ systems show the CT bands observed in an acetonitrile solution have sharpened considerably in the LB films and shifted hypsochromically. In acetonitrile the CT transition for the R(4)Q3CNQ system is observed at 708 $\pm$ 4 nm whereas for C_6H_{13}(4)Q3CNQ to $C_{14}H_{29}$(4)Q3CNQ the LB transition is hypsochromically shifted to 612 $\pm$ 2 nm (Table 6.09) with a HWHM of 37 $\pm$ 2 nm (Table 6.13). A further hypsochromic shift to 563 $\pm$ 3 nm in the LB transition is observed for the $C_{15}H_{31}$(4)Q3CNQ to $C_{18}H_{37}$(4)Q3CNQ adducts with a HWHM of 22 $\pm$ 2 nm. This behaviour of the R(4)Q3CNQ system is well documented[3,5,13] and is attributed to the sudden change in molecular orientation exhibited by the long chain analogues. A colour change from blue to purple is also observed for these long chain analogues.

The acetonitrile CT transition for the R(4)P3CNQ system is observed at 641 $\pm$ 3 nm and a large hypsochromic shift to 540 $\pm$ 6 nm with a HWHM at 30 $\pm$ 3 nm is observed for the LB band (Table 6.13).

Table 6.09 Uv/Vis data for gamma substituted quinolinium TCNQ adducts.

Zwitterion	λ_{max} of LB film (nm)	λ_{max} in MeCN (nm)
$C_4H_9(4)Q3CNQ$	-	705
$C_5H_{11}(4)Q3CNQ$	-	706
$C_6H_{13}(4)Q3CNQ$	614	705
$C_8H_{17}(4)Q3CNQ$	614	708
$C_{10}H_{21}(4)Q3CNQ$	612	710
$C_{11}H_{23}(4)Q3CNQ$	612	710
$C_{13}H_{27}(4)Q3CNQ$	611	710
$C_{14}H_{29}(4)Q3CNQ$	612	712
$C_{15}H_{31}(4)Q3CNQ$	560	712
$C_{16}H_{33}(4)Q3CNQ$	566	712
$C_{18}H_{37}(4)Q3CNQ$	566	710
$Bz(4)Q3CNQ$	668	708

Table 6.10 Uv/Vis data for gamma substituted picolinium TCNQ adducts.

Zwitterion	λ_{max} of LB film (nm)	λ_{max} in MeCN (nm)
$C_4H_9(4)P3CNQ$	-	638
$C_5H_{11}(4)P3CNQ$	-	638
$C_6H_{13}(4)P3CNQ$	-	638
$C_8H_{17}(4)P3CNQ$	535	642
$C_{10}H_{21}(4)P3CNQ$	535	638
$C_{11}H_{23}(4)P3CNQ$	538	638
$C_{13}H_{27}(4)P3CNQ$	538	640
$C_{14}H_{29}(4)P3CNQ$	544	640
$C_{15}H_{31}(4)P3CNQ$	546	640
$C_{16}H_{33}(4)P3CNQ$	546	641
$C_{18}H_{37}(4)P3CNQ$	547	644
$Bz(4)P3CNQ$	-	641

The α-bridged zwitterions exhibited a much smaller hypsochromic shift from the acetonitrile solution to the LB film (Tables 6.11, 6.12 and Figures 6.07 - 6.09). The acetonitrile CT transition occurs at 697 ± 3 nm for the R(2)Q3CNQ system and the LB band is shifted to 652 ± 6 nm with the HWHM at 48 ± 2 nm (Table 6.13). The R(2)P3CNQ system has an acetonitrile CT transition at 592 ± 5 nm shifted to 575 ± 5 nm with the HWHM at 50 ± 2 nm (Table 6.13).

Table 6.11 Uv/Vis data for alpha substituted quinolinium TCNQ adducts.

Zwitterion	λ_{max} of LB film (nm)	λ_{max} in MeCN (nm)
$C_4H_9(2)Q3CNQ$	-	695
$C_5H_{11}(2)Q3CNQ$	-	694
$C_6H_{13}(2)Q3CNQ$	655	698
$C_8H_{17}(2)Q3CNQ$	655	708
$C_{10}H_{21}(2)Q3CNQ$	655	698
$C_{11}H_{23}(2)Q3CNQ$	658	698
$C_{13}H_{27}(2)Q3CNQ$	654	699
$C_{14}H_{29}(2)Q3CNQ$	657	697
$C_{15}H_{31}(2)Q3CNQ$	655	698
$C_{16}H_{33}(2)Q3CNQ$	650	698
$C_{18}H_{37}(2)Q3CNQ$	647	700
$C_{20}H_{41}(2)Q3CNQ$	-	700
$Bz(2)Q3CNQ$	708	696

The differing molecular orientations of the α-and γ- bridged chromophores can explain the changes in the absorbance spectra. Ashwell et al[3,14] have suggested that the R(4)Q3CNQ analogues have an intermolecular CT band at approximately 614 nm and that the intramolecular CT band is observed in the long chain homologues at ca 560 nm. The more perpendicular alignment of the shorter chain R(4)Q3CNQ analogues leads to the intermolecular CT transition as the intramolecular transition moment and the electric

vector are orthogonal. The longer chain analogues, tilted towards the plane of the substrate give rise to the higher energy intramolecular transition.

The α-bridged adducts would therefore appear to exhibit intramolecular CT transitions at $\approx$ 655 nm and 575 nm for the quinolinium (Figure 6.08 and 6.09) and picolinium analogues respectively, as they are tilted even further towards the plane of the substrate. The low energy shoulder on these peaks at $\approx$ 840 nm and 810 nm for the quinolinium and picolinium analogues respectively could therefore be reasonably assigned to an intermolecular transition. Evidence for this has further support. It was possible to deposit LB films of the R(2)Q3CNQ systems from very concentrated solutions (> 1mg/ml) that exhibited a wide LB band (HWHM > 100 nm) at $\approx$ 845 nm with a shoulder at $\approx$ 700 nm. The lower energy transition at 845 nm could be attributed to the intermolecular CT band and the shoulder peak to the higher energy intramolecular transition.

It has been shown that the $C_{15}H_{31}$(4)Q3CNQ analogue[3] can be deposited at near collapse pressure (40 mN/m) and the LB absorbance band can be shifted to that of the shorter chain analogues ($\approx$ 615 nm), which was attributed to the intermolecular CT band. Both CT bands have been observed from the Kramers-Kronig - transformed, single-crystal absorption spectra of CH_3(2)P3CNQ.[15] The bands were assigned as the intramolecular CT band at the higher energy transition of 538 nm and the intermolecular CT band was assigned to the lower energy transition of 806 nm and in general agree with the LB films studied here.

Table 6.12 Uv/Vis data for alpha substituted picolinium TCNQ adducts.

Zwitterion	λ_{max} of LB film (nm)	λ_{max} in MeCN (nm)
C_4H_9(2)P3CNQ	-	590
C_5H_{11}(2)P3CNQ	-	590
C_6H_{13}(2)P3CNQ	-	588
C_8H_{17}(2)P3CNQ	-	588
$C_{10}H_{21}$(2)P3CNQ	578	590
$C_{11}H_{23}$(2)P3CNQ	581	591
$C_{13}H_{27}$(2)P3CNQ	574	592
$C_{14}H_{29}$(2)P3CNQ	573	592
$C_{15}H_{31}$(2)P3CNQ	571	592
$C_{16}H_{33}$(2)P3CNQ	574	592
$C_{18}H_{37}$(2)P3CNQ	570	594
Bz(2)P3CNQ	-	597

The transfer ratio (η) (see Chapter 4) was used to determine the structure type of the LB films deposited. Previous studies (see Chapter 4) had indicated that the γ-bridged analogues either were deposited as predominantly Y-type[1,13] or Z- type[2-4,6].

Ashwell et al[6] observed a large second order susceptibility exhibited by $C_{16}H_{33}$(4)Q3CNQ which would have to indicate a non-centrosymmetric film where a Z-type structure would dominate, for this large SHG to be observed.
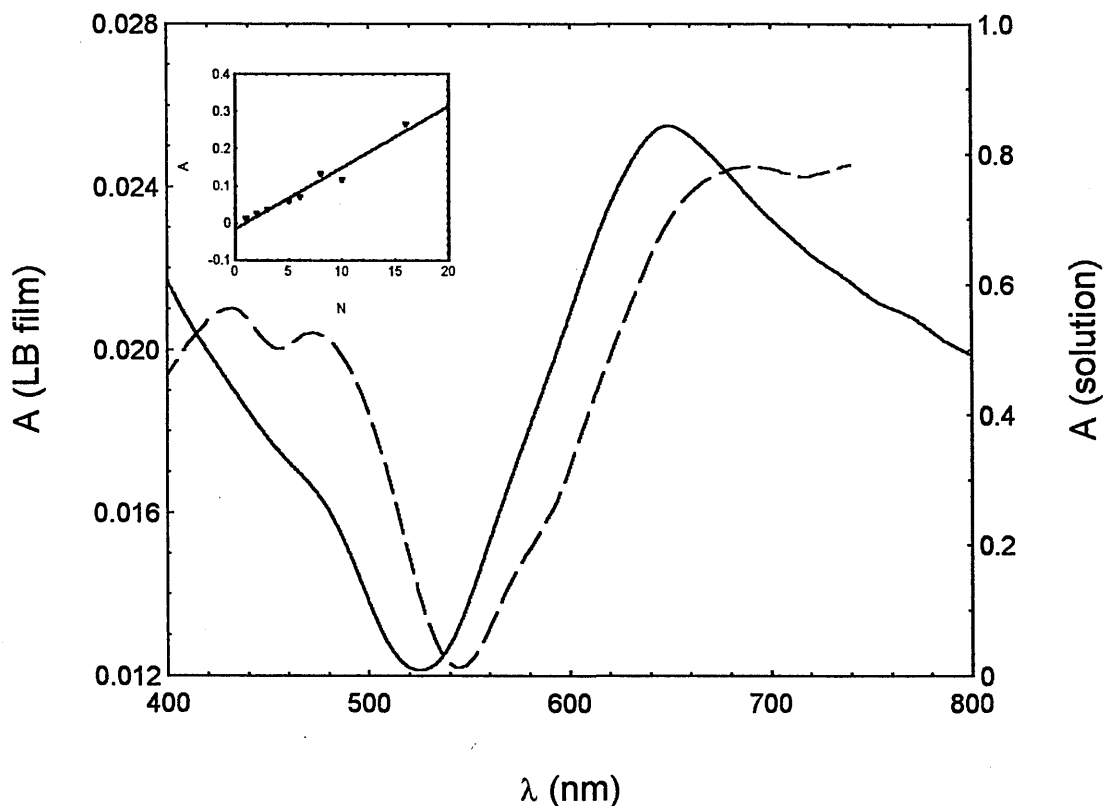
Figure 6.07 Absorption spectra of 2 monolayers of $C_{16}H_{33}(2)-Q3CNQ$ (solid line) and a dichloromethane solution of $C_{16}H_{33}(2)-Q3CNQ$ (dashed line). The inset shows the linear relationship between the number of monolayers and absorbance at 650 nm.

For Y-type deposition to occur, the material would need to be deposited on both the up and down strokes, whereas for Z-type, the material would need to be transferred on the up stroke only. From the transfer ratios of

$C_{16}H_{33}(4)Q3CNQ$ (Table 6.14) it can be seen that although deposition is occurring on both the up and the down strokes, the majority of the zwitterion is being picked up on the upstroke. Therefore a more accurate description of the LB film structure in this particular case would be a predominantly Z-type one. However the transfer ratios shown for $C_{10}H_{21}(4)Q3CNQ$ (Table 6.15) indicate a more even deposition of material on both the up and down strokes and thus could be described as a predominantly Y-type structure.

Table 6.13 A table showing Absorbance per monolayer and half-width at half maximum for LB films of the α- and γ- bridged quinolinium/picolinium zwitterions.

| Zwitterion	Absorbance per monolayer	HWHM	Colour of LB film
C_6H_{13}(4)Q3CNQ			
↓	0.02 ± 0.004	35 ± 4	blue
$C_{14}H_{29}$(4)Q3CNQ			
$C_{15}H_{31}$(4)Q3CNQ			
↓	0.02 ± 0.002	22 ± 2	purple
$C_{18}H_{37}$(4)Q3CNQ			
C_8H_{17}(4)P3CNQ			
↓	0.018 ± 0.004	30 ± 2	blue
$C_{18}H_{37}$(4)P3CNQ			
C_6H_{13}(2)Q3CNQ			
↓	0.015 ± 0.002	48 ± 2	blue
$C_{18}H_{37}$(2)Q3CNQ			
C_8H_{17}(2)P3CNQ			
↓	0.013 ± 0.002	50 ± 2	blue
$C_{18}H_{37}$(2)P3CNQ			
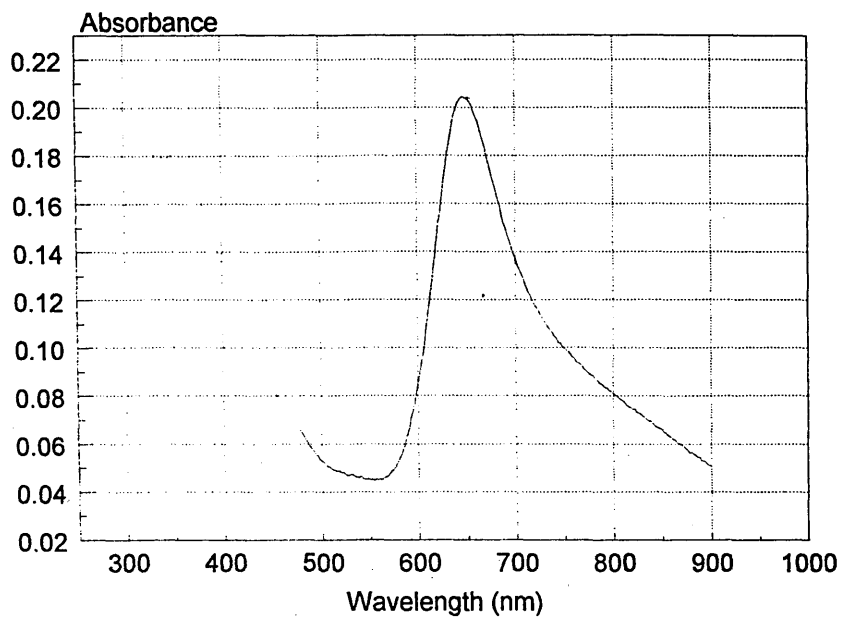
**Figure 6.08 UV/Vis spectra of a 15 layer $C_{16}H_{33}(2)Q3CNQ$ LB film**
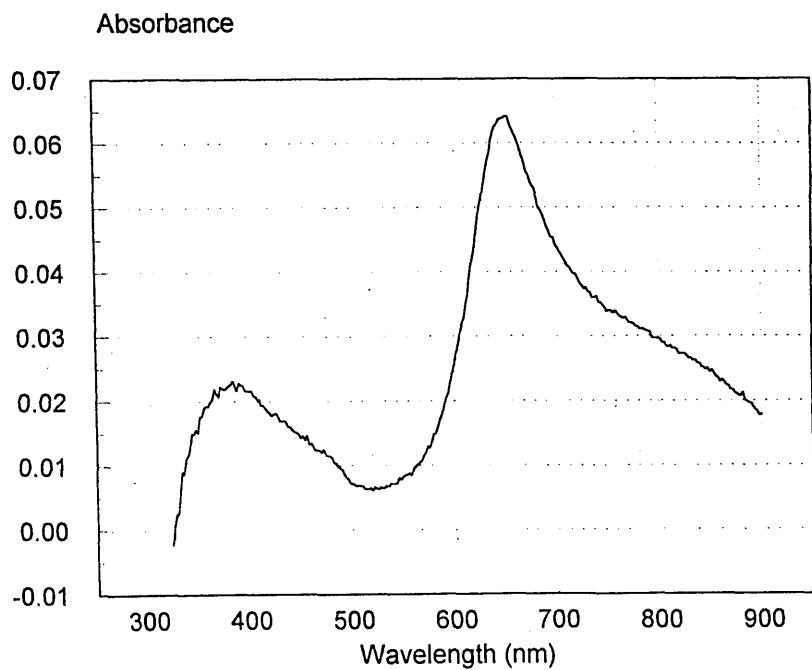
Figure 6.09 Vis spectra of a 5 layer $C_{10}H_{21}(2)Q3CNQ$ LB film

Again this property of the R(4)Q3CNQ homologous series appears related to the alkyl chain lengths and basically the short chain homologues ($\leq C_{14}H_{29}$) produce predominantly Y-type centrosymmetric LB films and the longer chain homologues ($\geq C_{15}H_{31}$) produce predominantly Z-type noncentrosymmetric films.

SHG studies on $C_{10}H_{21}(4)$Q3CNQ[6] have shown that the SHG is suppressed and thus the molecules must be adopting a centrosymmetric structure, thus supporting the results obtained here. However it has been suggested that this suppression of the SHG could be attributed to anti parallel packing arrangements, and not a Y-type structure, of the chromophore (see Figure 6.10). It was thought that the chromophores (short chain) would pack with the positively charged heterocycle adjacent to the negatively charged dicyanomethanide.
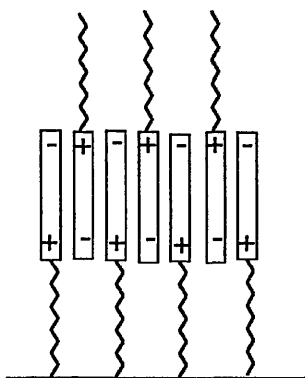
Figure 6.10 Suggested anti parallel packing for the $C_{10}H_{21}(4)$Q3CNQ adduct (tilt angles not shown) [6].

Neutron reflectivity and SPR studies on the $C_{10}H_{21}(4)$Q3CNQ adduct gave thicknesses of ≈ 3.4 nm for the Langmuir and LB layers respectively. This dimension is considerably longer than the van der Waals molecular length of ≈ 2.7 nm giving credibility to an anti parallel arrangement. However this increased molecular length could also indicate

contamination of the film, a bilayer or a defective film containing aggregation of the molecules that can be deposited in the LB film itself.

From the transfer ratios of $C_{16}H_{33}(2)Q3CNQ$ (Table 6.16) it can be seen that LB film structure is initially Y-type, however as more monolayers are laid down, the LB film develops a Z-type character, until it becomes predominantly Z-type. As with the other α-bridged adducts the influence of the alkyl chain is not great and the pattern of increasing Z-type character with layer number is observed in both R(2)Q3CNQ and R(2)P3CNQ systems (Figure 6.11).

There appears to be a relationship between the tilt of the molecules in the Langmuir film and the subsequent deposition structure, as the more flatly packed long chain R(4)Q3CNQ materials and α-bridged analogues all deposit in a Z-type manner.

	Dip Direction		Layer Number	Transfer Ratio
The loss of	↑		1	1.2
centrosymmetry	↓		2	0.8
in a				
$C_{16}H_{33}(2)Q3CNQ$	↑		3	1.2
film				
	↓		4	0.0
	↑		5	1.1

Figure 6.11 The loss of Y-type character with increasing layer number as observed in an LB film of $C_{16}H_{33}(2)Q3CNQ$

Layer Number	Transfer Ratio	Direction Of Slide
1	1.4	UP
2	0.6	DOWN
3	1.2	UP
4	0.7	DOWN
5	1.0	UP
6	0.7	DOWN
7	1.1	UP
8	0.7	DOWN
9	1.2	UP
10	0.7	DOWN
11	1.2	UP
12	0.6	DOWN
13	1.2	UP
14	0.7	DOWN
15	0.8	UP

Table 6.14 Transfer ratios in a 15 layer $C_{16}H_{33}(4)Q3CNQ$ LB film

Layer Number	Transfer Ratio	Direction Of Slide
1	1.4	UP
2	1.0	DOWN
3	1.2	UP
4	0.9	DOWN
5	1.0	UP
6	0.7	DOWN
7	1.1	UP
8	1.1	DOWN
9	1.2	UP
10	1.0	DOWN
11	1.2	UP
12	0.8	DOWN
13	1.0	UP
14	1.1	DOWN
15	1.0	UP

Table 6.15 Transfer ratios in a 15 layer $C_{10}H_{21}(4)Q3CNQ$ LB film

Layer Number	Transfer Ratio	Direction of Slide
1	1.2	UP
2	0.8	DOWN
3	1.2	UP
4	0.0	DOWN
5	1.1	UP
6	0.6	DOWN
7	1.2	UP
8	0.0	DOWN
9	1.2	UP
10	0.8	DOWN
11	1.1	UP
12	0.0	DOWN
13	1.0	UP
14	0.2	DOWN
15	1.6	UP

Table 6.16 Transfer ratios in a $C_{16}H_{33}(2)Q3CNQ$ LB film

6.4 Surface Plasmon Resonance

SPR studies[16] were carried out using the Kretchman configuration[17] of apparatus mounted on a computer controlled rotating table. Microscope slides, coated on one side with a 44 nm thick, vacuum evaporated, Au film, were attached to the glass prism using methyl benzoate as index matching fluid. Reflectivity data were obtained as a function of the incident angle, relative to the film, using p-polarising monochromatic light (HeNe laser, λ = 633 nm).
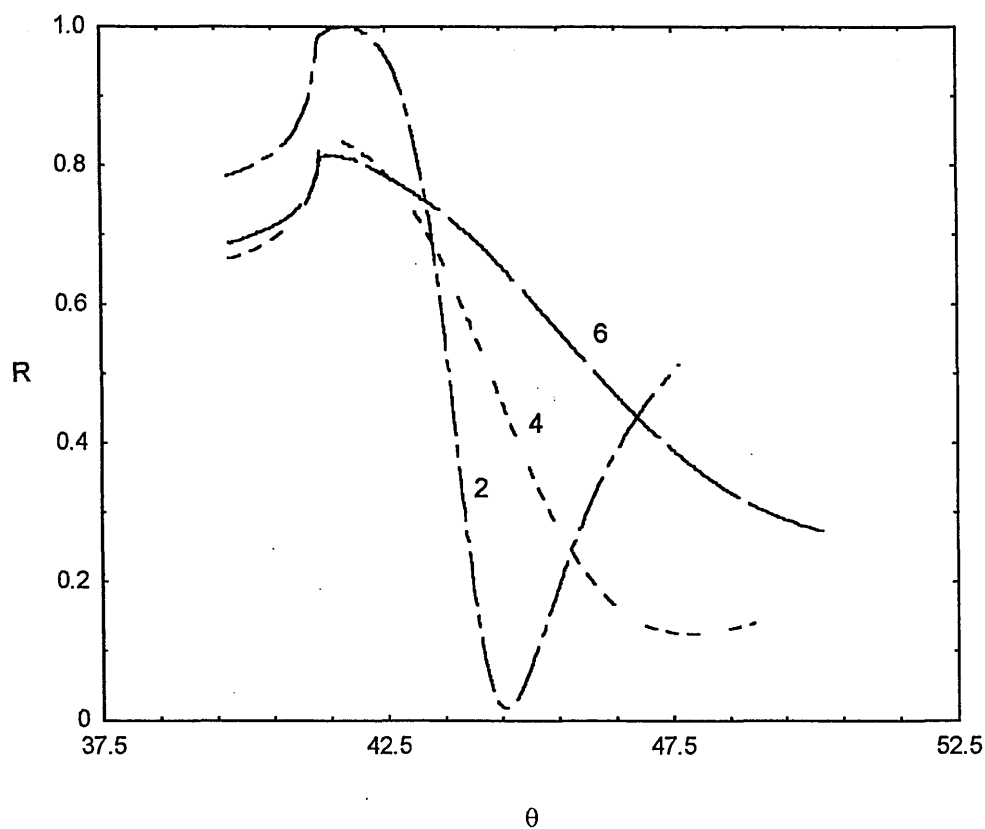

Figure 6.13 Normalised surface plasmon resonance reflectivity curves for 2 layers, 4 layers and 6 layers of $C_{16}H_{33}(2)Q3CNQ$ deposited on a 44 nm thick gold layer.

Figure 6.13 shows a set of surface plasmon curves obtained from 2,4 and 6 layer $C_{16}H_{33}(2)Q3CNQ$ LB films displaying the variations in reflected intensity, **R**, as a function of the incident angle, θ. All three sets of data were normalised using reflectivity data initially obtained at the entrance and exit faces of the prism. The curves become broader and the minimum of the reflected intensity rises to a higher non-zero value as the number of LB layers is progressively increased. This indicates that the resonance becomes increasingly damped with the increase in the number of LB layers, leading to higher values of depth and half-width resonance. The incident angle at which the resonance occurs is also found to be shifting to a larger value of approximately 1° per monolayer. This corresponds to a value of 1.4×10^6 ms^{-1} for a change in the phase velocity of the surface oscillations. Further analysis was carried out by the least squares fit of experimental data to Fresnal's theory for a four layered system.

The average thickness per layer from the SPR analysis was found to be 1.75 $\pm$ 0.15 nm. The angle, α, of molecular stacking in the LB film is estimated to be 33° from the empirical relation :-

$$\alpha = tan^{-1}[d/L]$$

where **d** is the average monolayer thickness and **L** is the van der Waals length of the TCNQ adduct (2.7 nm)[6]. Values for refractive index (**n**) and extinction coefficient (**k**), obtained at 633 nm, were found to be 1.47 $\pm$ 0.17 and 0.48 $\pm$ 0.08 respectively.

The angle of molecular stacking (ca. 33°) in the $C_{16}H_{33}(2)Q3CNQ$ LB film was found to be slightly larger than the tilt angle in the Langmuir film (ca. 27°). This would imply that the molecules pack more tightly in the deposited films than they do on the subphase and this can also explain why the transfer ratios on the upstrokes were greater than 1 (Table 6.16).

This molecular thickness of 1.75 $\pm$ 0.15 nm for the $C_{16}H_{33}(2)3CNQ$ LB film compares to that reported (1.6 $\pm$ 0.1 nm) by Ashwell et al[6] for phase 2 of $C_{16}H_{33}(4)Q3CNQ$ LB film.

6.5 Reflection Absorption Infra-red Spectroscopy (RAIRS)

RAIRS or grazing-angle Fourier transform infrared spectra are shown here for multilayer LB films of $C_{10}H_{21}(4)Q3CNQ$ and $C_{16}H_{33}(2)Q3CNQ$ respectively (Figures 6.14 and 6.15) on Al coated glass substrates, using p-polarised light. The main features of the spectra include absorbancies at 2920 cm^{-1} for the antisymmetric -CH$_2$- stretches, 2140 cm^{-1} for the symmetric C-H stretches and two -C$\equiv$N stretches at 2175 and 2140 cm^{-1}.

The CN stretches are similar to those seen in the solid quinolinium/picolinium zwitterions (Section 3.1.3.2), where the dicyanomethanide 3-carbon unit, over which the negative charge is delocalised, appears at a lower stretching frequency (higher wave number). This is because the delocalisation of charge reduces the strength of the bond and thus the stretching frequency is lowered correspondingly. Thus in the RAIRS spectra the negatively charged CN groups appear at 2175 cm^{-1} and the neutral CN group appears at 2140 cm^{-1}.

For the multilayer of $C_{10}H_{21}(4)Q3CNQ$ (Figure 6.14) the C-H, -CH$_2$- and both CN signals are very strong and would indicate that cyano and alkyl groups do not lie in the plane of the substrate but are somewhat tilted from it. These strong signals tentatively support the molecular orientation data shown in Table 6.05 that the tilt angles in the short chain R(4)Q3CNQ analogous series are approaching the perpendicular (90°). Although this tilt angle data applies to Langmuir films, the transfer ratios exhibited by this material i.e. greater than unity (Table 6.15), suggests that the molecules pack more tightly in the LB film than in the Langmuir film and thus a further increase in their tilt angles would be expected.
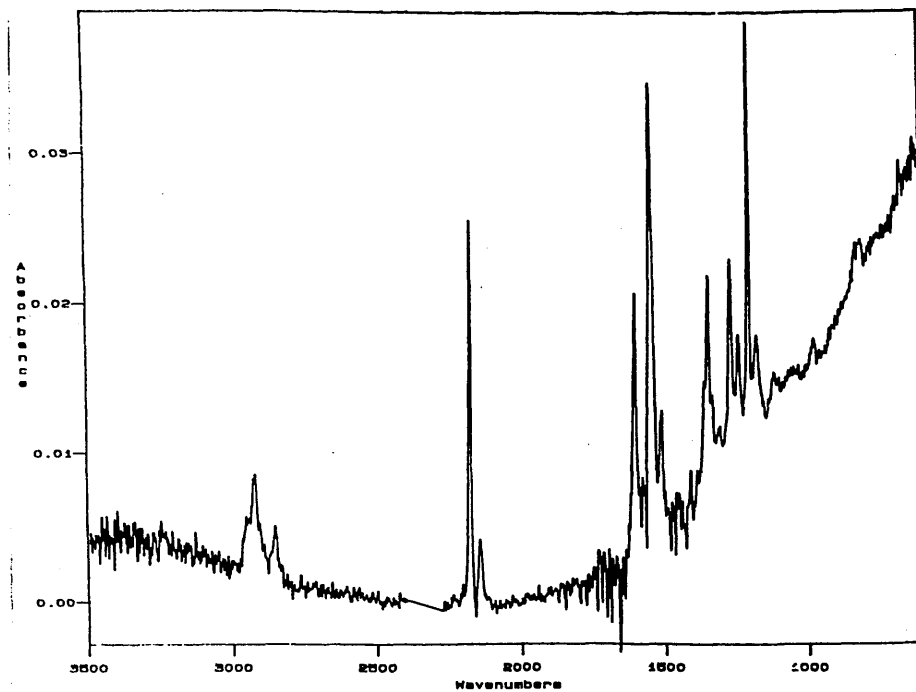
Figure 6.14 RAIRS spectrum of a 15 layer $C_{10}H_{21}$(4)Q3CNQ LB film on aluminium.
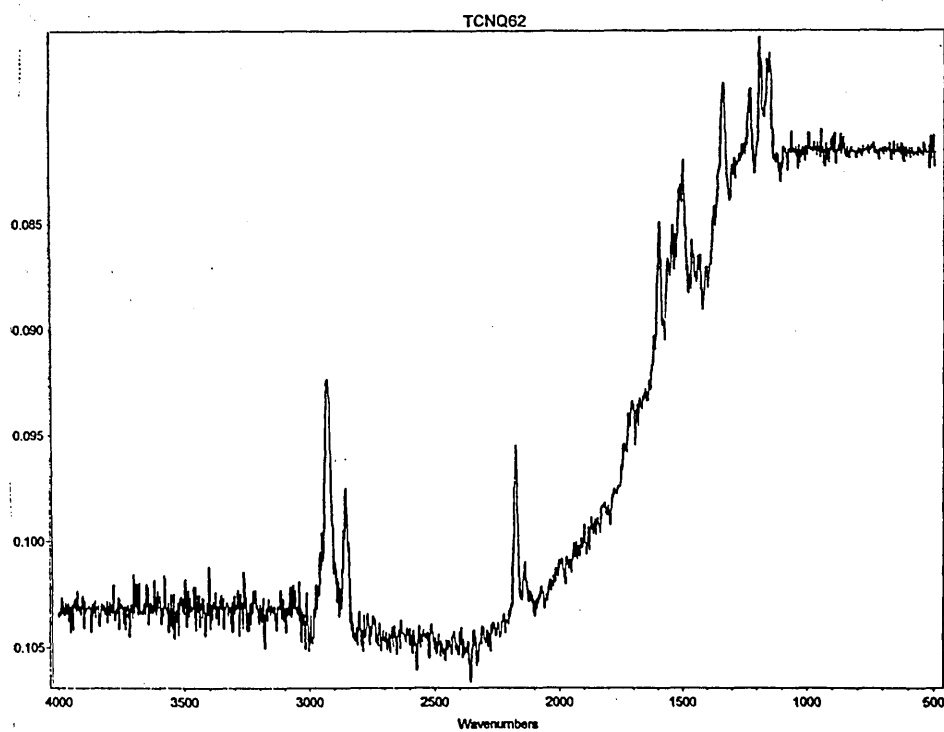

Figure 6.15 RAIRS spectrum of a 15 layer C16H33(2)Q3CNQ LB film on aluminium.

For the multilayer of $C_{16}H_{33}(2)Q3CNQ$ (Figure 6.15) a slightly different pattern emerges as the symmetric C-H and antisymmetric $-CH_2$ signals are very strong but the two CN signals although clearly visible, are much weaker than observed in the short chain R(4)Q3CNQ (Figure 6.14) and R(4)P3CNQ homologues. This supports the 'flatter' molecular orientation exhibited by the α-bridged adducts (Table 6.07) as the CN groups from the chromophore will be approaching the plane of the substrate.

6.6 A Preliminary LB film study of N-hexadecylpyridinium benzimidazolate - TCNQ charge transfer complex.

LB films of the betaine-TCNQ CT complex [54] were prepared from spreading dilute dichloromethane solutions (0.1 - 0.05 mg/ml) onto the water subphase. The quality of the initial films were poor and this was improved by annealing the film. This was achieved by expanding and compressing (never exceeding collapse pressure) the Langmuir films a number of times, which encouraged a more efficient molecular packing of the molecules within the film. This was demonstrated in the pressure area isotherms of the material (Figures 6.16 and 6.17) where it can be seen that prior to annealing, the isotherms were 'broken' and exhibited characteristics of the two separate components. The TCNQ component would be expected to form the flatter featureless part at $\pi < 20$ nN/m and after the 'break', a steeper rising part at $\pi > 20$ mN/m could be attributed to the chromophore with the hexadecyl group. Annealing yielded a generally featureless isotherm (Figure 6.17) with film collapse occurring above 40 mN/m which was characteristic of a more efficiently packed film.

The isotherm showed an area per molecule as 45 $Å^2$ at 20 mN/m and 25 $Å^2$ at film collapse (> 40 mN/m). LB films were fabricated by passing clean hydrophilically treated

microscope slides through the condensed film (held at 20 mN/m) at speeds of 8 mm/min. The transfer of the monolayers occurred on the upstroke only, to yield Z-type, light blue films with transfer ratios of 90 - 110 %.

Isotherm of C16 betaine - TCNQ
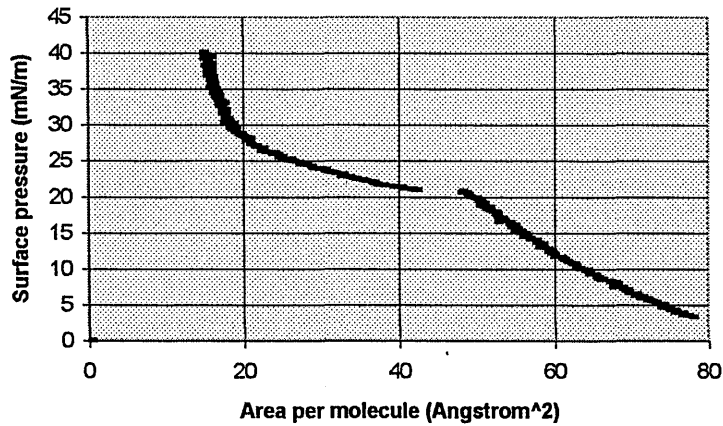
Figure 6.16 Isotherm of [54] prior to annealing

Isotherm of C16 betaine - TCNQ b
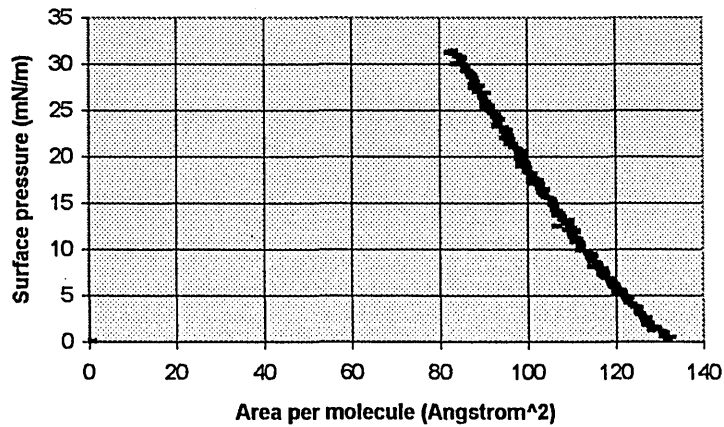
Figure 6.17 Isotherm of [54] after annealing

6.7 Summary

From a synthetic angle, the main body of this work has yielded the extensive analogous series of α- and γ- bridged quinolinium/picolinium TCNQ adducts.

The behaviour of these materials on the subphase and their resultant LB film fabrication has indicated that the γ-bridged systems behave significantly differently from the α-bridged systems.

The LB film forming properties of the γ-bridged systems are dependent upon chain length and it was observed that short chain γ-bridged quinolinium adducts, (where R $\leq$ $C_{14}H_{29}$) and the R(4)P3CNQ analogous series occupied minimum areas per molecule. They exhibited molecular orientations that were virtually perpendicular to the substrate and were deposited predominantly as Y-type (centrosymmetric) LB films. In contrast the long chain γ-bridged quinolinium adducts (where R $\geq$ $C_{15}H_{31}$) occupied much greater molecular areas, were more horizontally orientated towards the substrate and were deposited as predominantly Z-type (non-centrosymmetric) LB films.

The LB film forming properties of the α-bridged systems were not dependant on chain length and it was observed that both R(2)Q3CNQ and R(2)P3CNQ series occupied large molecular areas with the chromophores tilted towards the plane of the substrate and were deposited as predominantly Z-type (non-centrosymmetric) LB films.

The non-centrosymmetric LB film structures of the novel R(2)Q3CNQ and R(2)P3CNQ adducts hint at possible NLO applications, especially SHG, and this would provide a suitable focus for future work.

6.8 Chapter Six References

1.   N. A. Bell, R. A. Broughton, J. S. Brooks, T. A. Jones and S. C. Thorpe, *J. Chem. Soc. , Chem. Commun. ,* 325, 1990.

2.   G. J. Ashwell, *Thin Solid Films,* **186,** 155, 1990.

3.   G. J. Ashwell, E. J. C. Dawnay, A. P. Kuczynski, M. Szablewski, I. M. Sandy, M. R. Bryce, A. M. Grainger and M. J. Hasan, *J. Chem. Soc. , Faraday Trans. ,* **86,** 1117, 1990.

4.   G. J. Ashwell, E. J. C. Dawnay and A. P. Kuczynski, *J. Chem. Soc. , Chem. Commun. ,* 1355, 1990.

5.   N. A. Bell, R. A. Broughton, J. S. Brooks and S. C. Thorpe, *Int. J. Electronics,* **76,** 751, 1994.

6.   G. J. Ashwell, G. Jefferies, E. J. C. Dawnay, A. P. Kuczynski, D. E. J. Lynch, Y. Gongda and D. G. Bucknall, *J. Mater. Chem. ,* **5,** 975, 1995.

7.   R. M. Metzger, B. Chen, U. Hopfner, M. V. Lakshmikantham, D. Vuillaume, T. Kawai, X. Wu, H. Tachibana, T. V. Hughes, H. Sakurai, J. W. Baldwin, C. . Hosch, M. P. Cava, L. Brehmer and G. J. Ashwell, *J. Am. Chem. Soc. ,* **119,** 10455, 1997.

8.   G. J. Ashwell, J. R. Sambles, A. S. Martin, W. G. Parker and M. Szablewski, *J. Chem. Soc. , Chem, Commun. ,* 1355, 1990.

9.   G. J. Ashwell, D. D. Eley, S. C. Wallwork, M. R. Willis, G. F. Peachy and D. B. Wilkos, *Acta Crystallogr. B,* **33,** 843, 1977.

10.   R. M. Metzger, N. E. Heimer and G. J. Ashwell, *Molecular Crystals Liquid Crystals,* **107,** 133, 1984.

11.   A. V. Nabok, A. K. Ray, A. K. Hasan, J. R. Travis and M. J. Cook, *Supramolecular Sci. ,* 407, 1997.

12.   N. K. Adam, " *The Physics and Chemistry of Surfaces",* Oxford University Press.

13.   R. A. Broughton, Sheffield Hallam University, PhD Thesis, 1993.

14. G. J. Ashwell, M. Malhotra, M. R. Bryce and A. M. Grainger, *Synth. Met.* , **41**, 3172, 1991.

15. S. Akhtar, J. Tanaka, R. M. Metzger and G. J. Ashwell, *Mol. Cryst. Liq. Cryst.* , **139**, 353, 1986.

16. A. K. Ray, O. Omar, C. S. Bradley, N. A. Bell, D. J. Simmonds, S. C. Thorpe and R. A. Broughton, *Optical Materials*, in press.

17. E. Kretschmann and H. Raether, *Z. Naturforsch.* , **23a**, 2135, 1968.

Acknowledgements

I would like to express my warmest thanks to Dr Norman Bell of the School of Science for his never ending support and encouragement throughout this work and a special thanks to Dr Richard Broughton of the Health and Safety Executive for his enlightening 'discussions' and guidance.

I would also like to thank Dr Derek Simmonds and Professor David Allen for their advice and help with the organic synthesis part of this work. A special thanks is also due to Dr Steve Thorpe of the Health and Safety Laboratory without whose help and support much of this work would have been impossible.

My time in Sheffield has been a long and very happy one, during which I have gained many friends, who are too numerous to name here. However, I would just like to say a big thanks to the following:- John (Biz), Smithy, Paul (Criminal), Simon H, Steve (Uncle), Jackie, Simon S, Anita, Clive, Doog, Ben, Hilke and Emma.

Last but not least, I would like to thank my family, especially my long suffering parents who have had to put up with someone who refused to forsake student life for nearly a decade.